Technical Report ITL-95-4
June 1995

US Army Corps of Engineers
Waterways Experiment Station

Parametric Evaluation of Construction and Analysis Procedures Using Nonlinear, Incremental Structural Analysis

by Barry D. Fehl, WES
Kevin Z. Truman, Gary Warmka, Washington University

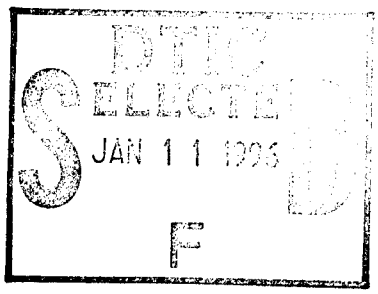

Original contains color plates: All DTIC reproductions will be in black and white

Prepared for Headquarters, U.S. Army Corps of Engineers

DISCLAIMER NOTICE

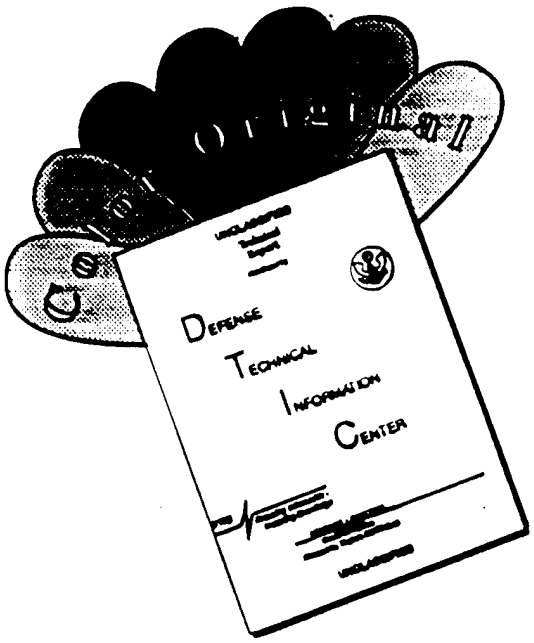

THIS DOCUMENT IS BEST QUALITY AVAILABLE. THE COPY FURNISHED TO DTIC CONTAINED A SIGNIFICANT NUMBER OF COLOR PAGES WHICH DO NOT REPRODUCE LEGIBLY ON BLACK AND WHITE MICROFICHE.

Technical Report ITL-95-4
June 1995

Parametric Evaluation of Construction and Analysis Procedures Using Nonlinear, Incremental Structural Analysis

by Barry D. Fehl

U.S. Army Corps of Engineers
Waterways Experiment Station
3909 Halls Ferry Road
Vicksburg, MS 39180-6199

Kevin Z. Truman, Gary Warmka

Washington University
Department of Civil Engineering
One Brookings Drive
St. Louis, MO 63130

Final report

Approved for public release; distribution is unlimited

Prepared for U.S. Army Corps of Engineers
Washington, DC 20314-1000

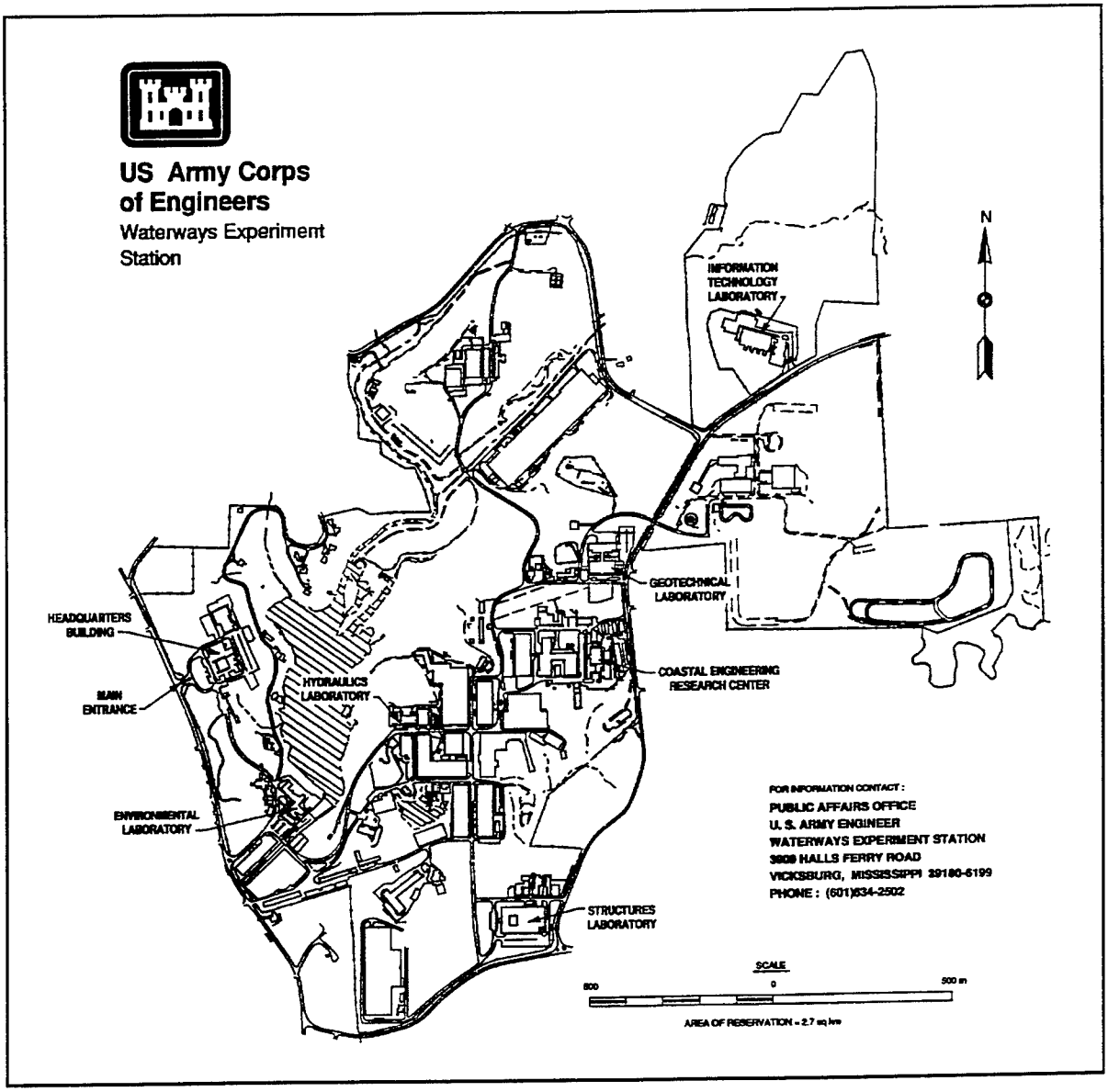

Waterways Experiment Station Cataloging-in-Publication Data

Fehl, Barry D., 1957-

Parametric evaluation of construction and analysis procedures using nonlinear, incremental structural analysis / by Barry D. Fehl, Kevin Z. Truman, Gary Warmka ; prepared for U.S. Army Corps of Engineers.

208 p. : ill. ; 28 cm. -- (Technical report ; ITL-95-4)

Includes bibliographic references.

1. Concrete construction -- Deterioration. 2. Structural analysis (Engineering) 3. Strains and stresses. I. Truman, Kevin Zane. II. Warmka, Gary R. III. United States. Army. Corps of Engineers. IV. U.S. Army Engineer Waterways Experiment Station. V. Information Technology Laboratory (US Army Corps of Engineers, Waterways Experiment Station) VI. Title. VII. Series: Technical report (U.S. Army Engineer Waterways Experiment Station) ; ITL-95-4.

TA7 W34 no.ITL-95-4

Contents

Preface

The investigation described in this report was conducted as part of the development of ETL 1110-2-365, Nonlinear, Incremental Structural Analysis of Massive Concrete Structures, 31 August 1994. The work was performed by the Computer-Aided Engineering Division (CAED), Information Technology Laboratory (ITL), U.S. Army Engineer Waterways Experiment Station (WES), and Washington University, St. Louis, MO. Funds for publication of the report were provided from those available for the Computer-Aided Analysis of Massive Concrete Structures Work Unit of the Structural Engineering Program of the Civil Works R&D Program.

The investigation was accomplished under the general supervision of Dr. N. Radhakrishnan, Director, ITL, and under the direct supervision of Mr. H. Wayne Jones, Chief, CAED. This report was prepared by Mr. Barry D. Fehl, CAED, and Dr. Kevin Z. Truman and Mr. Gary Warmka, Washington University. The authors acknowledge members of the Massive Concrete Structures Computer-Aided Structural Engineering Committee who reviewed this report and provided comments.

At the time of publication of this report, Dr. Robert W. Whalin was Director of WES. Commander was COL Bruce K. Howard, EN.

Conversion Factors, Non-SI to SI Units of Measurement

Non-SI units of measurement in this report can be converted to SI units as follows:

Multiply	By	To Obtain
Btu (International Table) per pound (mass) · degree Fehrenheit	4,186.8	joules per kilogram kelvin
Btu (International Table) inch per hour-square inch-degree Fahrenheit	20.7688176	watts per meter kelvin
degrees (angle)	0.01745329	radians
Fahrenheit degrees	5/9	Celsius degrees or kelvins[1]
feet	0.3048	meters
inches	0.0254	meters
miles (U.S. statute)	1.609347	kilometers
pounds (force) per square inch	6,894.757	pascals
pounds (mass) per cubic feet	16.01846	kilograms per cubic meter
pounds (mass) per cubic inch	27,679.899	kilograms per cubic meter

[1] To obtain Celsius (C) temperature readings from Fahrenheit (F) readings, use the following formula: C = (5/9) (F - 32). To obtain kelvin (K) readings, use: K = (5/9) (F - 32) + 273.15.

1 Introduction

Background

Nonlinear, incremental structural analysis (NISA) is an analysis method used on Corps of Engineers projects to evaluate massive concrete structures with respect to their aging characteristics and their construction sequence. The NISA process used to perform the studies reported herein has been used since the early 1980's when the U.S. Army Engineer District, St. Louis, took the initiative to have the U.S. Army Engineer Waterways Experiment Station (WES) develop a state-of-the-art method for evaluating thermal stresses of mass concrete structures to be applied to the Melvin Price Locks and Dam project (Truman, Petruska, and Ferhi 1992). It was through this study that the tools and methods for performing a NISA were established, including the selection of the finite element code ABAQUS (Hibbitt, Karlsson, and Sorensen 1989) and a constitutive model to be used with ABAQUS.

Since the first study, several other projects have had evaluations performed using the NISA methodology. Lock and Dam No. 4 on the Red River (Garner, Hammons, and Bombich 1991), Olmsted Locks and Dam on the Ohio River (Garner et al. 1992; Merrill, Fehl, and Garner 1995; Fehl and Merrill in preparation; Fehl et al. in preparation) and McAlpine Lock Replacement also on the Ohio River (Fehl, Riveros, and Garner in preparation) have all been evaluated using the NISA process. Each study has provided some insight on improving NISA methods and making the NISA a more valuable tool.

Since the NISA process was an innovative method for performing analysis of massive concrete structures, initially there were no guidance documents available for designers. Subsequent to the NISA performed for the Melvin Price project, Engineering Technical Letter (ETL) 1110-2-324 was written and published in March 1990 and established certain procedures to follow when performing a NISA. Since ETL 1110-2-324 was written primarily from experience gained from the Melvin Price project NISA, it was discovered that applying procedures in the ETL to other projects provided limitations in the analyses which were not appropriate. To account for these types of discrepancies, a new ETL was written to

replace ETL 1110-2-324. ETL 1110-2-365 was published in August 1994 and incorporated experience gained from performing NISA's on the analyses mentioned previously.

Objective

The primary objective of this report is to document work that was performed during the development of ETL 1110-2-365 for future reference. As part of this objective, conclusions and recommendations will be provided based on the results of the analyses to be used by designers and researchers to assist in making judgements when performing NISA's in the future. It is important for the database of information to be as broad as possible when dealing with a complex analysis procedure such as NISA, and this report is intended to increase our knowledge regarding analysis of massive concrete structures.

Parametric studies are often performed in many areas of engineering to evaluate the performance of an individual parameter or group of parameters. Analyzing different load cases for a structure is essentially a parametric study. Numerous parametric studies have been performed using the NISA approach to estimate the effects of parameters such as concrete placing temperatures, creep, shrinkage, and lift heights.

The parametric studies discussed in this report were performed during the development of ETL 1110-2-365 to assist in developing the guidance contained in the document. The studies performed were starting construction during different seasons of the year (Chapter 3), an evaluation of plane stress analysis versus plane strain analysis versus generalized plane strain analysis (Chapter 4), the length of time between lift placements (Chapter 5), and the effects of temperature due to the heat of hydration and ambient conditions (Chapter 6).

The parametric studies performed for this study were performed on a model developed for Melvin Price Locks and Dam, Alton, IL, on the Mississippi River just north of St. Louis, MO. Melvin Price Locks and Dam is a navigation structure consisting of a gated dam and two locks. The nine gatebays use tainter gates to control the pool elevation upstream of the lock during normal river conditions. The main lock at the project is 1,200 ft long, and the auxiliary lock at the project is 600 ft long. Both locks were constructed as U-frame locks which means that walls and base slab of the lock act as a unit when loaded.

The monolith selected for analysis in the parametric studies was the lower miter gate monolith of the auxiliary lock. An isometric view of this monolith is shown in Figure 1. Not shown in the isometric view are large voids in the lock walls which were used to reduce the weight of the monolith to reduce the pile loads. Analyses were performed on this model as

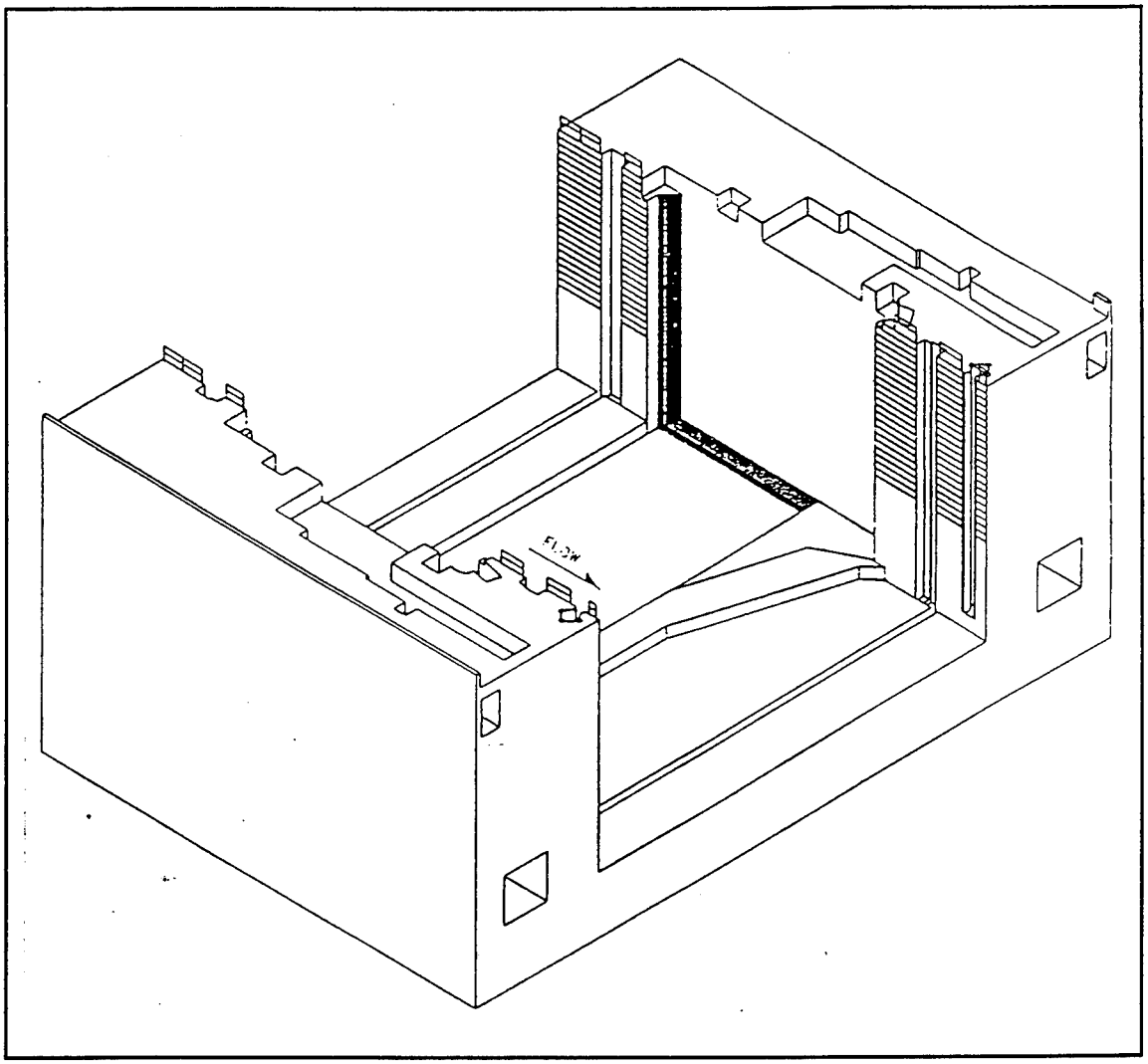

Figure 1. Isometric view of lower miter gate monolith at Melvin Price Locks and Dam

part of the NISA performed on the Melvin Price Locks and Dam project (Truman, Petruska, and Ferhi 1992).

Results of the various analyses will be documented through various graphical presentations. For results from heat transfer analyses, time-history plots showing temperature changes at a point as a function of time and contour plots showing temperatures at a given time will be shown. For the stress analysis, time-history plots of horizontal and vertical stress as a function time, contour plots of stresses at a given time, and, as necessary, crack plots showing the location of cracking as predicted by the constitutive model will be presented. Discussion will accompany the plots presented to distinguish the important points associated with the plots and to point toward the conclusions resulting from the analyses.

2 Modeling Parameters

Introduction

The model used in these parametric studies is an amalgamation of two NISA projects, Melvin Price and Olmsted Locks and the Dashield Lock Wall rehabilitation project. The geometry and some of the concrete properties for the lock monolith being modeled are those of a gate monolith for the auxiliary lock at Melvin Price Locks and Dam, Alton, IL. The adiabatic temperature rise (heat of hydration) data used in the heat transfer analysis were an average of the experimentally derived values for concrete mixtures proposed for the Olmsted Locks design and for the Dashield Lock Wall rehabilitation project. Many different concrete mixtures have been studied with regard to heat transfer properties since the early NISA studies performed on the Melvin Price Locks. The range in the adiabatic temperature rise data is quite large, therefore, it was decided to use a moderate heat generating mixture rather than one of the extremes. The heat transfer and mechanical properties for the soil, air, and ambient conditions are based on having a construction site in Alton, IL. The concrete mechanical properties are based on the experimentally derived properties of the Olmsted Locks.

Finite Element Model

The finite element (FE) model used in the parametric studies of this report, as well as in the Melvin Price NISA, is shown in Figure 2. A two-dimensional (2-D) strip taken at the upstream end of the monolith was used for determining the geometry of the model. Dimensions of the 2-D section are shown in Figure 3. Voids in the section consist of the culvert, the weight reducing voids, and the gallery. To reduce the number of elements required in the model, a symmetrical boundary condition was applied at the lock center line. The mesh was developed to model a construction sequence using 16 lift placements as shown in Figure 2. In addition to the model of the monolith shown in Figure 2, an FE model of the soil to a depth of 10 ft was also modeled in both the heat transfer and stress analyses (Truman, Petruska, and Ferhi 1992.) Since the lock is a

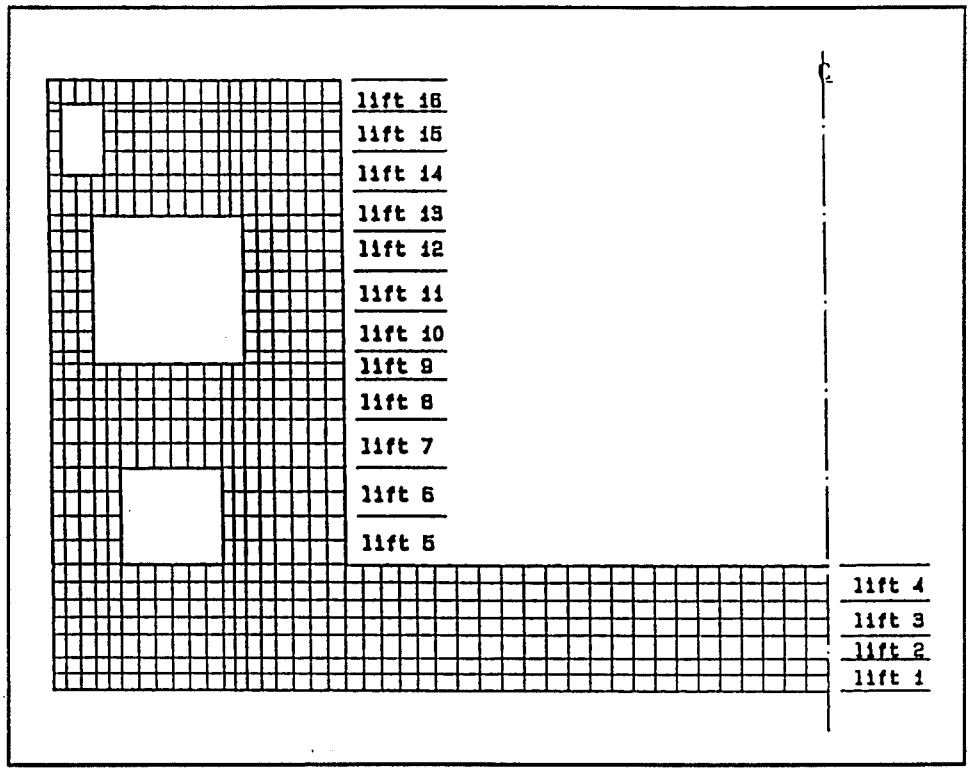

Figure 2. Finite element model and lift placement schedule of miter gate monolith

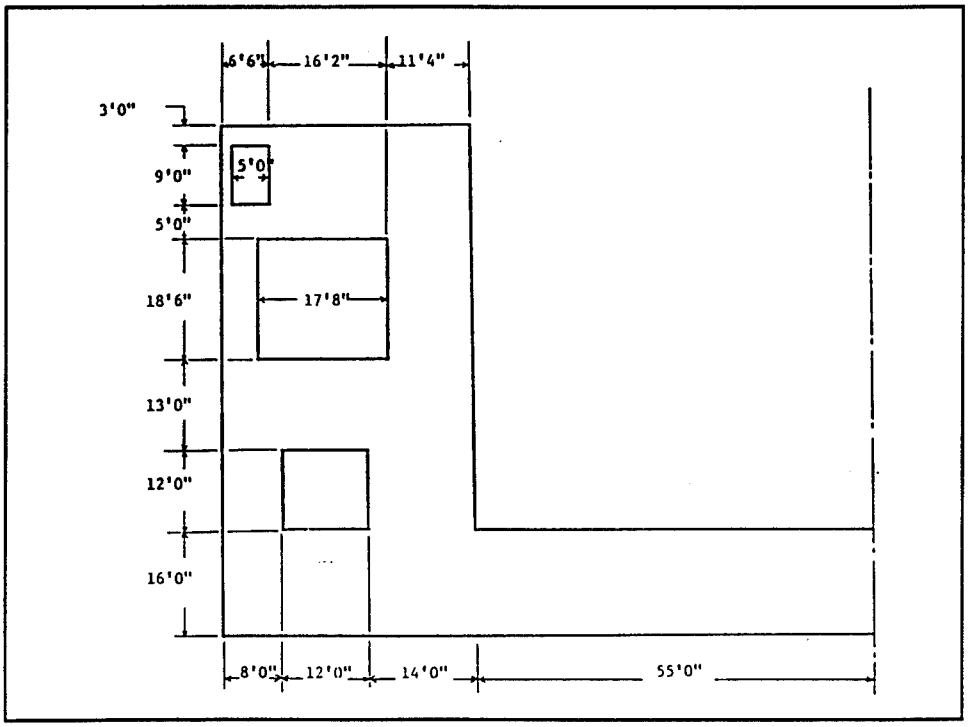

Figure 3. Geometry of miter gate monolith

pile-founded structure, piles were also included in the stress analysis model.

The density of the mesh is affected by the geometry of the structure, the location of the lift lines, and limits imposed by solution techniques used with ABAQUS in the heat transfer analysis. The limit imposed by ABAQUS restricts the element size as a function of the material density, specific heat, conductivity, and the minimum time increment used in the analysis. Further discussion of this limitation and the exact equation for computing the maximum element size is contained in ETL 1110-2-365 along with explanations on when these limits can be exceeded.

Heat Transfer Modeling Parameters

Ambient temperature

The data for the ambient temperature is the monthly average temperatures for Alton, IL, as provided by the National Weather Service. The daily average temperature data are shown in Figure 4. The maximum and minimum mean ambient temperatures for Alton are 80 and 32 °F, respectively. The mean ambient temperature data do not reflect daily variations in the ambient temperature data. For example, July 12 may reach a high

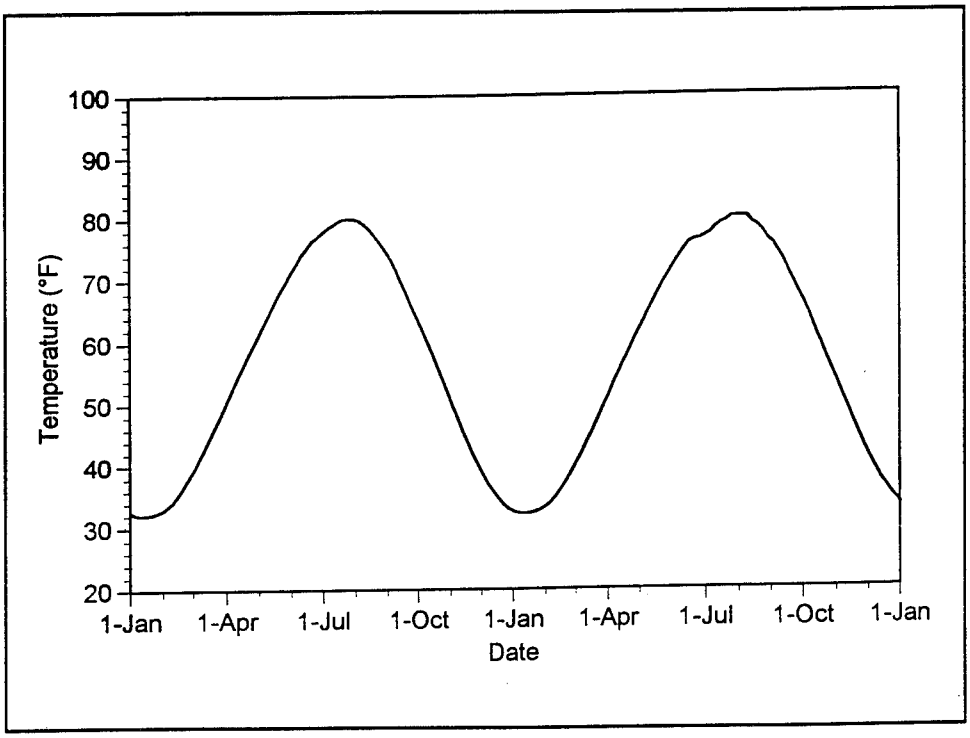

Figure 4. Average daily ambient curve

temperature of 95 °F and a low temperature of 65 °F, giving a daily average of 80 °F. This ambient temperature curve may be used for any construction start date. The data were used to extract digitized temperature data for every 5 days throughout a calendar year. The ABAQUS program uses interpolation and these 5-day values to generate the required temperatures for any time during the heat transfer analysis.

Heat of hydration

The heat due to hydration of the cementitious materials in concrete is modeled with the use of adiabatic temperature rise data. An adiabatic system is one in which heat is neither allowed to enter or leave. The adiabatic temperature rise is a direct measure of the change in temperature in a concrete mass when an adiabatic condition exists. The adiabatic temperature rise data are time dependent and serve as the internal heat generation mechanism in the heat transfer analysis. The amount and rate of heat generation is heavily dependent upon the cementitious materials in the mixture.

The adiabatic temperature rise data used in these studies are the average of the adiabatic temperature rise test data for the concrete mixture at Dashield Lock Wall rehabilitation project and concrete mixtures 6 and 11 from the Olmsted Locks and Dam project (Hammons et al. 1991) as shown in Figure 5. The Dashield concrete mixture has a high heat of hydration compared to many of the mixtures used in previous NISA studies. Since the main focus in these parametric studies was not concerning the

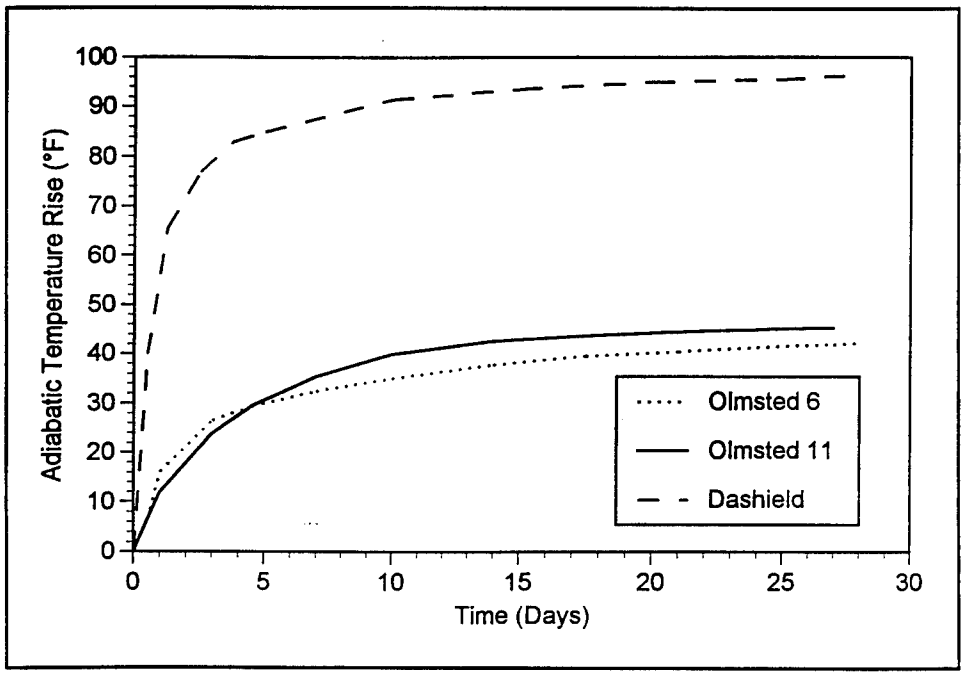

Figure 5. Adiabatic temperature rise data from Dashield and Olmsted projects

concrete properties, a concrete with a moderate heat of hydration was developed. The average adiabatic temperature rise curve used in the analysis uses the average of the Dashield and Olmsted mixture 6 data for the first 3 days and the average of the Dashield and Olmsted mixture 11 data for times later than 3 days. The average adiabatic temperature rise curve used in the parametric studies is shown in Figure 6. The maximum adiabatic temperature rise curve shown in Figure 6 is the Dashield experimental data. The minimum adiabatic temperature rise curve in Figure 6 is the Olmsted mixture 6 for the first 3 days and mixture 11 for any time later than 3 days.

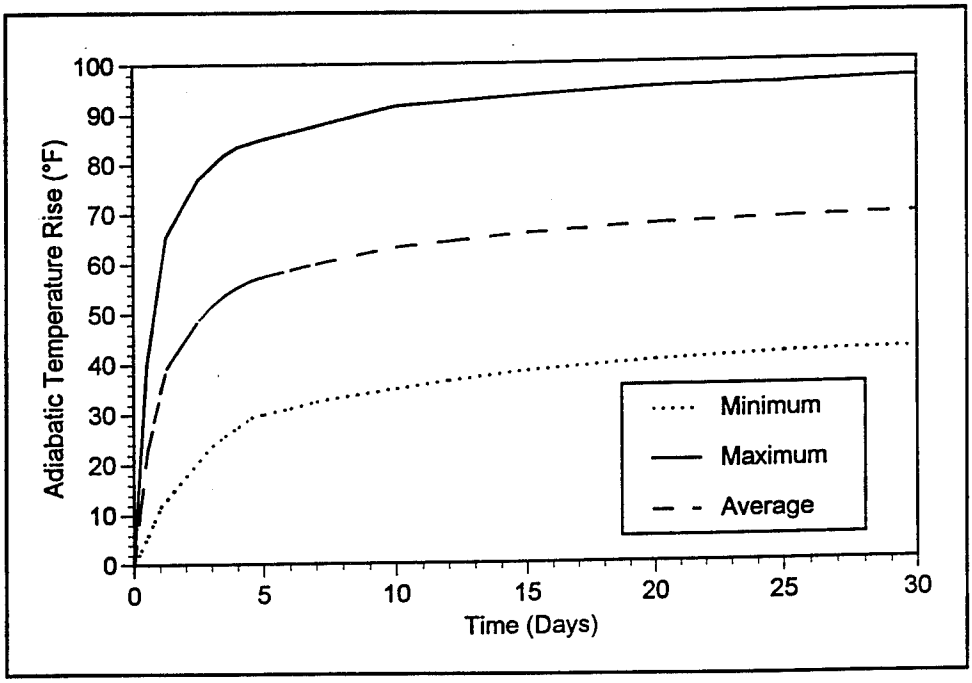

Figure 6. Maximum, minimum, and average adiabatic temperature rise curves considered for studies

Thermal conductivity, specific heat, and density

The concrete, soil, and air heat transfer properties for thermal conductivity, specific heat, and density were based on the Melvin Price Lock properties. Thermal conductivity is a measure of the quantity of heat flowing through a unit volume of material subjected to a unit temperature differential. Specific heat is the amount of heat required per unit mass to cause a unit rise of temperature. The density is the mass per unit volume. The density is required to interact with the specific heat and thermal conductivity since they are based on unit mass and unit volume measurements, respectively. The thermal conductivities and specific heat values and densities for the concrete, soil, and air are given in Table 1.

Table 1
Material Properties - Heat Transfer Analysis

Property	Variable	Value	Units
Concrete			
Conductivity	k	2.3494	Btu-in./day-in.^{2}-°F
Density	γ	0.0871	lb/in.^{3}
Specific Heat	c	0.2100	Btu/lb-°F
Foundation			
Conductivity	k	1.5840	Btu-in./day-in.^{2}-°F
Density	γ	0.0758	lb/in.^{3}
Specific Heat	c	0.4500	Btu/lb-°F
Air			
Conductivity	k	24,000	Btu-in./day-in.^{2}-°F
Density	γ	4.6E-5	lb/in.^{3}
Specific Heat	c	0.2400	Btu/lb-°F

Initial soil temperature distribution

Initial soil temperature distributions for the first 20 ft of soil were generated by performing a 365-day heat transfer analysis. The ambient temperatures are applied to the soil surface and a constant temperature of 55 °F at the 20-ft depth. The modeling and generation of initial soil temperature distributions have been discussed in previous publications (Truman, Petruska, and Ferhi 1992.) Two soil temperature distributions were developed to be used in these studies. The first was using a July 1 start date and the second was using a January 2 start date. The initial temperature of the top layer of the soil is dramatically different for the January 2 versus the July 1 start dates which is due to the difference in ambient conditions for the different dates. April and September initial soil temperature distributions were assumed to be identical to the July 1 values. The initial soil temperature distributions typically affect only the first lift of concrete. These effects can be as minor as slight changes in the stresses or as major as the creation of localized cracking. The temperature differential between the initial soil temperature distribution and the placement temperature of the April and September first lifts is not significant enough to cause cracking, therefore, the use of the July 1 initial soil temperature distribution will have a minor effect in the first lift stresses. The second and subsequent lifts are generally unaffected by the initial soil temperature distributions. The soil temperature distributions are shown in Figure 7.

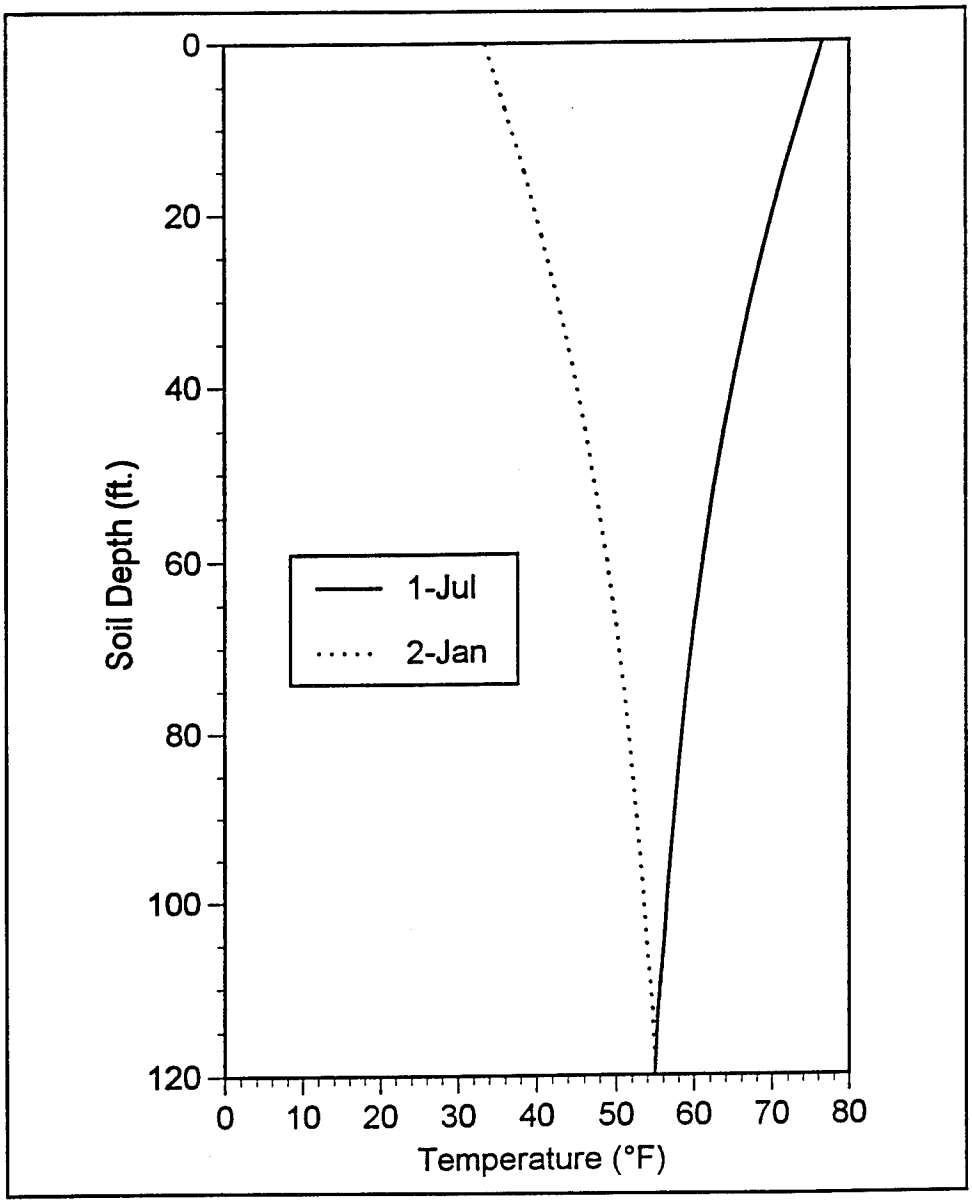

Figure 7. Initial soil temperature distribution

Film coefficients

Film coefficients are used to model convection. Convection is the process of the heat transfer that occurs between the air and the concrete. Every exposed surface, whether with or without forms and/or insulation, must have a film coefficient to model the convective process of heat removal due to wind passing over the surface (ETL 1110-2-365). The film coefficients for surfaces without forms or insulation are given in Table 2. The film coefficients for the formwork were developed for 3/4-in. plywood forms and a wind velocity of 10 mph for the exposed external surfaces and 1 mph for the culvert. The coefficients are different for the culvert, machine room, and the exterior surfaces due to the relationship of

Table 2
Film Coefficients

Description	Variable	Value	Units
Outer Walls			
Uninsulated Forms	h′	0.1411	Btu/day-in.^{2}-°F
Insulated Forms	h′	0.0322	Btu/day-in.^{2}-°F
Insulated Surface	h′	0.0393	Btu/day-in.^{2}-°F
Exposed Surface	h	0.6792	Btu/day-in.^{2}-°F
Machine Room Walls			
Uninsulated Forms	h′	0.0857	Btu/day-in.^{2}-°F
Insulated Forms	h′	0.0280	Btu/day-in.^{2}-°F
Insulated Surface	h′	0.0333	Btu/day-in.^{2}-°F
Exposed Surface	h	0.1650	Btu/day-in.^{2}-°F
Gallery/Culvert Walls			
Uninsulated Forms	h′	0.1253	Btu/day-in.^{2}-°F
Insulated Forms	h′	0.0313	Btu/day-in.^{2}-°F
Insulated Surface	h′	0.0379	Btu/day-in.^{2}-°F
Exposed Surface	h	0.4224	Btu/day-in.^{2}-°F

the film coefficient to the wind velocity. These coefficients must change during the analysis to reflect the removal of forms, removal of insulation, closing of the machine room, and placement of the top on the culvert. The air in the machine room, once closed, has no velocity; therefore, the film coefficient for its exposed surface is significantly reduced compared to that of the exposed surface of the outer walls. It is also assumed that once the top of the culvert is placed, the wind velocity of the air passing through the culvert is reduced compared to that of the wind passing over exposed surfaces of the outer walls, and the culvert exposed surface film coefficient is reduced. The film coefficients must be modified to reflect insulated and uninsulated formwork and insulated surfaces with no formwork. The method for modifying these coefficients is outlined in ETL 1110-2-365 which provides these equations:

$$h' = \frac{1}{\left(\frac{b}{k}\right)_{formwork} + \left(\frac{b}{k}\right)_{insulation} + \left(\frac{1}{h}\right)}$$

$$= \frac{1}{R_{formwork} + R_{insulation} + \left(\frac{1}{h}\right)}$$

where

h' = revised film coefficient including formwork and/or insulation

h = exposed surface film coefficient

b = thickness of the formwork or insulation

k = conductivity of the formwork or insulation

R = resistance of the formwork or insulation

The insulating effects of having formwork and/or insulation reduces the rate of heat transfer between the concrete and the surrounding air, therefore, the film coefficients are smaller than those for exposed surfaces.

Placement temperatures

The concrete placement temperature is primarily a function of the ambient conditions, the concrete mixture and the construction specifications. The parametric study for the start of construction was first performed with the January, April, July, and September each having a constant concrete placement temperature of 65 °F. The placement temperature was assumed to be constant to limit the number of variables that would be changing to quantify the effects of the changing start dates.

A second study was performed for the January start of construction using concrete placement temperatures indicative of actual construction specifications. The placement temperature for a given lift for the January construction start date study using the construction specification values was assumed to be between 40 and 65 °F. When the ambient temperature was below 40 °F, it was assumed that the concrete constituents were heated and that the placement temperature was 40 °F. When the ambient temperature was above 65 °F, it was assumed that the concrete constituents were cooled and the concrete was placed at 65 °F. When the ambient temperature was between 40 and 65 °F, it was assumed that the placement temperature was the ambient temperature. The results of this second study is compared to the results of the January start of construction using

a constant 65-°F placement temperature to quantify the effects of accurate modeling of placement temperatures.

Lift placement and formwork

For the parametric studies performed in Chapters 3 and 4, the lift placement interval was kept constant at 5 days. Chapter 5 presents results and a discussion of the effects of longer lift placement intervals. The forms were modeled as being in place for the first 2 days and removed for the remainder of the construction. The use of insulated forms and insulation without forms was indicative of typical specifications for this type of structure. If the lift was placed during the time period between November 1 and April 2, insulated forms were used, the top of the lift was insulated, and the exposed concrete was insulated after form removal. Typical specifications indicate a minimum insulation period of 45 days with the exception that no region need be insulated after April 1. Therefore, the insulation for a given lift was removed either 45 days after placement or on April 2, which ever came first.

Stress Analysis Modeling Parameters

Modulus of elasticity

The modulus of elasticity is typically defined as the ratio of normal stress to the corresponding load dependent strain. The modulus of elasticity used in a NISA is referred to as an aging modulus due to its dependency on the age of the concrete, as shown in Figure 8. The aging modulus is dependent upon the age and temperature of the concrete. The model used does not account for temperature effects due to the lack of data. The modulus is dependent upon the degree of hydration making it highly dependent upon the age of the concrete. There is limited data for the aging modulus of concretes for the first day after. Therefore, the aging modulus is assumed to be a linear function for the first day after placement. The linear function has a value of zero at the time of placement and the experimentally found value at the age of 1 day. The remainder of the aging modulus versus the age curve in Figure 8 is experimentally determined.

Poisson's ratio

Poisson's ratio is the ratio of lateral to the longitudinal strain resulting from a uniformly distributed axial stress. Poisson's ratio is dependent upon age and temperature, but the lack of experimental data prohibits the modeling of these effects. A constant value used in this study is a typical design value of 0.15.

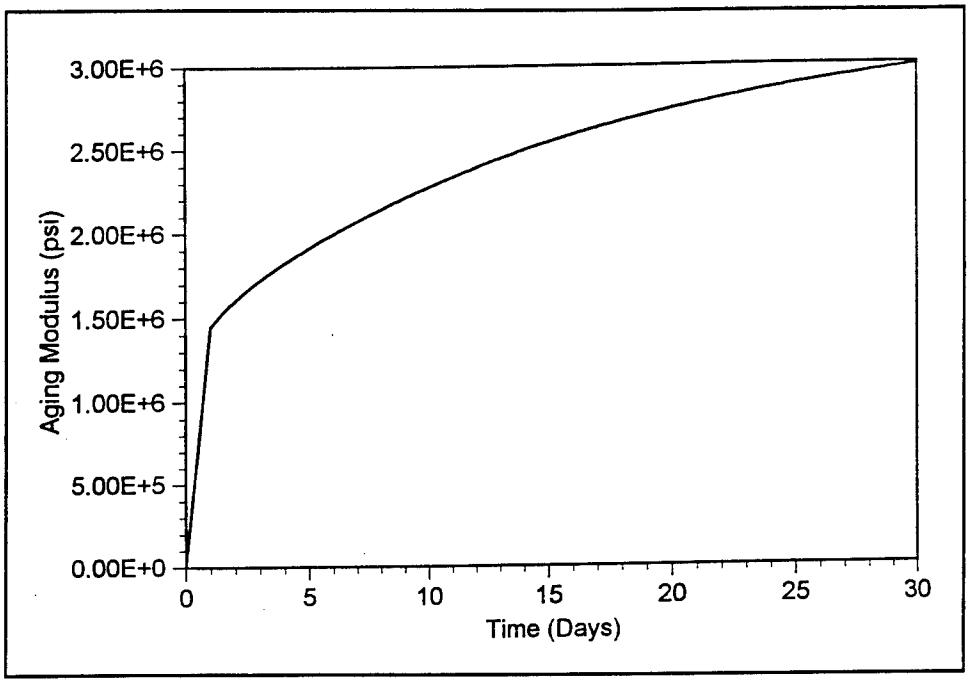

Figure 8. Aging modulus of elasticity curve

Autogenous shrinkage

Autogenous shrinkage is the shrinkage of concrete due to the hydration of the cementitious materials, and it can be significant in mass concrete structures. Autogenous shrinkage includes no shrinkage effects due to a loss or gain of moisture. Drying shrinkage is shrinkage associated with a loss of moisture and is typically associated with surface cracking. The current model is incapable of modeling drying shrinkage. Autogenous shrinkage is an age varying phenomenon and is modeled as a function of time as shown in Figure 9. The shrinkage curve shown can be scaled to reflect different levels of autogenous shrinkage. The curve shown in Figure 9 has already been scaled by the shrinkage factor given in Table 3.

Creep

Creep is the time-dependent deformation of the concrete due to a sustained load. Creep is highly dependent on the aging modulus and ultimate compressive strength of the concrete at the time of loading. Creep is modeled as an age and load dependent function as described in *UMAT - A Simplified Overview* (Truman and Fehl in preparation). The equation used to represent creep in the user defined material subroutine was scaled using the creep factor given in Table 3.

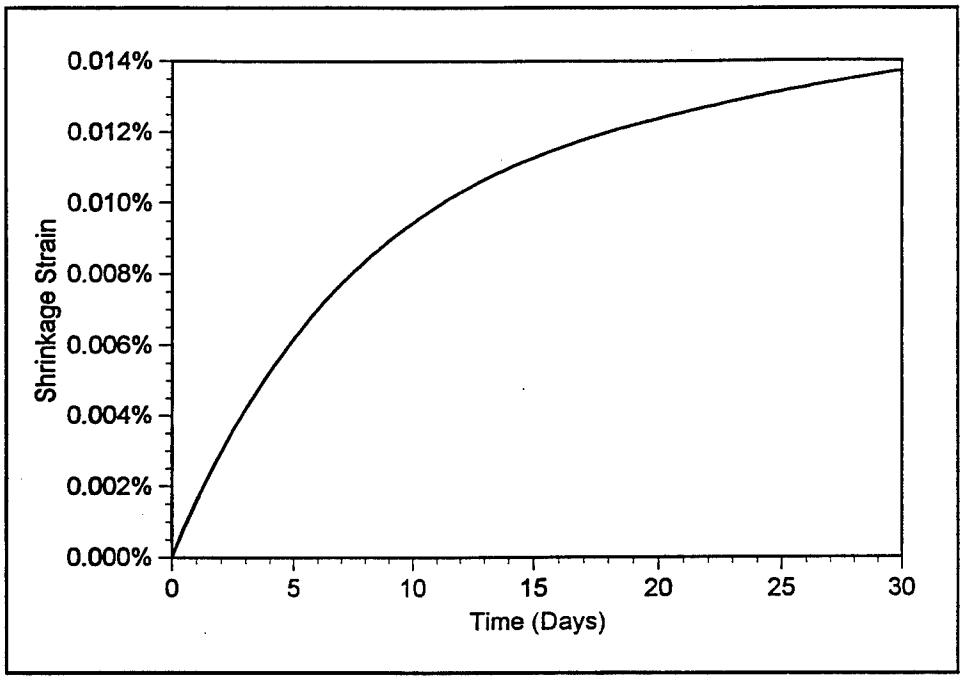

Figure 9. Autogenous shrinkage curve

Table 3
Material Properties - Stress Analysis

Description	Variable	Value	Units
3-day Crushing Strength	$f'_b(3)$	675.0	psi
Cracking Strain	ε_o	1.oE-4, 0.5E-4	
3-day Modulus	E(3)	2.1E6	psi
Poisson's Ratio	ν	0.15	
Coefficient of Thermal Expansion	α	4.0E-6	in./°F
Shrinkage Factor		1.10	
Creep Factor		0.9	

Coefficient of thermal expansion

The coefficient of thermal expansion is the change in a given dimension due to a unit change in temperature in the direction of the dimensional change. This quantity is highly dependent upon the type and quantity of aggregate in the concrete mixture. The coefficient of thermal expansion used in these analyses is given in Table 3.

Tensile strain capacity

The tensile strain capacity is required for the implementation of the cracking model. The failure or cracking criterion is discussed in Addendum B, Appendix A, ETL 1110-2-365. Actual cracking of concrete is age and rate of loading dependent. The rate of loading is assumed to be slow in the case of most mass concrete structures. Therefore, the cracking criterion model does not account for the rate of loading and is modeled only as age dependent.

Since the rate of loading is assumed to be slow, the tensile strain capacity of the concrete is determined from a slow load test as discussed in ETL 1110-2-365. The studies discussed in Chapters 3 and 4 use a tensile strain capacity of 50 microstrains, whereas, the other studies used a value of 100 microstrains. The value of 50 microstrains would be considered low or a minimum and was used in the start of construction parametric studies to give a worst case for cracking and to provide clear indications of critical regions where cracking could occur. The value of 100 microstrains would be a typical value for mass concrete structures. It was used in the lift interval studies of Chapter 5 to give typical crack patterns with respect to the varied lift placement intervals.

Gravity loads

Gravity effects are modeled in two different ways. When the concrete is first placed, the concrete does not have adequate strength to support itself without failing the cracking criterion. In reality the concrete is held in place by the forms for a minimum of 2 days, thereby, providing the needed support and time for the concrete to gain strength without cracking. Modeling the structural properties, placement and connectivity of the formwork becomes complicated and unnecessary. Therefore, the gravity effects of a newly placed lift on a previous lift is simulated by using a uniformly distributed load along the top of the previous lift. Two days after placing the new lift, the uniformly distributed load is removed. By the second day, the new lift has gained adequate strength to carry its own weight and is loaded with a body force. The density for the concrete used in the body force application is given in Table 3.

Thermal loads

The thermal related stresses are generated by finding the thermal gradients or change in neighboring nodal temperatures. The nodal temperatures are provided from the heat transfer analyses. The heat transfer analysis results reflect the ambient conditions, insulation, heat generation, and soil temperature effects which all affect the final stress distributions in the structure.

Foundation

The soil and pile foundation are used to provide both early- and late-time support to the structure. The piles offer little or no support until the concrete ages and becomes structurally capable of spanning the distance between the piles. The soil is modeled with finite elements that are used to provide support at every node along the base of the structure. If this first lift is not adequately supported at early times, the concrete will have a stress-strain state that could violate the crack criterion. Therefore, the concrete in this first lift would be considered as cracked throughout the remainder of the stress analysis. The use of the soil elements minimizes the potential of premature or inaccurate cracking in the first lift. As the analysis progresses, the piles become the major load carrying component of the foundation.

The piles are modeled as vertical springs. The spring locations closely reflect the actual pile locations for the miter gate monolith of the auxiliary lock at Melvin Price Locks. The pile stiffnesses were derived by finding equivalent pile stiffnesses for a unit strip of the monolith. The piles were assumed to be uniformly distributed in the direction of flow (in and out-of-the plane). Therefore, the number of piles may be used to compute the total vertical stiffness and when this stiffness is divided by the length of the monolith, a stiffness for a unit length in the direction of flow may be obtained. In the direction transverse to the flow, the springs were located at the node closest to the design location of that pile as seen in Figure 10. The vertical stiffness per unit length in the direction of flow was evenly distributed to the number of piles in the direction transverse to the flow. The vertical stiffness of each pile was calculated as 19.751 k/in. per inch of thickness in the flow direction.

Summary

The modeling parameters have been chosen to serve several purposes. The need for useful parametric results with minimal changes in variables was one purpose. Changing one variable per analysis provides data which can be easily compared and synthesized with the knowledge that the changing variable is the cause for any differences in the results. A second purpose was to provide realistic modeling. Realistic modeling provides information regarding actual design specifications, proper modeling procedures, and the global effects of changing multiple variables.

The modeling parameters chosen primarily reflect those of the auxiliary lock at the Melvin Price Locks and Dam but have minor modifications to certain parameters to reflect accumulated experimental data. Experimentally derived heat generation data from Olmsted Locks and Dam and the Dashield Lock Wall rehabilitation project have been used to modify the heat generation properties of the concrete used in these analyses.

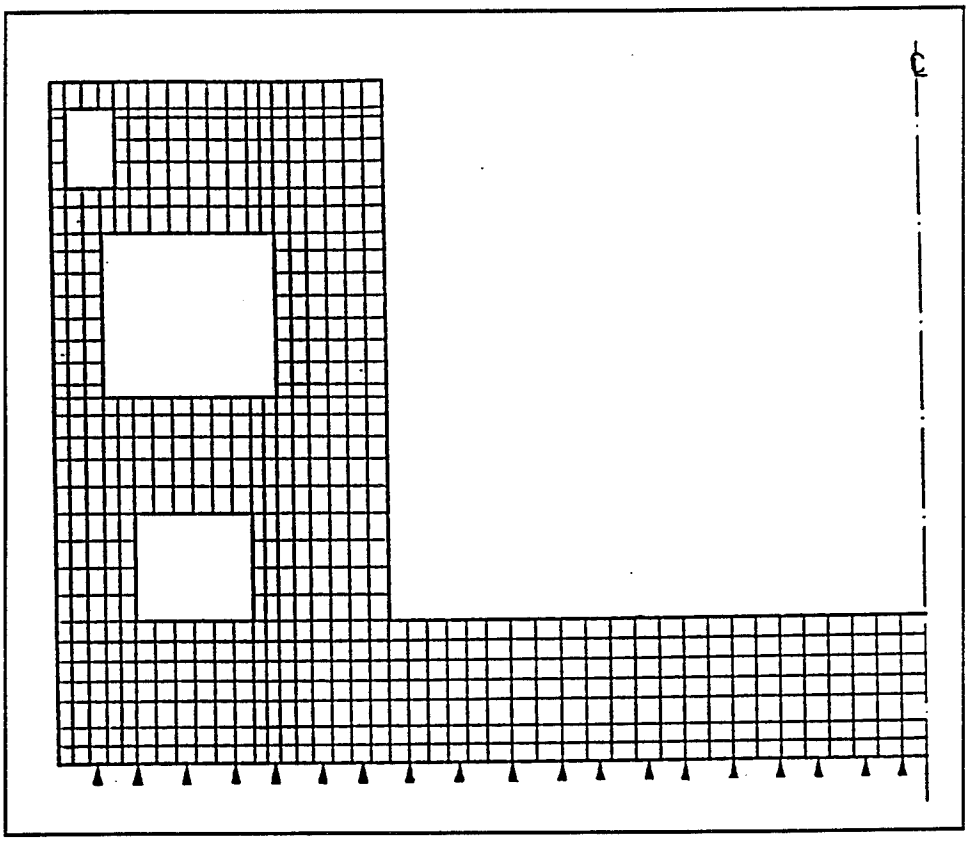

Figure 10. Pile locations

The derived heat generation properties represent a moderate heat generation concrete which was better suited for these parametric studies.

3 Construction Start Dates

Introduction

Four different dates were used to study the effects of seasonal construction start dates on the structural performance of massive concrete systems. In particular, this study was performed on a structural model representing AL-3, a gate monolith, for the Melvin Price Locks and Dam in Alton, IL. The dates for start of construction were January 2, April 2, July 1, and September 29. These dates were selected as representative dates for starting construction in each of the four seasons coupled with the need to maintain the constant 5-day time interval. Maintaining the 5-day time interval allows for direct comparison of the thermal and mechanical related responses. To have an unbiased parametric study regarding only the start dates, one study was performed where no other parameters were varied. This assumption provides realistic results for three of the four cases, April, July, and September, but unrealistic results for January. The January start of construction requires significant insulation and a changing concrete placement temperature in the placement temperatures due to the cold weather within the early stages of construction. The results presented are useful for the unbiased comparison of start dates as well as seeing the effects of improper construction procedures (no insulation) or improper modeling assumptions (ignoring insulation or varying placement temperatures). Since the January start date modeling did not accurately reflect January field conditions, an additional study was performed. The study, with a January 2 start of construction, included a change in the soil temperature profile, insulation of the concrete during cold weather, removal of the insulation when moderate ambient conditions arrived, and placement temperatures varying with the ambient conditions. This additional analysis closely models actual construction procedures as required for a January start of construction. This comparison of the results obtained from the two models using a January start of construction is beneficial for studying the effects of insulation and the need for realistic and accurate modeling of the construction process.

The results are presented in the form of nodal and element time-histories, as well as contour plots and crack surface diagrams. The nodal and element time-histories are very useful in tracking the construction and ambient

effects on the temperatures and stresses throughout time at a specific location. The contour plots give a snapshot in time and provide the state of the entire monolith at that specific instant in time. The temperature, stress, and crack potential contours are typically shown at 6-month intervals after the first concrete lift was placed. These intervals were chosen to show the seasonal effects after the monolith has been fully constructed. End of construction of the monolith occurs at 80 days (16 lifts placed at 5-day intervals). The crack surface diagrams show the locations and orientation of the cracks at a specific instant in time. The cracks seen in these diagrams indicate all cracks that have occurred through day 725 after the start of construction.

Thermal Analyses

Contour plots

The thermal results have several general trends regardless of the start date and age of the structure. These trends are very dependent upon the geometry and ambient conditions of the project. For instance, in Figure 11, the culvert is considered to be open with no insulation after the structure is complete; therefore, the temperatures surrounding the culvert and in the thinner wall tend to be very near ambient. On the other hand, the machine room is near the ambient temperature; therefore, the interior of the machine room has a temperature which is indicative of the larger concrete wall next to it. The thinner, exterior wall between the machine room and the ambient conditions can have a large temperature gradient reflecting the difference between the interior of the massive portion of the concrete and the ambient temperature. There tend to be higher temperatures within the more massive concrete portions such as above the machine room, between the machine room and the culvert, between the machine room and the lock chamber, and in the region of intersection between the chamber floor and the interior or chamber lock wall. The exterior surfaces typically have contours which parallel the surface and reflect the ambient conditions. The contours of the chamber floor tend to be parallel to the floor, since the top and bottom of the floor are the only means of heat transfer from the chamber floor. The contours in the floor intersect the center line at a right angle due to the symmetry boundary conditions at the center line of the structure. This is unlike the lower exterior corner of the monolith. The contours in this corner reflect the ambient condition on the exterior surface and the soil temperature on the bottom surface; therefore, the contours turn approximately 90 deg from horizontal within the lock floor to nearly vertical at the exterior wall. The typical line contour plots provide a very visual look at the temperature gradient, but the color contour plots shown in Figure 12 are generally simpler to numerically evaluate. The trends described using the line contour plots are easily seen in the color contour plots.

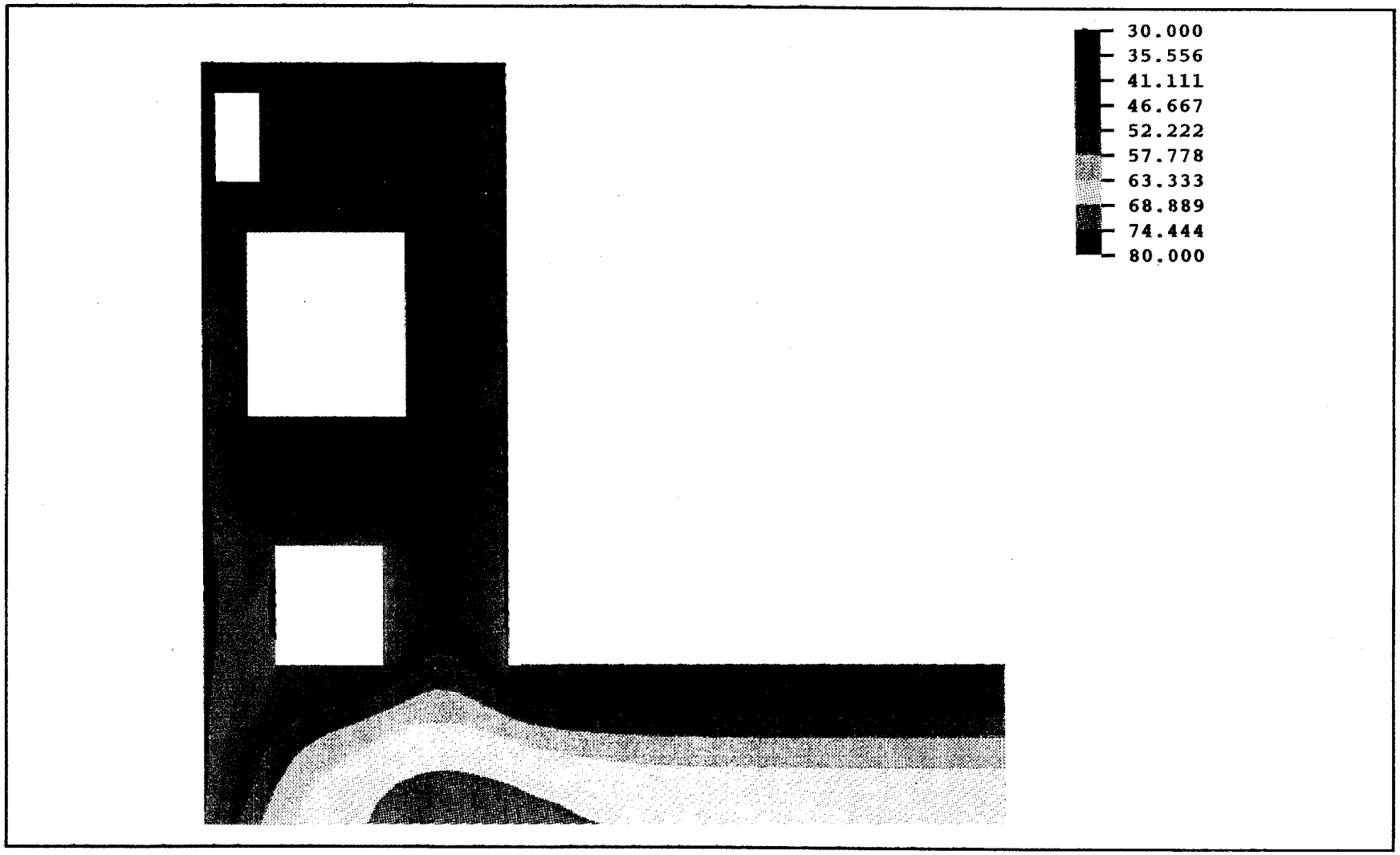

Figure 11. Typical line-temperature contour for 180 days after start of construction

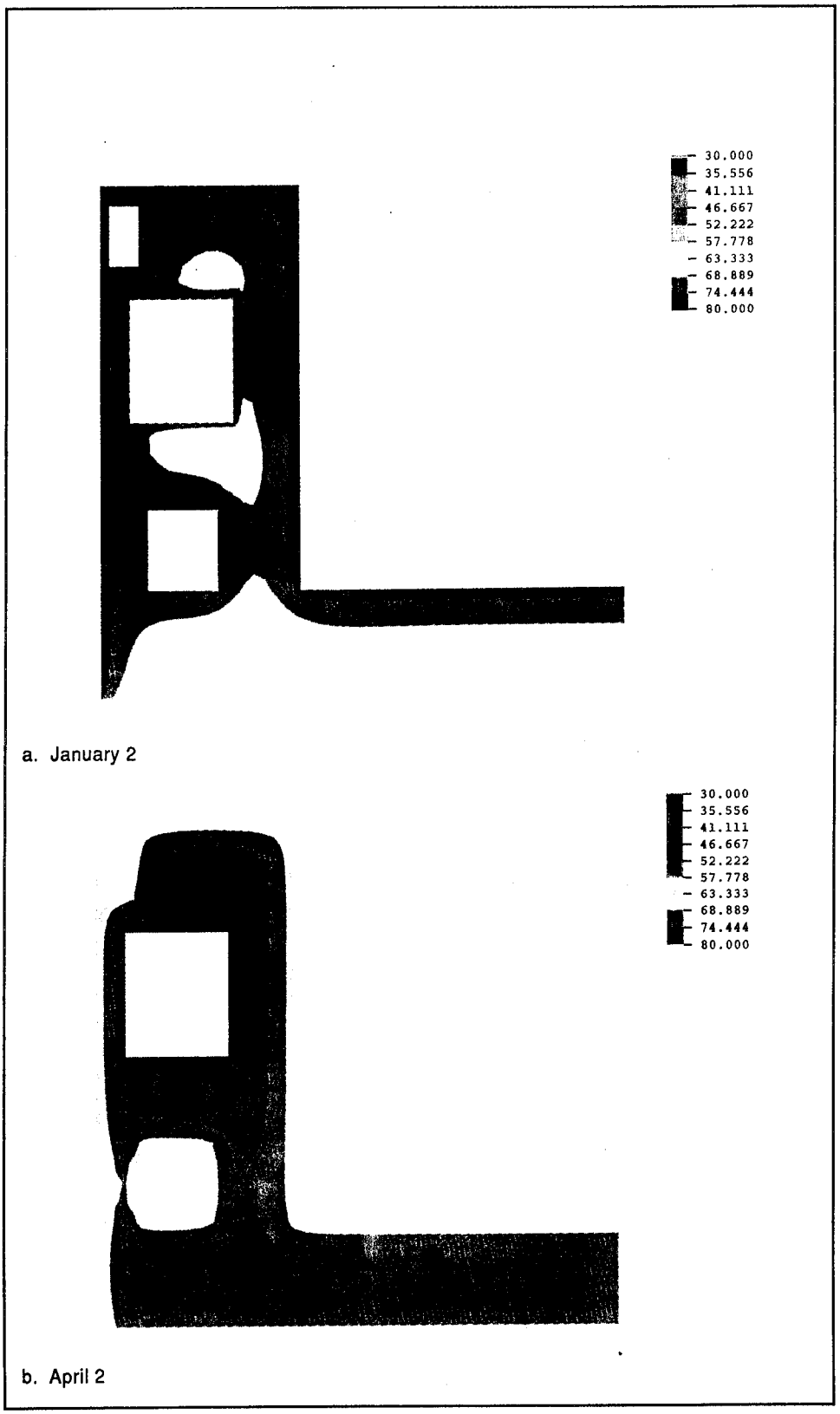

Figure 12. Temperature contours for 180 days after start of construction (step = 181, amp = 180) (Continued)

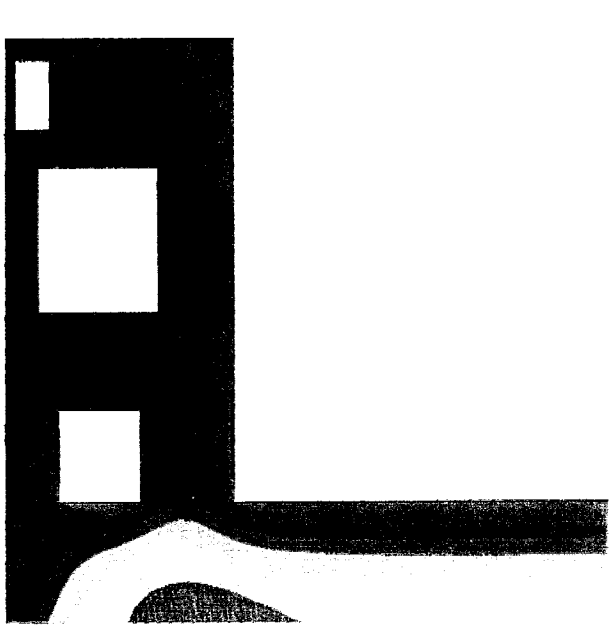

c. July 1

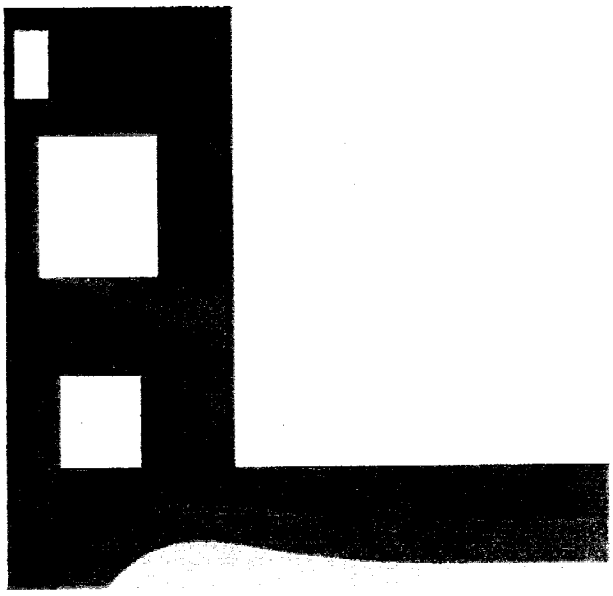

d. September 29

Figure 12. (Concluded)

These trends are apparent in all of the thermal contour plots shown after construction. The temperature contours change during construction due to the ever changing boundary conditions of insulation due to the formwork, placement of lifts causing the production of heat above the previously placed lifts, changing ambient conditions and changing geometry. These factors all have significant impact on the distribution of temperatures. Once the structure is complete, the temperature distribution is very much a function of the ambient conditions and the size of the structural elements comprising the mass concrete system. The temperature contours for 180 and 360 days after the start of construction are presented in Figures 12 and 13, respectively. The first fact to note is that the temperature inside the massive concrete systems after construction is completed is very dependent upon the ambient conditions. At 180 days after construction, April and January have the highest internal temperatures, near 80 °F. At 180 days after construction, the April monolith has just passed through the hottest ambient temperatures of the year and the January monolith is just entering the hottest month of the year. Conversely, at 180 days the July and September monoliths have cooler internal temperatures, since they are approaching or have just passed through the coldest ambient conditions of the year. The exterior surface temperatures for all four conditions reflect the ambient temperatures. The contours at 360 days after construction are useful in noting the thermal lag inherent in mass concrete systems. The interior temperature above the machine room for the September monolith after 1 year is 74 °F while it is only 63 °F for the July monolith after 1 year. The September monolith has just passed through the hottest season of the year and the July monolith is just entering the hottest season. This is easily seen by looking at the exterior surface temperatures. The top of the slab temperature for the July monolith is 77 °F, and the top of slab temperature for the September monolith is 67 °F. This thermal lag is also apparent in the January and April monoliths. April has a minimum internal temperature above the machine room which is approximately 10 °F cooler than that of the January monolith. It is clear that the thermal effects are now being driven by the ambient conditions. The contours for 1.5 years (545 days) are almost identical to those for 180 days, and the contours for 2 years (725 days) are nearly identical to those for 360 days. Therefore, the heat generated during construction seems to dissipate within 180 days after construction.

As seen from the contours, there are several areas which tend to have high thermal gradients, regions of closely spaced colors. These areas are potential locations of higher stresses. The chamber side or interior lower corner of the gallery, the thin wall between the machine room and the exterior surface, the chamber side or interior corners of the culvert, the top of the slab, and the interior wall of the chamber are all areas with high thermal gradients. These areas within the monoliths will typically be the areas where crack potentials will be high or where cracking will occur.

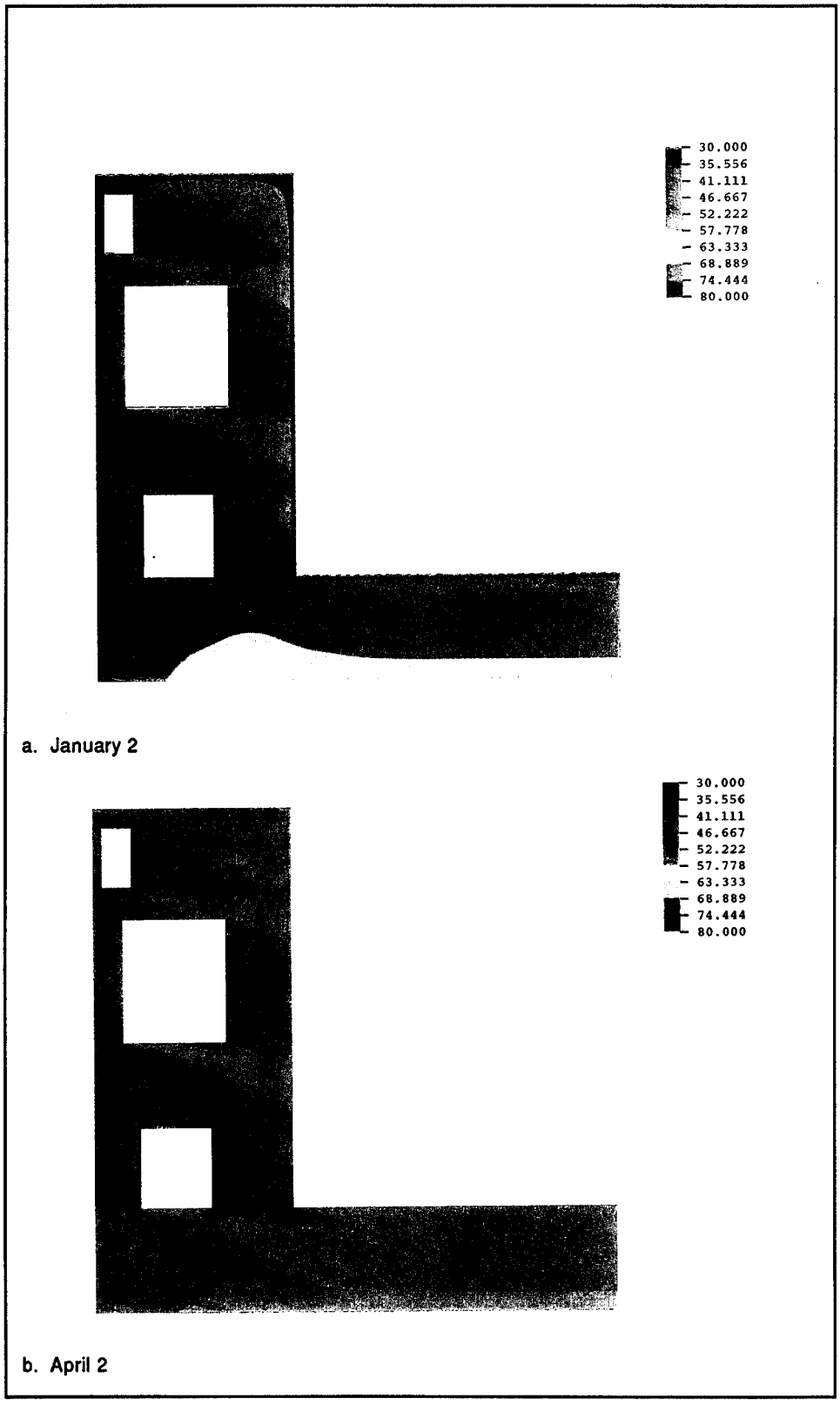

Figure 13. Temperature contours for 360 days after start of construction (step = 217, amp = 360) (Continued)

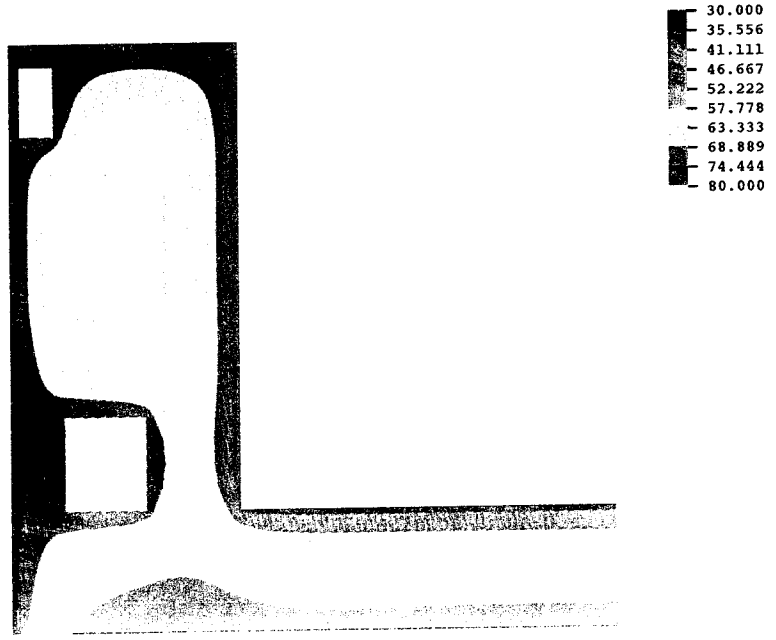

c. July 2

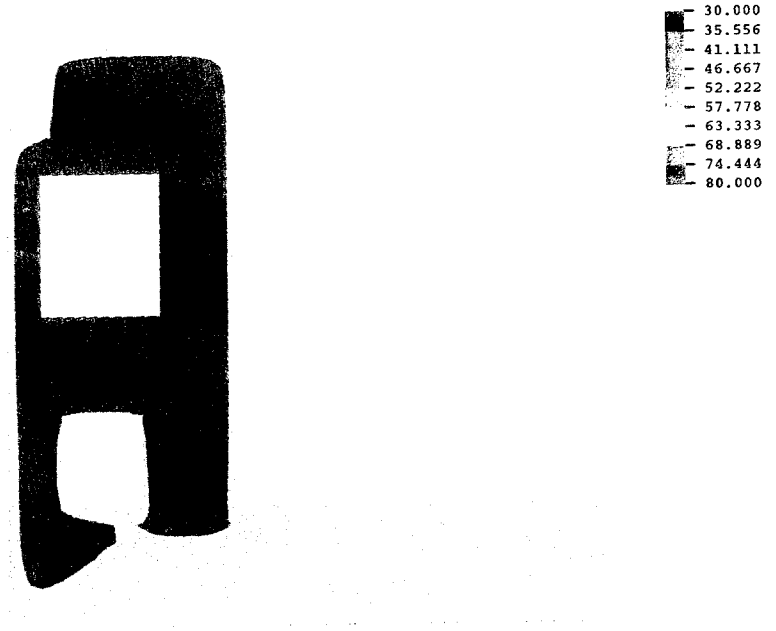

d. September 29

Figure 13. (Concluded)

Time-history plots

Six nodes have been chosen to illustrate different types of thermal behavior during and after construction within the gate monolith shown in Figure 14. Temperature history plots for these six nodes are shown using chronological time with zero being July 1. These nodal temperature time-histories were developed using a common placement temperature of 65 °F, the average heat of hydration curve, and the July 1 soil temperature distribution. The July 1 soil temperature distribution seems unrealistic for January, April, and September start dates, but this assumption typically affects only the first lift. Other assumptions include the removal of formwork after 2 days, a 5-day lift placement schedule, and no insulation. Since all parameters except the start dates remained constant, the time-histories show only the effects of construction start dates or construction with different ambient temperatures. A more accurate model taking into account the approximate placement temperature and a realistic insulation procedure is discussed later in the chapter to explore the effects of insulation and placement temperatures.

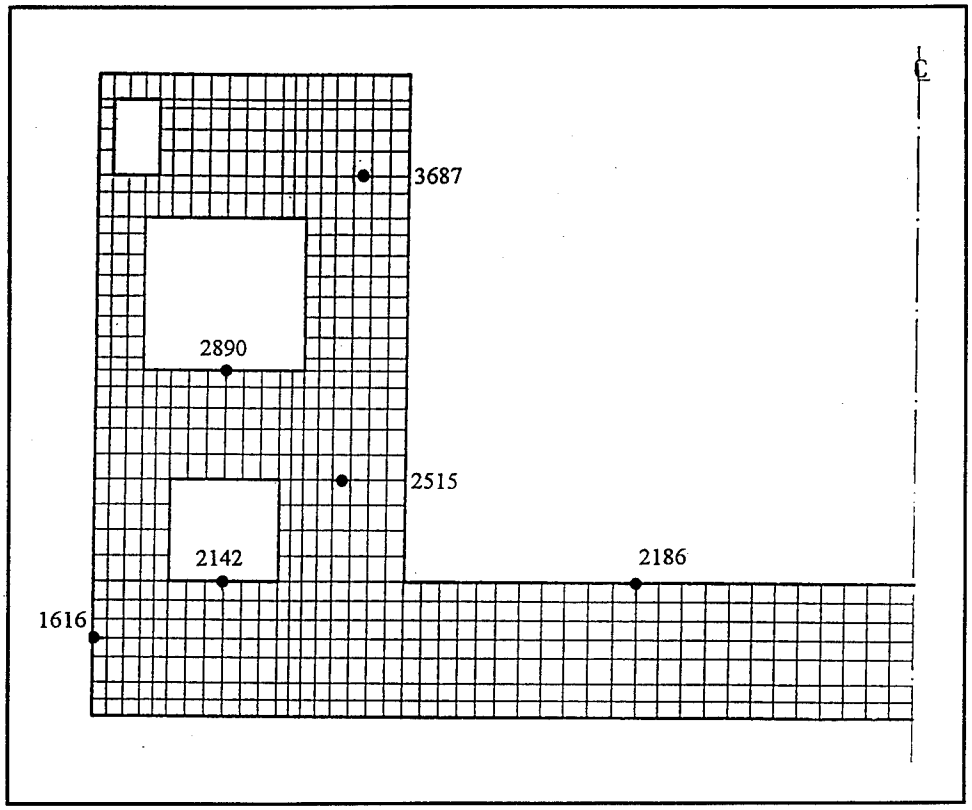

Figure 14. Nodes used to describe the thermal behavior of the monolith

Node 1616

Node 1616 is located on the vertical, exterior surface of the gate monolith as shown in Figure 14. As seen in Figure 15 and as expected, the temperatures for node 1616 are very dependent upon the ambient temperature. The initial spike in the temperatures are due to the insulating effects of the formwork. For these analyses, the formwork was removed after 2 days corresponding to the rapid drop in temperatures which approach the ambient values. The July 1 start date has an approximate temperature increase of 25 °F within the first day, while the September and April start dates had a temperature rise of approximately 15 °F. The January start date had a small temperature increase followed by a significant decrease in temperature when the forms were removed. This sudden drop in temperature at the surface would be cause for concern. The large drop in temperature at the surface with the heat generation continuing to occur within the concrete could create a large thermal gradient and high stresses. Therefore, insulation after removing the forms would most likely be needed.

Node 2142

Node 2142 is located at the top of lift 4 and on the bottom of the culvert floor as shown in Figure 14. The temperature time-histories for node 2142 are shown in Figure 16. Node 2142 does not have the insulating effects of formwork; therefore the spikes are no longer present. The additional fluctuations within the time-history are due to the placement of the walls on either side of node 2142. At 15 days, the culvert is closed and the film (heat transfer) coefficients change due to enclosing the top of the culvert as seen in Table 2. In each case, there is a slight rise in temperature once this film coefficient is changed. Shortly after enclosing the culvert, the nodal temperature begins to parallel or approach the ambient values. For this node, the January start date provides the largest change in temperature by dropping sharply within the first day. This indicates the need for insulating the top of the lift in these cold months.

Node 2186

Node 2186 is located at the top of the chamber floor at approximately the quarter point of the chamber width as shown in Figure 14. The temperature time-histories are shown in Figure 17 and are similar to those for node 2142, with the exception of the fluctuations in temperatures for node 2142 during the first 15 days. Node 2186 is uninsulated and the film coefficient never changes; therefore, for three of the four cases there is some initial heating of the node with a gradual transition to the ambient temperature. The January start date has a minimal or no heat gain and has a significant drop in temperature during the first day. Within 10 to 20 days, the temperature of this node is essentially the ambient value.

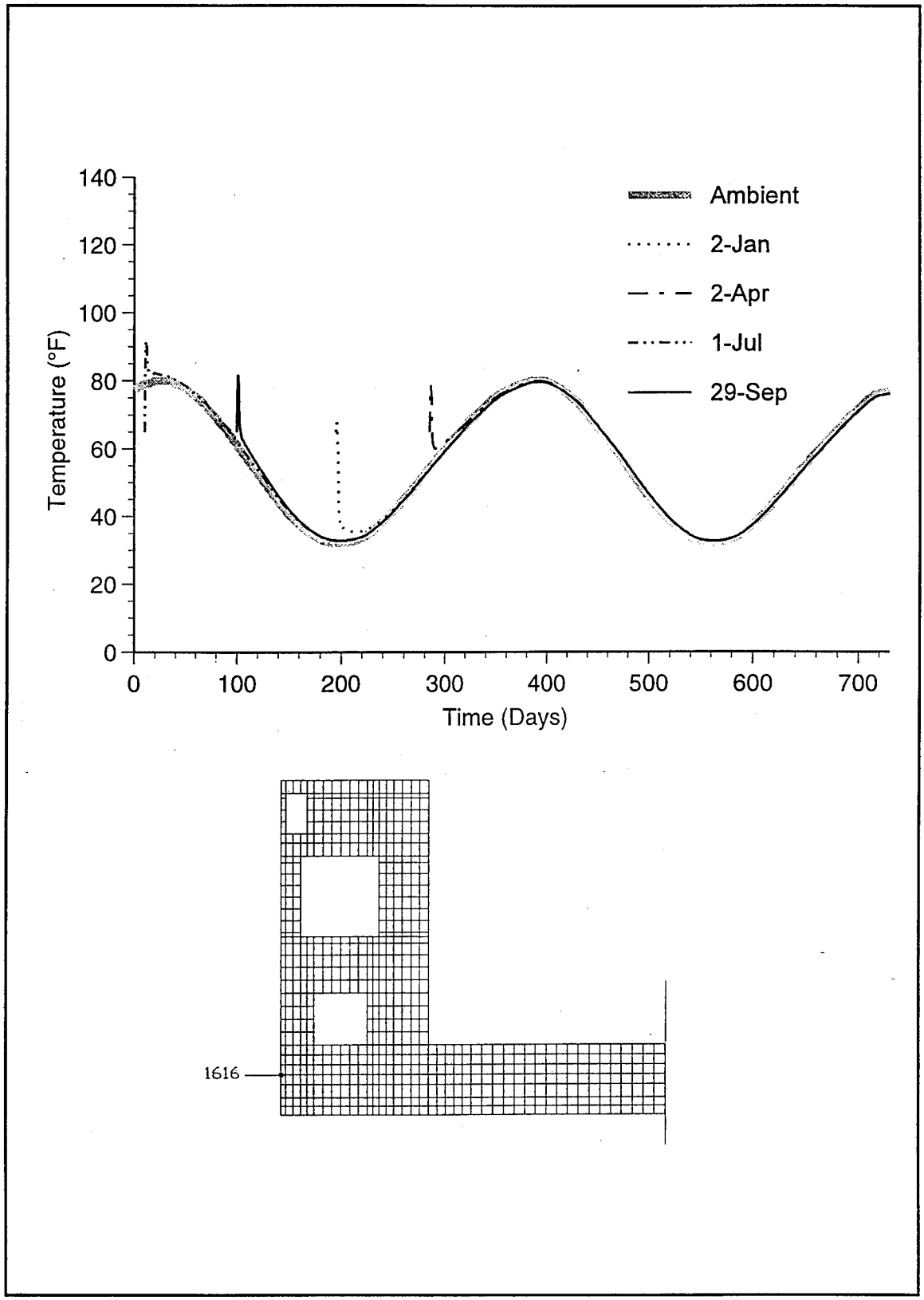

Figure 15. Temperature time-history for node 1616

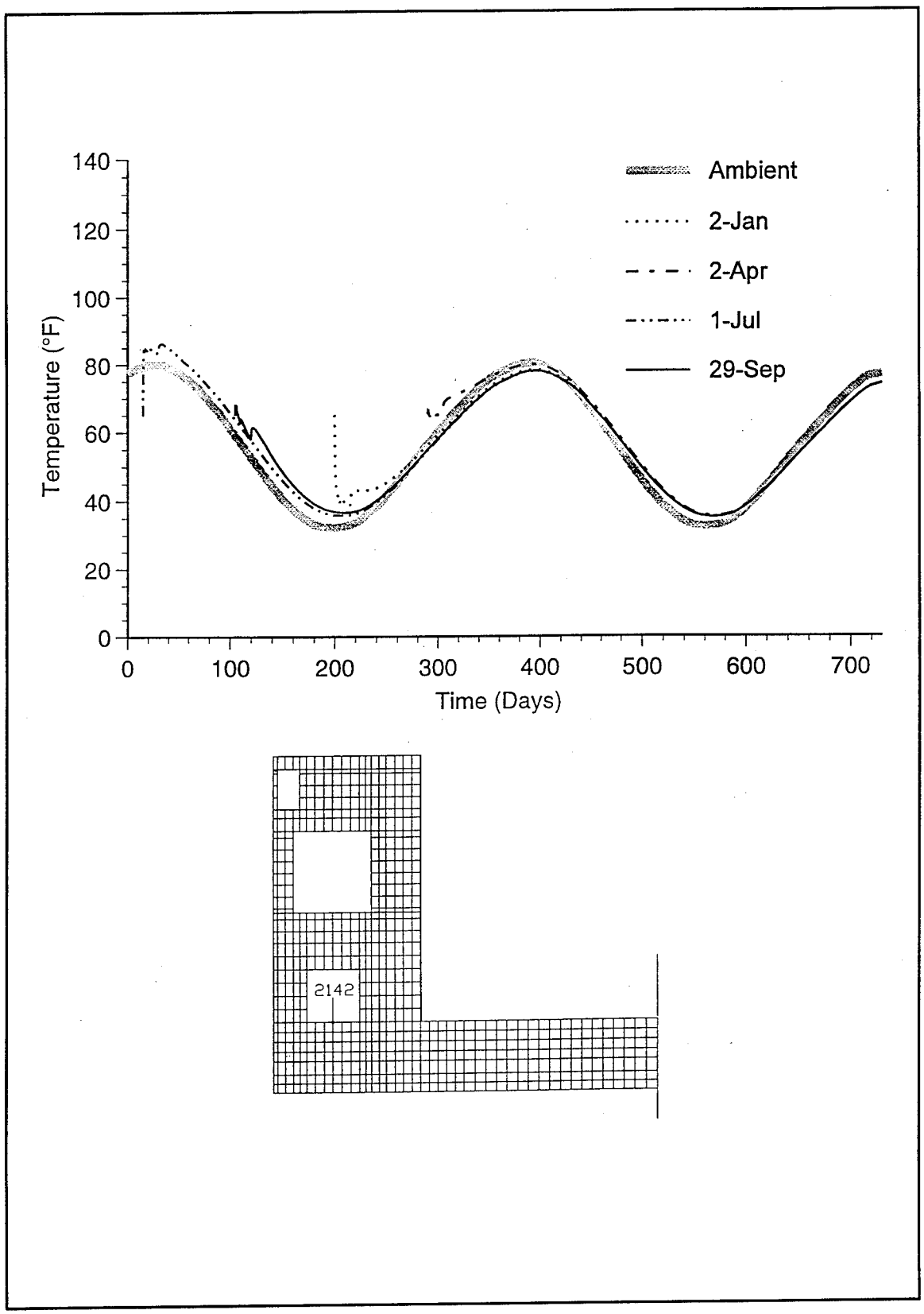

Figure 16. Temperature time-history for node 2142

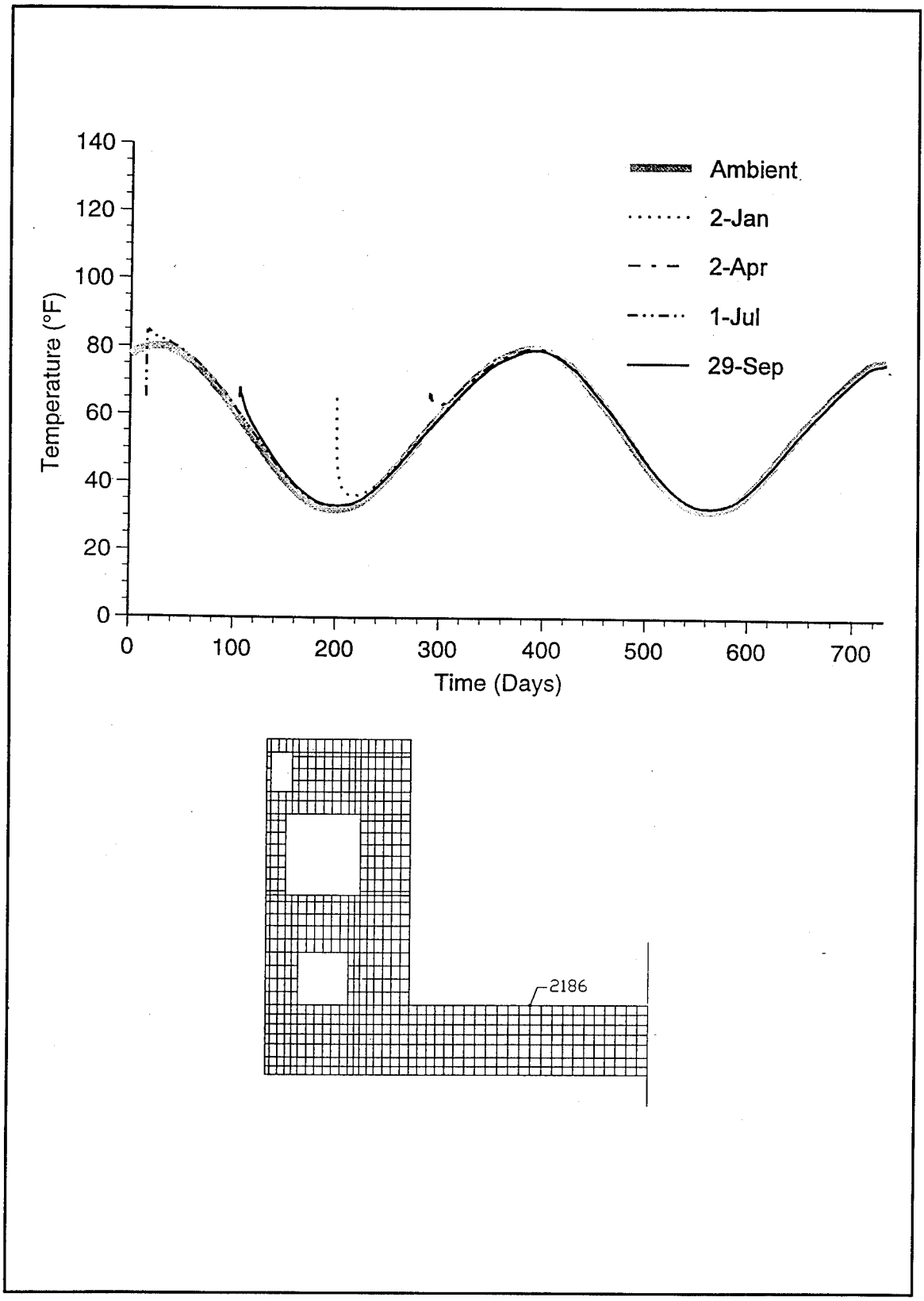

Figure 17. Temperature time-history for node 2186

Node 2515

Node 2515 is located at the top of lift 4 near the middle of the wall between the culvert and the chamber as shown in Figure 14. This node has a very different behavior than the previous nodes, as shown in Figure 18, due to the fact that the node is covered with a new lift of concrete after 5 days. Being at the top of a lift, the initial 5 days are similar to nodes 2142 and 2186, but after the next lift is placed the thermal behavior is quite different. For the July and April start dates, there is an initial increase in temperature in the first day with a slight decrease in temperature in the following 3 days due to the uninsulated top of the lift. The September and January start dates have an initial decrease beginning after the placement of the lift due to the dropping ambient temperature. After the fifth day a new lift is placed on top of node 2515, and the temperature increases dramatically for each start date. Each case has a temperature rise of approximately 35 to 40 °F. Since node 2515 is now an interior node, the temperatures tend to be slightly out-of-phase with the ambient temperatures, and the temperature never quite reaches the maximum or minimum ambient temperature.

Node 2890

Node 2890 is located on the bottom floor of the machine room as shown in Figure 14. The machine room adds another condition not seen with the previously discussed nodal locations and that is the closing of the machine room. Once the machine room is closed, no air flows through the room causing a buildup of heat within the room as seen in Figure 19. The culvert, although closed on four sides, still allows air to flow through the ends of the monolith allowing heat to escape. Each of the four start dates shows an increase in temperature during the first day with a sharp decrease in temperature to near ambient in the following 15 days. After 15 days, the capping lift is placed and the machine room becomes static, allowing little heat to escape. The temperature rises approximately 15 to 20 °F for the next day or two, at which time a slight decrease or leveling of the temperature occurs. Then at the 20^{th} day after placement of the lift containing node 2890, a new lift is placed on top of the machine room roof and it causes a minor increase in the temperature within the machine room. Since the room is completely surrounded by a substantial amount of concrete, the dissipation of this heat is slow and this causes the temperature of node 2890 to be out-of-phase with the ambient temperature and not quite capable of reaching extreme ambient temperatures.

Node 3687

Node 3687 is located in the center of a lift in a massive wall between the gallery and the chamber monolith. These interior nodes generally have a significant gain in temperature regardless of the placement date as seen in Figure 20. The interior nodes do typically have a slight increase

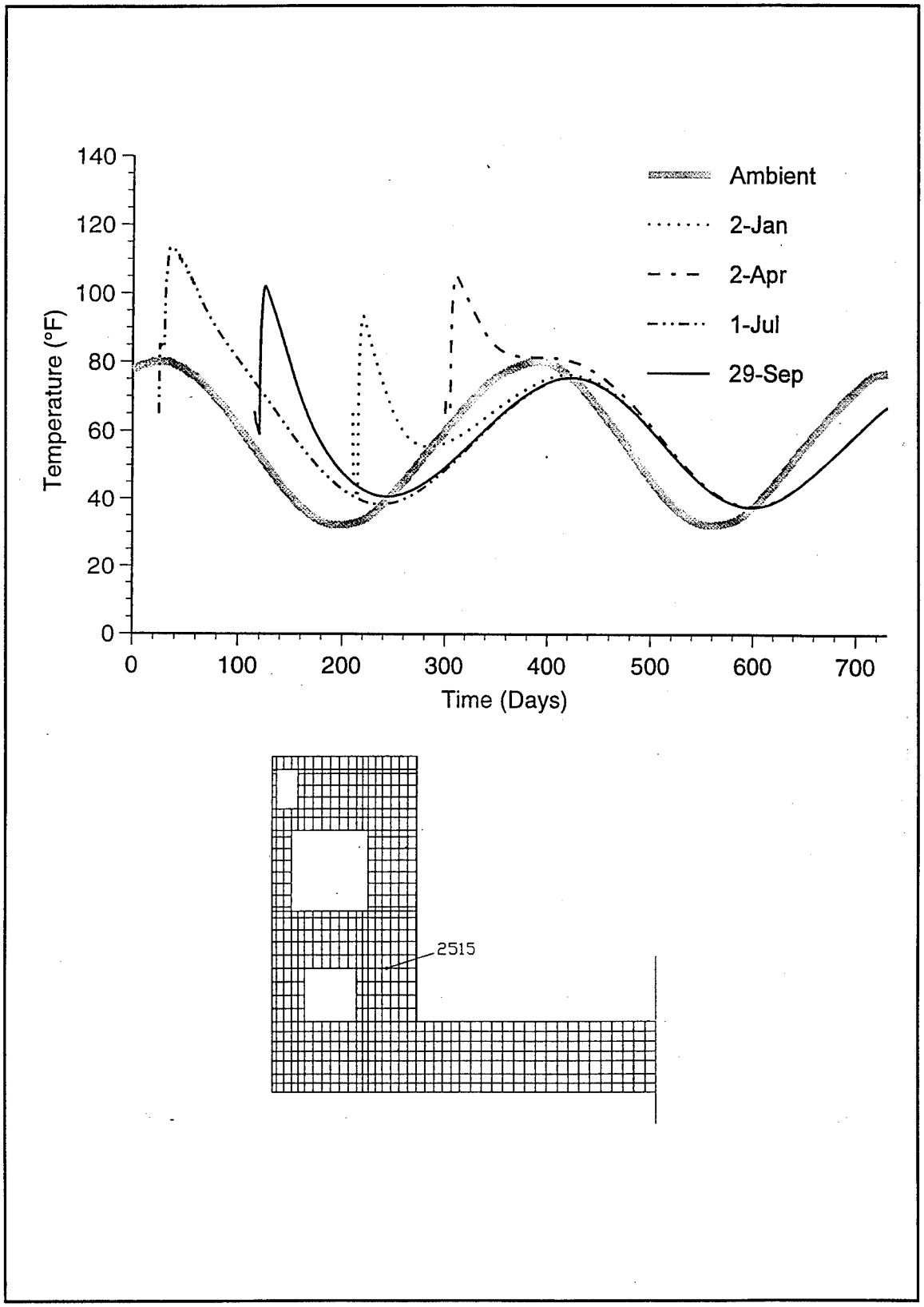

Figure 18. Temperature time-history for node 2515

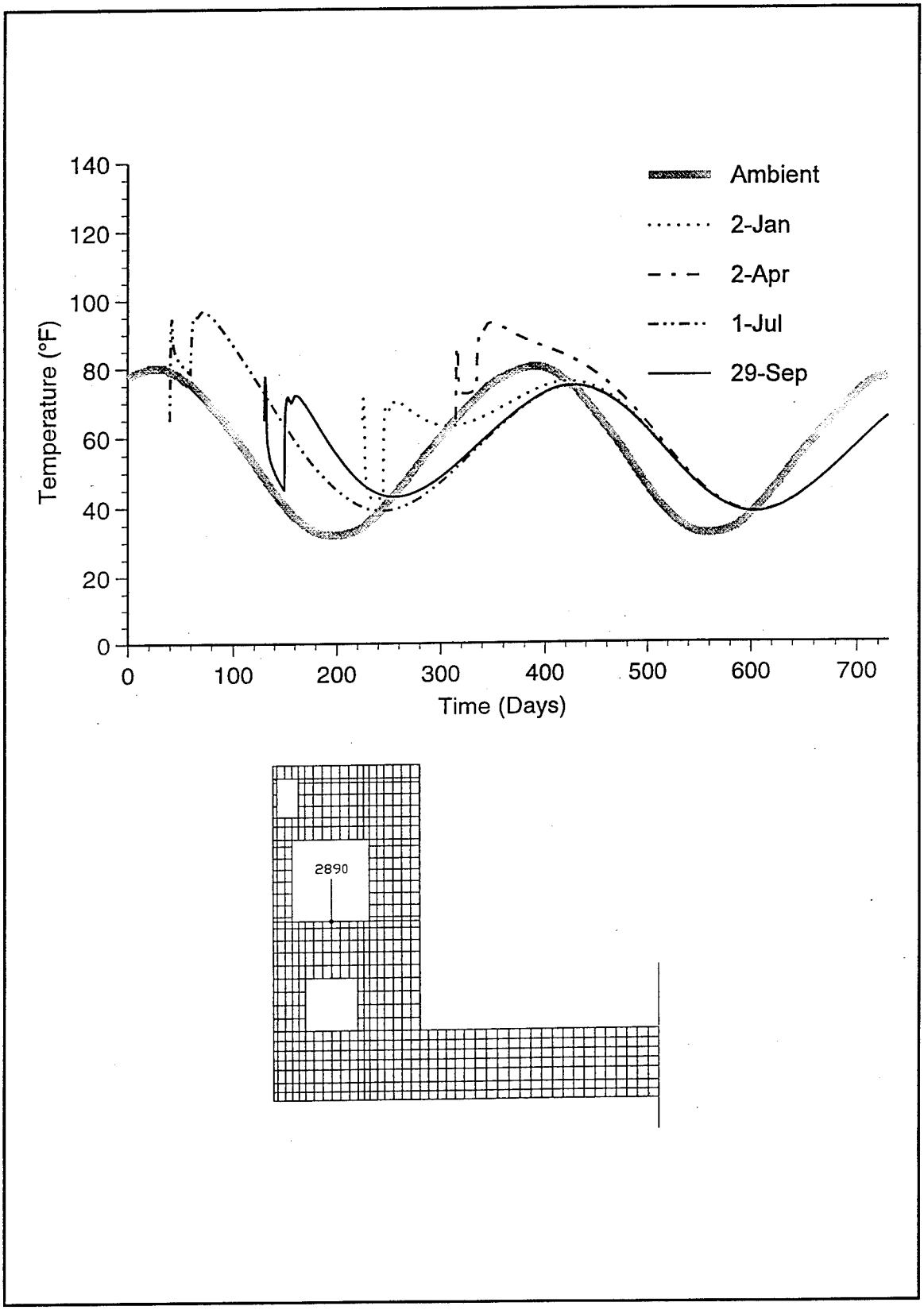

Figure 19. Temperature time-history for node 2890

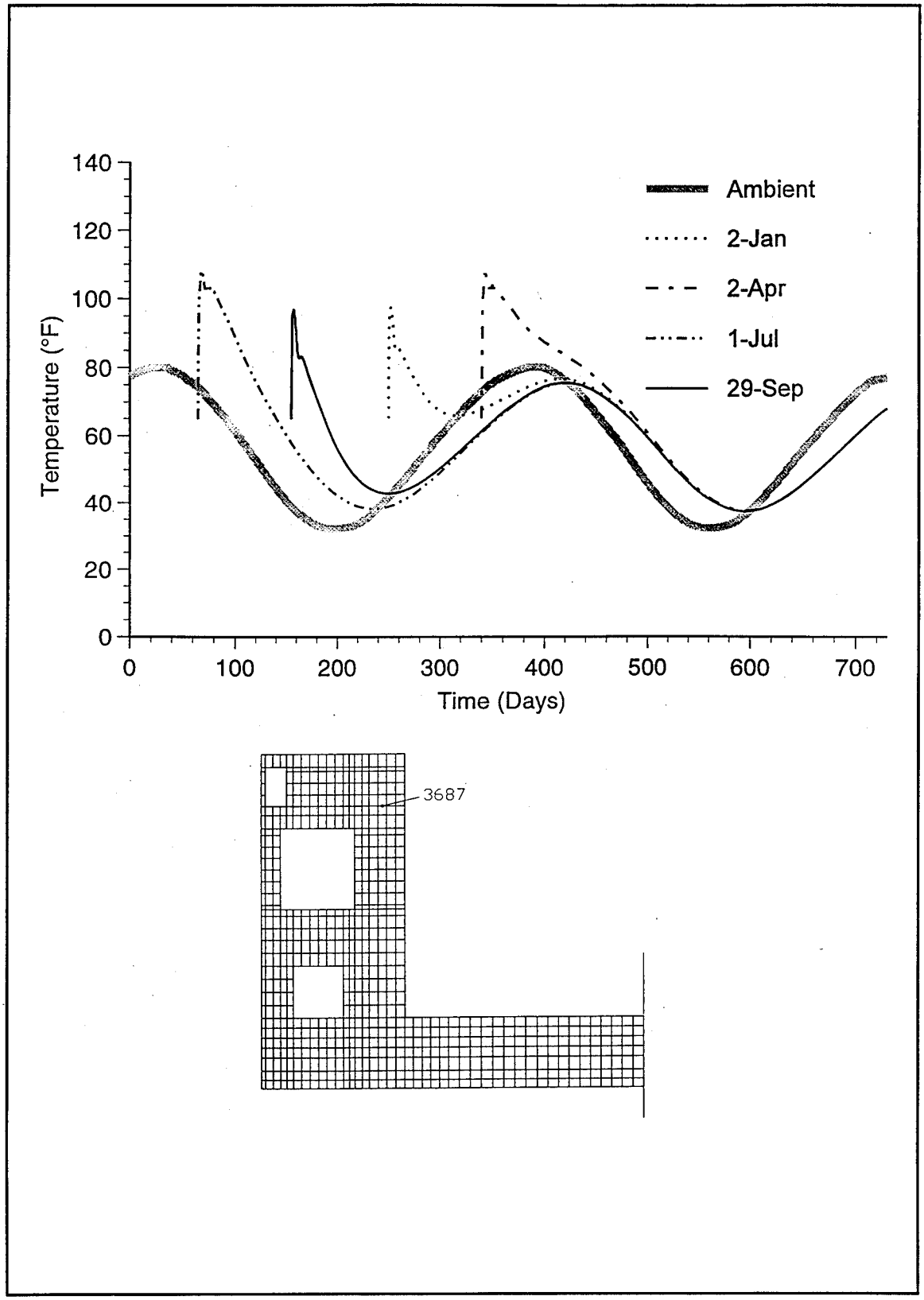

Figure 20. Temperature time-history for node 3687

or leveling of the temperatures after the next lift is placed. After the next lift or two is placed, the interior temperatures become out-of-phase with the ambient temperatures, and the interior temperatures never quite reach the extreme ambient temperatures as discussed for the other interior nodes.

Stress Analyses

Stresses are generated as element-dependent values; therefore, there is not a one-to-one correspondence to the nodes as presented in the thermal discussion. The stresses are presented with compression as negative values and tension as positive values. Stresses are also presented as horizontal or vertical stresses for ease of presentation and understanding. The stresses are presented versus the time from start of construction to easily compare the peak stress values for the elements.

Element 394 is a typical interior element that is never directly exposed to the ambient conditions as shown in Figure 21. The element is also located directly below the chamber wall making it an element with primarily vertical stresses. As seen in Figures 22 and 23, the construction start date has little effect on the stresses, since it is an interior element and there is a

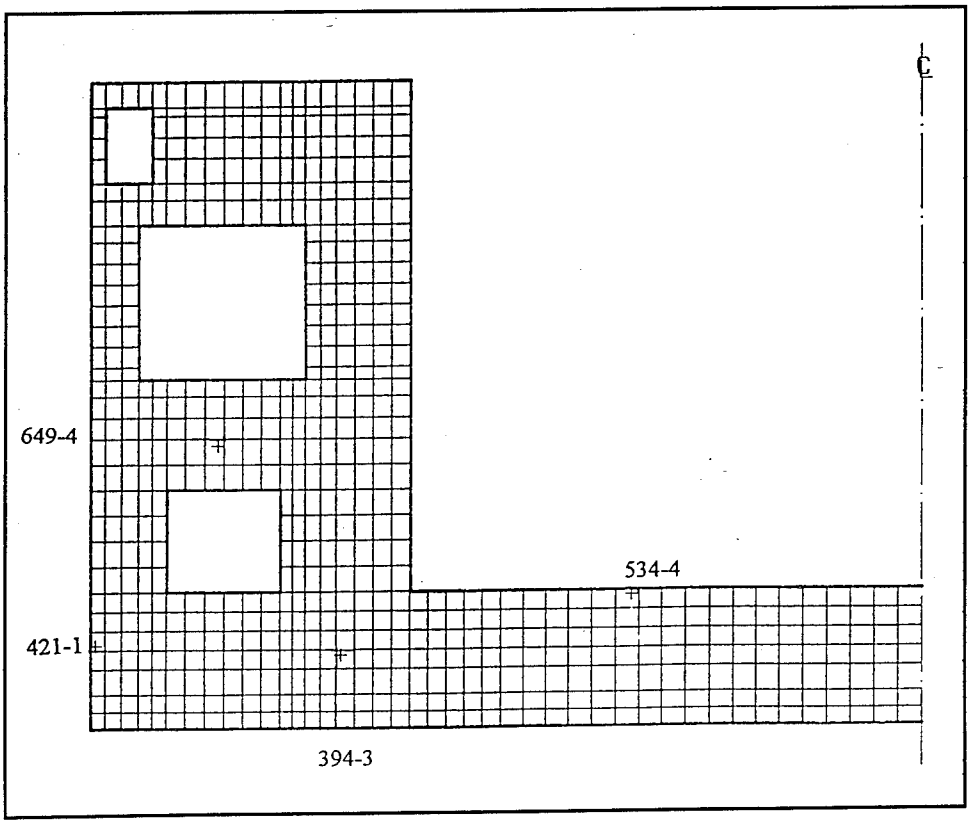

Figure 21. Elements used for time-histories

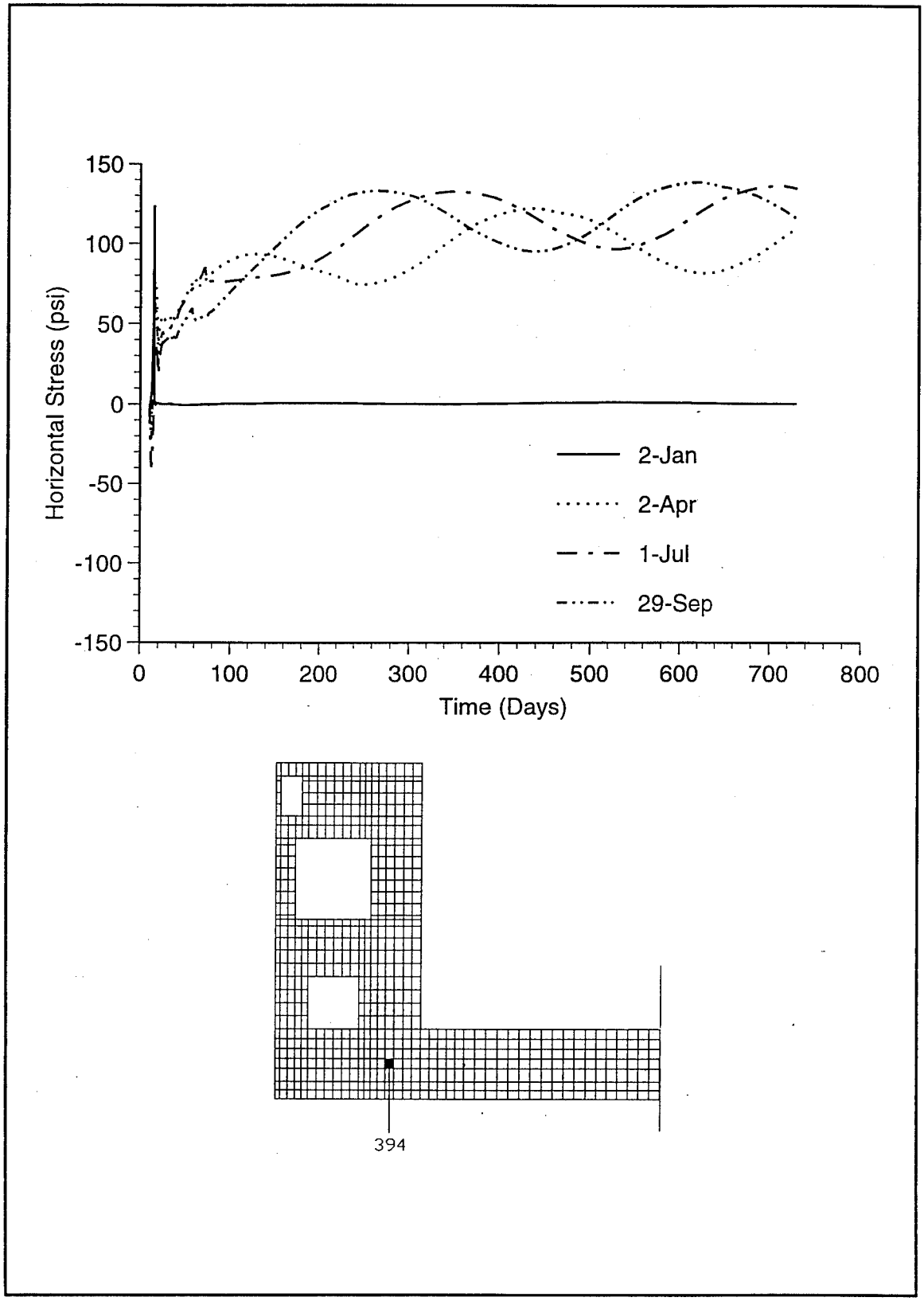

Figure 22. Horizontal stress time-history for element 394

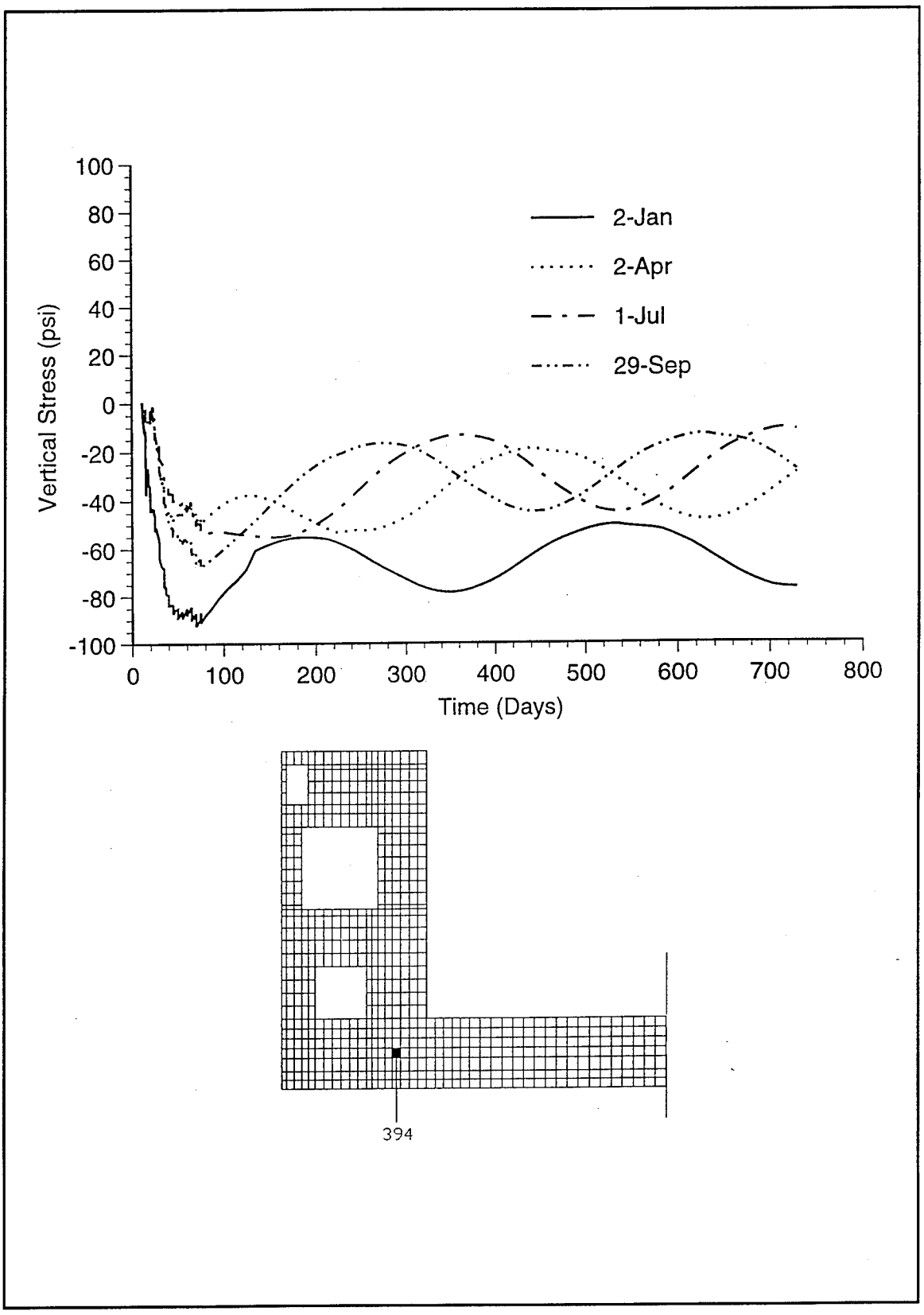

Figure 23. Vertical stress time-history for element 394

short period of time between lift placements. The stair-step effect in the vertical stresses is due to the gravity effects of placing a new lift every 5 days. Ambient effects take over after construction is complete with none of the vertical stresses reaching the maximum value of -100 psi present during the first day of placement.

Element 421 is an element which is adjacent to the node 1616 that was discussed in the thermal analysis section. Since this element is located on the vertical face of the exterior wall, the vertical stresses are of primary importance and are shown in Figure 24. Early-time stresses of approximately 50 psi tension are seen, but they are quickly reduced by the gravity-induced compressive stresses created by the addition of lifts. Then, a large increase in vertical stress takes place around day 50 and continues to increase until day 100, reflecting the additional concrete being placed in the monolith wall. At this point in the life of the structures, the stresses begin to oscillate due to the ambient temperature variations.

Element 534 shows the major effects associated with a large differential in placement temperatures and an adjacent ambient condition. The placement temperature of 65 °F is nearly the ambient temperature for the spring and fall start dates, but there is a large disparity in the January ambient temperature and the assumed placement temperature. Keep in mind that in "real" construction this disparity would be smaller, since the January concrete placement temperature would be near 40 °F. For illustration purposes and the sanctity of the parametric study, this model did not include the change in placement temperatures to quantify the effect of the start dates. As seen in Figure 25, the horizontal stress component at the top of the slab is much higher than any of the other locations. This element is essentially subjected to a thermal shock with the January start date. It is placed at 65 °F, then is left completely uninsulated, thus subjecting it to an extreme temperature of approximately 32 °F. This condition, as has been known for many years, creates a large tensile stress causing surface cracking.

Element 649 (Figure 26) is located at the top of lift 7 between the top of the culvert and the bottom of the machine room. The location of this element is interesting because the first 5 days are spent uninsulated, then the next heat generating lift is placed, and 25 days later the machine room is enclosed, thus affecting the heat gain and loss for this element. During the first 5 days, the element is subjected to a similar thermal shock as described for element 534, and high tensile stresses are created. Then the next lift is placed, providing heat to this element and causing it to enter a compressive state. Twenty five days later the machine room is enclosed, and an accumulation of heat coupled with the additional gravity effects thereby causes a slight rise in the tensile stresses.

The horizontal stress contours for 185, 365, 545, and 725 days after construction for each of the different start dates are shown in Figures 27 through 30. The color contours clearly show some residual effects occurring at the lift lines. Several of the contour plots also indicate high levels

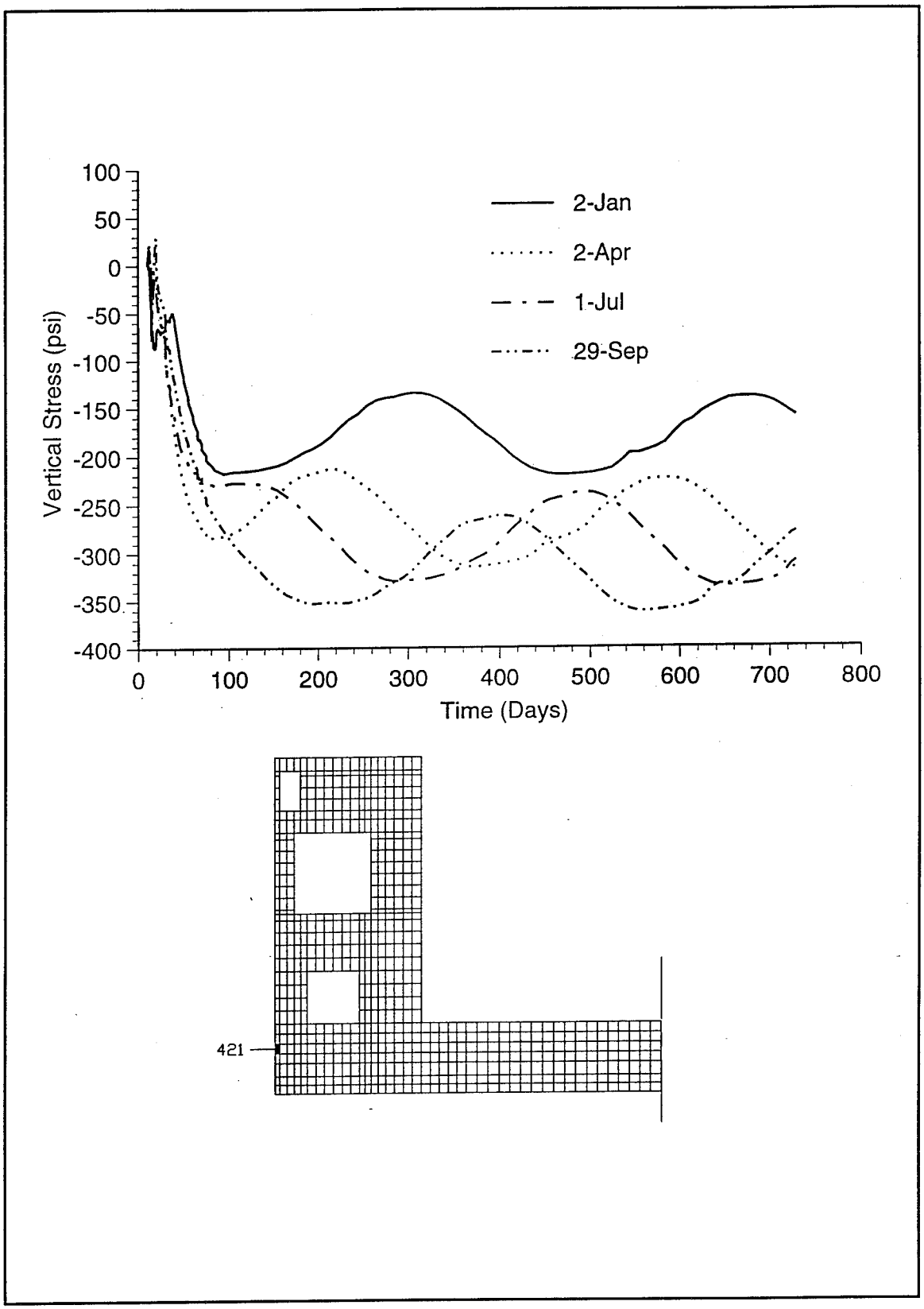

Figure 24. Vertical stress time-history for element 421

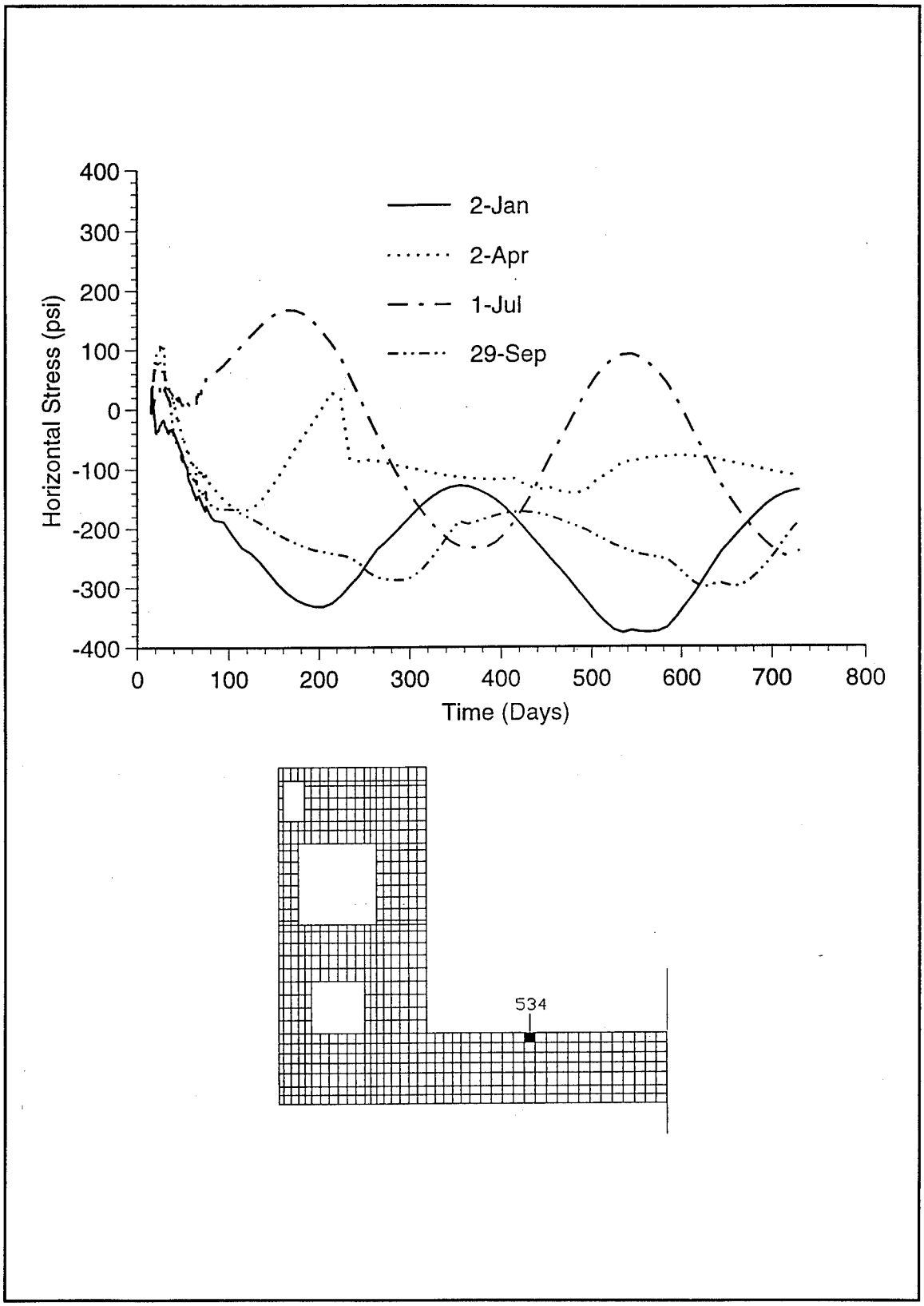

Figure 25. Horizontal stress time-history for element 534

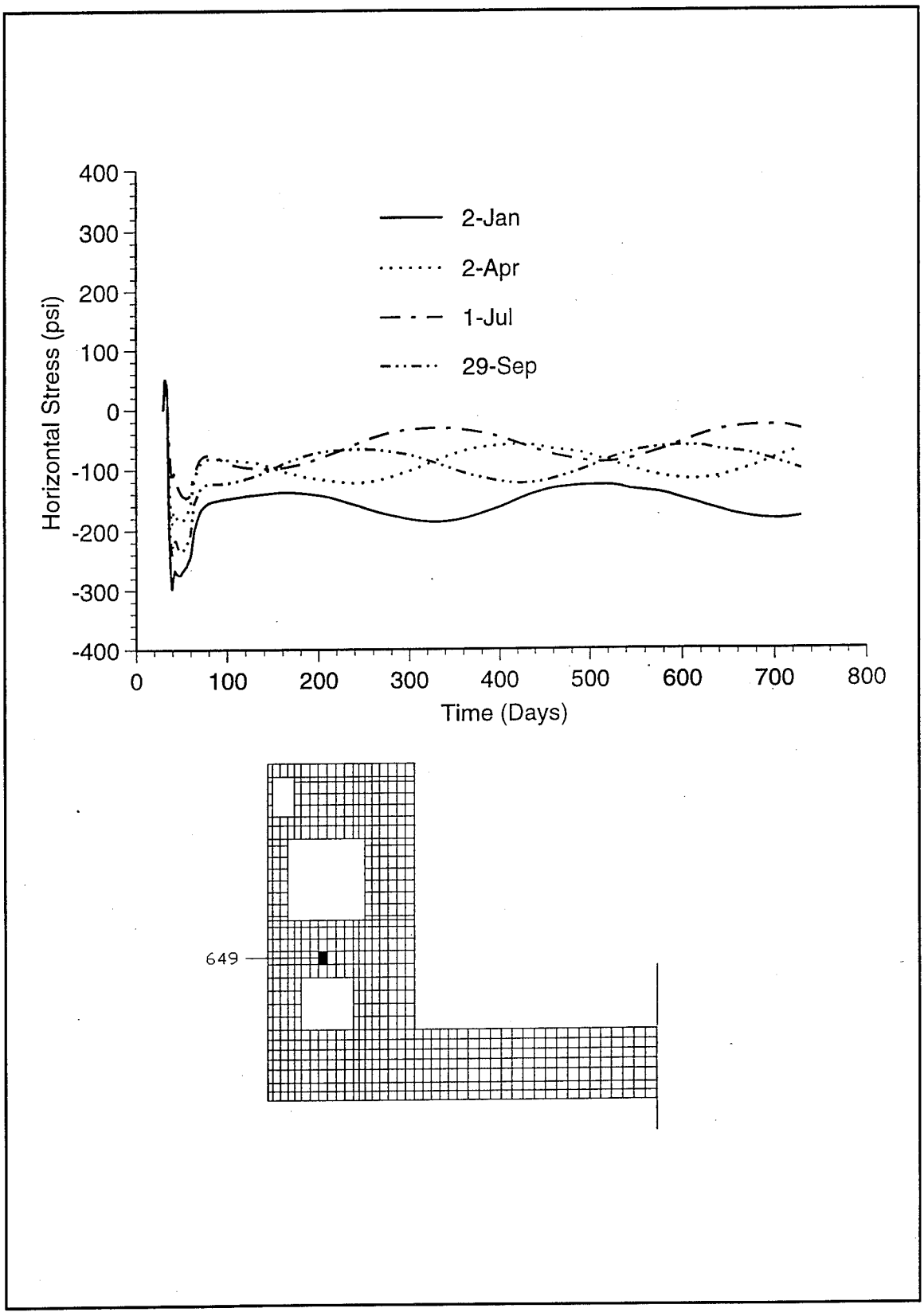

Figure 26. Horizontal stress time-history for element 649

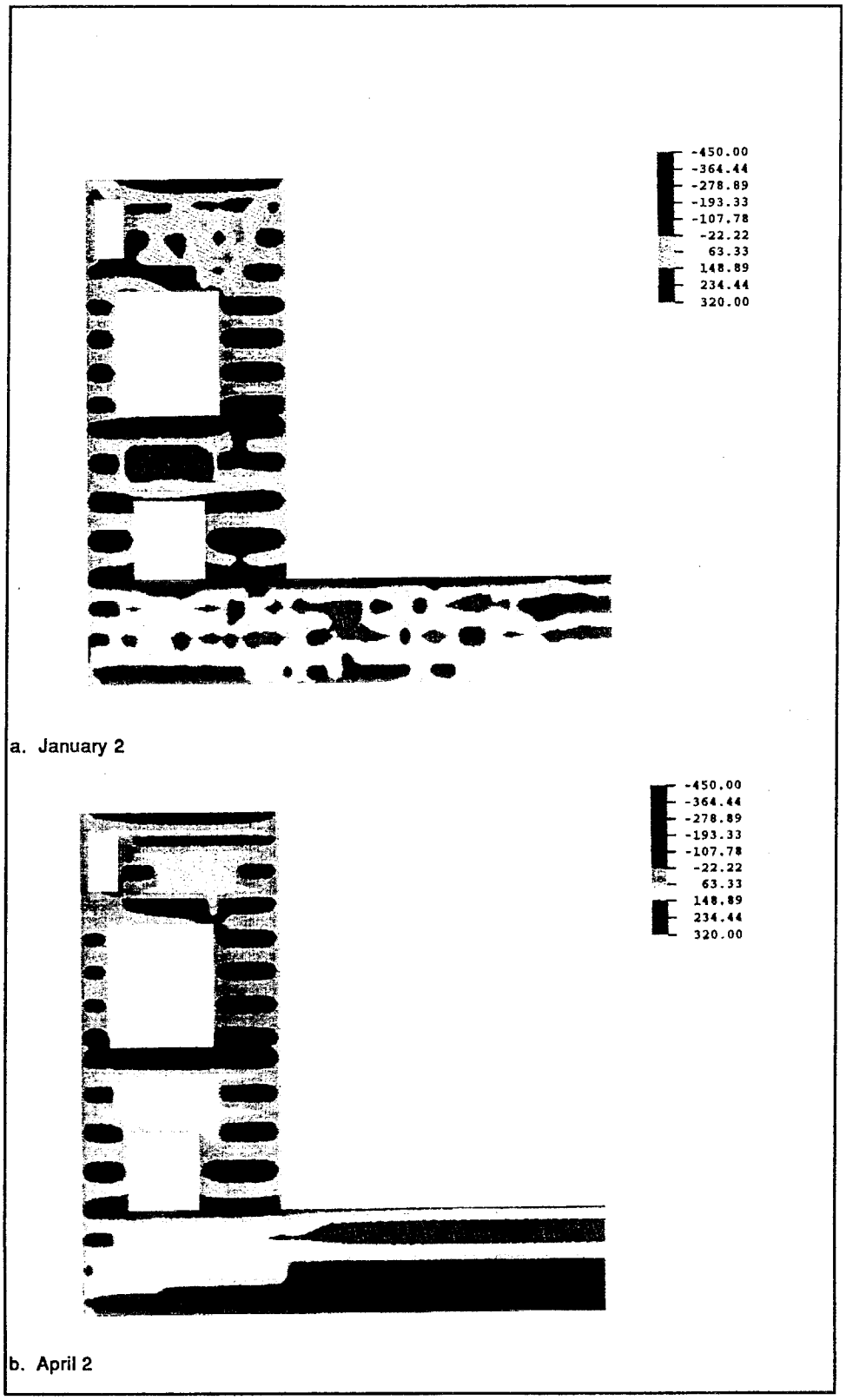

Figure 27. Horizontal stress contours for 180 days after start of construction (step = 187, amp = 185) (Continued)

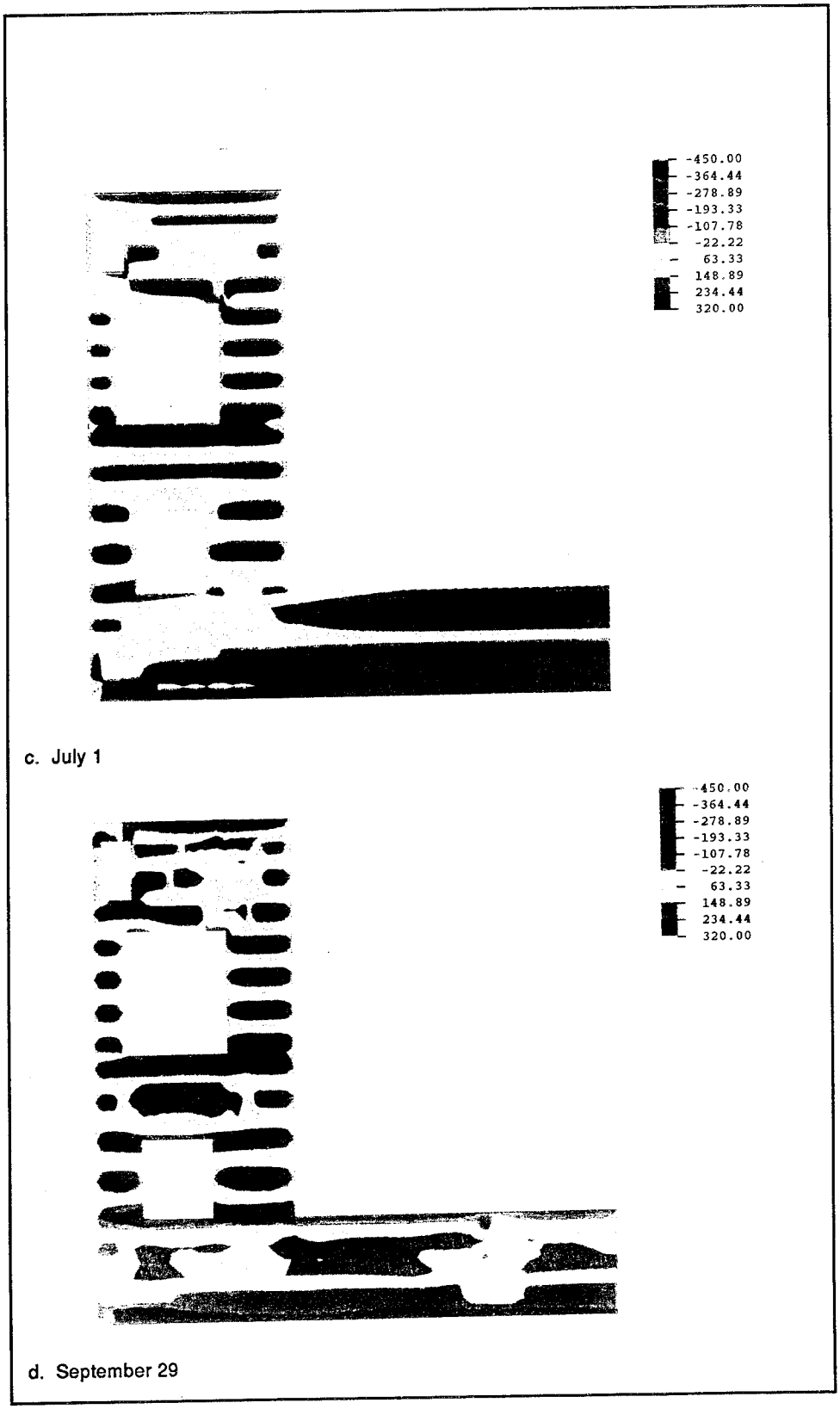

Figure 27. (Concluded)

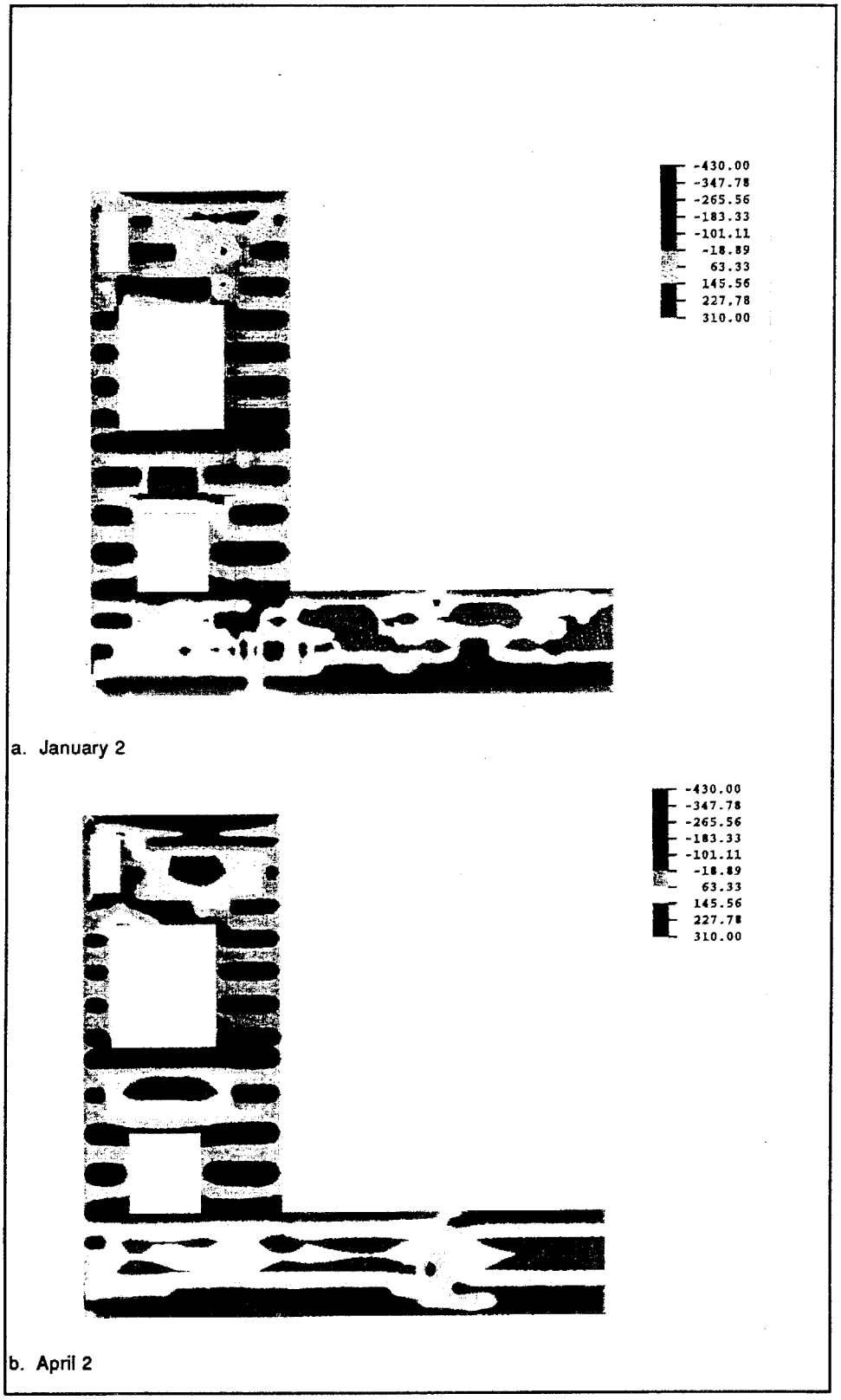

Figure 28. Horizontal stress contours for 360 days after start of construction (step = 205, amp = 365) (Continued)

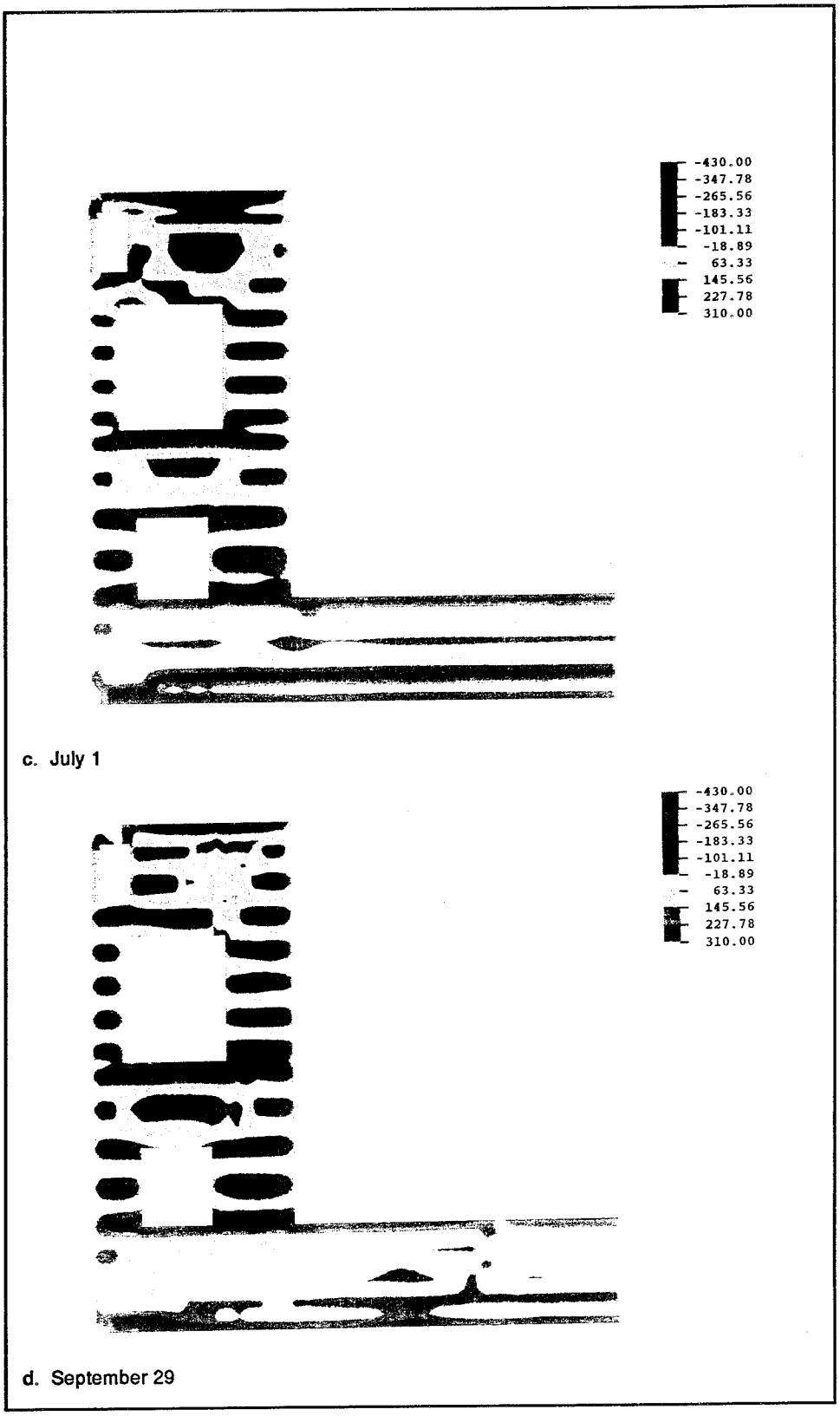

Figure 28. (Concluded)

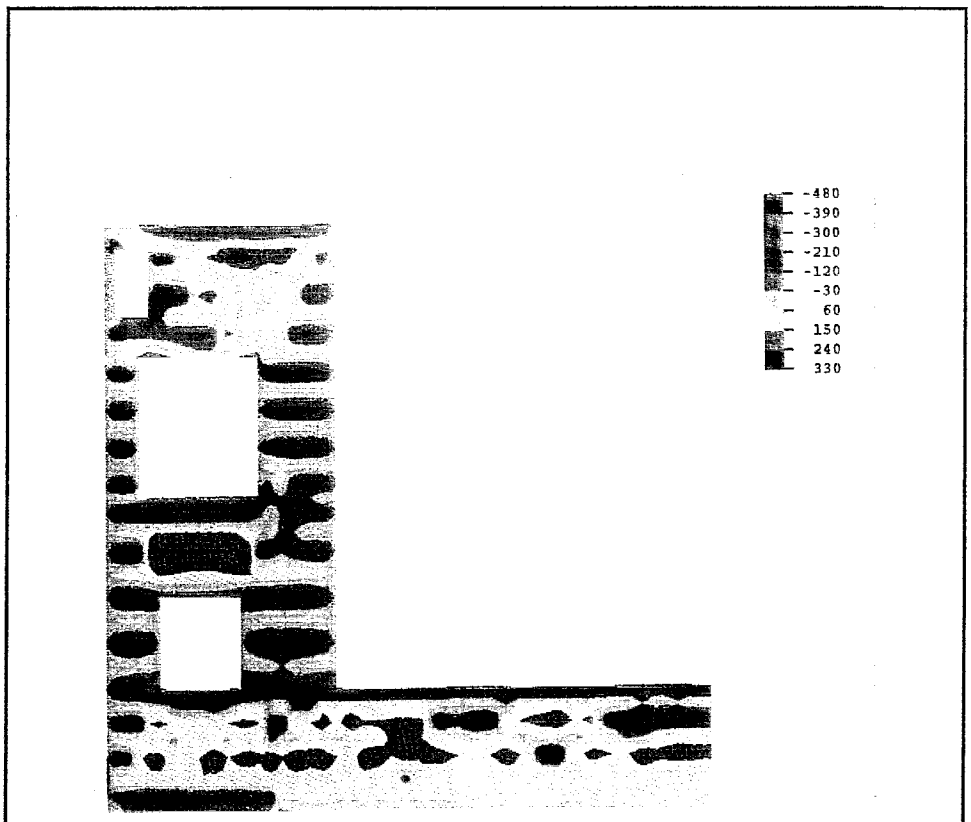

a. January 2

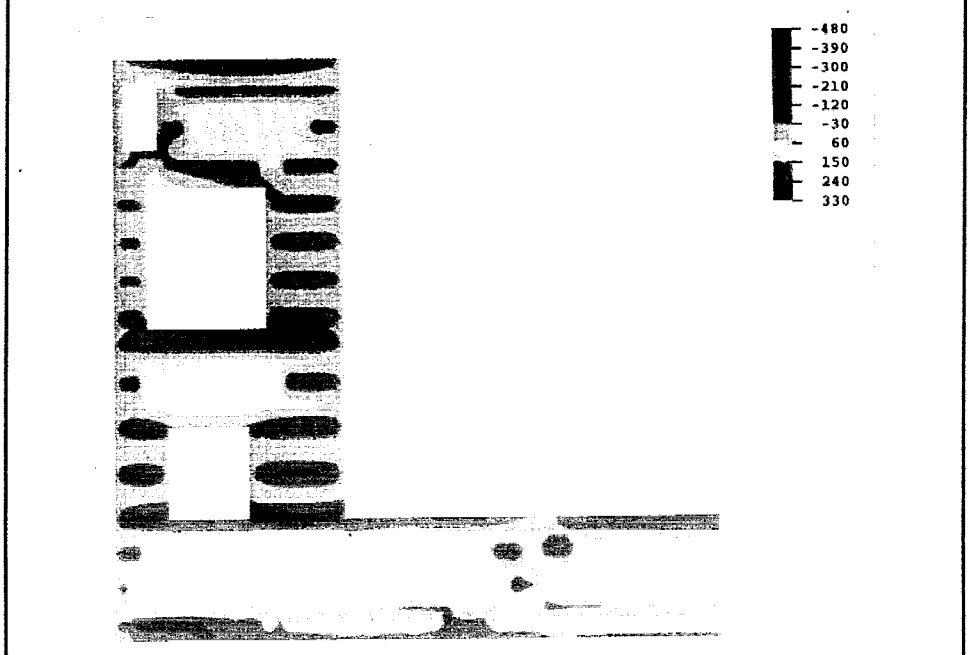

b. April 2

Figure 29. Horizontal stress contours for 545 days after start of construction (step = 223, amp = 545) (Continued)

Figure 29. (Concluded)

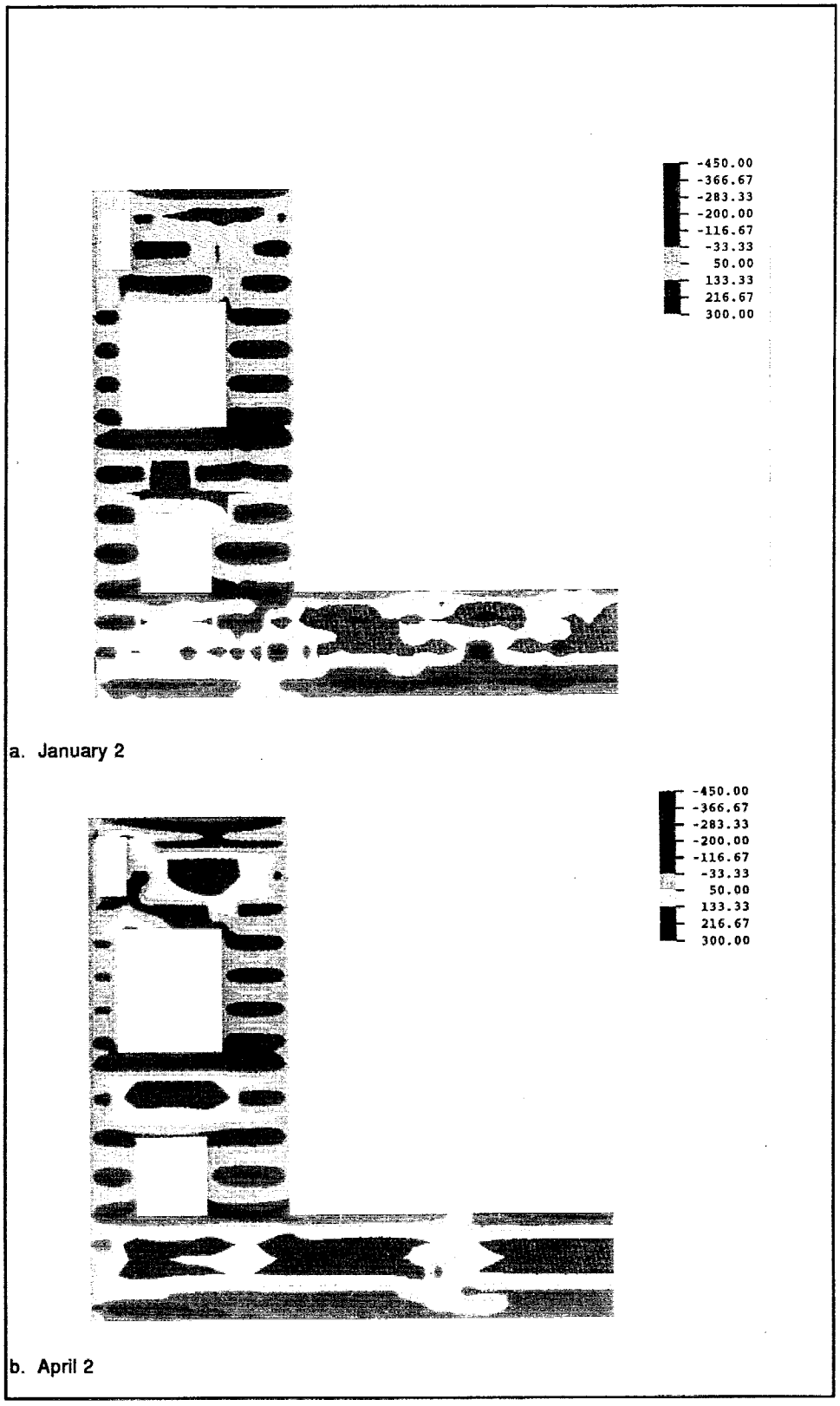

Figure 30. Horizontal stress contours for 725 days after start of construction (step = 241, amp = 725) (Continued)

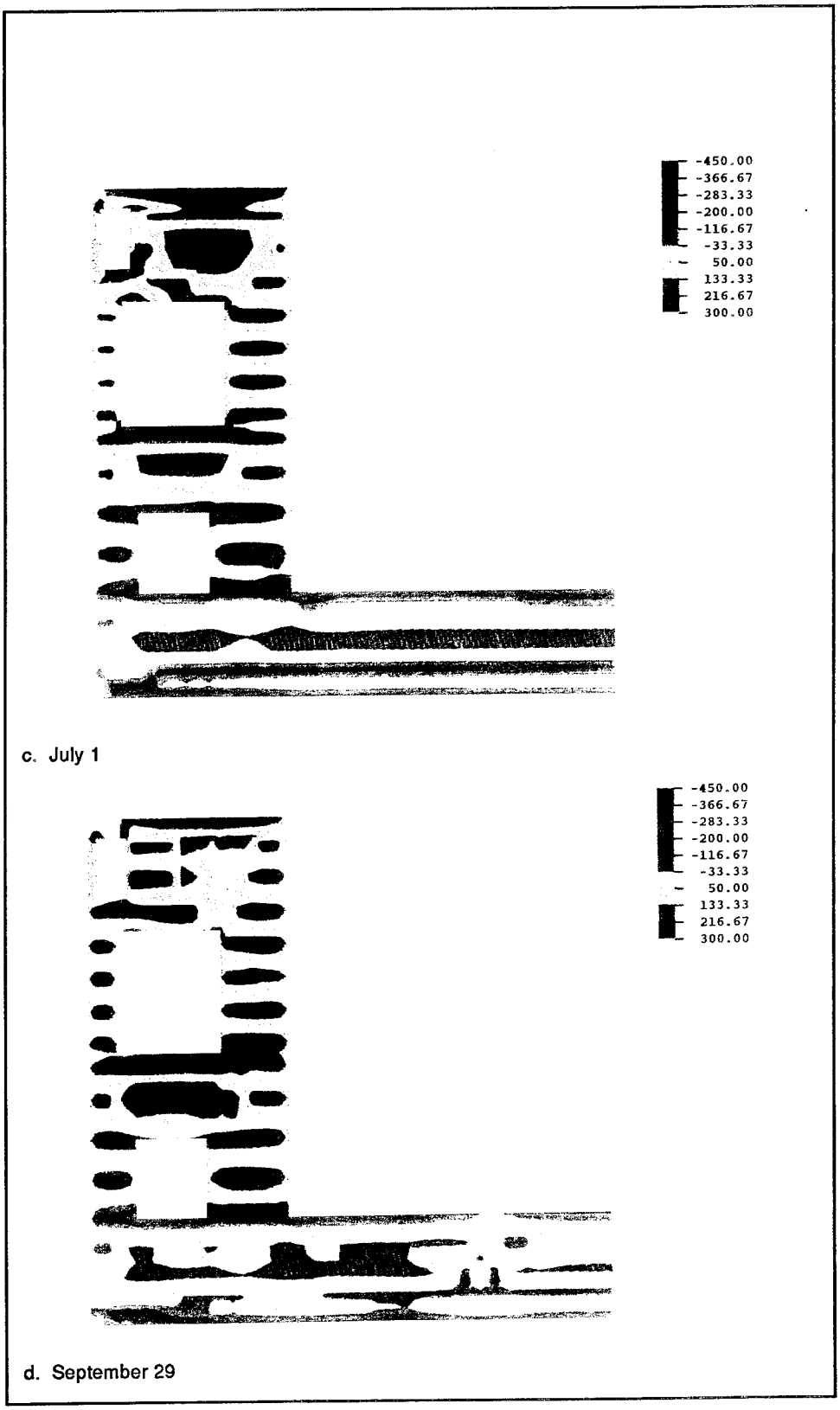

Figure 30. (Concluded)

of tensile stress within the floor slab and in the areas of larger concrete volumes such as between the culvert and the machine room. As seen from the figures, the tensile stresses may reach values as high as 300 psi.

Cracking Analyses

The crack surface plots for 725 days after the start of construction for the four different start dates are shown in Figure 31. The dots in these figures show the locations where cracking has occurred during the life of the structure. The January start-of-construction (without insulation) case shows cracking across the entire top of lift 1. These cracks are vertical, and therefore, are controlled once the second lift is placed. The bottom of the machine room floor, the exterior surface of the walls, and the bottom corners of the culvert are all areas that indicate cracking. The significant cracking along the top of lift 1 can be reduced by using insulation and proper placement temperatures as shown later in this chapter. The April start date has significant cracking in the slab but minimal cracking within the monolith walls. The lifts comprising the chamber floor were placed assuming a 65-°F placement temperature, but the April based ambient temperature is still in the 40- to 50-°F range, thereby creating a large thermal gradient at the top of a lift. This first lift cracking would be minimized if a placement temperature approaching the ambient condition was used. The cracking near the top of the chamber floor close to the center line of the structure is due to a combination of bending of the floor coupled with the thermal effects. The July start date has minimal cracking. The lower exterior corner of the monolith could use another pile or two in this region to help support this corner. This cracking was due to inadequate support. The September start-date analysis shows basically the same cracking pattern in the chamber floor as the April start date, but it also has significant cracking within the walls. This occurs since the upper part of the walls are placed in colder weather. The last lift is placed in late November when the ambient temperature is approaching the minimum. This coupled with the 65 °F placement temperature and no insulation creates a high potential for cracking to occur. Once again modeling the placement temperature as a function of the ambient temperature would eliminate much of the cracking. These final crack patterns found using constant parameters does give a perspective of the effect of start dates on the behavior of the structure. If all of the variables were changed to reflect realistic structures, it would be difficult to assess why or what were the causes for the behavior of the structure.

Figures 32 and 33 show crack potential plots for 185 days and 365 days after each of the different start dates. The contours for 185 days after start of construction indicate that the January, April, and September structures are highly susceptible to cracking. The July contours at 6 months show only an 85-percent propensity for cracking. The January start of construction indicates a high potential for cracking in many different regions while the April and September contours have high potential for

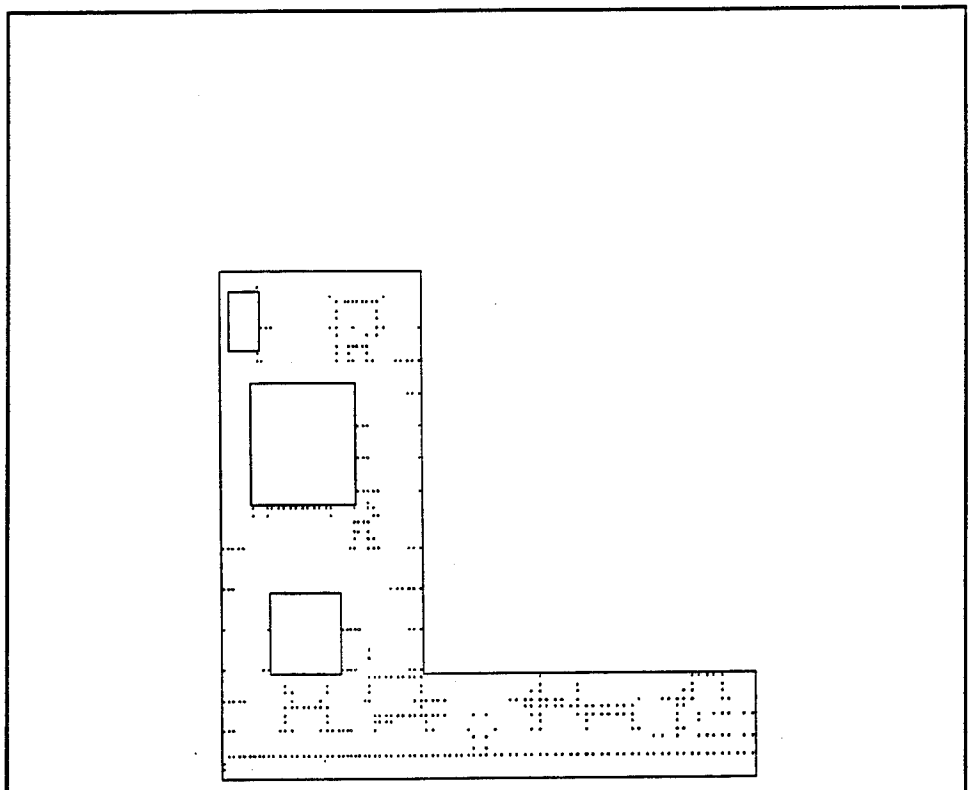

a. January 2

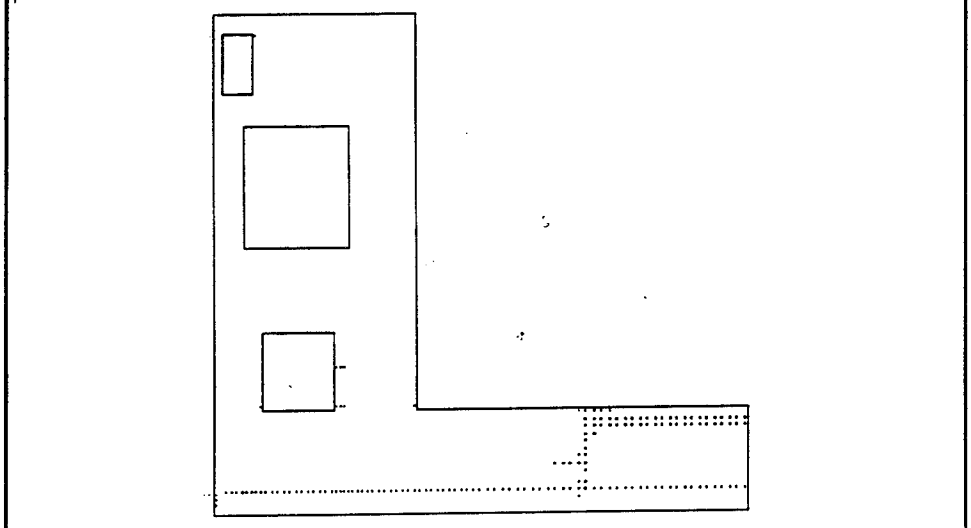

b. April 2

Figure 31. Crack surface diagrams for 725 days after start of construction (step = 241, amp = 725, scale = 1.00) (Continued)

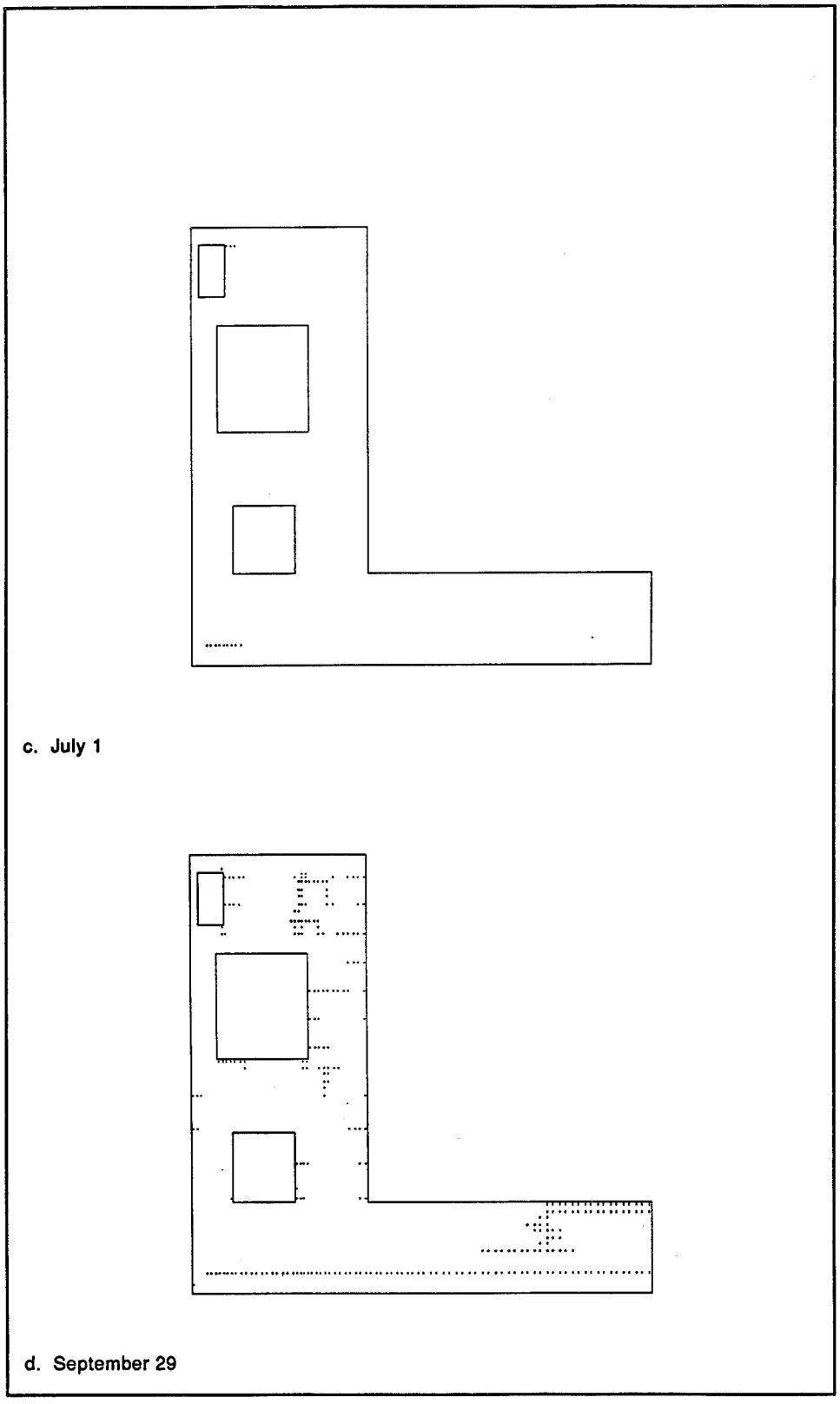

c. July 1

d. September 29

Figure 31. (Concluded)

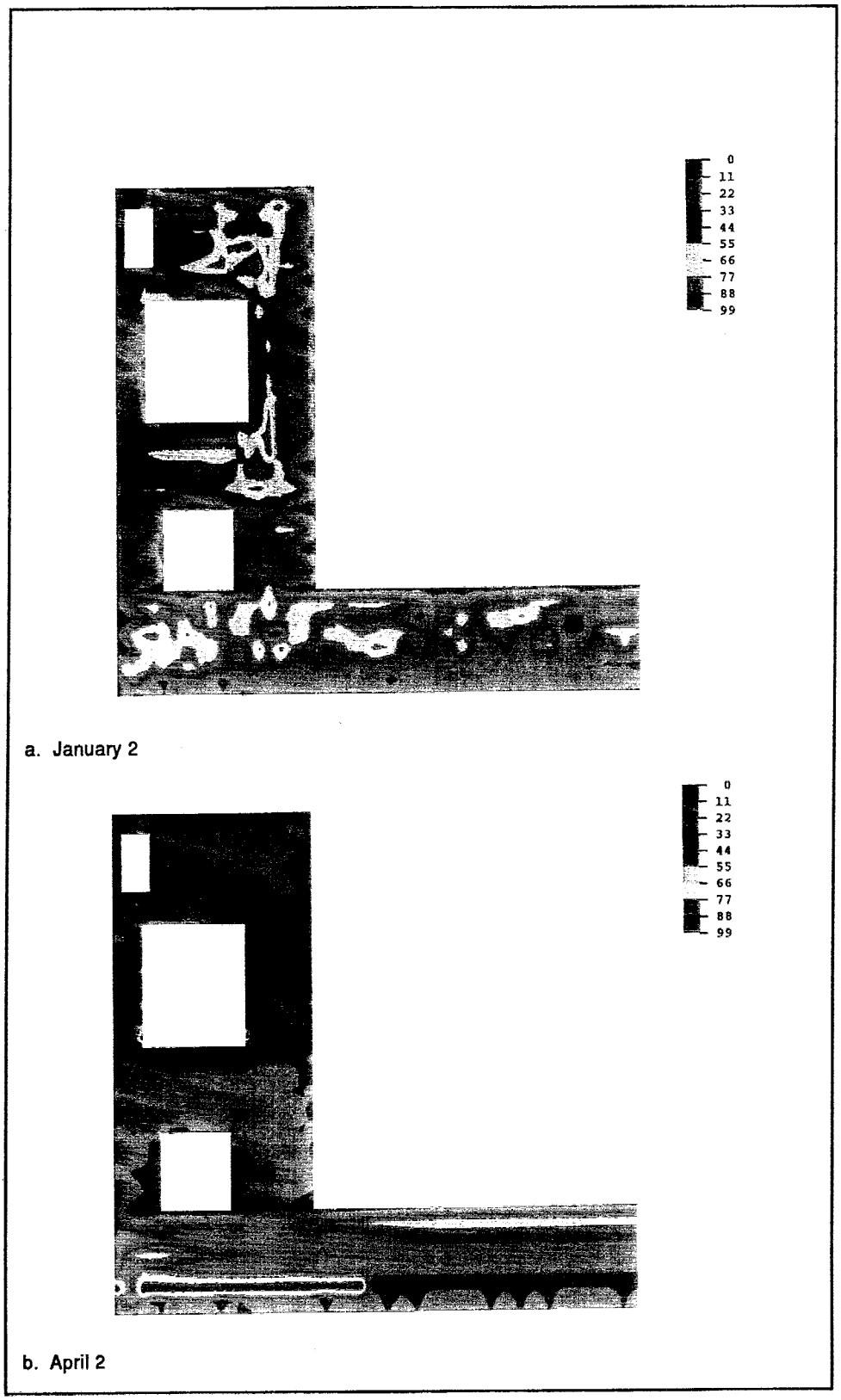

Figure 32. Crack potential contours for 180 days after start of construction (step = 187, amp = 185) (Continued)

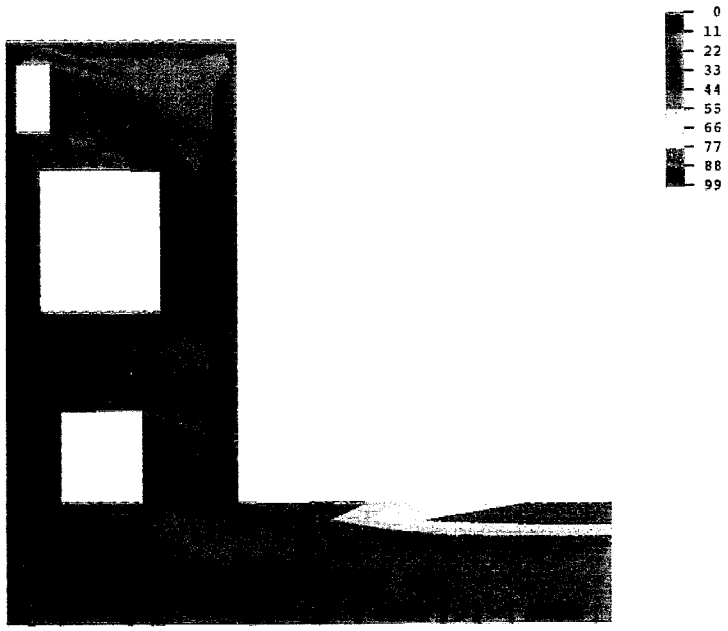

c. July 1

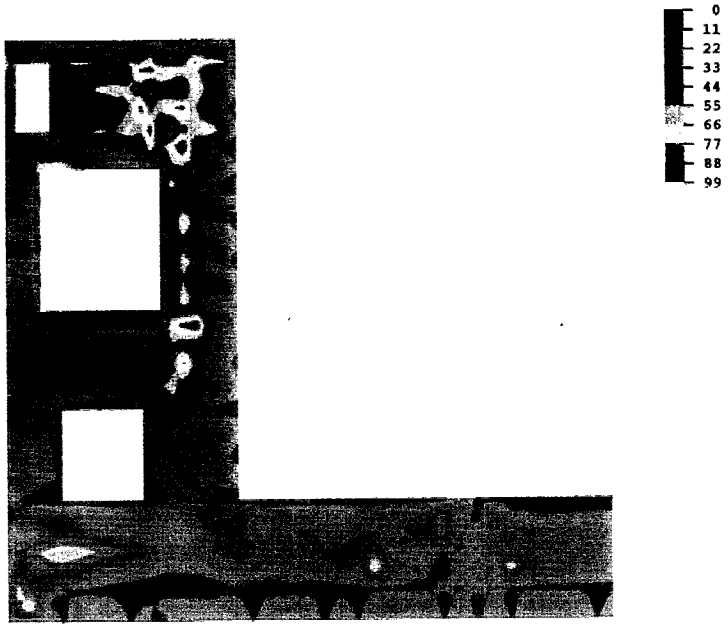

d. September 29

Figure 32. (Concluded)

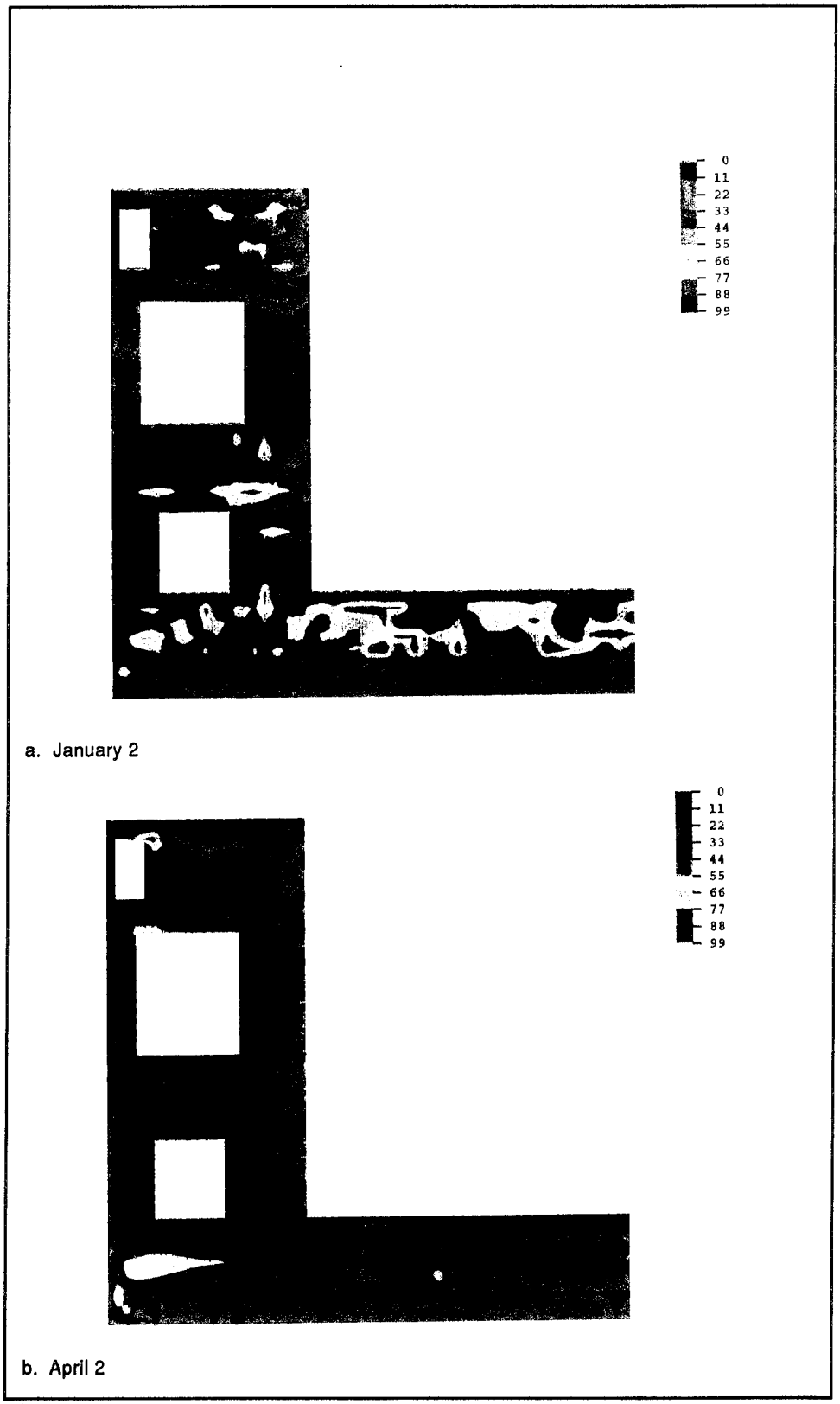

Figure 33. Crack potential contours for 365 days after start of construction (step = 205, amp = 365) (Continued)

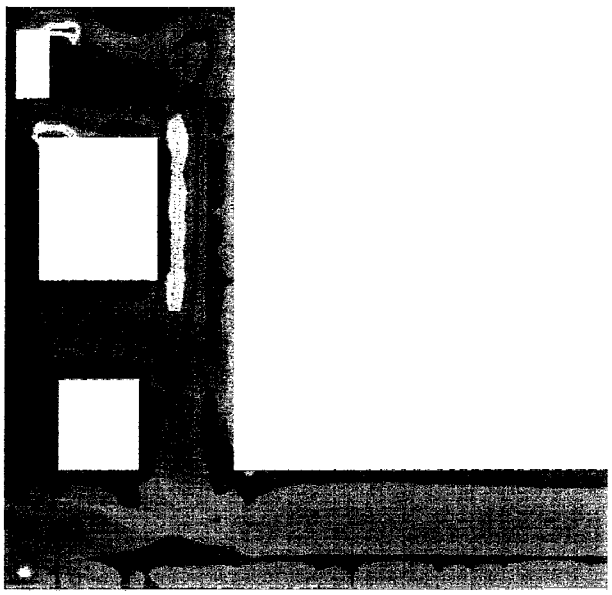

c. July 1

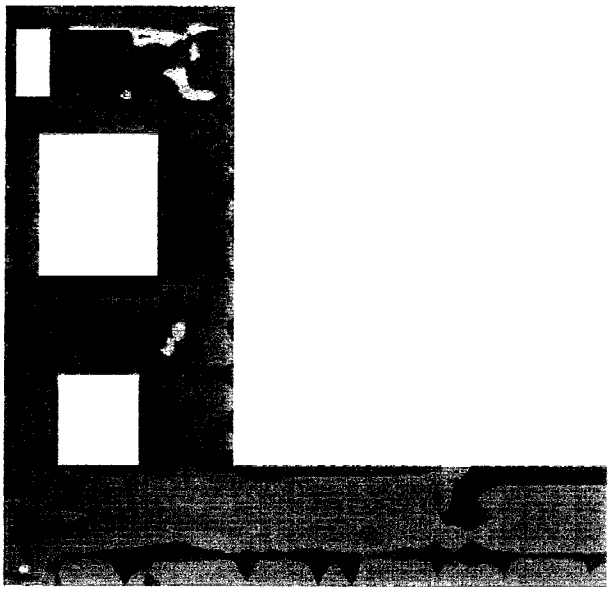

d. September 29

Figure 33. (Concluded)

cracking primarily in two regions. The April and September contours indicate that the bottom corners of the machine room and the slab under the wall have high potential for cracking. At day 365 after start of construction, the April and September crack potentials show moderately high potential for cracking near the gallery corners and in the bottom exterior corner of the slab. The January start of construction shows high potential for cracking in several different areas of the slab, namely, near the culvert and machine room corners, as well as, in the top of the structure. The July start of construction has a high potential for cracking near the gallery corners and the upper machine room corner nearest the exterior wall.

Figures 34 and 35 show the crack potential contours for 545 and 725 days. Note that these figures show results similar to the 185- and 365-day contours. The January start of construction provides the highest potential for cracking for the 545-day contours with several critical regions. All four start dates have crack potential above 80 percent at the end of 2 years, with the gallery corners and the bottom exterior corner of the slab being critical regions.

Summary of the Effects of Construction Start Dates

The effects of construction start dates have been a commonly asked question since the earliest NISA procedures were developed. From the results presented, it is apparent that cold weather construction must be protected. The concrete placed in cold weather can have a high potential for cracking. The start dates can significantly affect the behavior, but their effect is very much dependent upon the geometry of the structure, its ambient conditions, construction procedures, and construction sequence. The September start of construction had more cracking taking place in the monolith walls, since these lifts were being placed in mid-December; whereas, the April start of construction had cracking mostly within the monolith slab or floor. From these results one would conclude that cold-weather construction is the most critical and should be avoided. Once the proper construction precautions are taken and they are accurately modeled in the analysis, the cold-weather construction results can become tolerable.

Revised Modeling Parameters for a January Start Date

Four distinct analyses were completed for the January start date. All four analyses were performed using plane strain elements, but different thermal properties. The first analysis, Case 1, was performed using a placement temperature of 65 °F, the higher soil temperature distribution as shown in Figure 4, 2-day uninsulated formwork, and uninsulated lift tops.

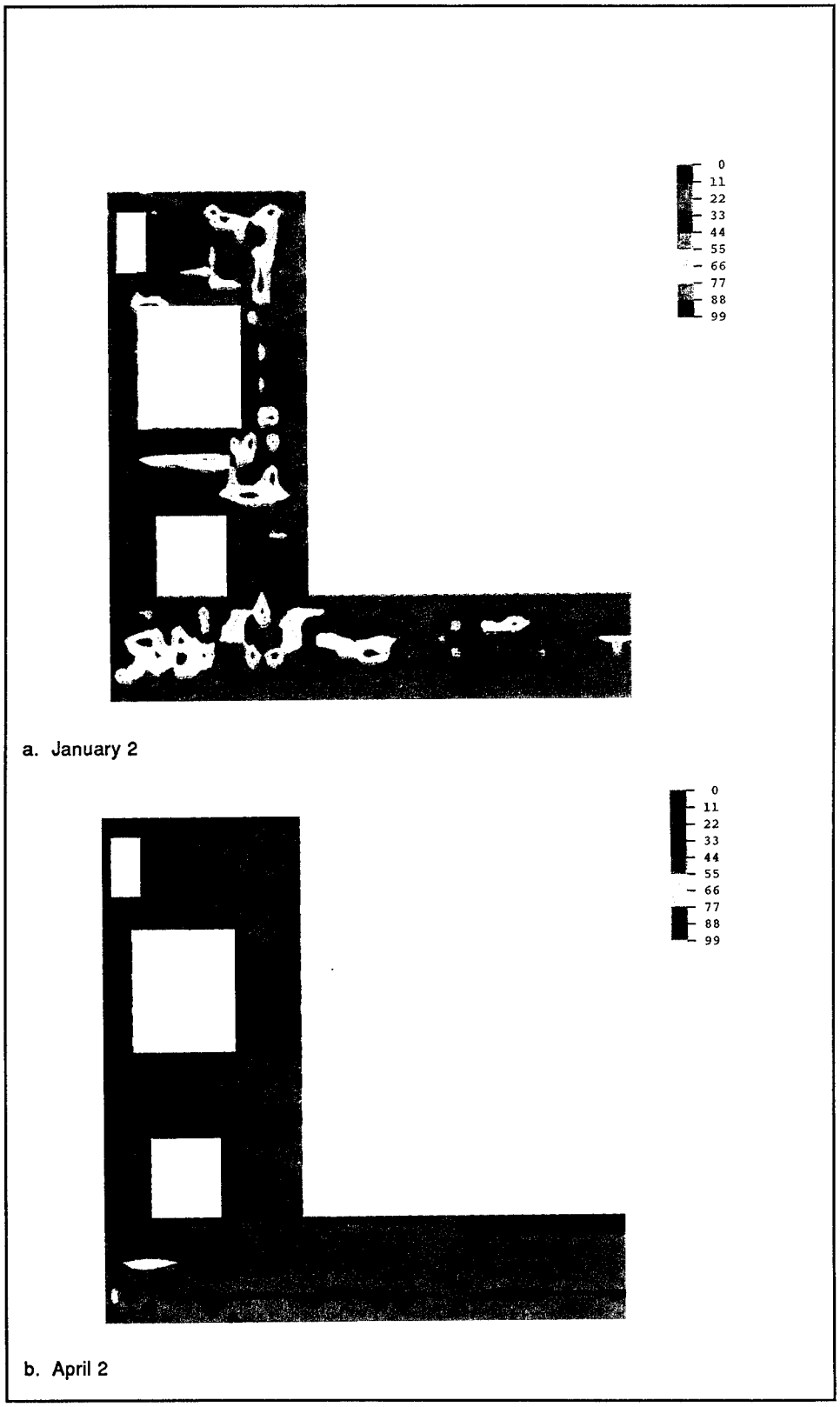

Figure 34. Crack potential contours for 545 days after start of construction (step = 223, amp = 545) (Continued)

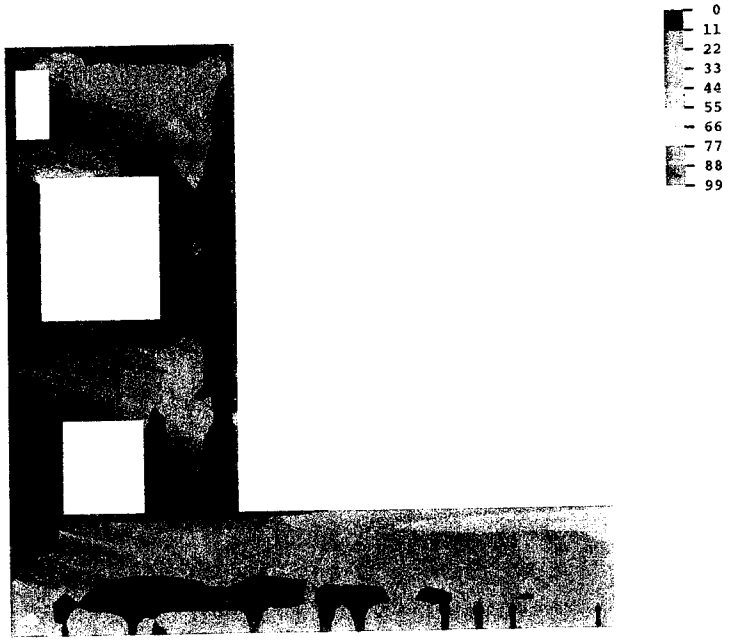

c. July 1

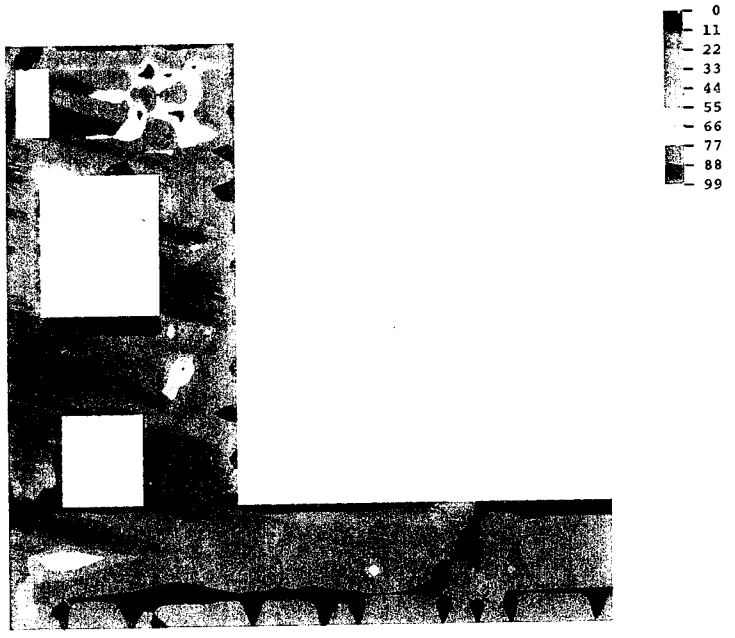

d. September 29

Figure 34. (Concluded)

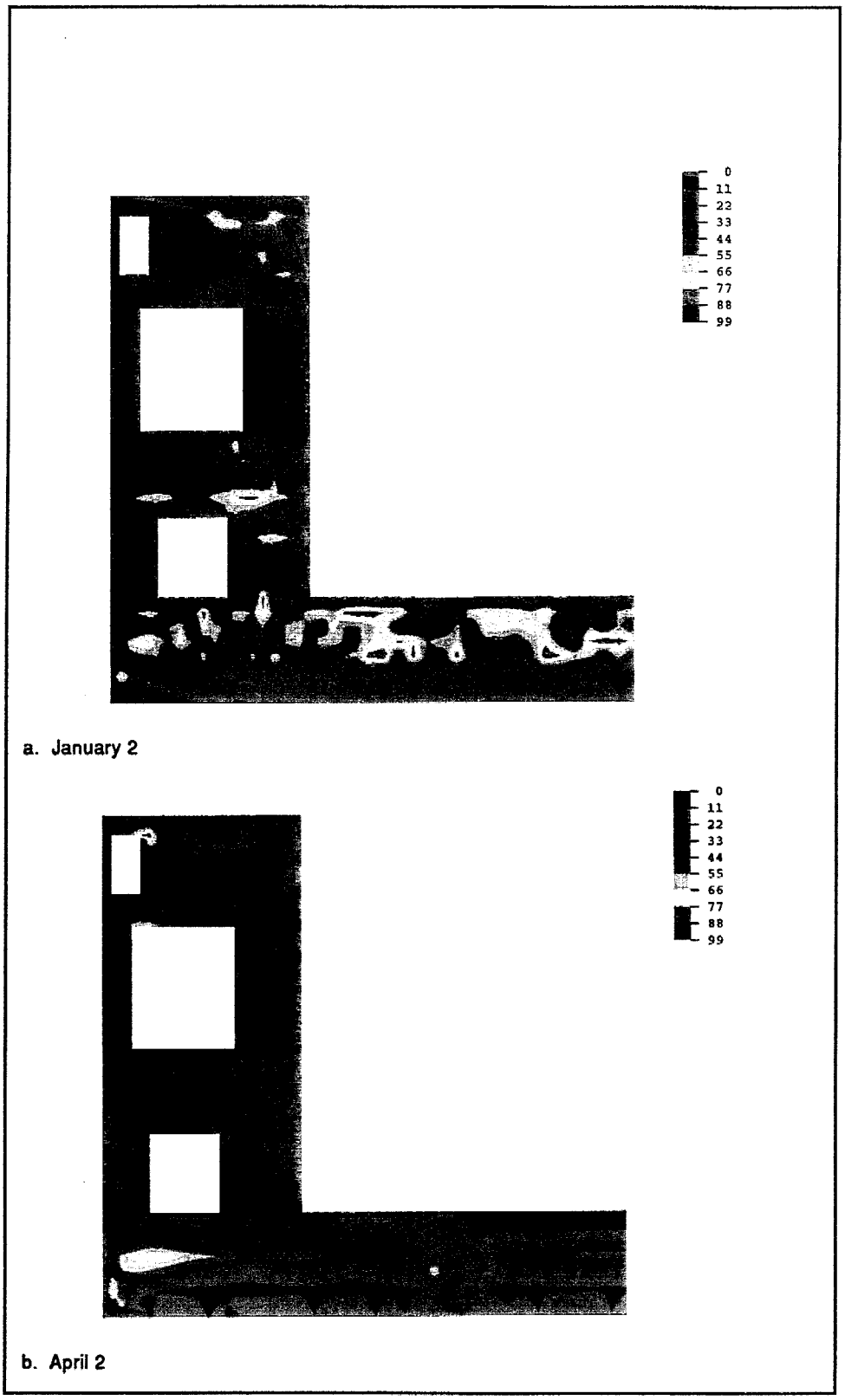

Figure 35. Crack potential contours for 725 days after start of construction (step = 241, amp = 725) (Continued)

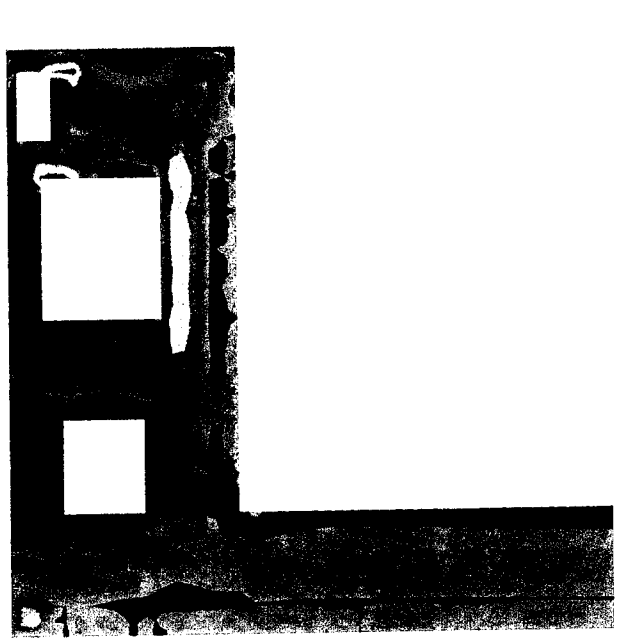

c. July 1

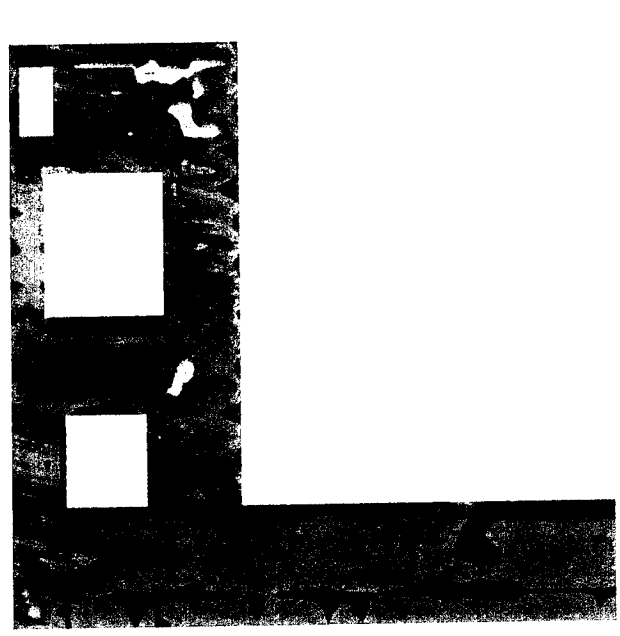

d. September 29

Figure 35. (Concluded)

This case corresponds to the January start date case used in the previous discussions. The second analysis, Case 2, was performed with the same parameters as the first, except that the soil distribution was the lower values shown in Figure 4. The third analysis, Case 3, was the same as Case 2 except if used placement temperatures that were between the minimum value of 40 °F and the maximum value of 65 °F. If the ambient temperature was between these values, the ambient temperature was the placement temperature. If the ambient temperature was outside this range, either the maximum or minimum was used as the placement temperature. This analysis also used insulated forms but did not insulate the top of the slab. In this case, the insulation was removed simultaneously with the formwork. The fourth analysis, Case 4, was performed with all of the attributes of the third analysis coupled with insulation of the top of the slab. Also, the insulation remained in place for 45 days or until April 1, whichever was the shorter time. The fourth analysis is an accurate simulation of the construction procedures for a lock monolith starting construction in January. The four analyses are progressive and provide insight into the effect of each variable as they changed from the January analysis used in the start-of-construction studies to the most realistic simulation of Case 4. The four cases highlight the benefits of insulation and having placement temperatures near the ambient values. The four analyses also reflect the need for accurate modeling, the benefits of progressively changing the variables to track their effects, and easily interpreting the results.

Temperature results

There does not appear to be any long-term residual thermal effects with the use of insulation. The 180-day thermal contours are nearly identical for all cases. Case 1 and Case 4 temperature contours for 180 days are shown in Figure 36. The two cases produce very similar 180-day temperatures, regardless of insulating parameters used in the analyses. This can also be seen in the 360-day contours shown in Figure 36. Although the temperatures become stable and ambient dependent, the construction temperature distributions are considerably different and cause very different behavior during construction.

Cracking patterns

The simplest comparison to show the difference in behavior is the final crack patterns. Figure 37 shows the final crack pattern for all four cases. Case 1 has significant cracking throughout the structure. Much of the cracking for Cases 1 and 2 occurs at the lift lines. The suspected cause is the high placement temperature coupled with the low ambient temperature. The complete line of cracks along the top of lift 1 is the most prominent set of cracks, but they are all vertical cracks due to the high thermal gradient along the top of the lift. The second case is almost identical to the first analysis with the exception of the cracking at the soil-structure interface. This cracking is due to the lower soil temperature distribution

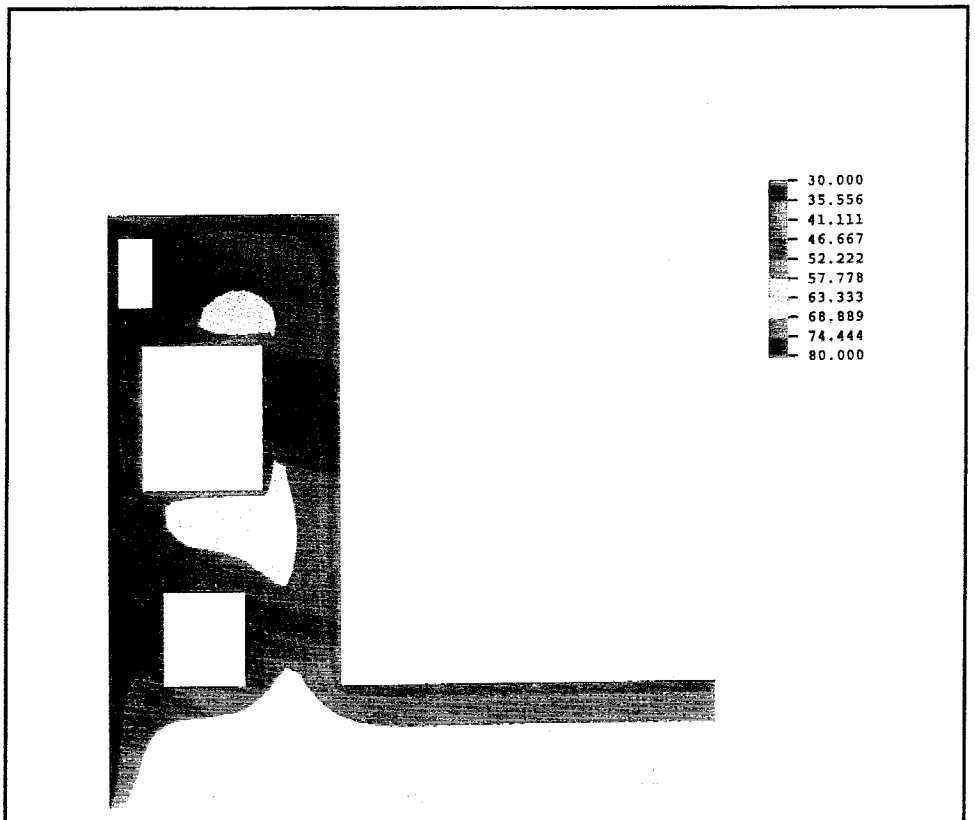

a. Uninsulated - 180 days (step = 181, amp = 180)

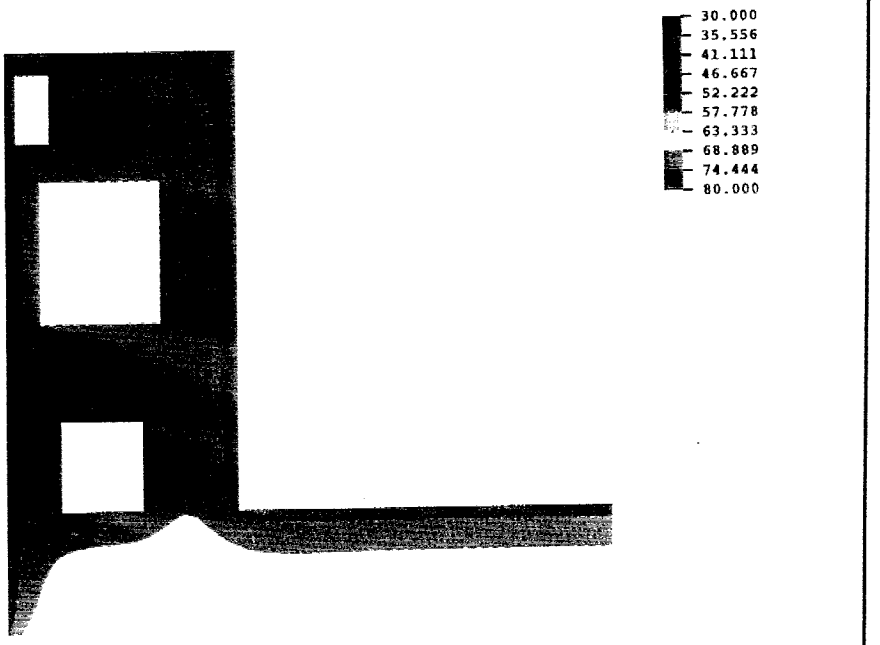

b. Insulated - 180 days (step = 181, amp = 180)

Figure 36. Temperature contours for 180 and 360 days after start of construction (Continued)

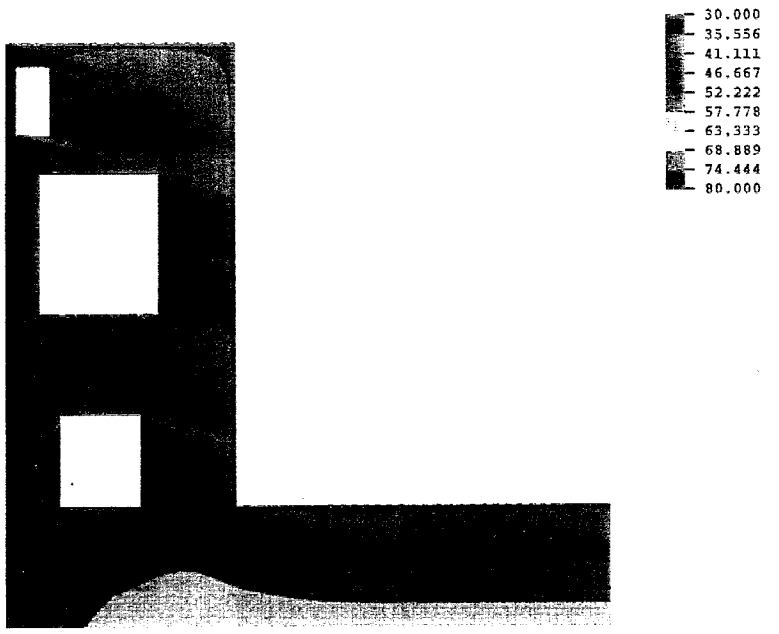

c. Uninsulated - 360 days (step = 217, amp = 360)

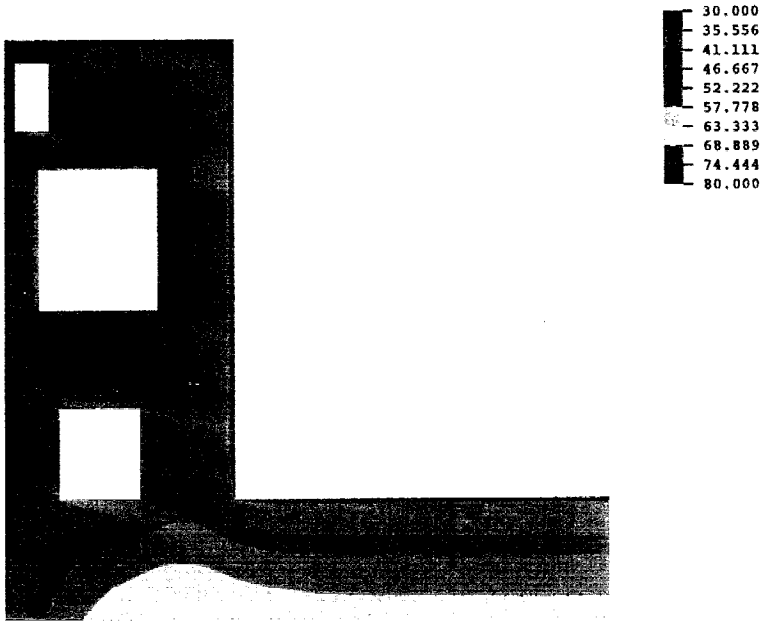

d. Insulated - 360 days (step = 217, amp = 360)

Figure 36. (Concluded)

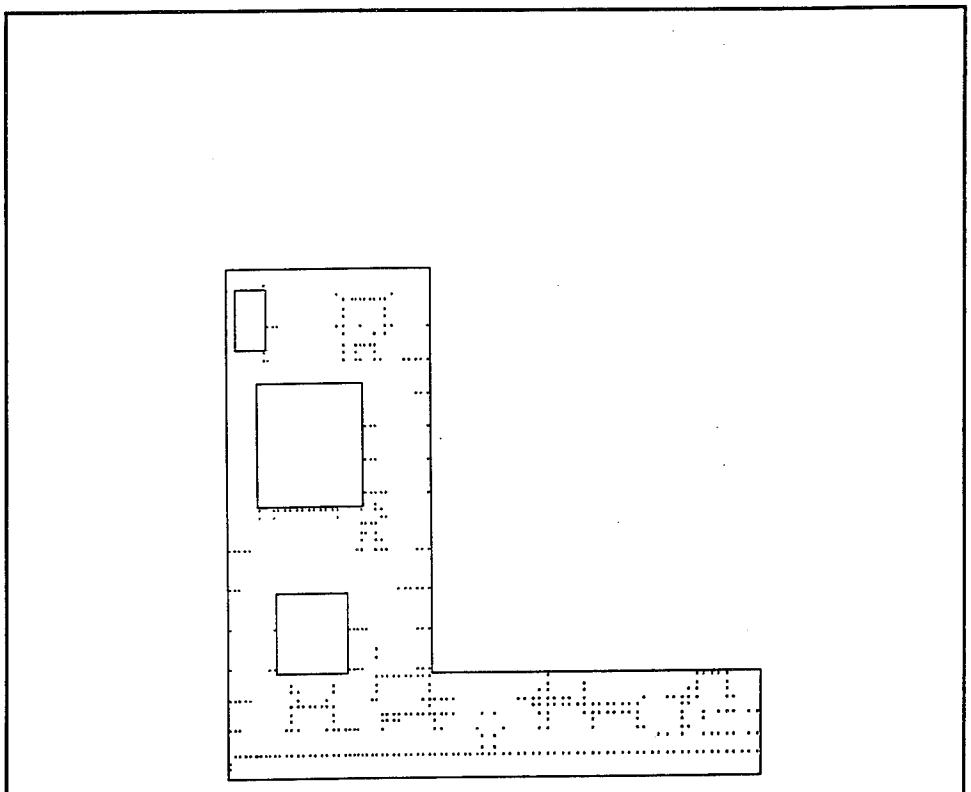

a. Case 1

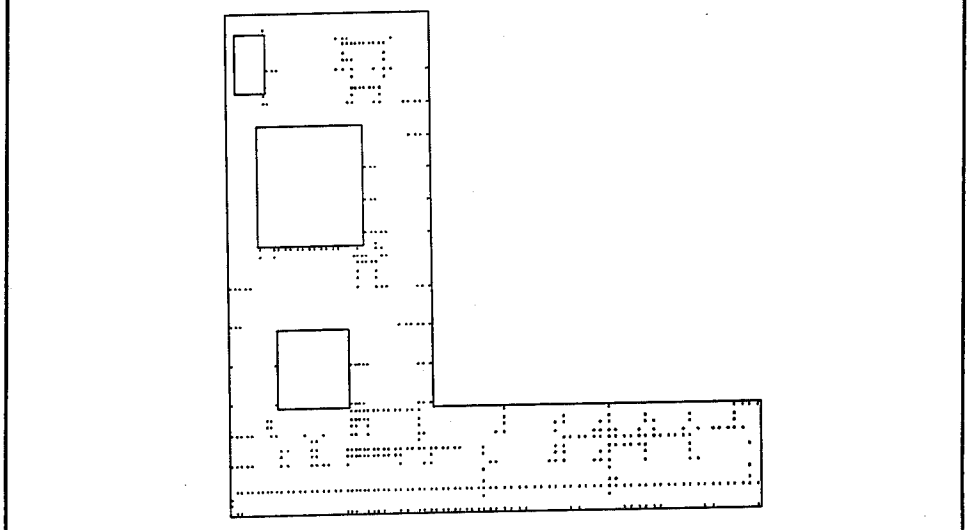

b. Case 2

Figure 37. Crack surface diagrams for 725 days after start of construction (step = 241, amp = 725, scale = 1.00) (Continued)

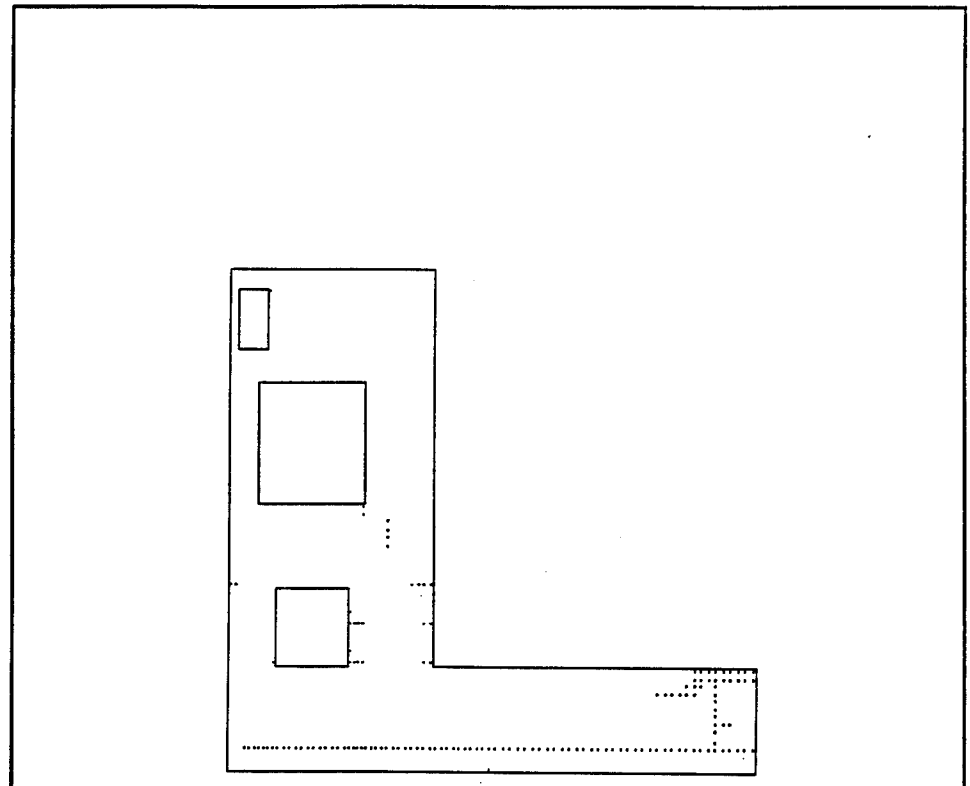

c. Case 3

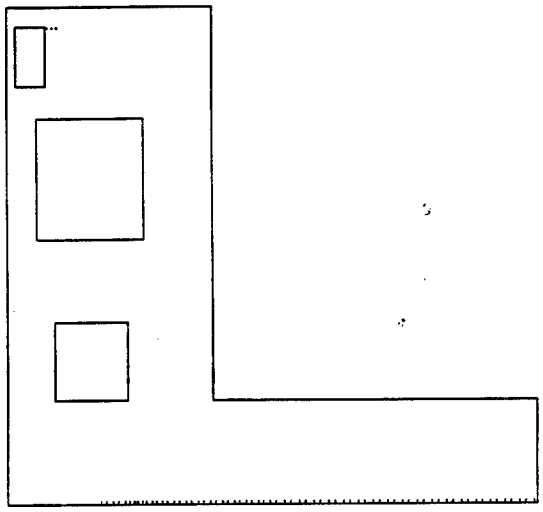

d. Case 4

Figure 37. (Concluded)

coupled with a higher placement temperature. In the first analysis, both the soil and the first lift had similar temperatures during placement. The second analysis kept the 65-°F placement but significantly reduced the soil temperature at placement causing a high thermal gradient along this interface. The third case has significantly reduced cracking. It still contains the long line of cracks along the top of the first lift which is caused by having an uninsulated top of the lift. Note that most of the cracks near the exterior surface of the monolith have vanished with the exception of those near the chamber floor and the culvert. Most of the cracks within the slab have also vanished since the placement temperature of the concrete was closer to or was the ambient temperature. This greatly reduced the thermal gradient near the top of each lift eliminating a major portion of the cracking. The combined thermal and bending of the chamber floor provides the right conditions for cracking near the center of the chamber floor. The fourth case eliminates almost all of the cracking except cracking near the spring supports and a small crack at the gallery corner. It is suspected that the soil is a substantial heat sink and, by insulating the top of the slab, the heat travels into the soil to create a high thermal gradient between the soil and the slab. This high gradient could cause the significant cracking along the soil-structure interface. The use of insulation on the top of the lifts combined with the proper ambient conditions provides a structure which is virtually crack free.

Cracking potentials

Figure 38 shows the crack potential for the four analyses in early July. Red indicates regions of highest potential for cracking. Cases 1 and 2 which are identical with the exception of the soil temperature distributions indicate that cracking could occur near the corners of the machine room nearest the chamber, isolated areas of the chamber floor, and several regions under the culvert. Since these two cases did not have insulation, the monoliths have undergone severe thermal changes creating residual effects leading to high cracking potentials. If these simulations were more indicative of the construction, the designers would have to seriously consider remedial measures to reduce the cracking and cracking potentials. Case 3 shows markedly reduced cracking potentials with 80 to 93 percent being the highest value other than regions that have previously cracked. Regions of concern would include the top, chamber corner of the gallery, the bottom, chamber corner of the machine room, and the intersection of the slab and chamber wall. A 90-percent potential would require close scrutiny and possible changes in reinforcement, but it may not require extensive remedial actions. Case 4 which is the most realistic model used in the analyses has a slightly different pattern than the other cases. The critical regions seem to be the top, chamber corner of the gallery, the exterior wall of the machine room, and the soil-structure interface. Remedial actions such as an insulation barrier along the soil-structure interface could be used to reduce the cracking and the crack potentials in this region. The high potential of the thin exterior machine room wall is due to the residual effects of high heat buildup within the machine room prior to removal of

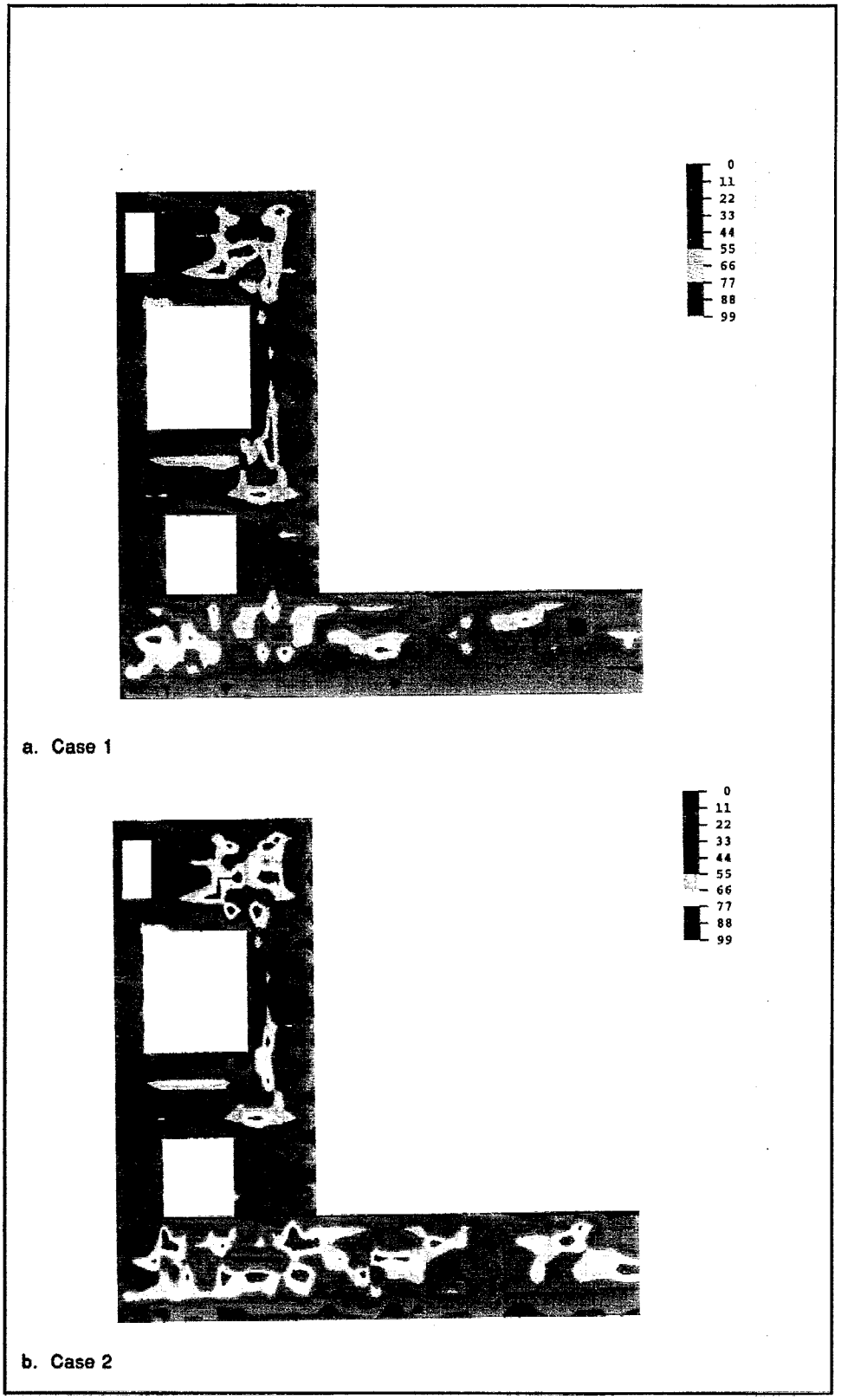

Figure 38. Crack potential contours for 185 days after start of construction (step = 187, amp = 185) (Continued)

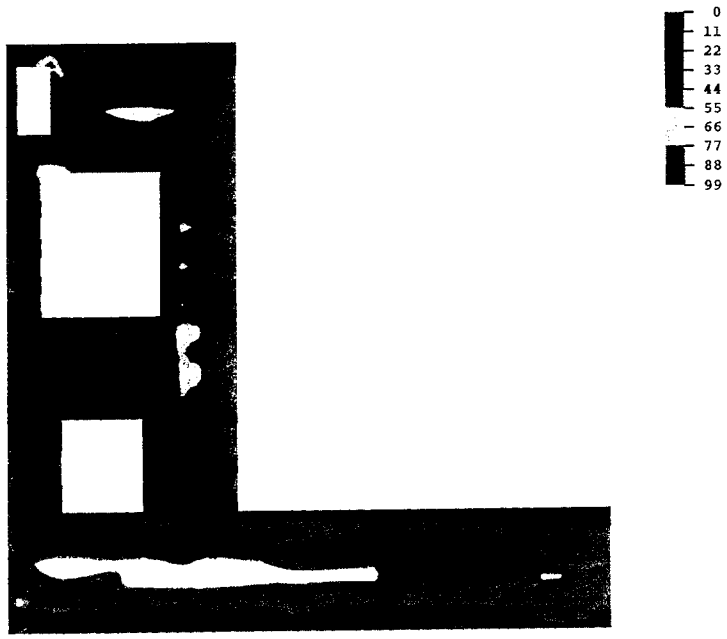

c. Case 3

d. Case 4

Figure 38. (Concluded)

the outer insulated forms. This could possibly be solved by keeping the insulated forms in place longer than the one used in the model.

Figure 39 shows the crack potentials for the four analyses at approximately 1 year after construction. The crack potentials for the first two cases have reduced by approximately 5 percent. The regions of highest potentials have not appreciably changed from day 185 to day 365. Some surfaces show higher potentials due to the ambient conditions, but most of the higher potentials are still located in the more massive regions or near areas of stress concentrations. Case 3 has increased its cracking potential from 93 to 99 percent. The chamber floor surface and the interior of the slab and chamber wall intersection show very high potentials. The potentials of Case 4 drop from 99 to 56 percent, with the highest potentials being at the corner of the gallery and near the center of the chamber floor.

Figures 40 and 41 are crack potential contour plots for July 1 of the following year, 545 days (1.5 years), and December 28, 725 days (2 years), after construction, respectively. The contours for each of the cases are not significantly different from the contours presented in Figures 35 and 36. The regions of possible cracking are nearly the same locations but have reduced in size.

Stress contours

The horizontal stress contour for each of 365 and 545 days after the start of construction are shown in Figures 42 and 43, respectively. These contours were chosen since the 365-day tensile stresses were typically higher than the 725-day values for January, and the 545-day values were typically higher than the 185-day values. The highest tensile stresses reach approximately 330 psi for Case 1 during July and a minimum tensile stress of approximately 170 psi for Case 4 during July. As discussed previously, areas of tensile stress concentrations are reflected in the crack potentials. The most significant result is the homogeneity that occurs within the Case 4 results. The horizontal stress contours reflect bending within the chamber floor and minor horizontal stresses in the walls. Case 4, with the most stringent insulation procedures, seems to have minimized the residual effects at the lift lines. The accurate modeling of the construction procedures using insulation and correct placement temperatures indicate that acceptable stress levels and controlled cracking can be obtained even during cold-weather construction.

The vertical stress contours for each of 365 and 545 days after the start of construction are shown in Figures 44 and 45, respectively. These contours were chosen since the 365-day tensile stresses were typically higher than the 725-day values for January and the 545-day values were typically higher than the 185-day values that were used for July start-of-construction comparisons. The maximum vertical tensile stress was 220 psi for Case 1 in July. The maximum tensile stress of Case 4 was 141 psi compared to the 220 psi for Case 1. Case 4 has a vertical stress distribution that is

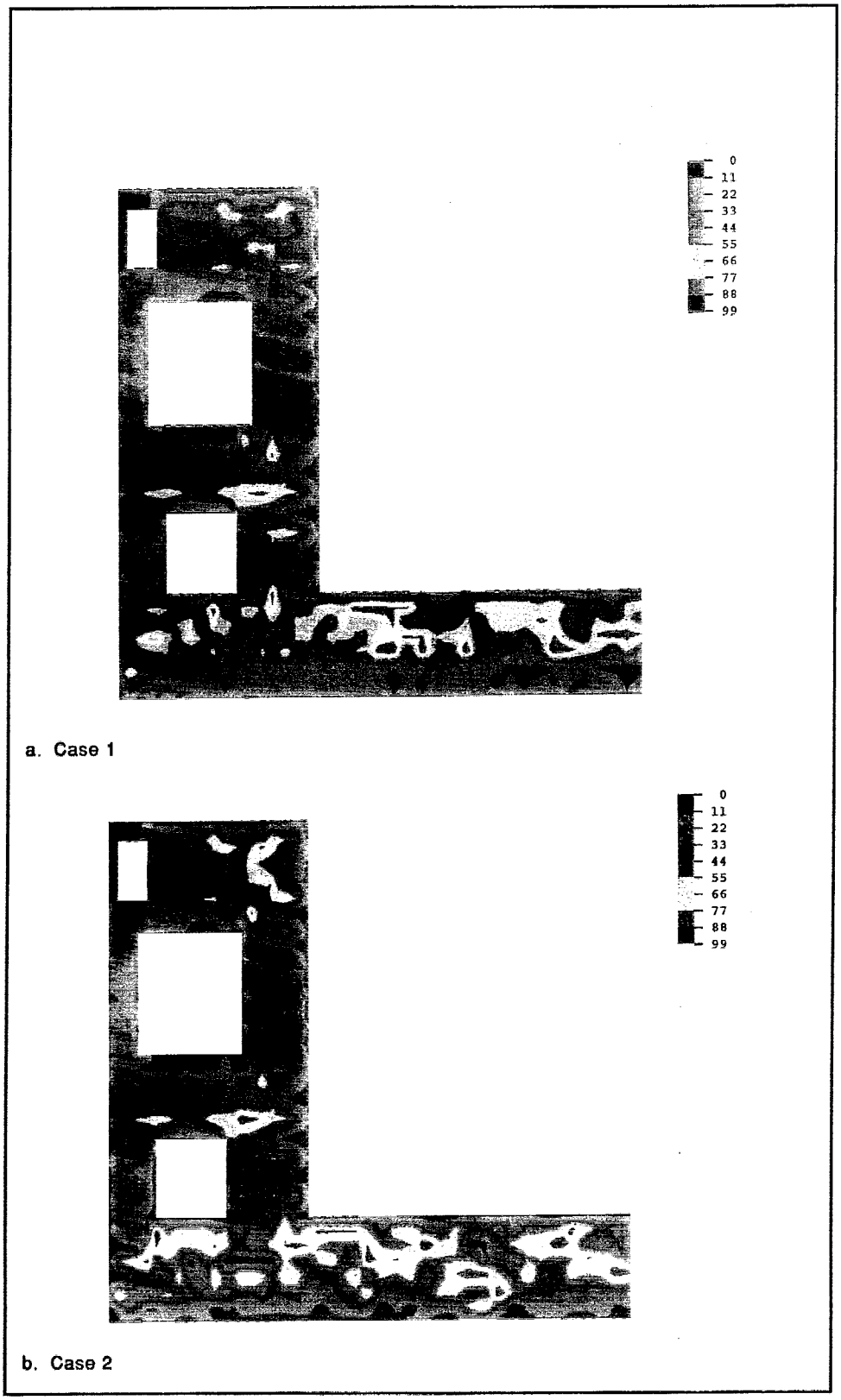

Figure 39. Cracking potential contours for 365 days after start of construction (step = 205, amp = 365) (Continued)

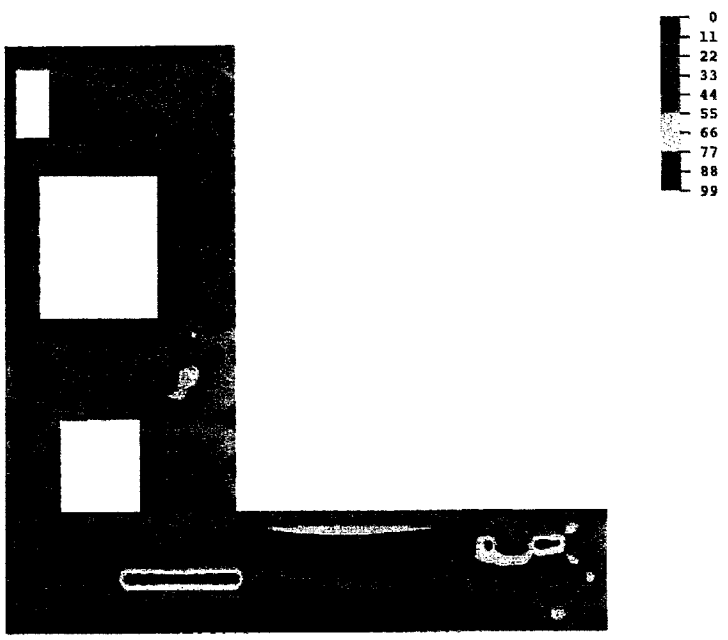

c. Case 3

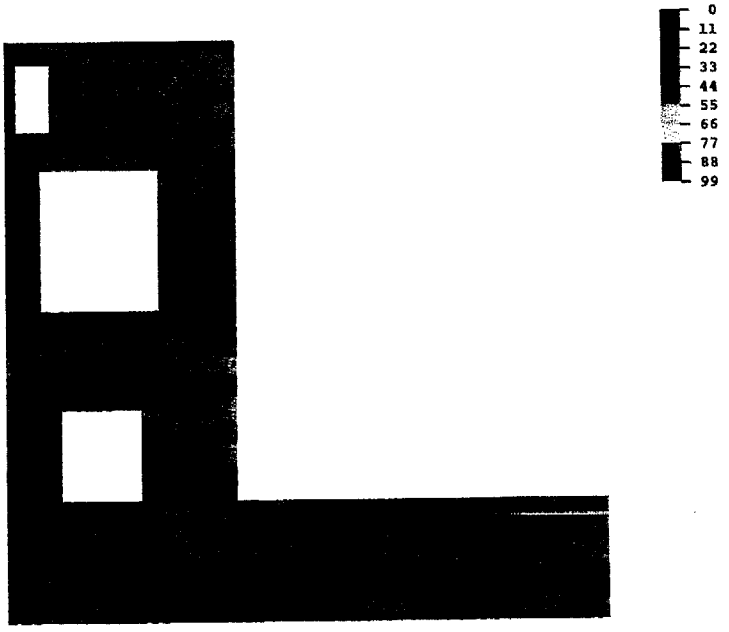

d. Case 4

Figure 39. (Concluded)

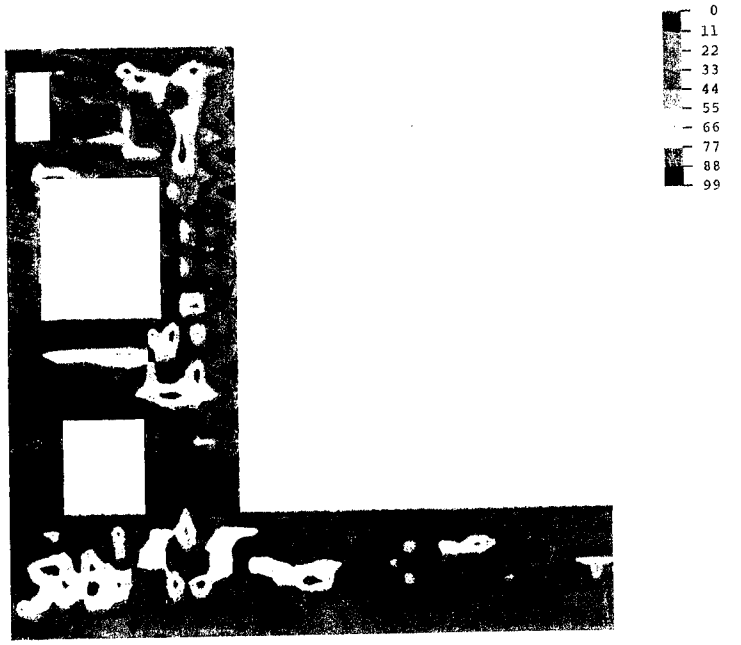

a. Case 1 (step = 223, amp = 545)

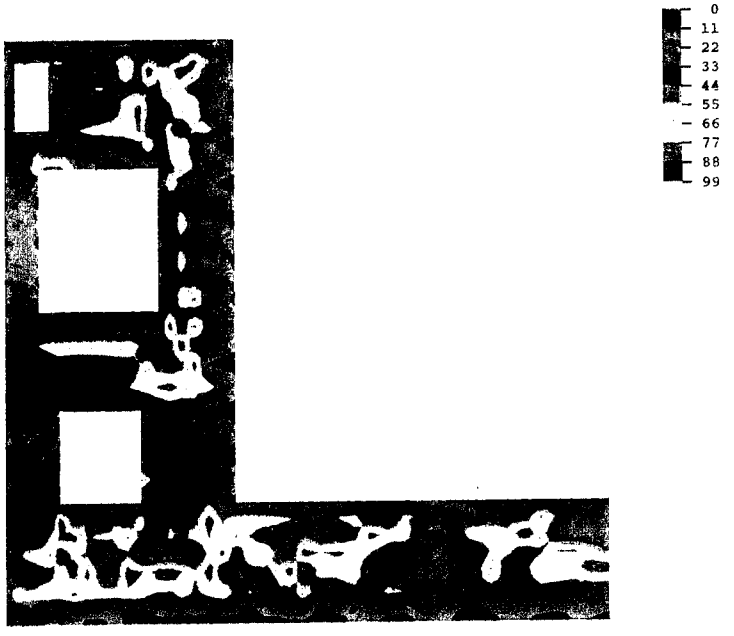

b. Case 2 (step = 223, amp = 545)

Figure 40. Cracking potential contours for 545 days after start of construction (Continued)

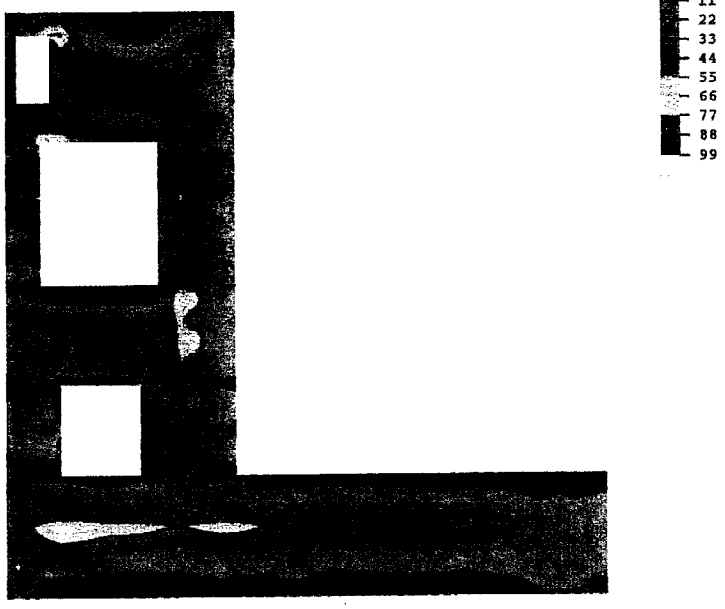

c. Case 3 (step = 223, amp = 545)

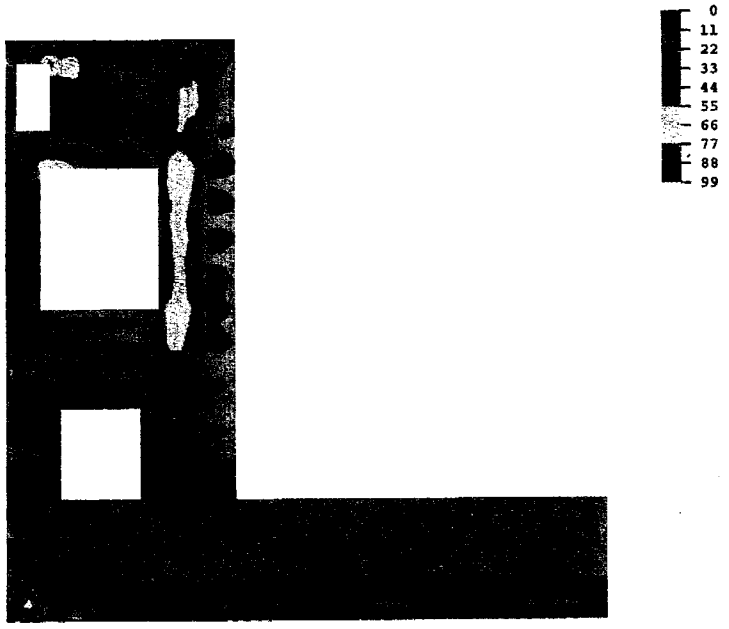

d. Case 4 (step = 223, amp = 540)

Figure 40. (Concluded)

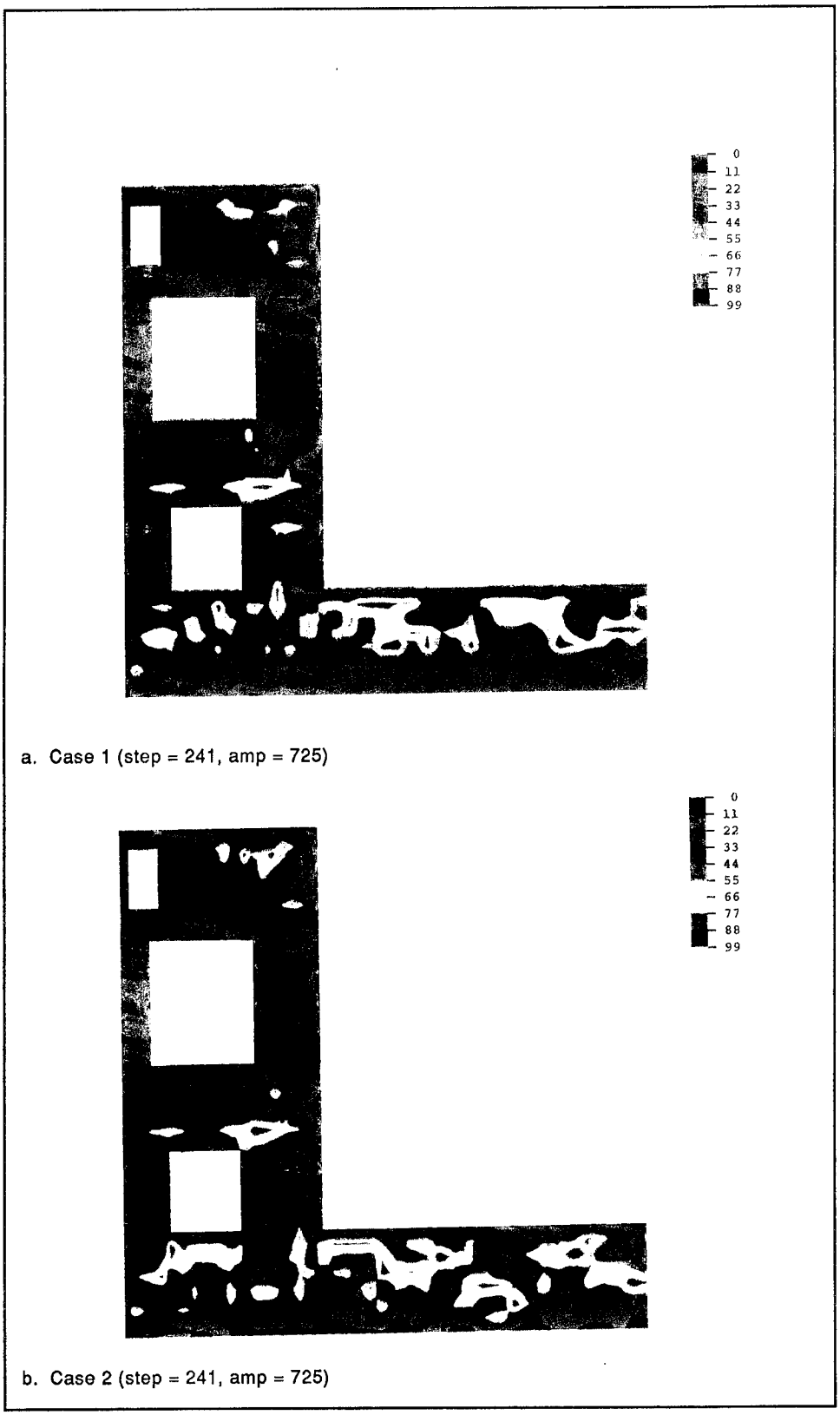

a. Case 1 (step = 241, amp = 725)

b. Case 2 (step = 241, amp = 725)

Figure 41. Cracking potential contours for 725 days after start of construction (Continued)

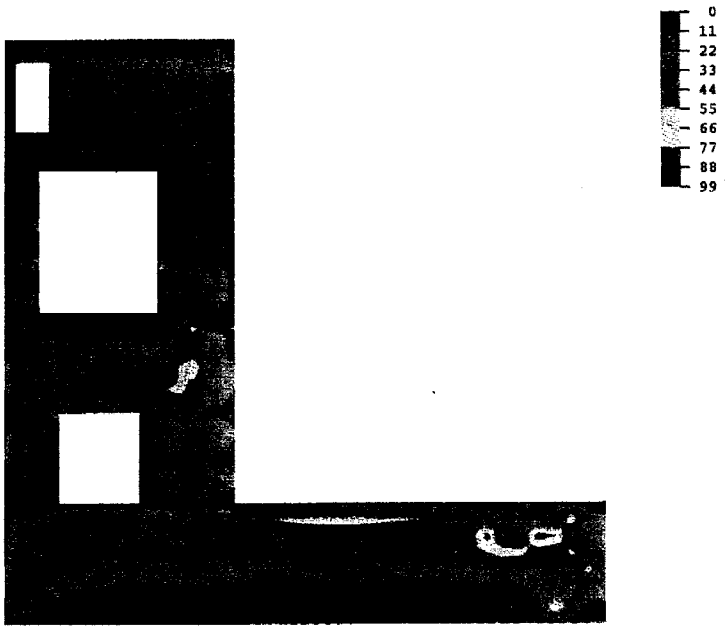

c. Case 3 (step = 241, amp = 725)

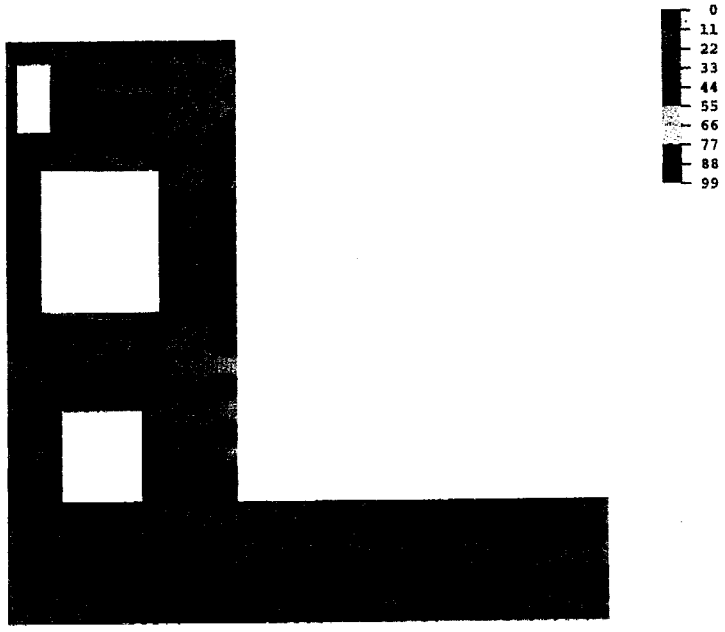

d. Case 4 (step = 241, amp = 720)

Figure 41. (Concluded)

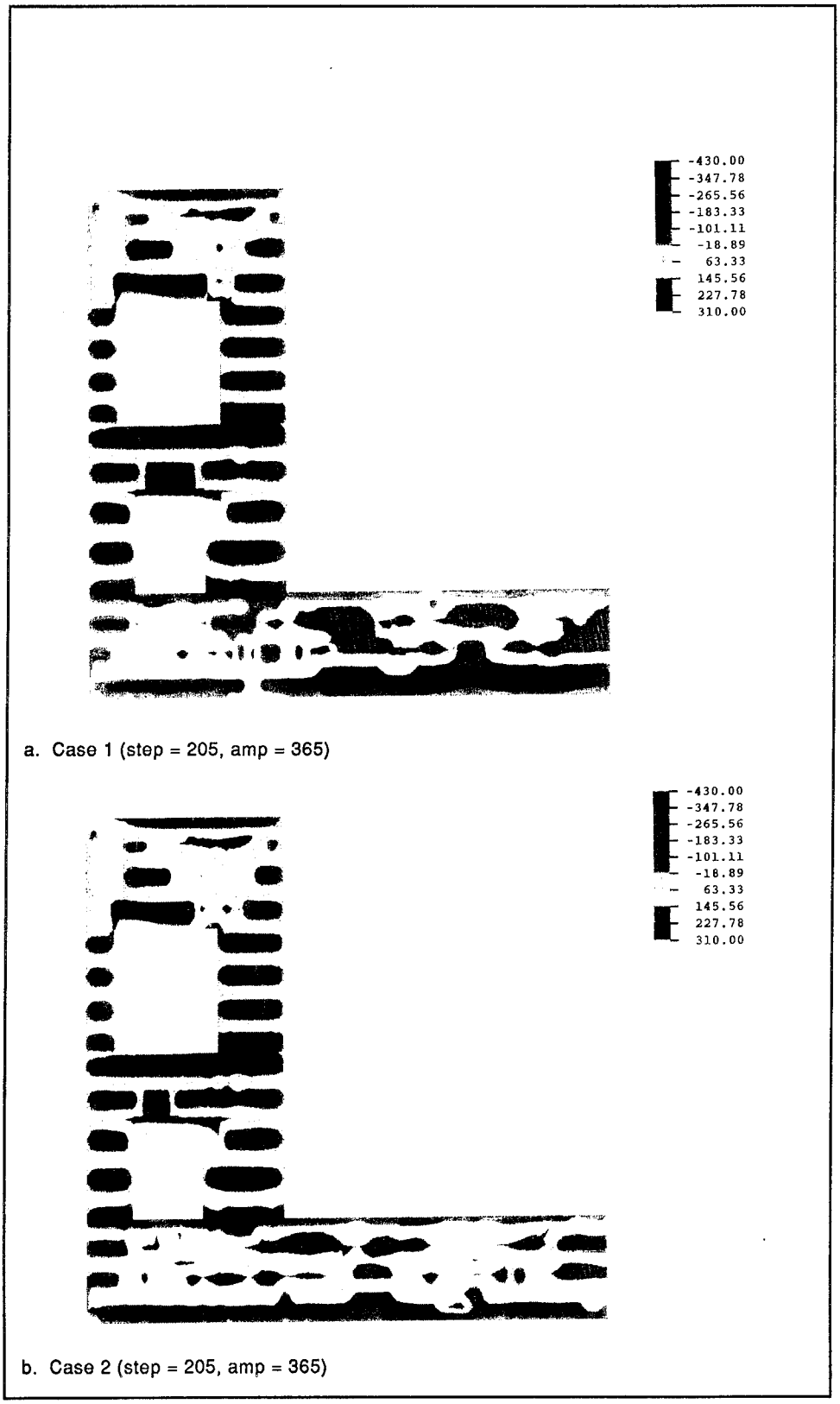

Figure 42. Horizontal stress contours for 365 days after start of construction (Continued)

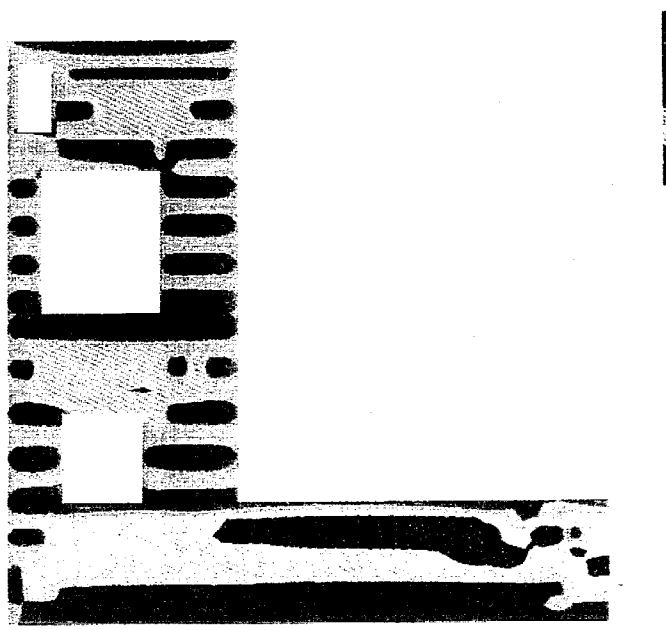

c. Case 3 (step = 205, amp = 365)

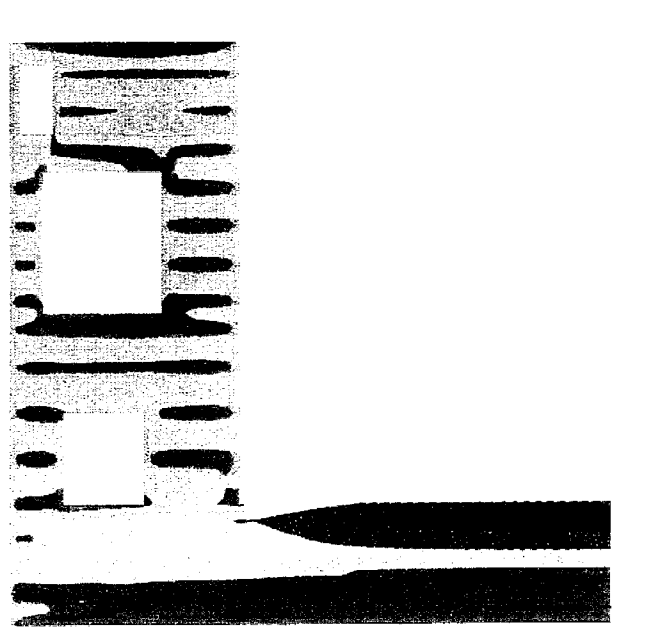

d. Case 4 (step = 205, amp = 360)

Figure 42. (Concluded)

a. Case 1 (step = 223, amp = 545)

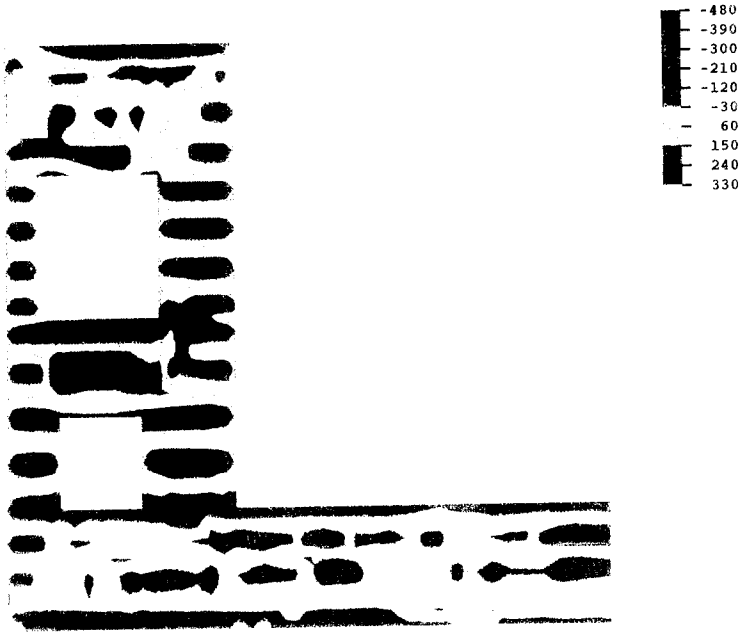

b. Case 2 (step = 223, amp = 545)

Figure 43. Horizontal stress contours for 545 days after start of construction (Continued)

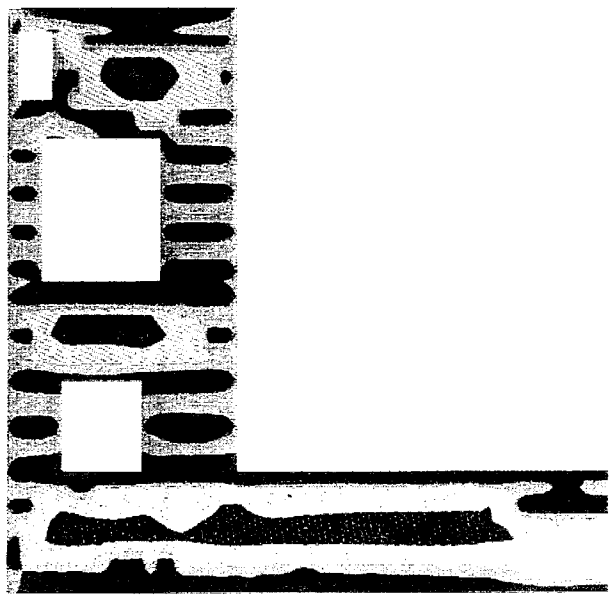

c. Case 3 (step = 223, amp = 545)

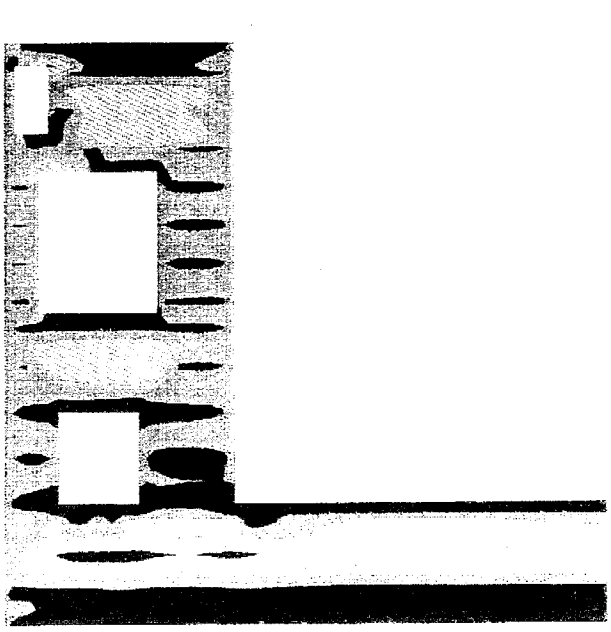

d. Case 4 (step = 223, amp = 540)

Figure 43. (Concluded)

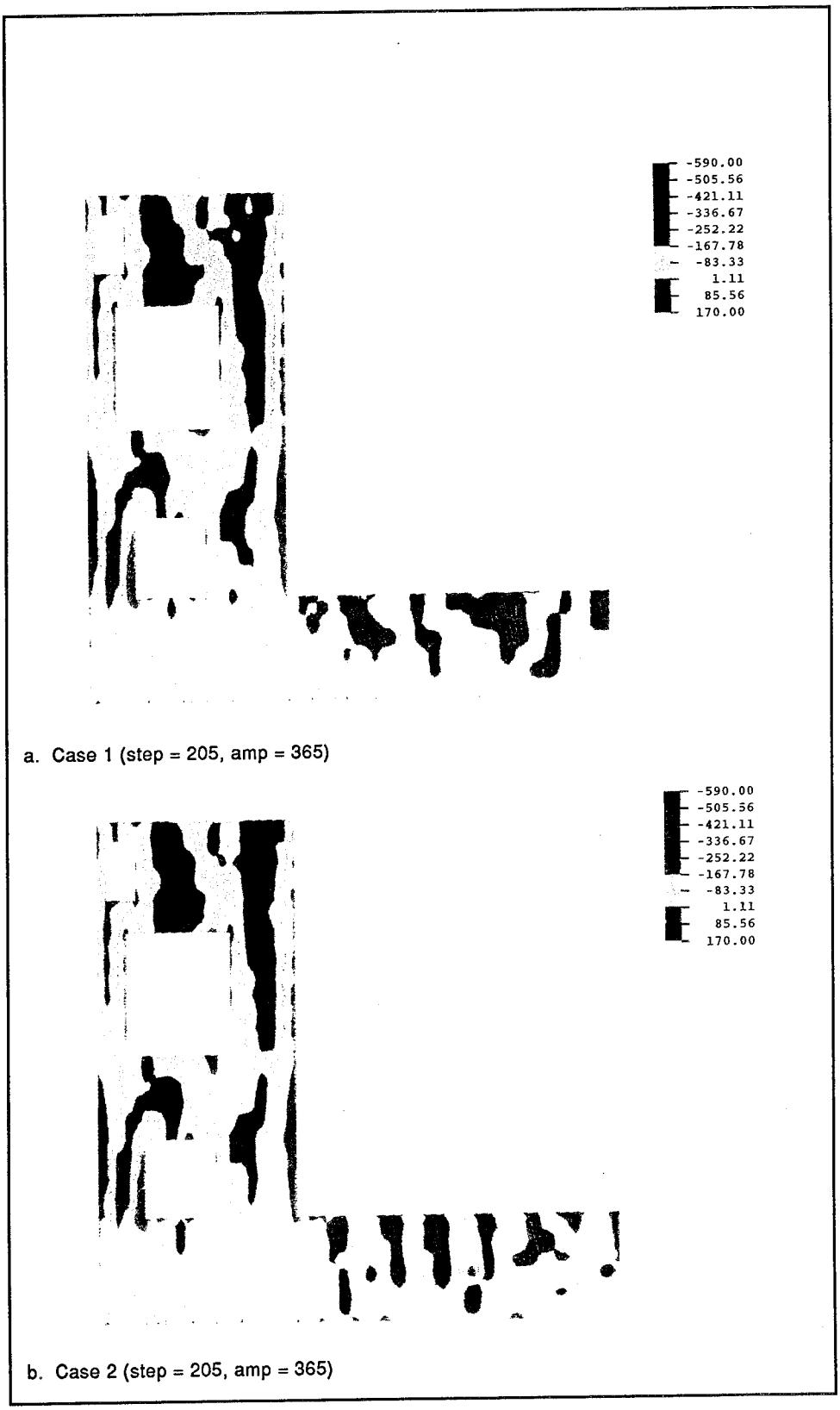

Figure 44. Vertical stress contours for 365 days after start of construction (Continued)

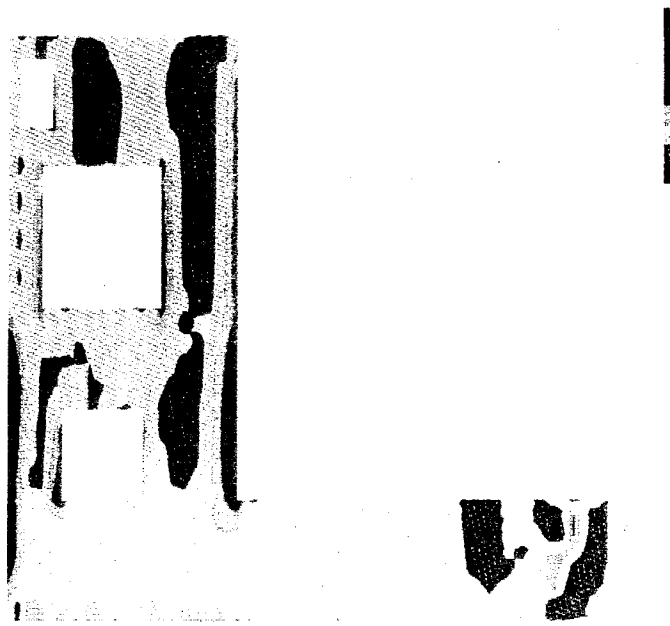

c. Case 3 (step = 205, amp = 365)

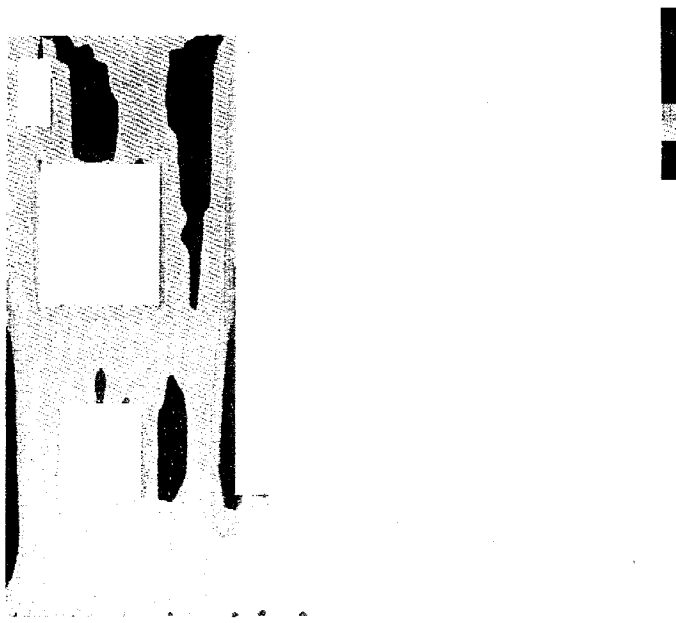

d. Case 4 (step = 205, amp = 360)

Figure 44. (Concluded)

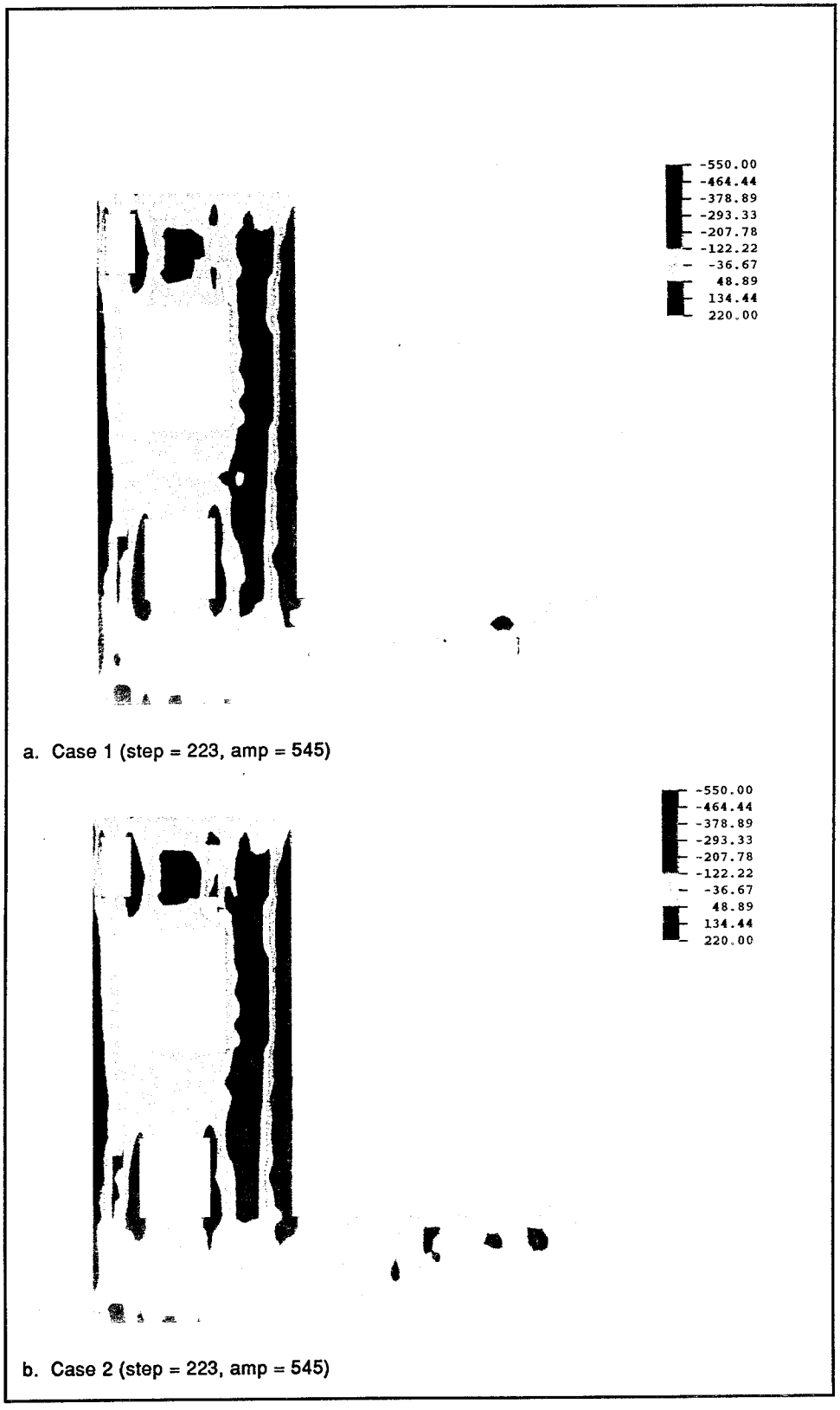

Figure 45. Vertical stress contours for 545 days after start of construction (Continued)

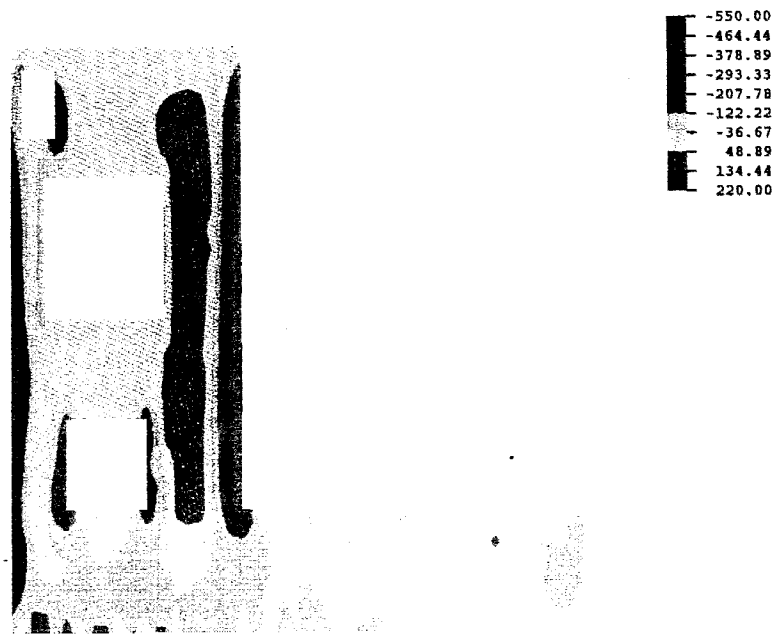

c. Case 3 (step = 223, amp = 545)

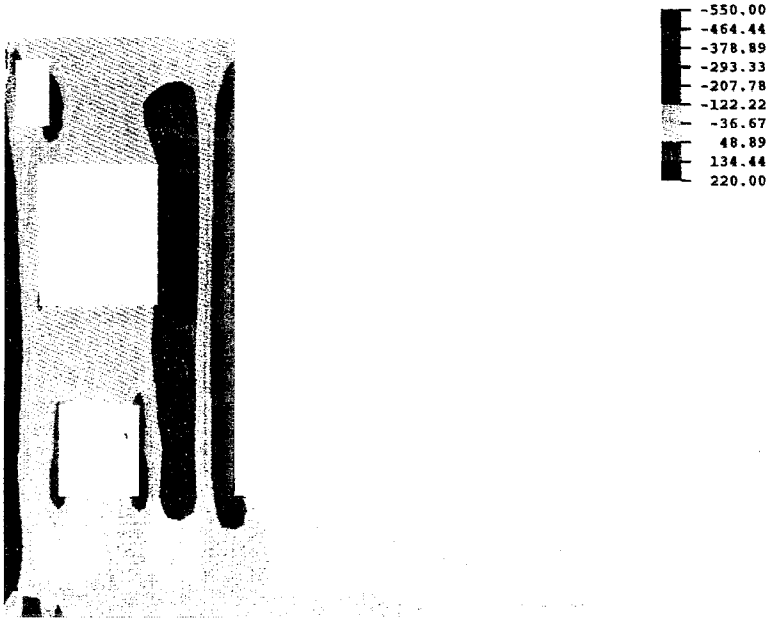

d. Case 4 (step = 223, amp = 540)

Figure 45. (Concluded)

more uniform than the other cases. None of the cases have significantly high tensile stresses, but controlling the thermal gradients using insulation and ambient-driven placement temperatures does provide a better behaved structure.

Summary

Use of realistic modeling of the construction procedures significantly changes the amount of cracking and the crack potentials for the January start of construction. By having realistic placement temperatures, soil temperatures, and insulation procedures, the lock monolith model went from severely cracked to minimally cracked. As long as the January construction procedures include proper insulation, it is generally less critical than the fall or spring starts of construction without insulation. The behavior of the January, Case 4 model, would suggest that the September model or construction should include insulation procedures as well. This study definitely supports the current insulating procedures used in construction of lock monoliths.

The April and September start-of-construction results are the worst cases. Once the January model included insulation, these start dates had the worst cracking conditions. Early in NISA studies, it was thought that the July start date would be critical due to the large buildup of heat, but the large thermal gradients produced by the ambient conditions are critical and should be considered when performing a NISA. From the results presented, it is apparent that geometry, ambient conditions, and construction procedures all play a large role in the thermal behavior. As expected but now verified by NISA procedures, geometric singularities, high heat generating concretes, and cold weather are all potential sources of crack production in massive concrete systems. NISA now provides a tool for exploring and quantifying the effects of these sources for cracking, thereby, providing a mechanism for analyzing different alternatives for the minimization or elimination of cracking in massive concrete structures.

4 Plane Stress, Plane Strain, Generalized Plane Strain

Introduction

A series of analyses on the auxiliary lock for the Melvin Price Locks was performed using three different finite element formulations. Since 2-D models are being used for most NISA studies, the question of whether plane stress or plane strain elements are appropriate is constantly being debated. ABAQUS, the program used to perform the analyses, offers a third choice of generalized plane strain.

Plane stress and plane strain formulations have been available and have been commonly used for the past several decades, whereas, generalized plane strain has been less commonly used. Plane stress assumes a 2-D stress field with the out-of-plane direction being stress free. This formulation is most appropriate for thin structures with no restraints in the out-of-plane direction or when near the end of a massive structure such as a lock monolith where the free end of the monolith is unloaded. Plane strain assumes a 2-D strain field with the out-of-plane direction being strain free. The plane strain formulation is appropriate for thick structures where the out-of-plane direction is highly restrained. This formulation is also appreciated when it is in the middle of a massive structure such as a lock monolith where the movement of longitudinally adjacent nodes would be limited. The generalized plane strain formulation attempts to have an analysis capable of capturing behavior which is in between the extremes of plane stress and plane strain. This formulation allows the structure to displace in the out-of-plane direction. The planes on each side of the 2-D slice representing the structure are independently free to rigidly displace and/or rotate. This relative, rigid motion allows both stress and strain to be generated in the out-of-plane direction. The results that follow were generated to distinguish the relative difference in the results produced by the three formulations and to begin the accumulation of data that could eventually lead to guidance for choosing specific analysis methods for mass concrete structures.

Common Parameters

The analyses performed to compare plane stress, plane strain, and generalized plane strain results were performed with identical input parameters with the exception of the element type. The common parameters consist of a July start-of-construction, a concrete placement temperature of 65 °F, the Alton, IL, ambient temperature curve, form removal after 2 days, a 5-day lift interval, the average adiabatic temperature rise data, and a July soil temperature distribution, as discussed in Chapter 2. The dimensions and lift sequence are the same as shown in Figure 2.

Cracking Analysis

The crack surface plots as of the 725th day for each of the three models are shown in Figure 46. The plane strain model produced the fewest cracks with cracking occurring in the lower exterior corner of the monolith and the top interior corner of the gallery. The plane stress model produced cracks in exactly the same locations, but with several more cracks being present in the lower exterior corner of the monolith. The generalized plane strain model also had cracking in these locations, but it also indicated cracking in several new areas; the region between the gallery and the machine room, the lower exterior corner of the machine room, the exterior corners of the gallery, and most significantly, the center line of the chamber floor. Neither of the more conventional analysis methods predicted cracking at the center line of the chamber floor. The crack potentials, Figure 47, for the top of the chamber floor at its center line do reach values in the 85-percent range for the plane strain analysis and the 97-percent range for the plane stress analysis at the 185th day after construction. The crack potentials for the generalized plane strain monolith at the chamber center line, shown in Figure 47, are relatively small since the center line of this model has already had significant cracking take place. Therefore, the region is shown to be susceptible to cracking by all of the analyses, but the crack criteria has not been violated in either the plane strain or plane stress analyses. The severity of the cracking as predicted by the generalized plane strain analysis would have to be heavily considered in the design of this structure. The plane strain result, 85-percent crack potential, may not be considered critical by current criterion, but the plane stress result, 97-percent crack potential, would be considered critical. Therefore, the analyses, all showing high potential for cracking in the center slab region of the structure, could require different actions according to current design criterion. For this monolith and the given assumptions, the plane stress and generalized plane strain results have higher crack potentials at 365, 545, and 725 days after construction than the plane strain results. It is important to use both the crack surface plots coupled with the crack potentials to analyze the structure for cracking.

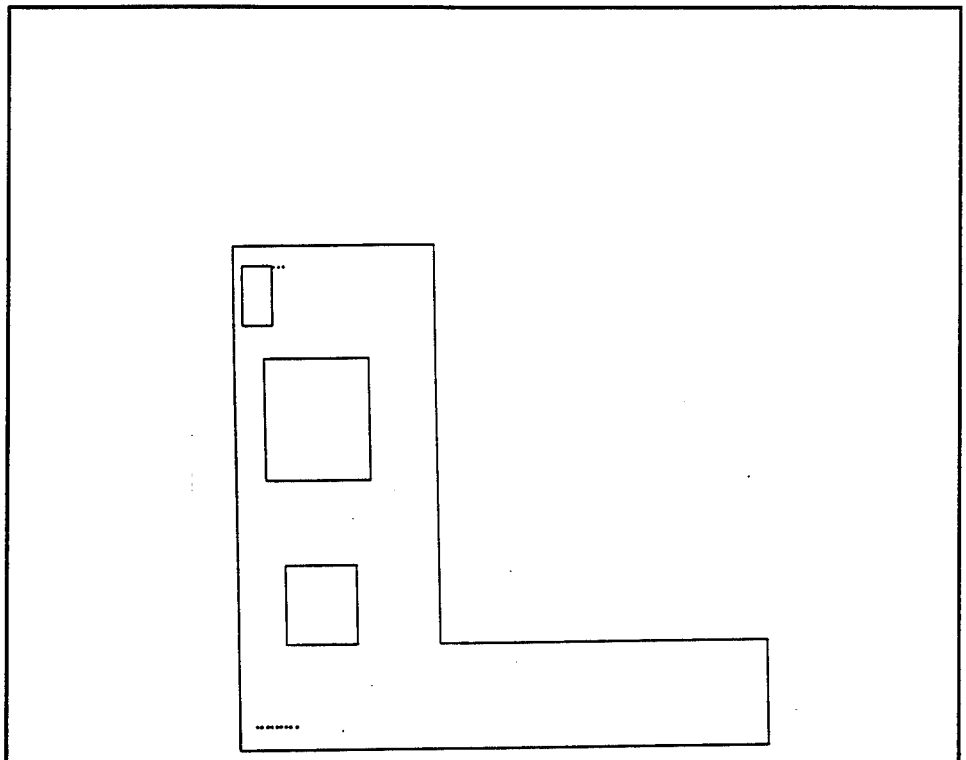

a. Plane strain

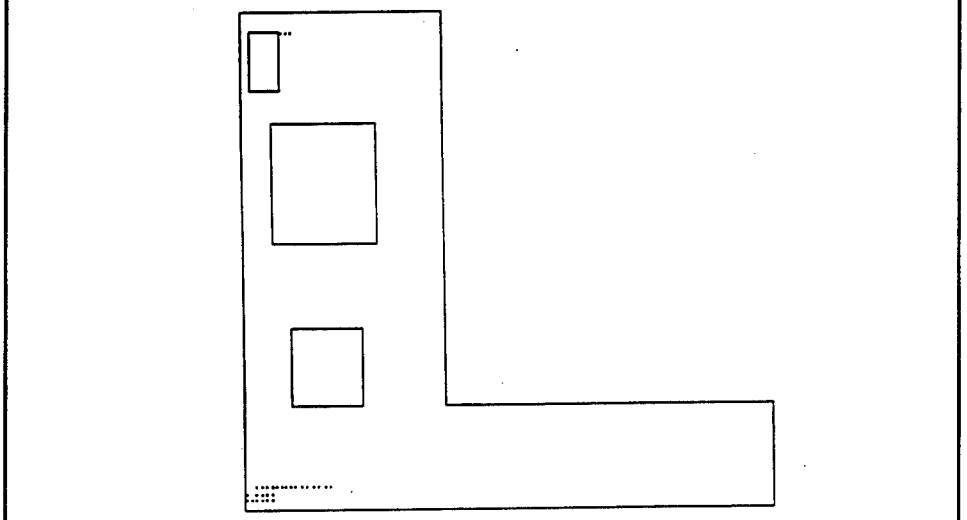

b. Plane stress

Figure 46. Crack surface diagrams for 725 days after start of construction (step = 241, amp = 725, scale = 1.00) (Continued)

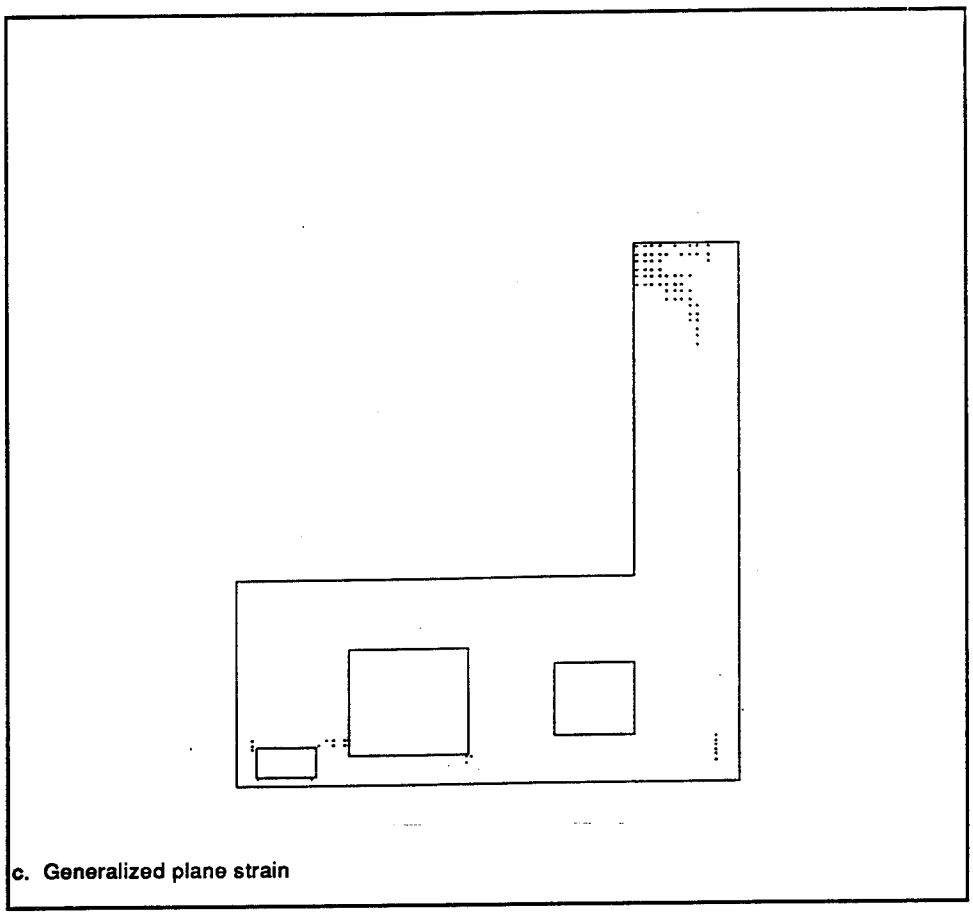

c. Generalized plane strain

Figure 46. (Concluded)

Stress Analyses

The stresses generated by each of the three models show only minor differences. Plane strain and generalized plane strain tend to produce nearly identical stresses at most locations. Generalized plane strain produced stresses that were above the values for those of plane stress and plane strain as shown in Figures 48 to 51 except in locations where cracking occurred. Deviations in the stresses in Figures 48 and 49 are directly related to cracking in nearby elements. Element 340, Figure 48, is near the lower left corner of the monolith where the plane stress model predicted more cracking than the other two modes. The additional cracking relieved the tensile stress in this element for the plane stress model, whereas, the other two models still predict tensile stresses in the 50-psi range. The generalized plane strain analysis predicts cracking for element 494, as seen in Figure 49, while the other analyses do not. The crack potentials for the plane stress and plane strain analyses are quite high at this point in time, approximately 140 days, and in this location, but the crack criteria was not violated. (This can be seen in the 185-day crack potentials shown in Figure 47.) It is interesting that the minimum tensile stress for element 494 for all three analyses is nearly identical, regardless of the cracking, but

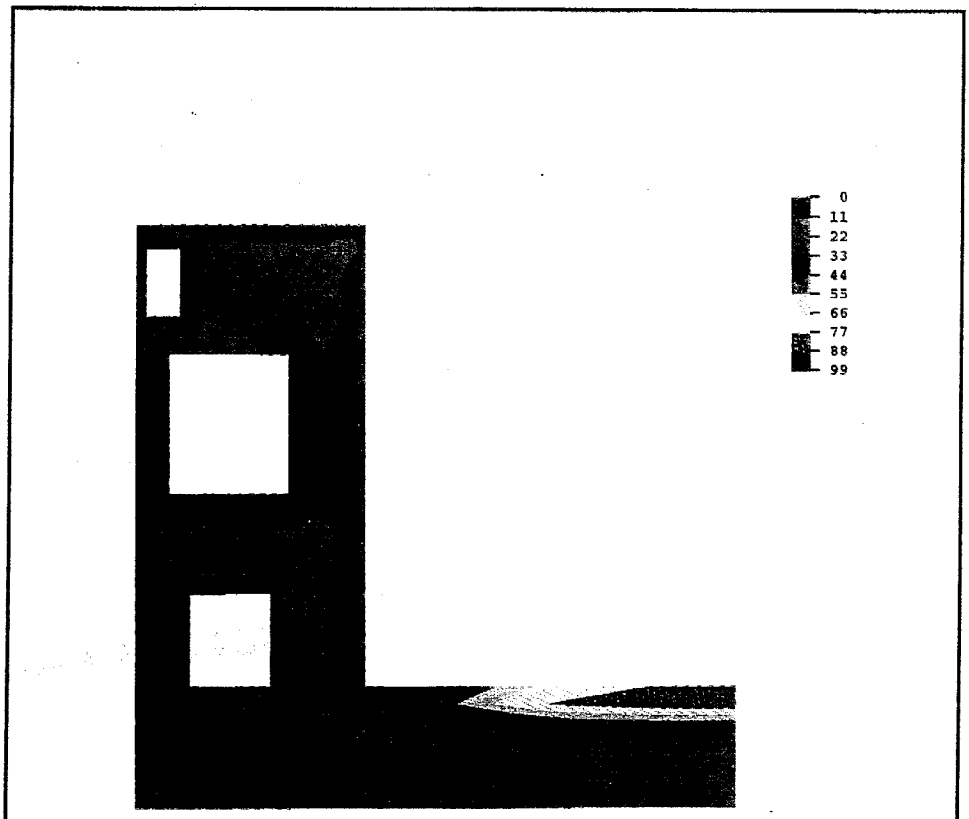

a. Plane strain

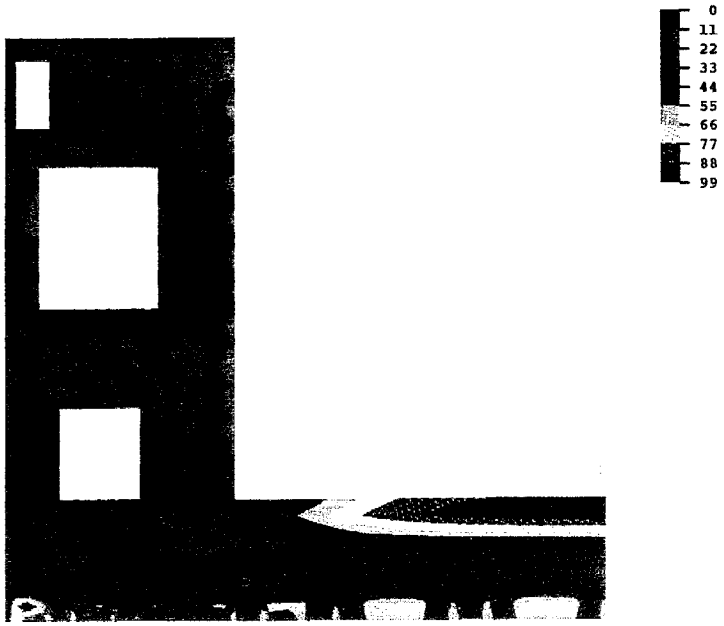

b. Plane stress

Figure 47. Crack potential contours for 185 days after start of construction (step = 187, amp = 185) (Continued)

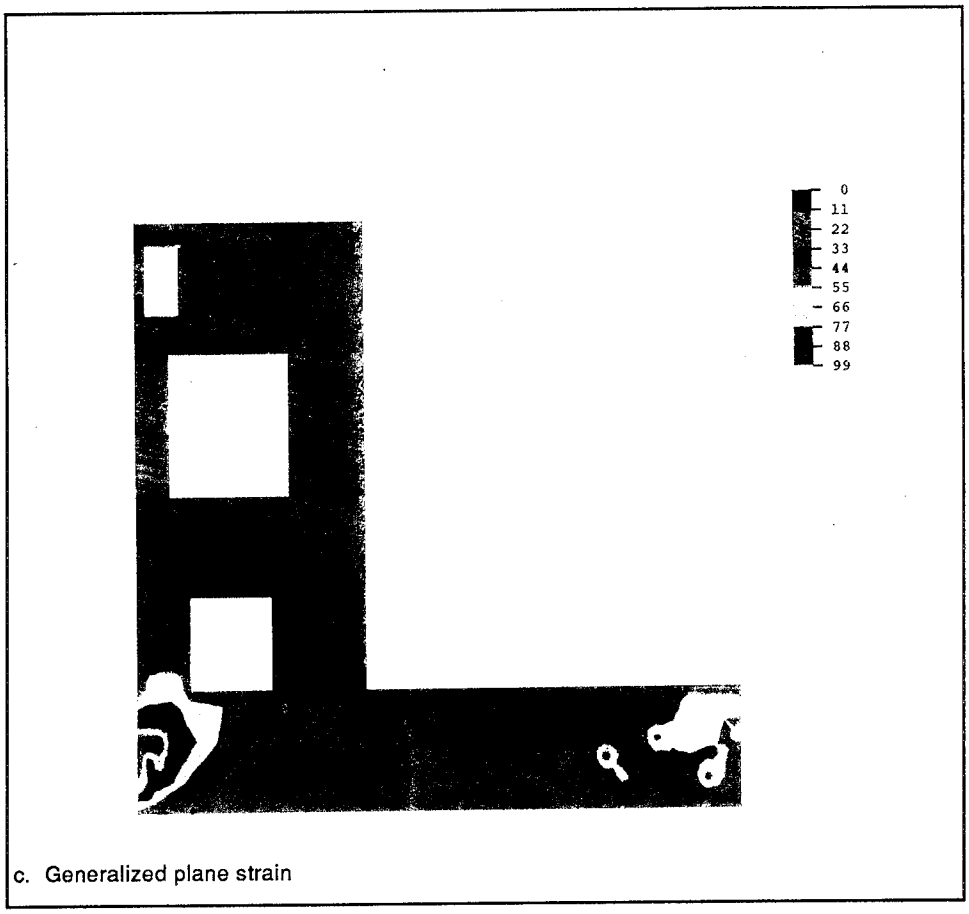

c. Generalized plane strain

Figure 47. (Concluded)

the cracking definitely relieves the maximum tensile stress. Stresses in nearby elements can be quite different while further removed elements' stresses will remain virtually unchanged. The high level of internal restraint or redundancy within a massive concrete structure accounts for the behavior remaining localized.

Figures 52 and 53 show the horizontal and vertical stress contours for 185 days after the start of construction. The respective contours are very similar with the exception of the contours near the center line of the chamber floor where the generalized plane strain analysis predicts cracking. The plane stress and plane strain analyses have predicted maximum horizontal stresses close to 300 psi in this region while the generalized plane strain is predicting stresses near zero (post cracking stresses). The plane stress and plane strain analyses are predicting nearly zero vertical stresses at the chamber floor center line, while the generalized plane strain analysis is predicting 100 to 200 psi in tension as a result of the cracking.

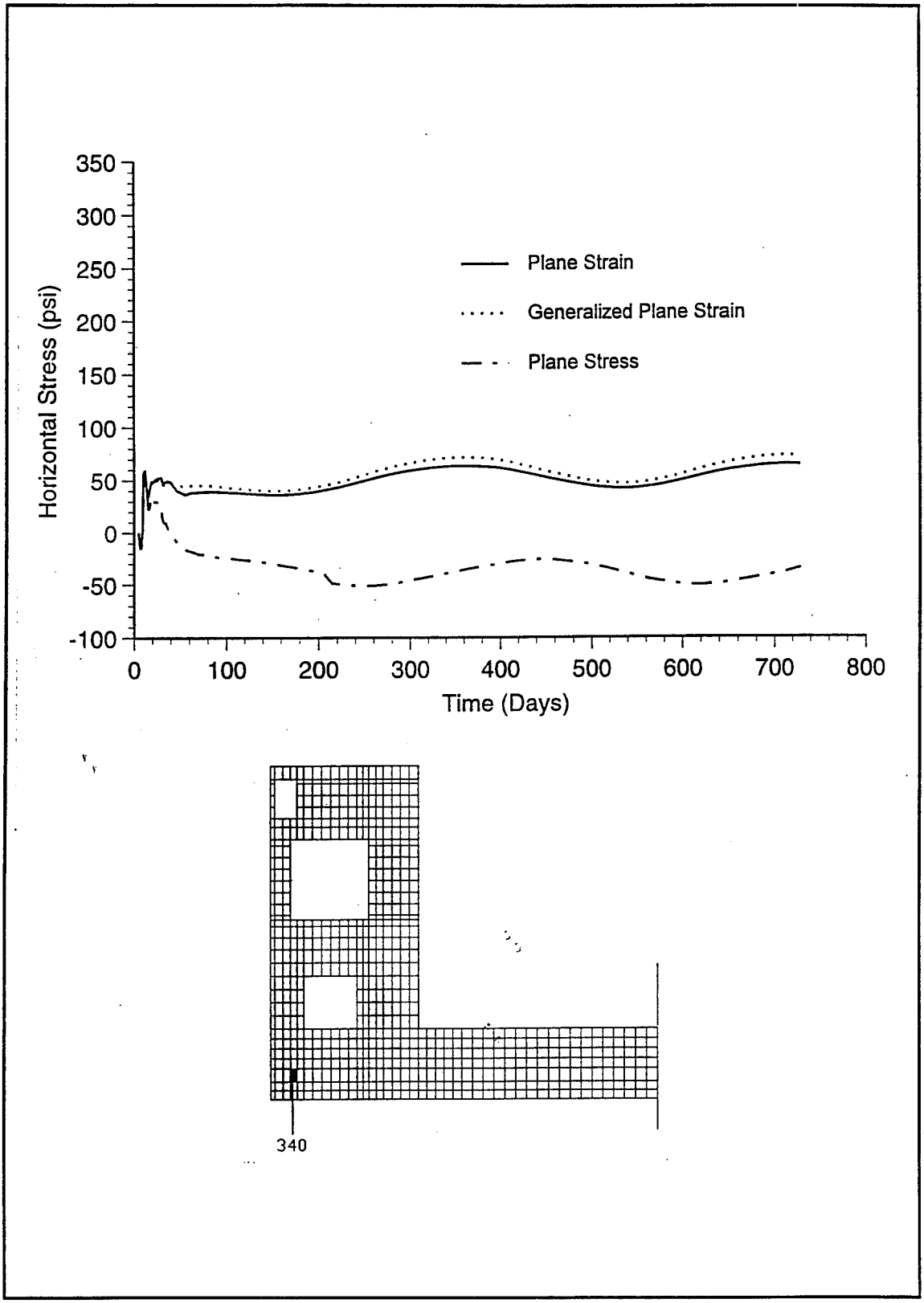

Figure 48. Horizontal stress time-history for element 340

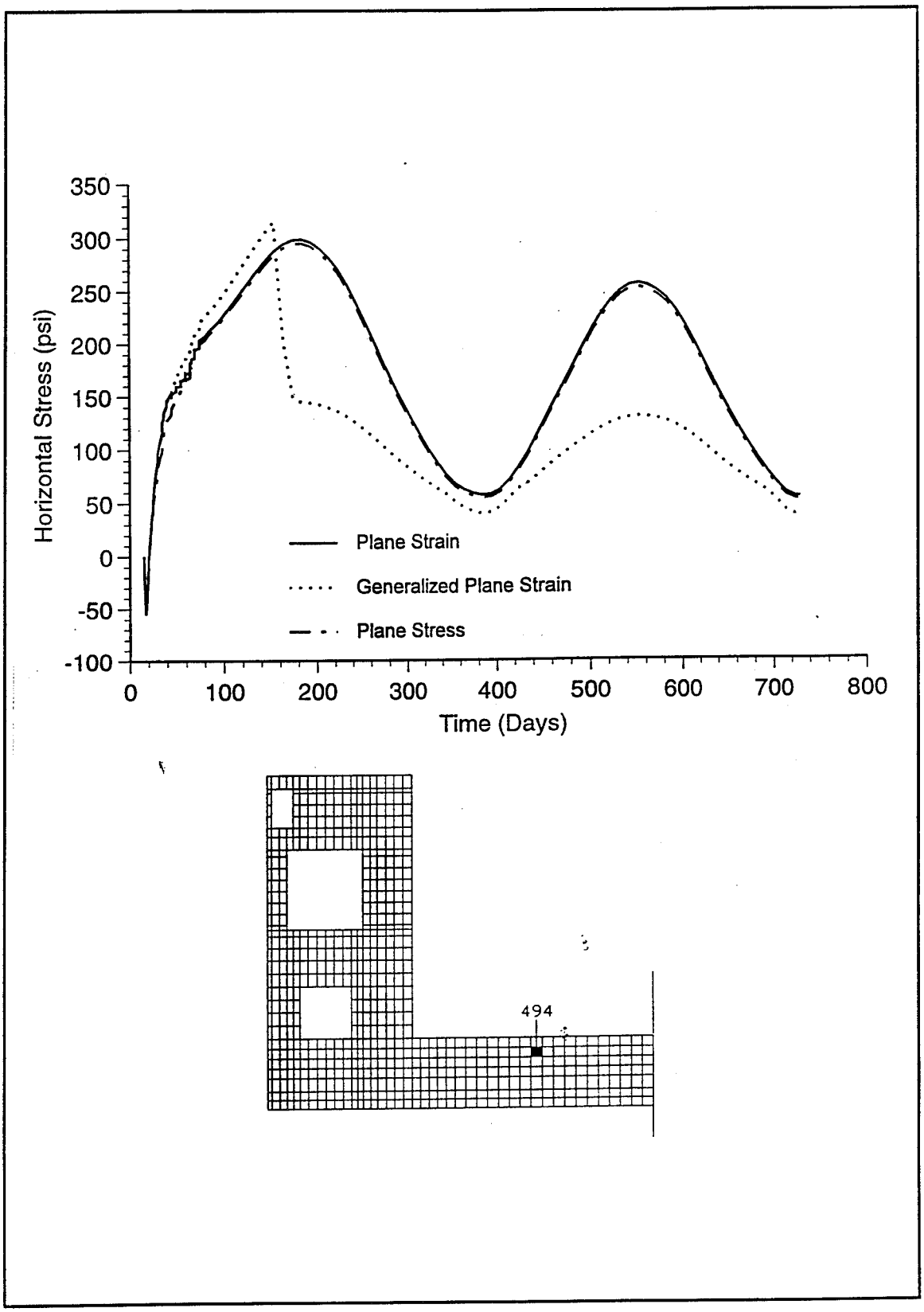

Figure 49. Horizontal stress time-history for element 494

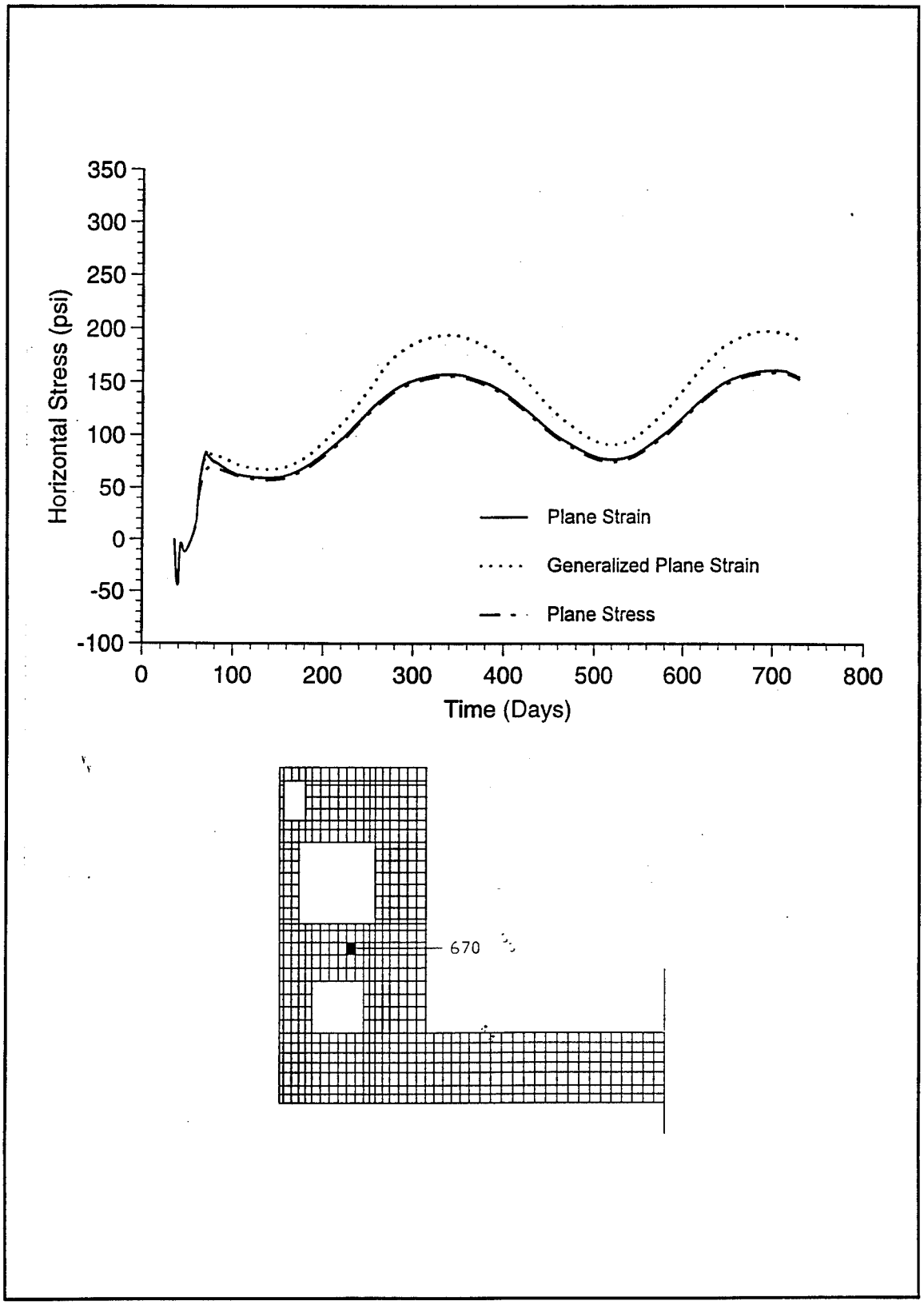

Figure 50. Horizontal stress time-history for element 670

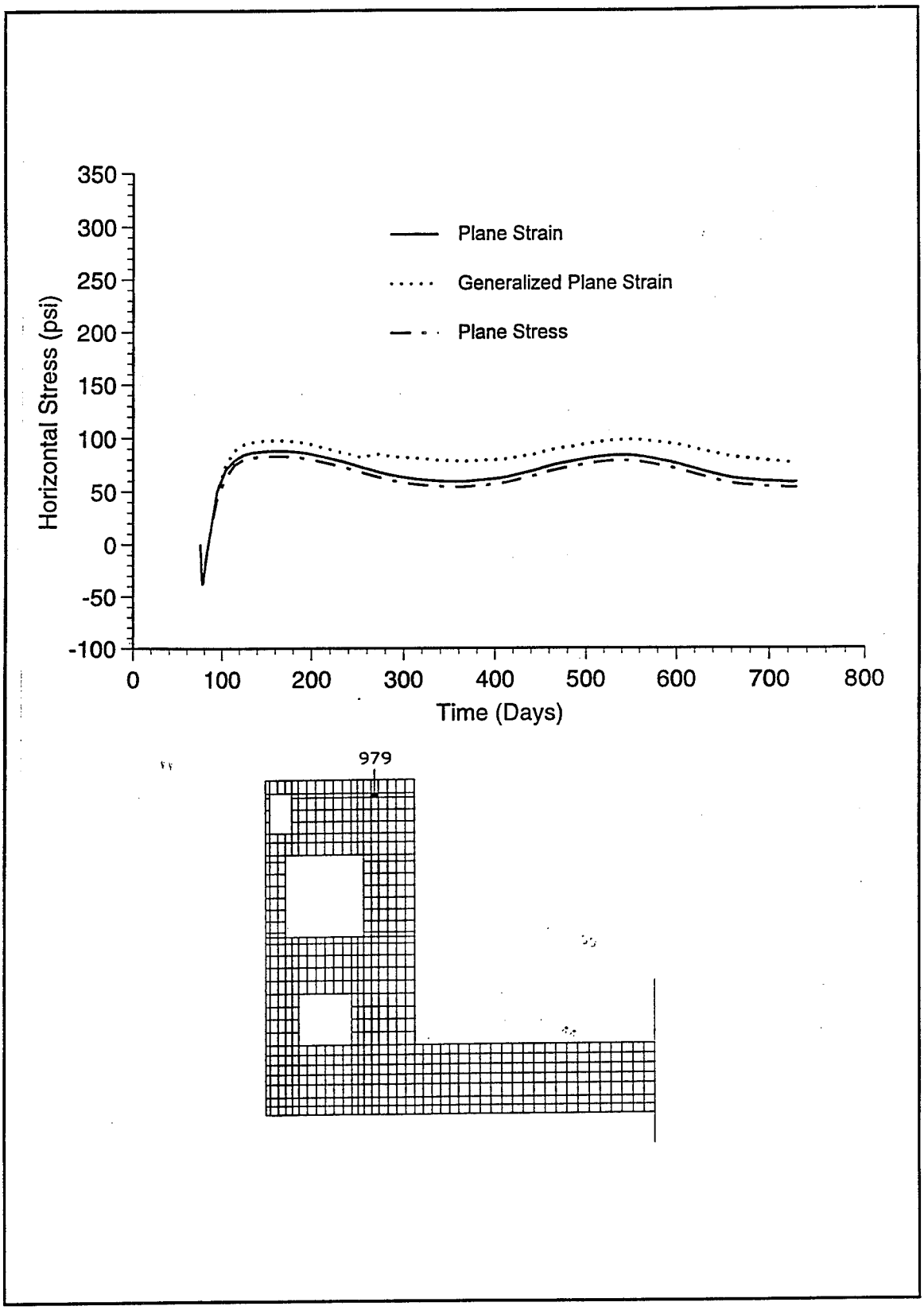

Figure 51. Horizontal stress time-history for element 979

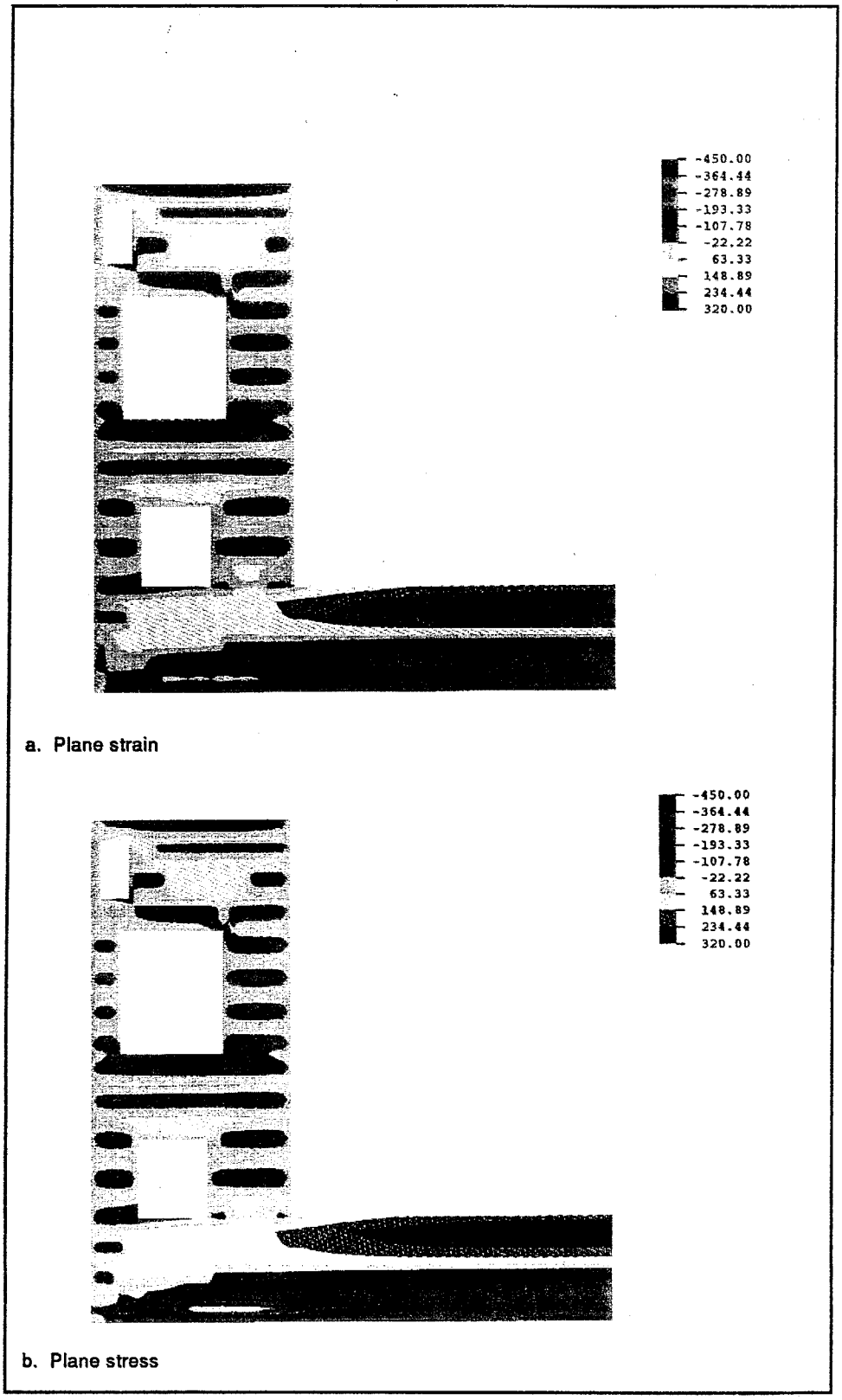

Figure 52. Horizontal stress contours for 185 days after start of construction (step = 187, amp = 185) (Continued)

c. Generalized plane strain

Figure 52. (Concluded)

Summary

Fortunately, all three models predicted cracks in common regions with additional cracked regions being indicated by the generalized plane strain model. These additionally predicted cracks in the generalized plane strain analysis results were also indicated as high-crack potential regions by the other two formulations. If the high-crack potential regions are considered significant, the three analyses would most likely lead to similar designs for the prevention of cracking.

The stress results from the three analyses were not significantly different with the exception of the localized regions where cracking was assumed to have occurred. In regions away from the cracked elements, the stresses were very consistent. In localized regions where cracking occurred, the relieving of tensile stress is very apparent. If the designer of such a structure were to control the cracking, the stress results in these regions would be very similar and any of the finite element analyses would appear to be appropriate.

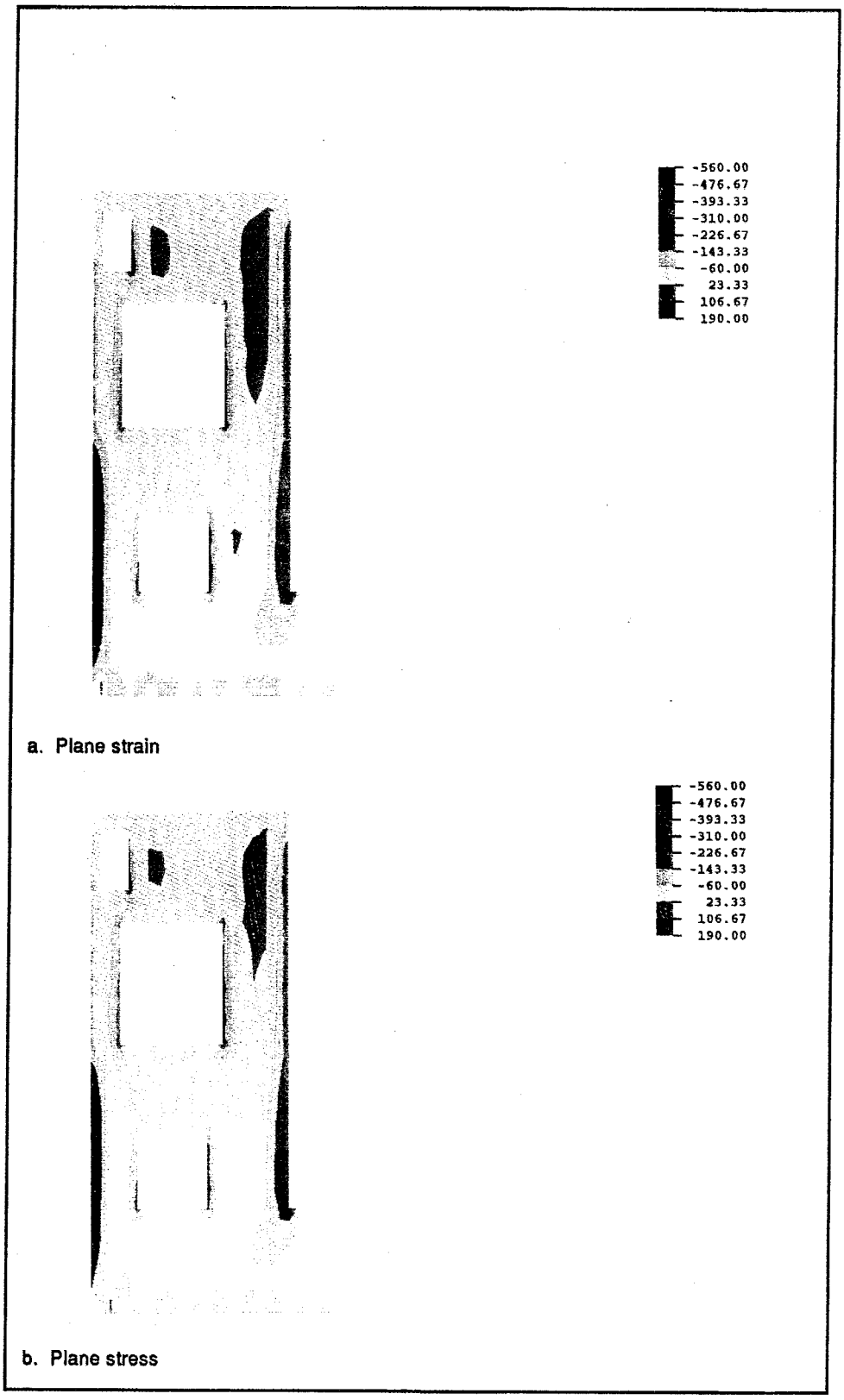

Figure 53. Vertical stress contours for 185 days after start of construction (step = 187, amp = 185) (Continued)

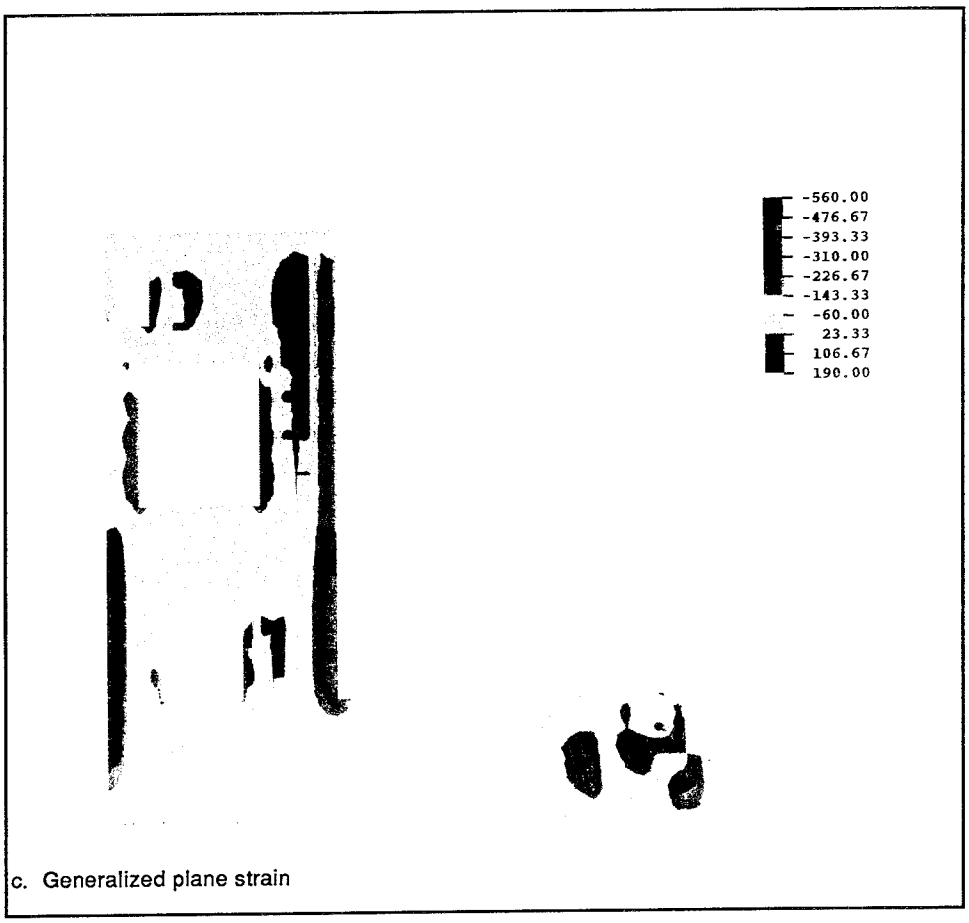

Figure 53. (Concluded)

The results from the stress and crack analyses for each finite element formulation are still inconclusive as to which is the "correct" formulation to use for massive concrete structures. In fact, as discussed in the introduction, different element formulations are most likely appropriate for different locations within a lock monolith such as the one analyzed from Melvin Price Locks. Full three-dimensional (3-D) crack and stress analyses must be performed and compared to the 2-D analyses in order to fully answer the question of which 2-D model should be used to provide the "best" results. Despite the uncertainities about which formulation should be used, based on the results presented, generalized plane strain will provide the most conservative approach.

5 Lift Intervals

Introduction

Due to the massive nature of structures such as locks and dams, construction of these structures requires building them in lifts as shown in the model description in Chapter 2. To ensure that an existing lift of concrete has sufficient strength prior to placement of the lift above it, most projects require that there be 5 days between the placement of lifts. This 5-day specification is a minimum; therefore, during actual construction, the time between placement of the lifts may be more than 5 days due to weather conditions or because placing concrete at another location at the project is on the critical path for completion. Typically when a NISA has been performed in the past, the 5-day minimum interval between lift placements has been used primarily because it was felt that it was the most conservative case. Since it was assumed that the heat of hydration was the primary source of thermal stresses, it was reasoned that the sooner the next lift is placed the more heat will be retained in the structure. This in turn would produce higher thermal stresses.

Using the 5-day minimum as specified is intuitively the worst condition for producing the highest temperatures, but the results of the stress analysis may not be as inherently obvious. Using a 5-day minimum interval does not consider the fact that a longer time interval between lift placements can create a worse stress condition. The existing lift would be stiffer if the interval is longer than 5 days and would thereby provide more restraint. Changes in the interval between lifts will also have an effect on the temperature gradient within a lift as well as the structure which also has an effect on stresses that result. The effects of using different intervals between lift placements will be evaluated in this portion of the parametric study for both temperature and stress analyses. Table 4 gives dates of lift placements for each lift.

A plane stress approach will be used in the study to compare analyses using 5, 10, and 15 days between lift placements. For this study, the time between placement of lifts will be the only parameter to be changed. As a result of leaving all other parameters constant, some conditions will be used in the 10- and 15-day analyses which will not occur in the field.

Table 4
Dates of Lift Placements

Lift No.	Lift Placement Dates		
	5 Days	10 Days	15 Days
1	Jul 1	Jul 1	Jul 1
2	Jul 6	Jul 11	Jul 16
3	Jul 11	Jul 21	Jul 31
4	Jul 16	Jul 31	Aug 15
5	Jul 21	Aug 10	Aug 30
6	Jul 26	Aug 20	Sep 14
7	Jul 31	Aug 30	Sep 29
8	Aug 5	Sep 4	Oct 14
9	Aug 10	Sep 14	Oct 29
10	Aug 15	Sep 24	Nov 13
11	Aug 20	Oct 4	Nov 28
12	Aug 25	Oct 14	Dec 13
13	Aug 30	Oct 24	Dec 28
14	Sep 4	Nov 3	Jan 12
15	Sep 9	Nov 13	Jan 27
16	Sep 14	Nov 23	Feb 11

First, as described in Chapter 2, when the ambient air temperature drops below the minimum placing temperature, then concrete is assumed to be placed at the current air temperature. All analyses used a placing temperature of 65 °F despite the fact that the 10- and 15-day interval analyses had lifts which were placed when ambient temperatures were below 65 °F. Second, for analyses which extend into the winter months for a location such as Alton, IL, insulation should be included in the analysis. As can be seen in Table 4, both the 10- and 15-day analyses extend into the winter months, but for these analyses no insulation was included. While neglecting realistic conditions is undesirable as stated in Chapter 3, in some cases such as this study, it sometimes becomes necessary so that the impact of the one parameter can be fully understood.

The evaluation of the parametric study will begin with examining the temperature results. The effects on the temperatures will be presented using time-history plots of temperature at select nodes and by comparing

temperature contours from the three analyses at given times. The results of the stress analyses will then be explored. Contours of cracking potentials and horizontal and vertical stresses will then be compared at various times throughout the analyses. Again, time histories of stress at various points in the structure will be shown.

The primary purpose of the study is to evaluate the effect of changing the time between lift placements. Since evaluating this parameter is the primary objective, most of the discussion will center on the differences between the various analyses. Some discussion will touch on the general monolith behavior but most of the discussion will highlight the differences from one analysis to the next and why the differences exist.

All of the parameters used in this portion of the analyses are described in Chapter 2 for the heat transfer and stress analyses.

Heat Transfer Analyses

Time-history plots

Initial comparisons for the heat transfer analyses are shown in Figures 54 through 61 where temperatures from the three analyses are compared at various nodes in the structure. A quick review of the nodes presented shows that by day 300 of the analyses very little if any difference exists in nodal temperatures between the three analyses. Another item of note is that once a lift has been in place approximately 100 days for the case using 15-day intervals, the temperatures in the lift are nearly equal to temperatures for the other two cases using 5- and 10-day intervals.

Initially there are differences in the temperature increases and decreases at each node which can be attributed in most of the cases to the lifts being placed at different times. This becomes very pronounced at nodes located at the top of the wall, such as nodes 2812 (Figure 59), 3670 (Figure 60) and 3826 (Figure 61). These differences are less notable for nodes located near surfaces such as nodes 2101 (Figure 56) and 2539 (Figure 57), where the temperatures follow the ambient air temperature and the initial behavior of the three different analyses is nearly identical. This behavior does not coincide because the times of year the lifts are placed are different. Some of the difference occurring between the three cases can also be attributed to the fact that the 10- and 15-day cases allow a lift to dissipate more heat prior to the placement of the next lift. This effect can be seen in Figure 54 for node 1166 which is located in the first lift. Because it is in the first lift, all three cases start at the same time. As can be seen in the plot, the temperature drops off considerably in the early times for the 10- and 15-day case when compared to the 5-day case.

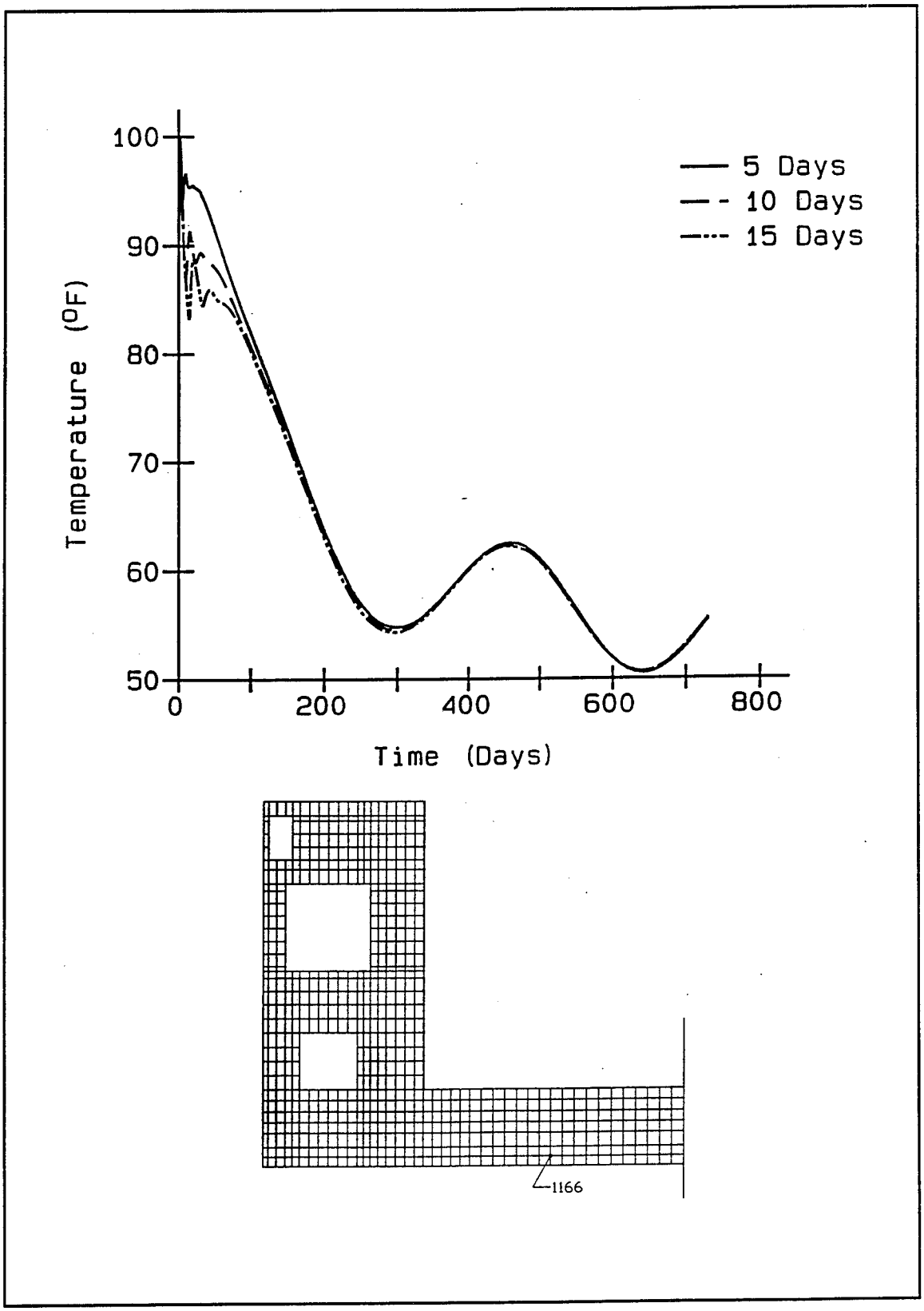

Figure 54. Temperature time-histories at node 1166

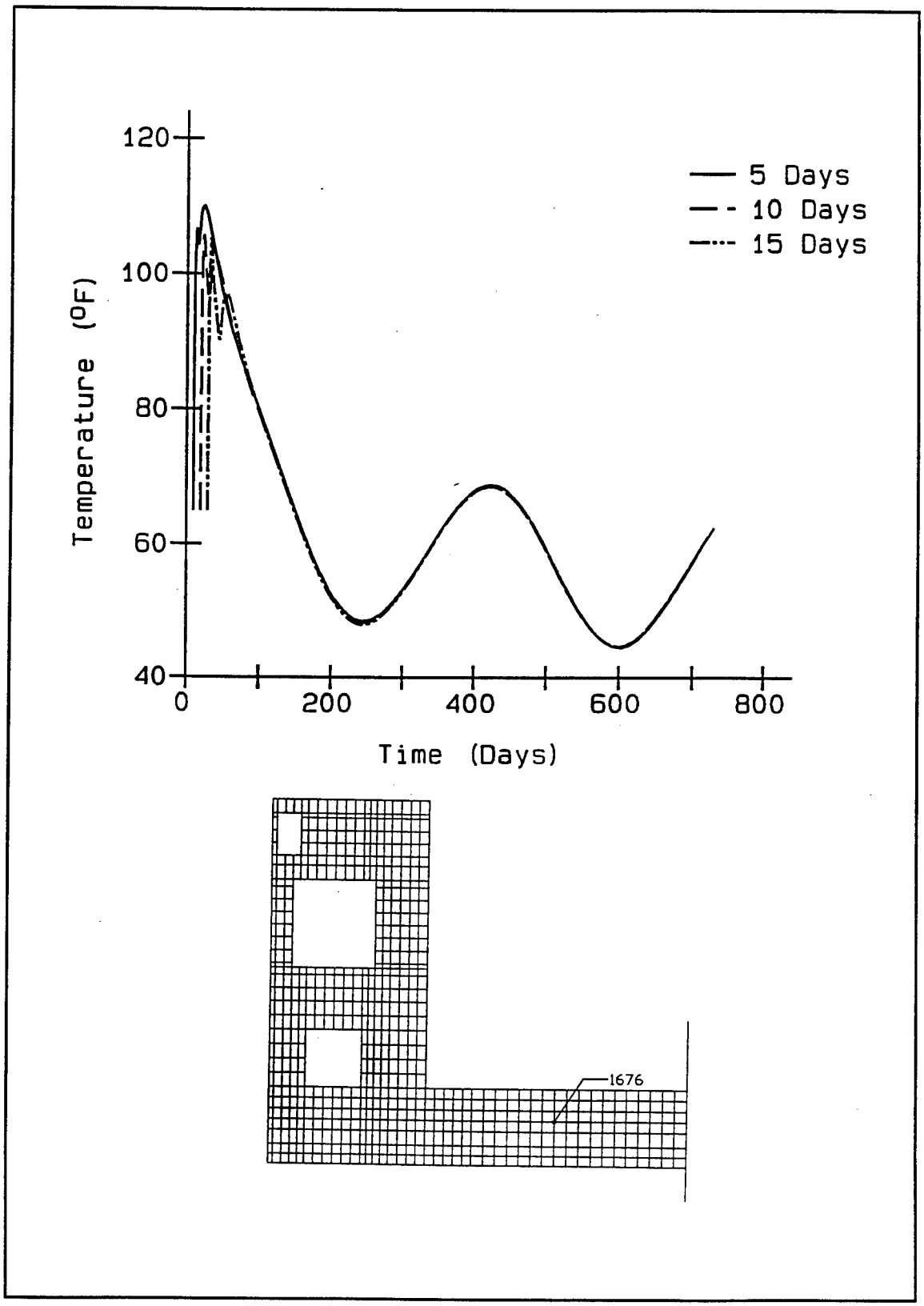

Figure 55. Temperature time-histories at node 1676

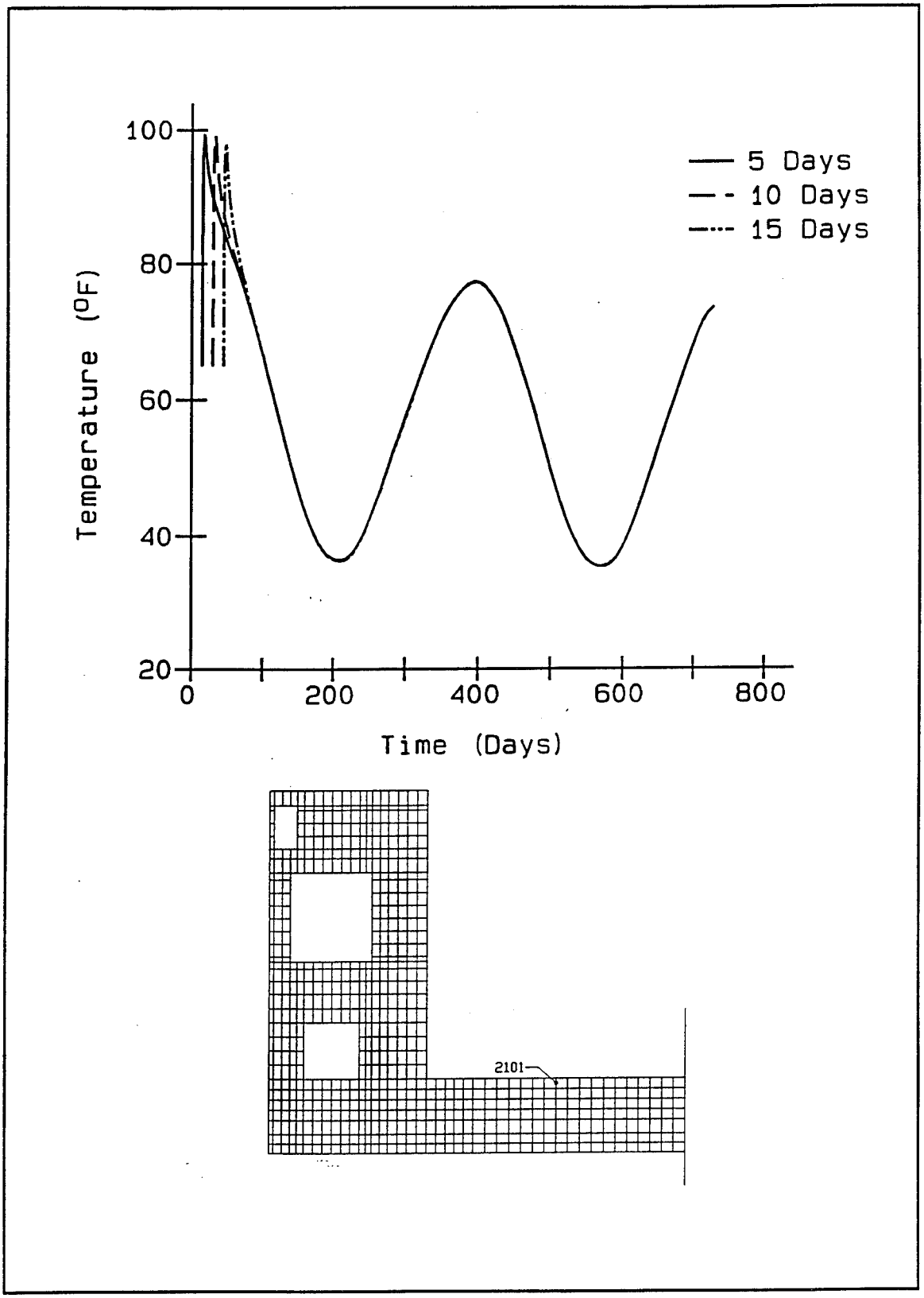

Figure 56. Temperature time-histories at node 2101

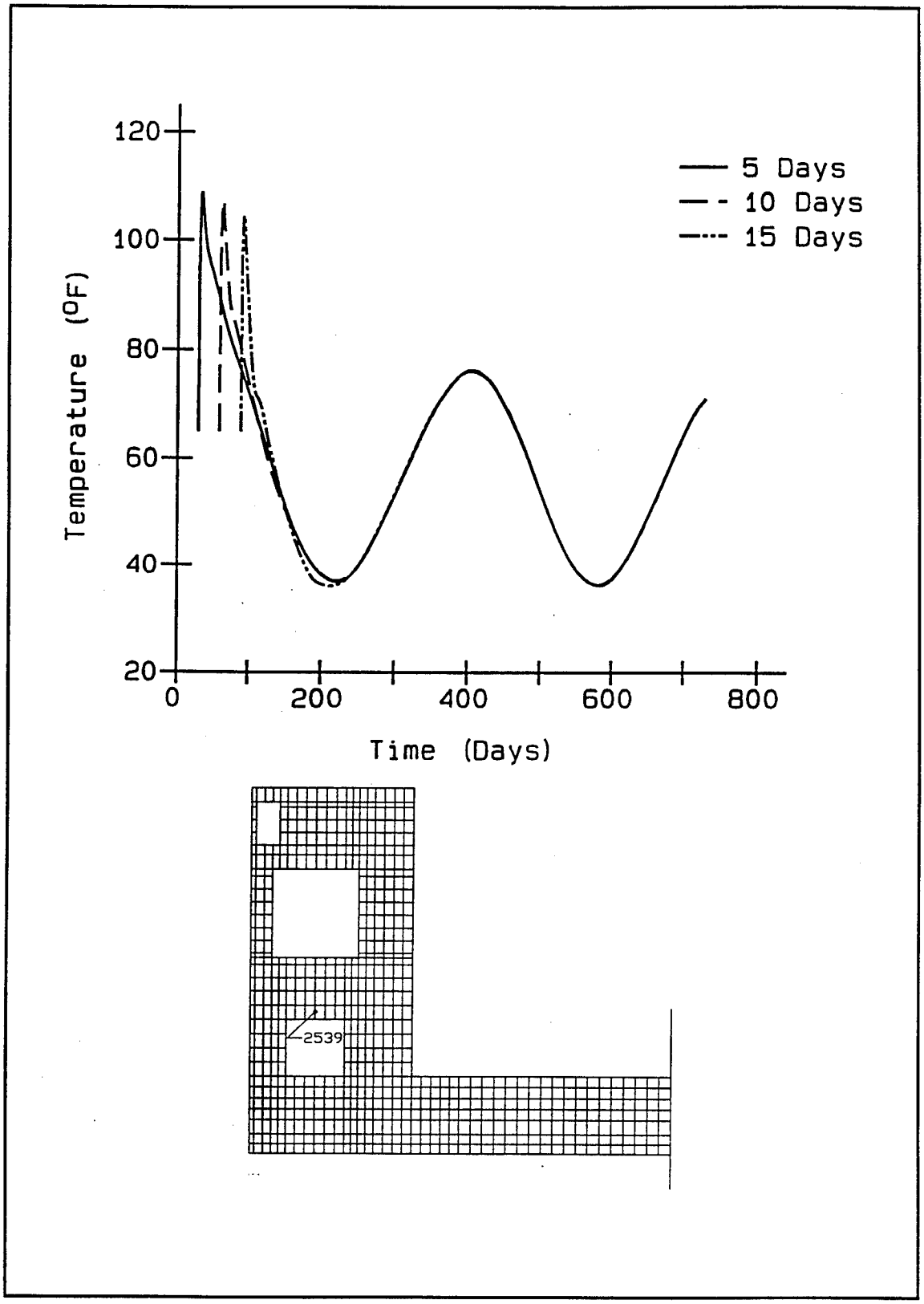

Figure 57. Temperature time-histories at node 2539

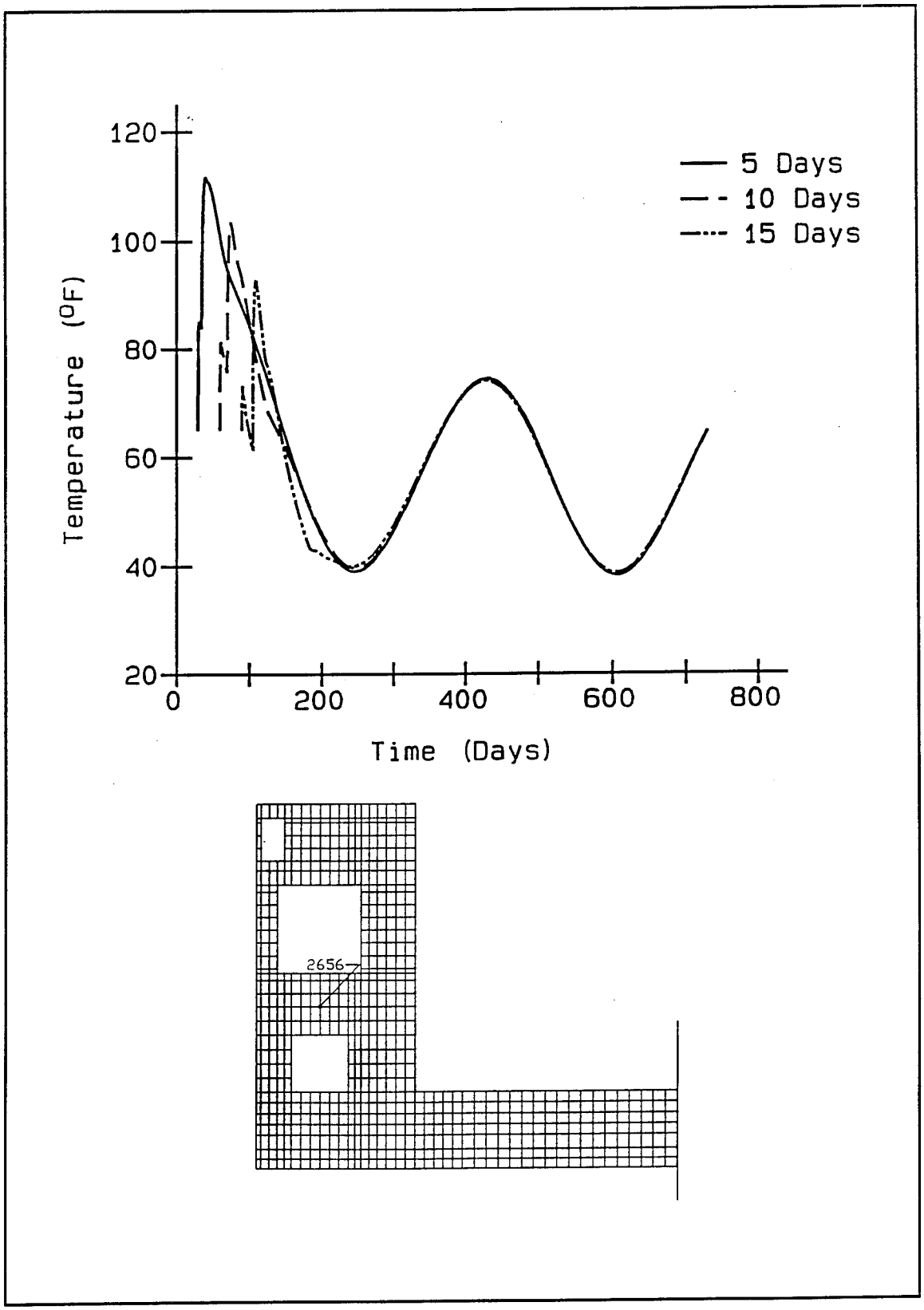

Figure 58. Temperature time-histories at node 2656

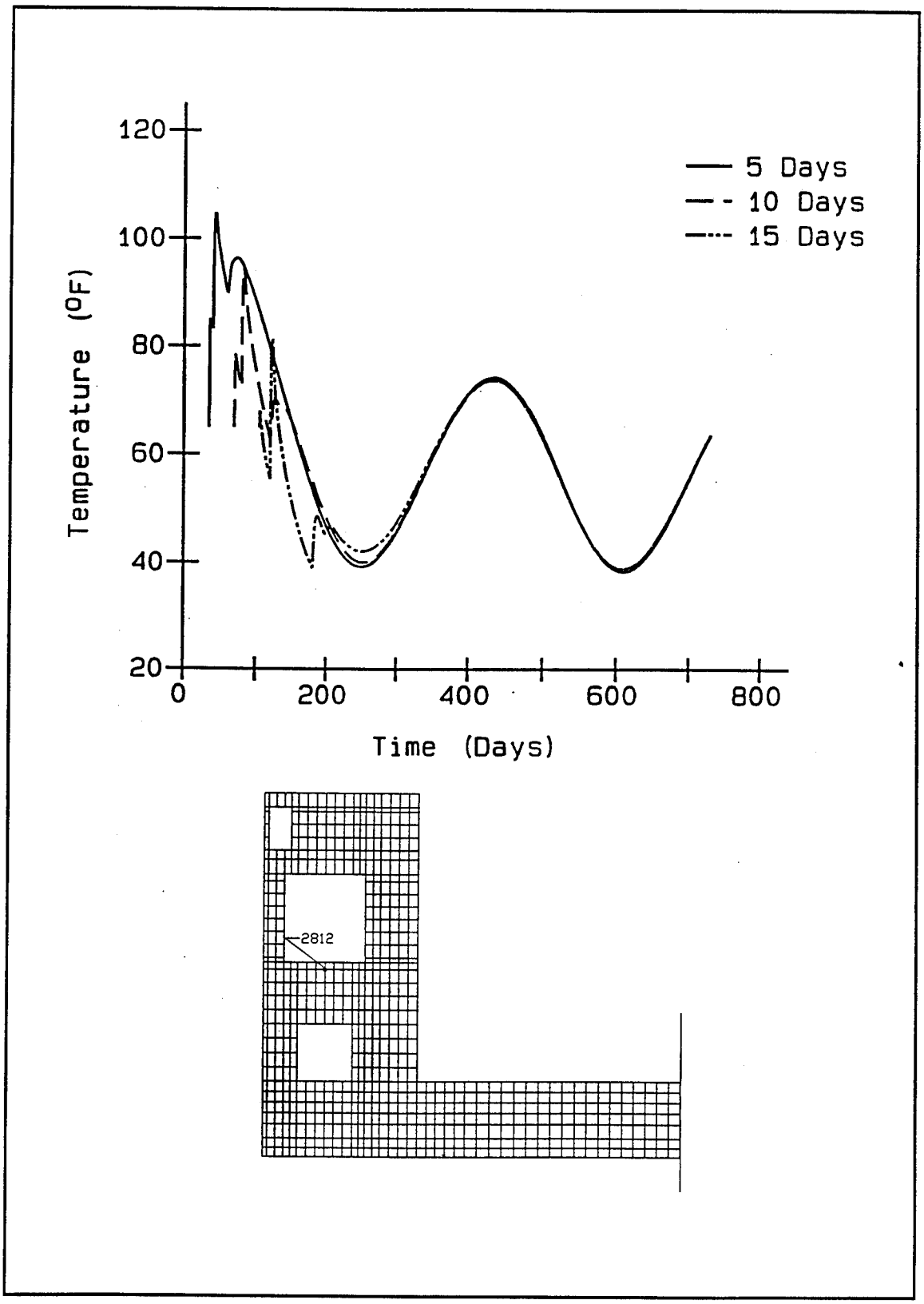

Figure 59. Temperature time-histories at node 2812

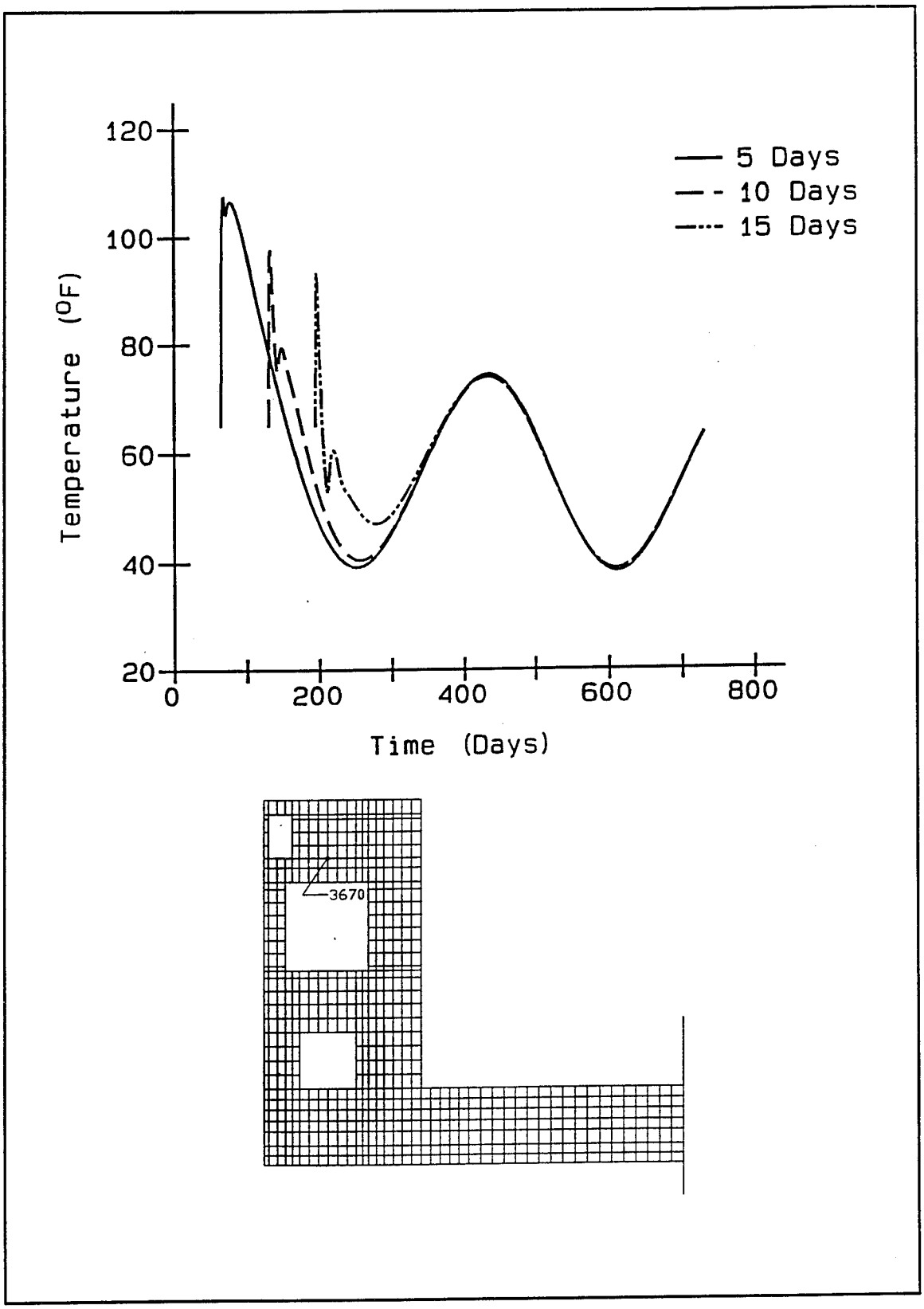

Figure 60. Temperature time-histories at node 3670

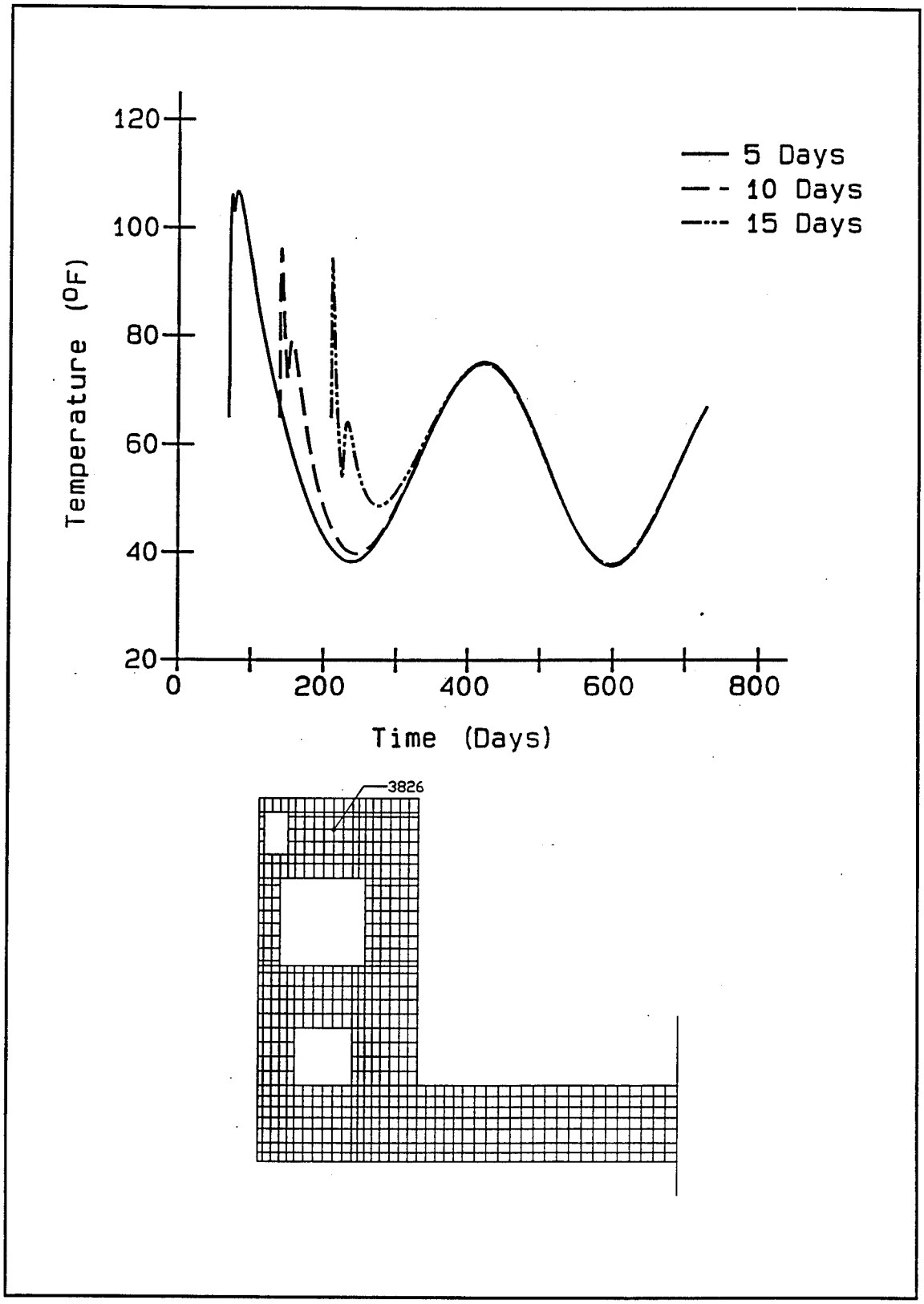

Figure 61. Temperature time-histories at node 3826

Figures 62 through 64 are time-histories of nodes through the thickness of the slab. Each figure represents a different analysis. Figure 56 is for 5-day intervals, Figure 57 is for 10-day intervals, and Figure 64 is for 15-day intervals. As in comparisons shown at individual nodes, if the three figures are compared, it can be seen that there is initial variation between the plots, but by day 100 all three plots are almost identical.

Temperature contours

Figures 65 through 68 are temperature contours taken at various times during the analyses. Figure 65 presents the results at day 180 of the analyses and, as might be expected from looking at the time-history plots, the contours in the base of the monolith are almost identical. Differences do exist in the top of the monolith due to later placement of the lifts in the second and third analyses. For the 10-day analysis (Figure 65b), heat that was generated above the void of the monolith has not completely dissipated, and for the 15-day analysis (Figure 65c), the top three lifts have not yet been placed. Comparison of the results of the three analyses in Figures 66 (at day 360), 67 (at day 540), and 68 (at day 720) shows virtually no difference from one contour to the next. Again, this agrees with the data reported in the time-history plots.

Finally, if the plots shown in Figure 66 are compared to the plots shown in Figure 68, the two sets of plots are nearly identical. These figures are showing temperatures for the monolith at approximately the same time of the year with Figure 66 showing results 1 year after the start of construction and Figure 68 showing results 2 years after the start of construction. Some of the differences in the contours can be attributed to the fact that the scales for the two sets of plots are slightly different.

Stress Analyses

Cracking potential contours

Initial comparisons between the three analyses are shown in Figures 69 through 72 which are contour plots of the cracking potential. Figure 69 shows plots taken 180 days after the start of construction. Similarities between analyses are evident particularly in the base of the monolith where the shapes of the contours are similar and the maximum values are located in the same area of the slab, which is near the symmetry boundary. Cracking potentials are low for all three analyses in the wall portion of the monolith. The major difference in the three analyses at day 180 is that the potentials for the 10- and 15-day interval analyses are approximately 50 to 75 percent higher than the potentials for the 5-day interval analysis.

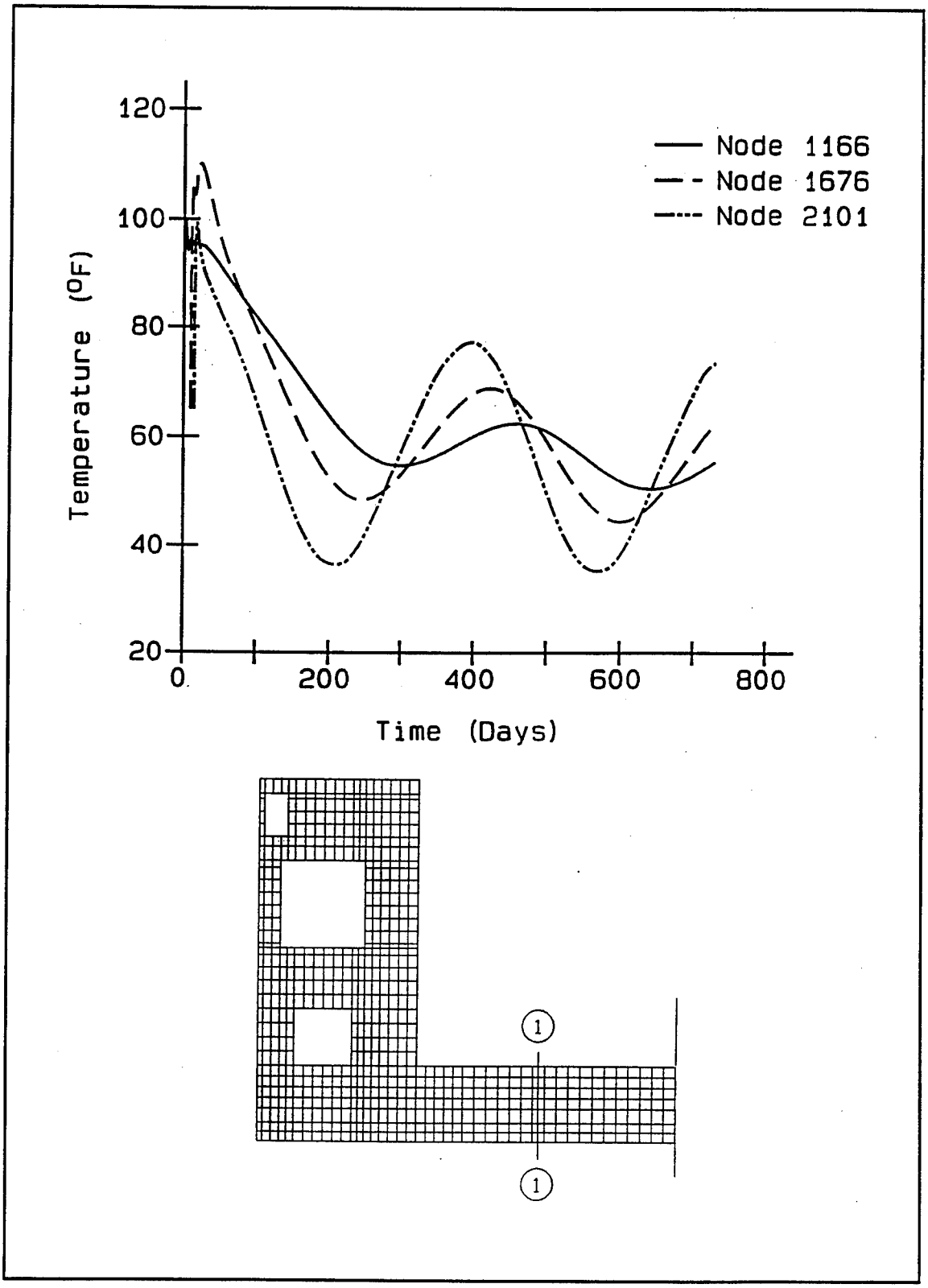

Figure 62. Temperature time-histories at section 1 through slab for 5-day interval analysis

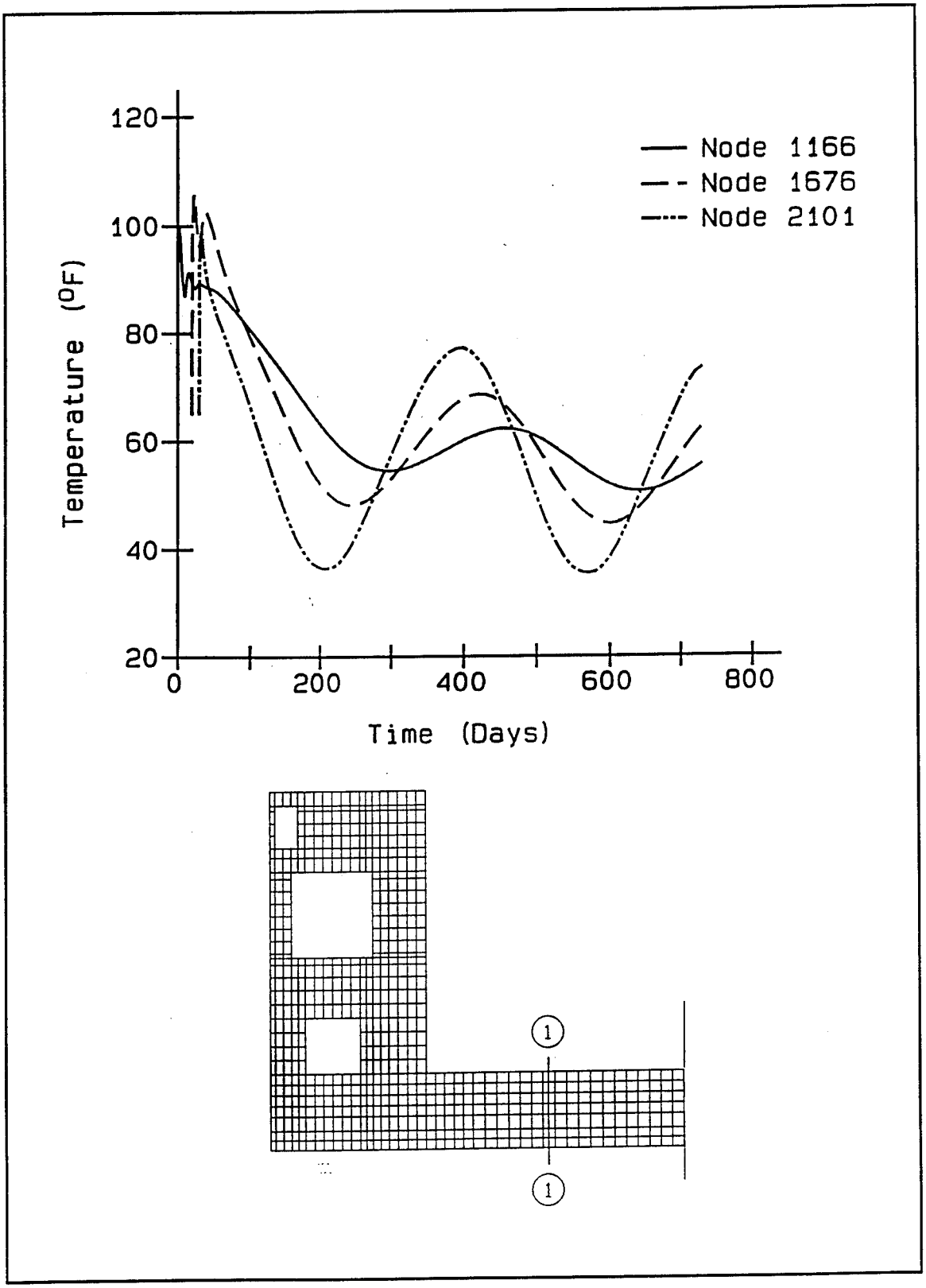

Figure 63. Temperature time-histories at section 1 through slab for 10-day interval analysis

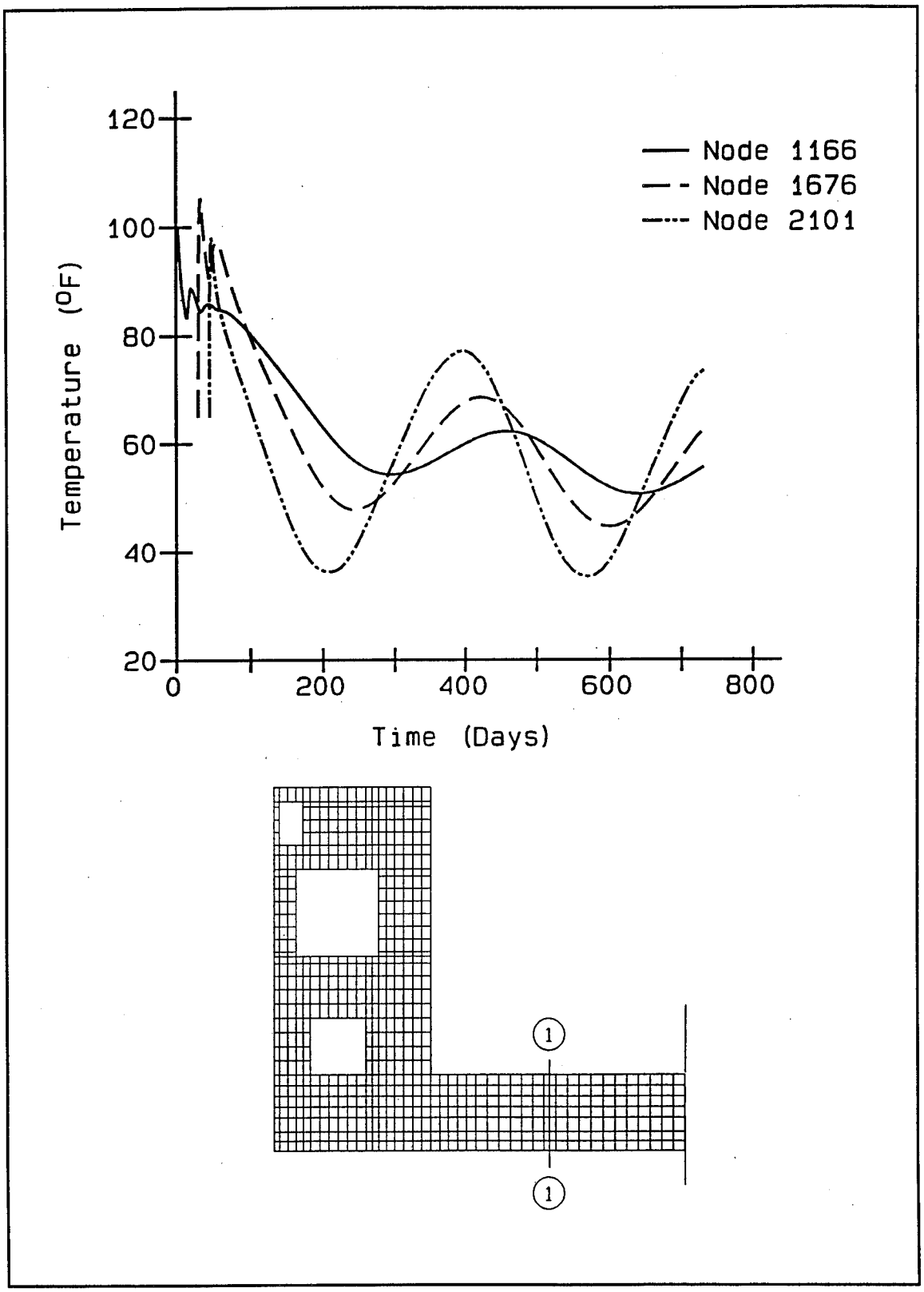

Figure 64. Temperature time-histories at section 1 through slab for 15-day interval analysis

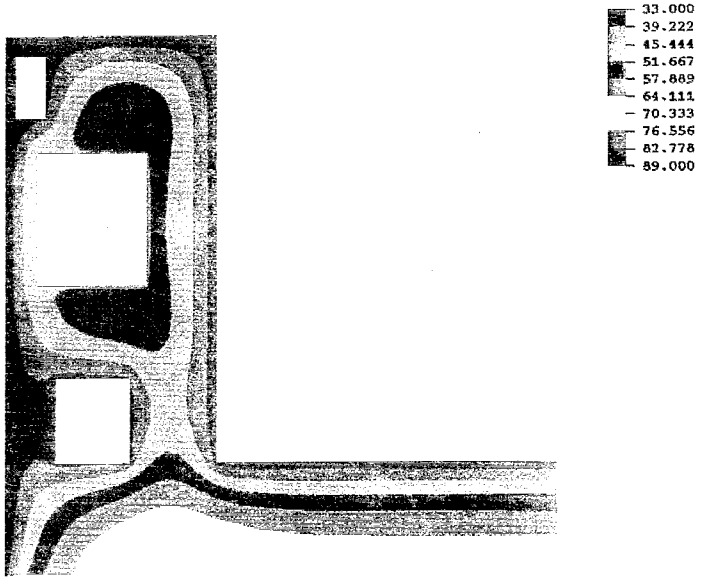

a. 5-day intervals (step = 181, amp = 180)

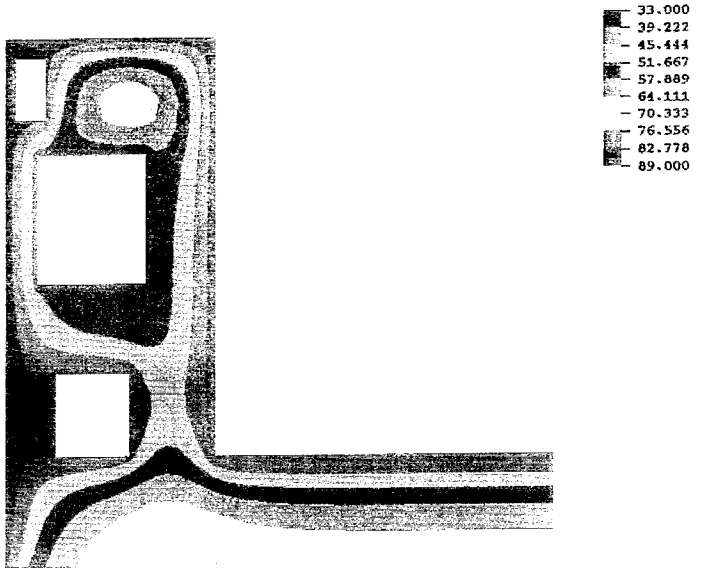

b. 10-day intervals (step = 325, amp = 180)

Figure 65. Temperature contours at 180 days after start of construction (Continued)

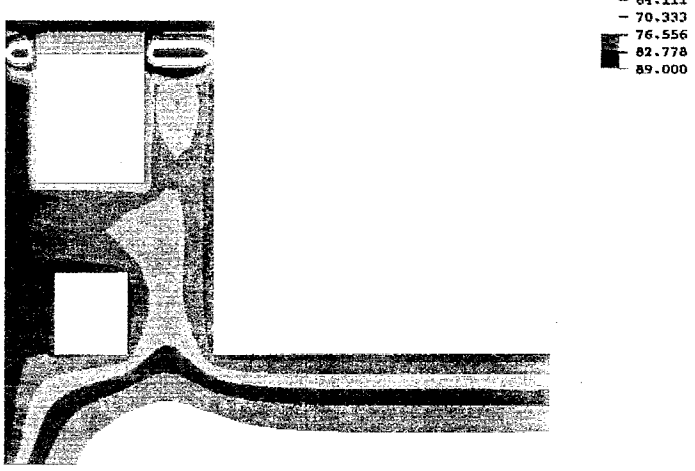

c. 15-day intervals (step = 241, amp = 180)

Figure 65. (Concluded)

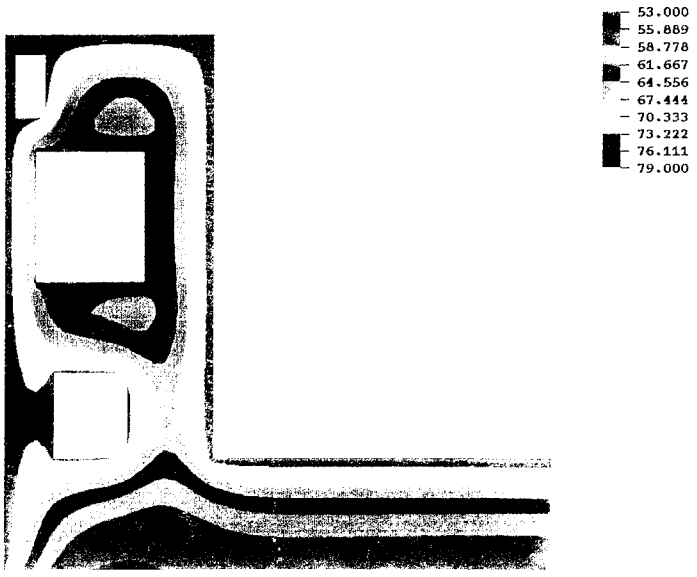

a. 5-day intervals (step = 217, amp = 360)

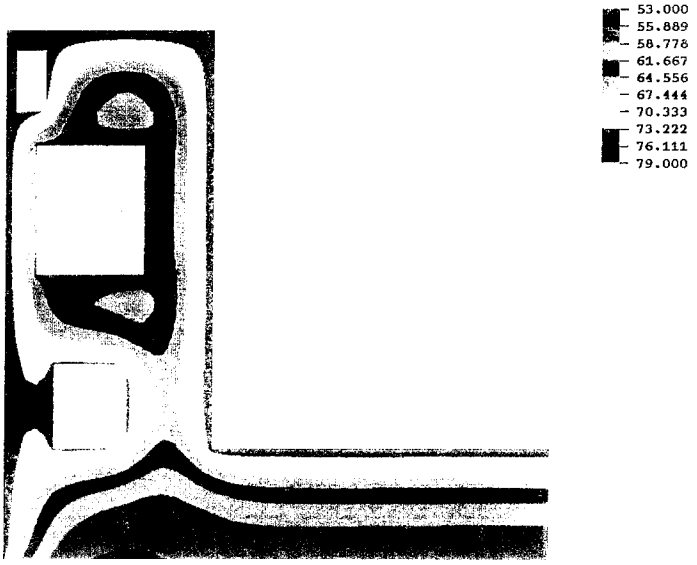

b. 10-day intervals (step = 355, amp = 360)

Figure 66. Temperature contours at 360 days after start of construction (Continued)

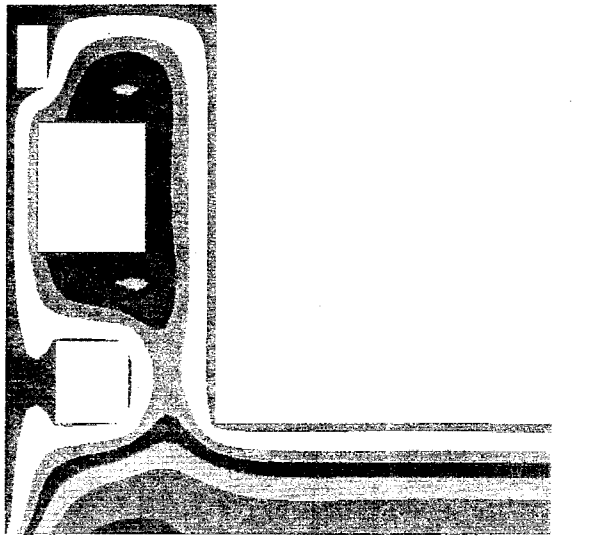

c. 15-day intervals (step = 339, amp = 360)

Figure 66. (Concluded)

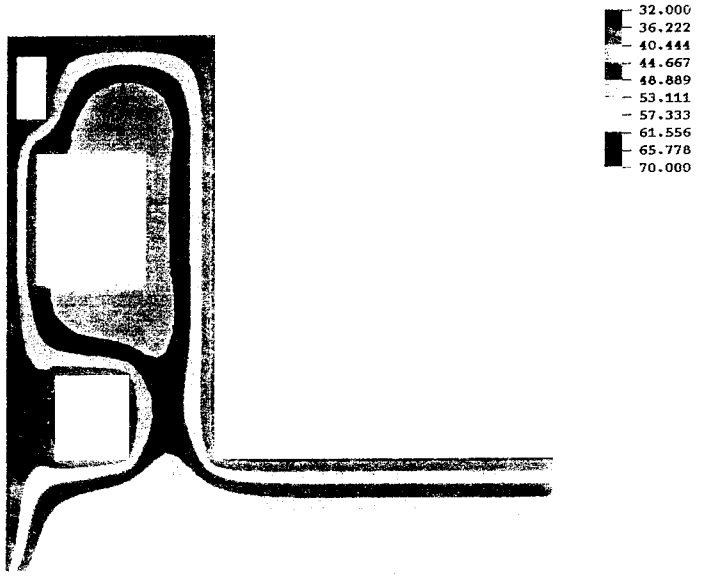

a. 5-day intervals (step = 253, amp = 540)

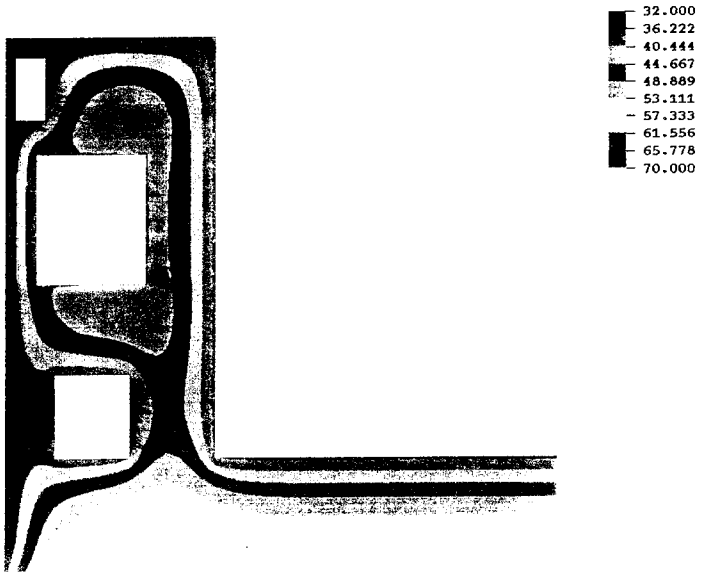

b. 10-day intervals (step = 373, amp = 540)

Figure 67. Temperature contours at 540 days after start of construction (Continued)

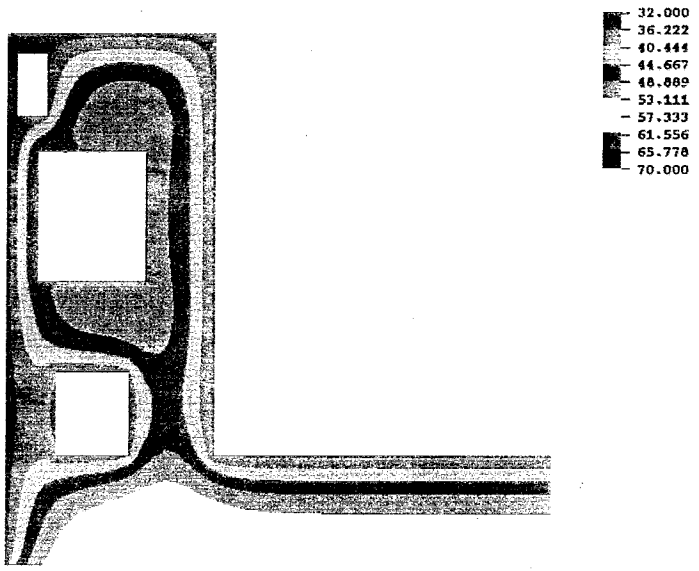

c. 15-day intervals (step = 357, amp = 540)

Figure 67. (Concluded)

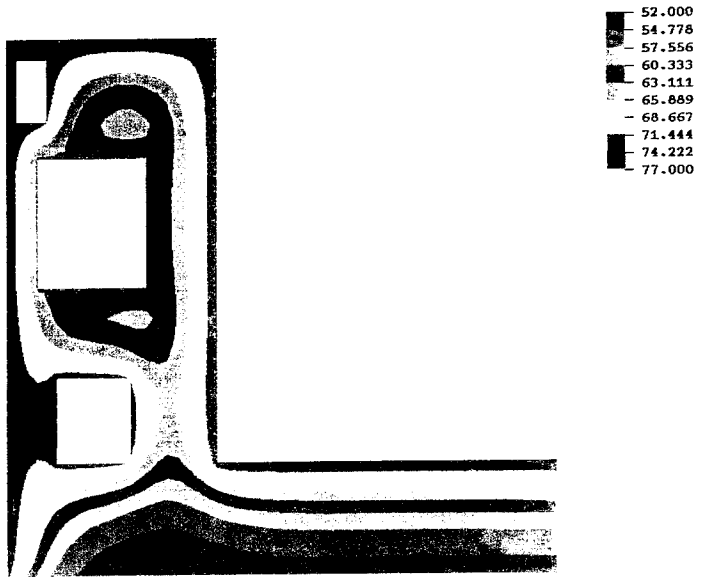

a. 5-day intervals (step = 289, amp = 720)

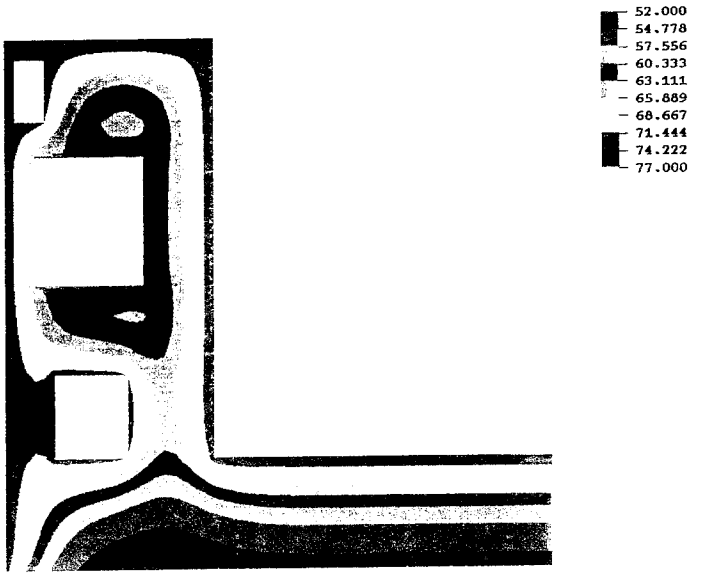

b. 10-day intervals (step = 391, amp = 720)

Figure 68. Temperature contours at 720 days after start of construction (Continued)

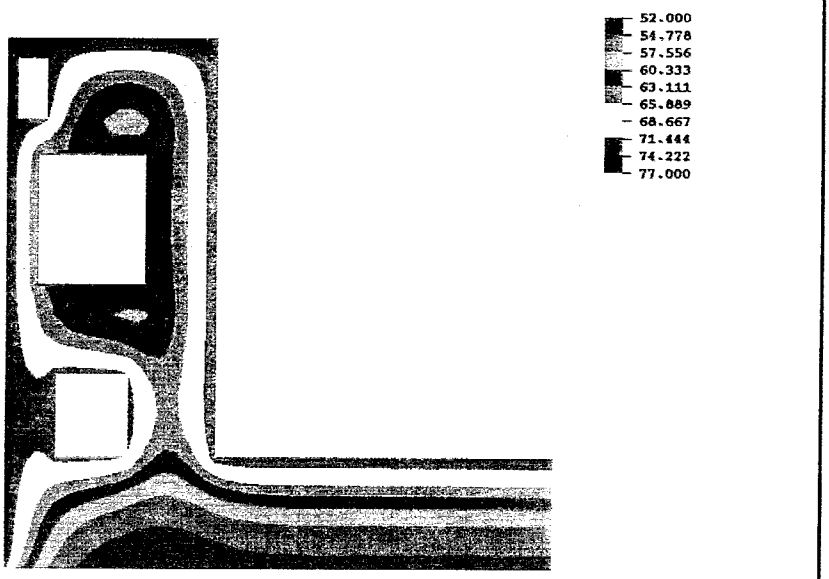

c. 15-day intervals (step = 375, amp = 720)

Figure 68. (Concluded)

a. 5-day intervals (step = 187, amp = 185)

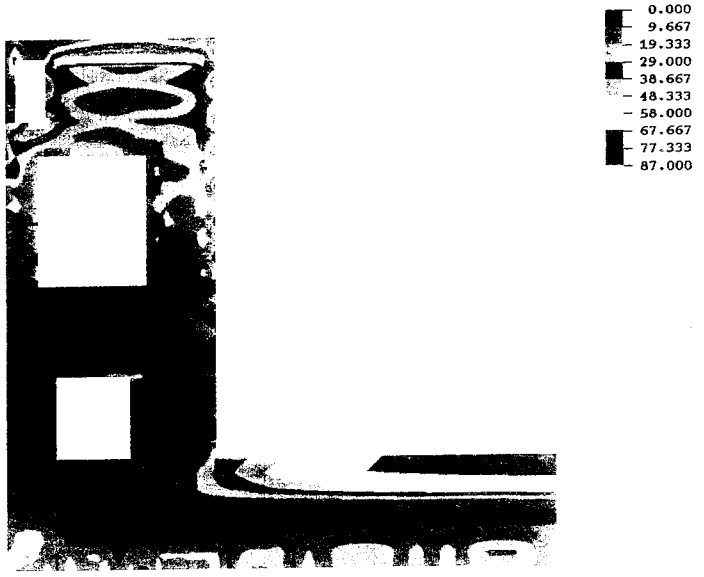

b. 10-day intervals (step = 339, amp = 185)

Figure 69. Cracking potential contours at 180 days after start of construction (Continued)

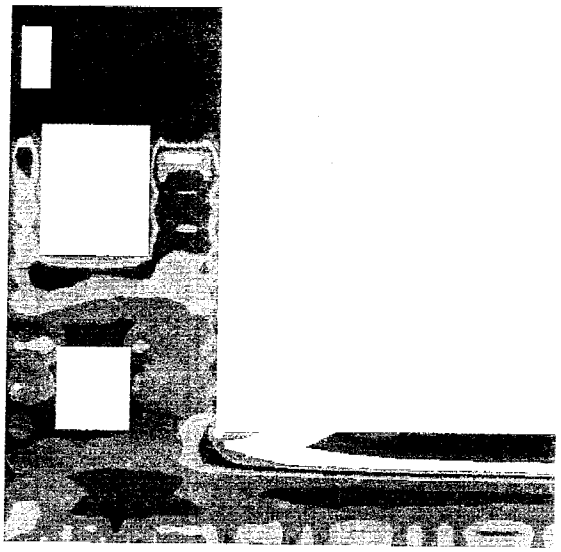

c. 15-day intervals (step = 156, amp = 180)

Figure 69. (Concluded)

a. 5-day intervals (step = 205, amp = 365)

b. 10-day intervals (step = 354, amp = 360)

Figure 70. Cracking potential contours at 360 days after start of construction (Continued)

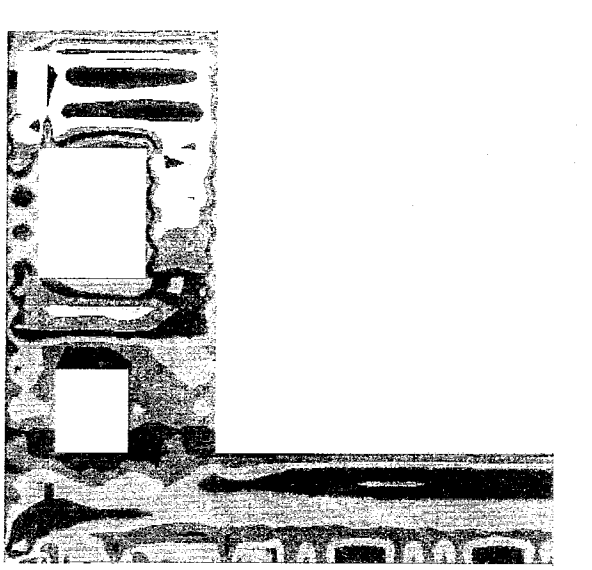

c. 15-day intervals (step = 218, amp = 360)

Figure 70. (Concluded)

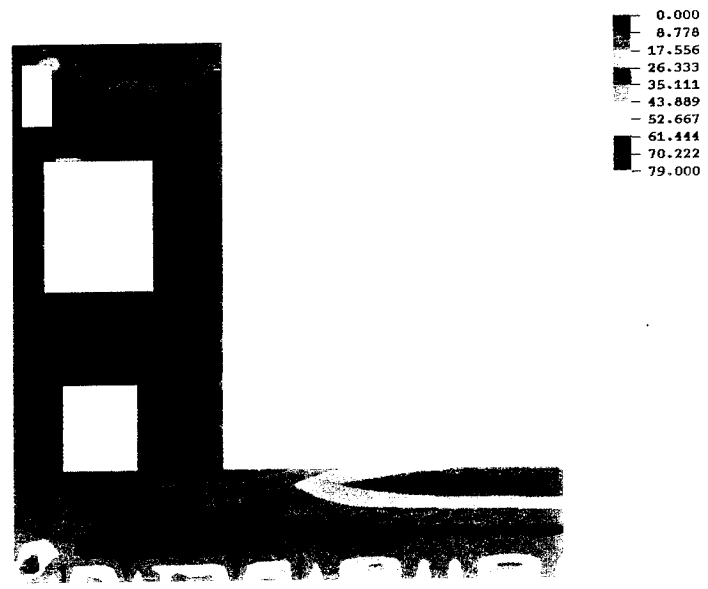

a. 5-day intervals (step = 223, amp = 545)

b. 10-day intervals (step = 363, amp = 540)

Figure 71. Cracking potential contours at 540 days after start of construction (Continued)

c. 15-day intervals (step = 227, amp = 540)

Figure 71. (Concluded)

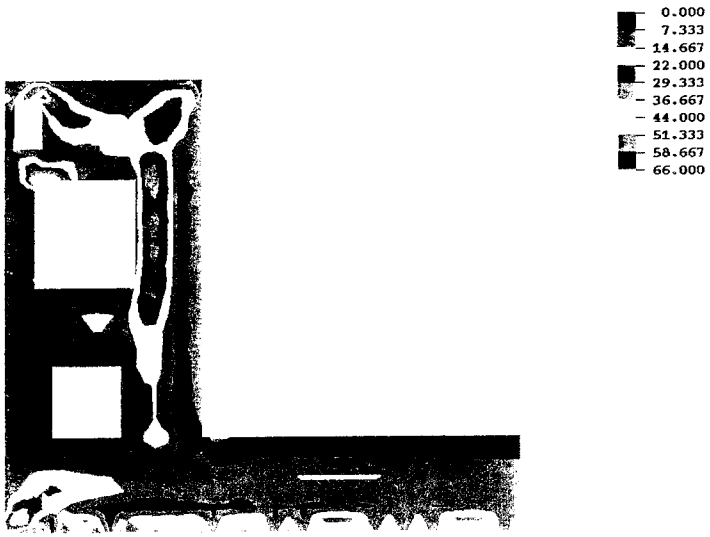

a. 5-day intervals (step = 241, amp = 725)

b. 10-day intervals (step = 372, amp = 720)

Figure 72. Cracking potential contours at 720 days after start of construction (Continued)

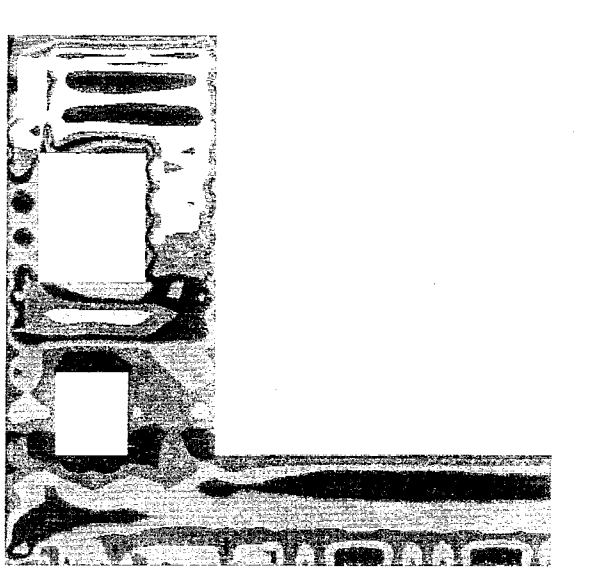

c. 15-day intervals (step = 236, amp = 720)

Figure 72. (Concluded)

Figure 70 presents the potentials at day 360 of the analysis. The potentials in the slab are low for all three analyses which should be expected since day 360 is near the middle of summer. It has been documented (Garner et al. 1992) that slabs are sensitive to ambient conditions and that cold temperatures applied to the top of the slab provide the worst conditions. In general, the cracking potentials are not particularly high at any location in the monolith with the maximum potential being 66 percent for the 15-day interval analysis. It should also be noted that the maximum potential for the 10- and 15-day interval analyses occurs near the base of lift 15, but for the 5-day interval analysis, the maximum occurs near the top of the gallery. Larger gradients also appear to occur for the 10- and 15-day analyses than for the 5-day analysis.

By day 540 (Figure 71), the cracking potentials for the 5-day analysis are very low (less than 35 percent). Comparing between the three different analyses, the general shape of the contours is the same for all three analyses for the slab portion of the monolith, but some differences do exist in contours in the wall of the monolith when the 5-day analysis is compared to the 10- and 15-day analyses. Another notable difference is that the maximum potential for the 10-day analysis occurs in the base of

the monolith while the maximum potential for the 15 day analysis occurs at the top of lift 15, near the top of the wall. For all three analyses if the plots at day 540 are compared to the plots at day 180 (Figure 69), the potentials are all lower 1 year later.

The last set of cracking potentials are shown in Figure 72 for day 720. If the plots in Figure 72 are compared to the plots in Figure 70 (day 360), the resulting contours are nearly identical. Therefore, the discussions for Figure 70 should also apply to Figure 72.

Stress contours

Contours of stress in the horizontal direction are presented in Figures 73 (day 180), 74 (day 360), 75 (day 540) and 76 (day 720). Comparison of these stresses produces many of the same comments made regarding the cracking potentials. This should not be surprising since the cracking potentials are in part a result of the stress state.

Looking first at Figure 73 at day 180, the maximum stresses are occurring approximately in the same location for all three analyses and in general the shape of the contours in the slab are very similar from one analysis to another. As with the cracking potentials, the stresses in the wall portion of the monolith are very low.

Figure 74, taken at day 360, shows that by this time in the analysis the behaviors of the three analyses are very similar based on the magnitudes of stress and the shapes of the contours. One item of note from Figure 74 is that the gradients of stress shown appear to be steeper for the 10- and 15-day intervals than the 5-day interval. This would indicate that the longer intervals do create some differences within the monolith due to larger differences in stiffness from one lift to the next. This same phenomenon appears again in Figure 75 for day 540 where once again contour shapes are similar from one analysis to another, although for this plot the 15-day analysis has a significantly higher tensile stress than the 5-day analysis. Finally in Figure 76, the contours from these plots at day 720 compare very favorably with the plots at day 360 (Figure 74) as was the case for the cracking potentials.

The final set of contours presented are for stresses in the vertical direction and these also are presented at day 180 (Figure 77), day 360 (Figure 78), day 540 (Figure 79), and day 720 (Figure 80). In general, the trends in behavior which were discussed for the cracking potential contours and the horizontal stress contours apply to the contours of vertical stress as well. The primary difference is in the shapes of the contours, which are different from what has been seen from the previous sets of contours. Gradients for the horizontal stresses are generally in the up-and-down direction, but stresses in the vertical direction create gradients in the side-to-side direction, particularly in the walls. A general comparison of tensile stresses in the vertical direction shows that the vertical stresses are 1.5 to 3 times lower

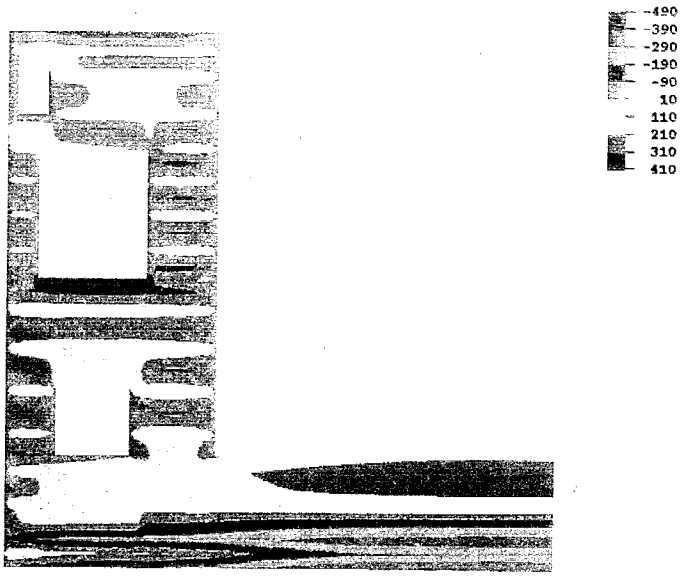

a. 5-day intervals (step = 187, amp = 185)

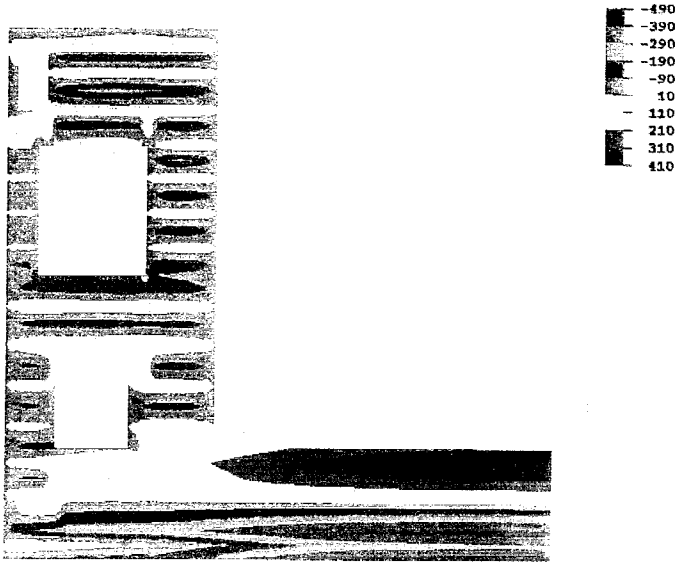

b. 10-day intervals (step = 339, amp = 185)

Figure 73. Horizontal stress contours at 180 days after start of construction (Continued)

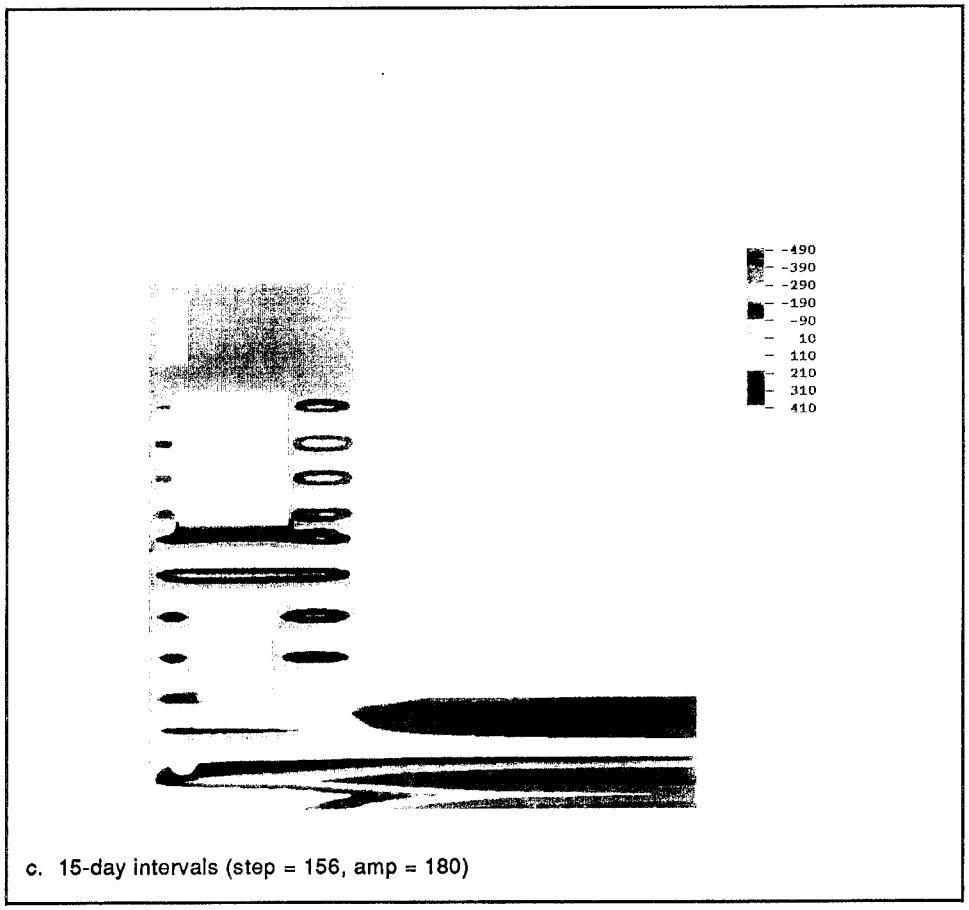

c. 15-day intervals (step = 156, amp = 180)

Figure 73. (Concluded)

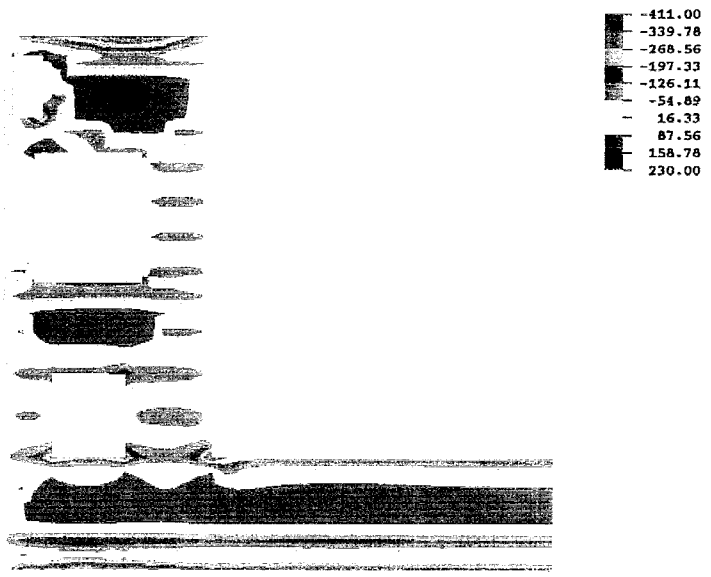

a. 5-day intervals (step = 205, amp = 365)

b. 10-day intervals (step = 354, amp = 360)

Figure 74. Horizontal stress contours at 360 days after start of construction (Continued)

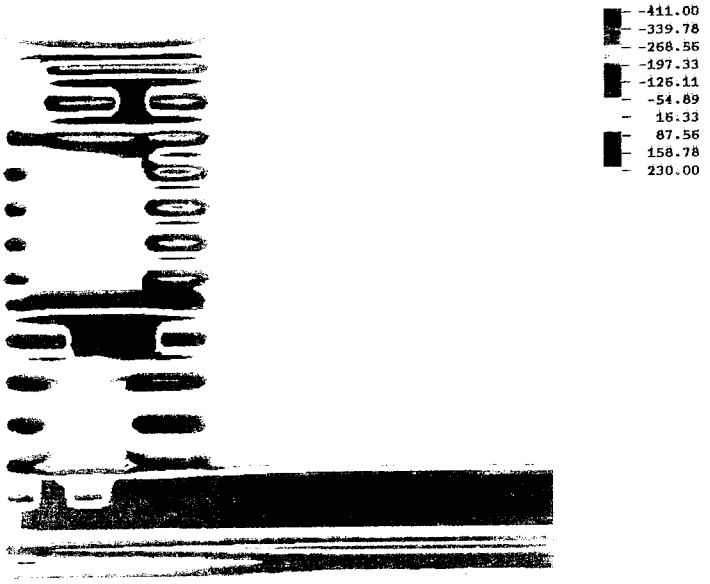

c. 15-day intervals (step = 218, amp = 360)

Figure 74. (Concluded)

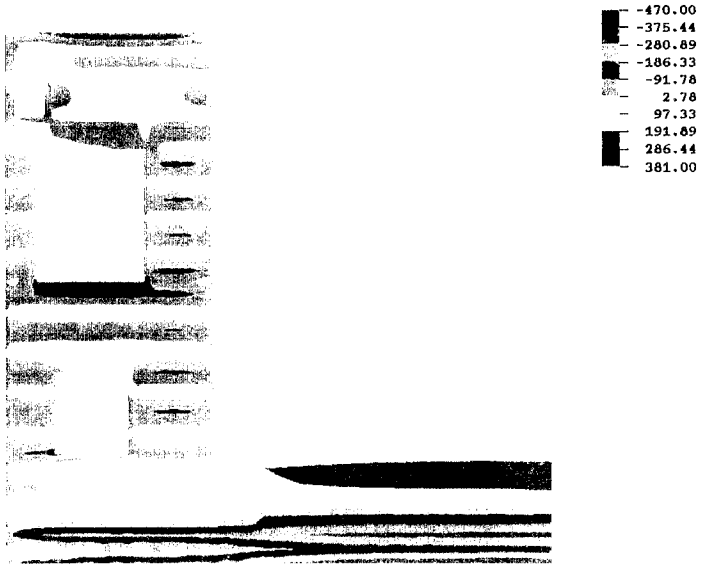

a. 5-day intervals (step = 223, amp = 545)

b. 10-day intervals (step = 363, amp = 540)

Figure 75. Horizontal stress contours at 540 days after start of construction (Continued)

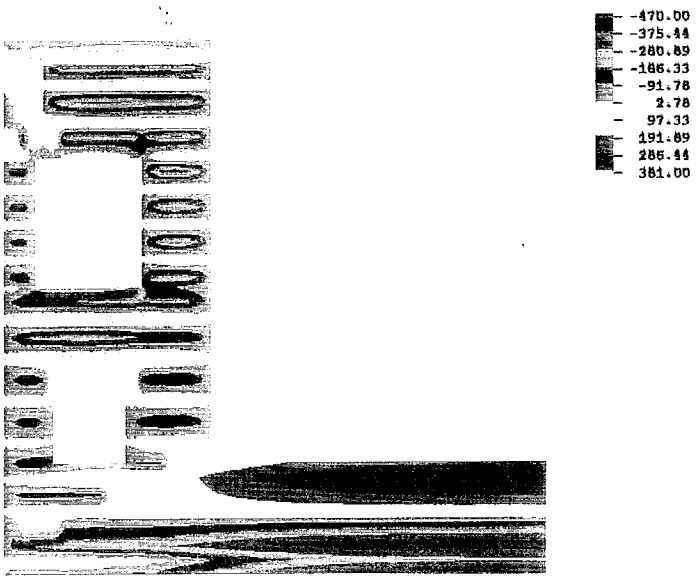

c. 15-day intervals (step = 227, amp = 540)

Figure 75. (Concluded)

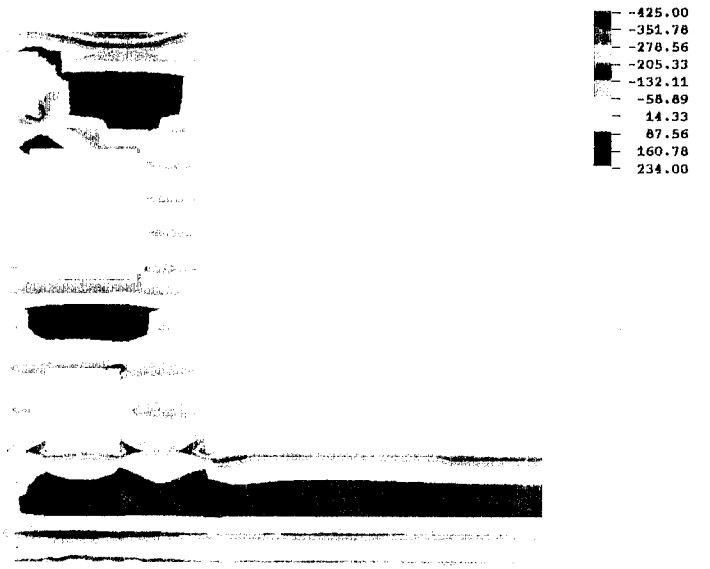

a. 5-day intervals (step = 241, amp = 725)

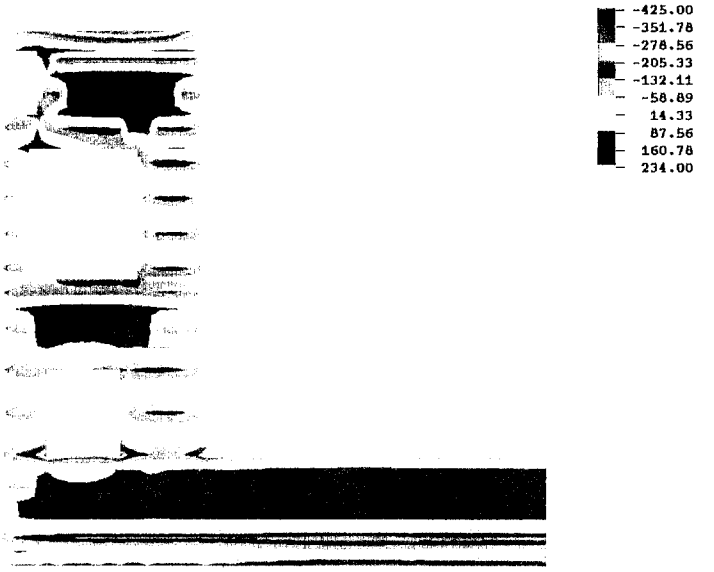

b. 10-day intervals (step = 372, amp = 720)

Figure 76. Horizontal stress contours at 720 days after start of construction (Continued)

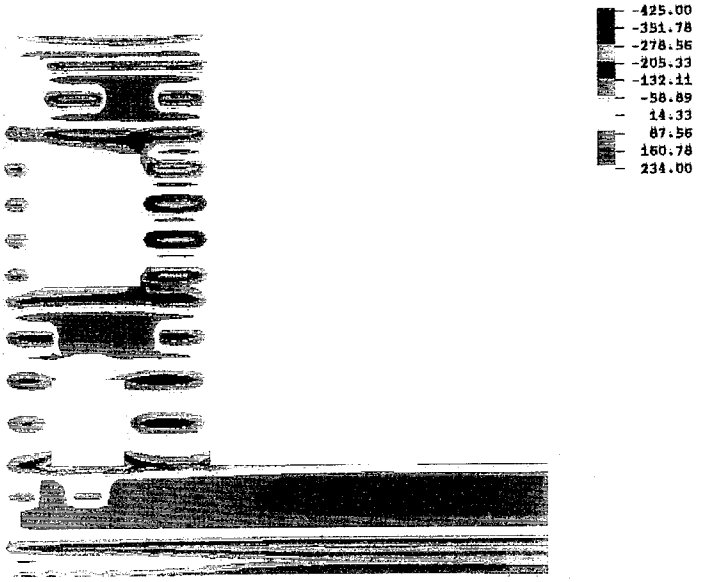

c. 15-day intervals (step = 236, amp = 720)

Figure 76. (Concluded)

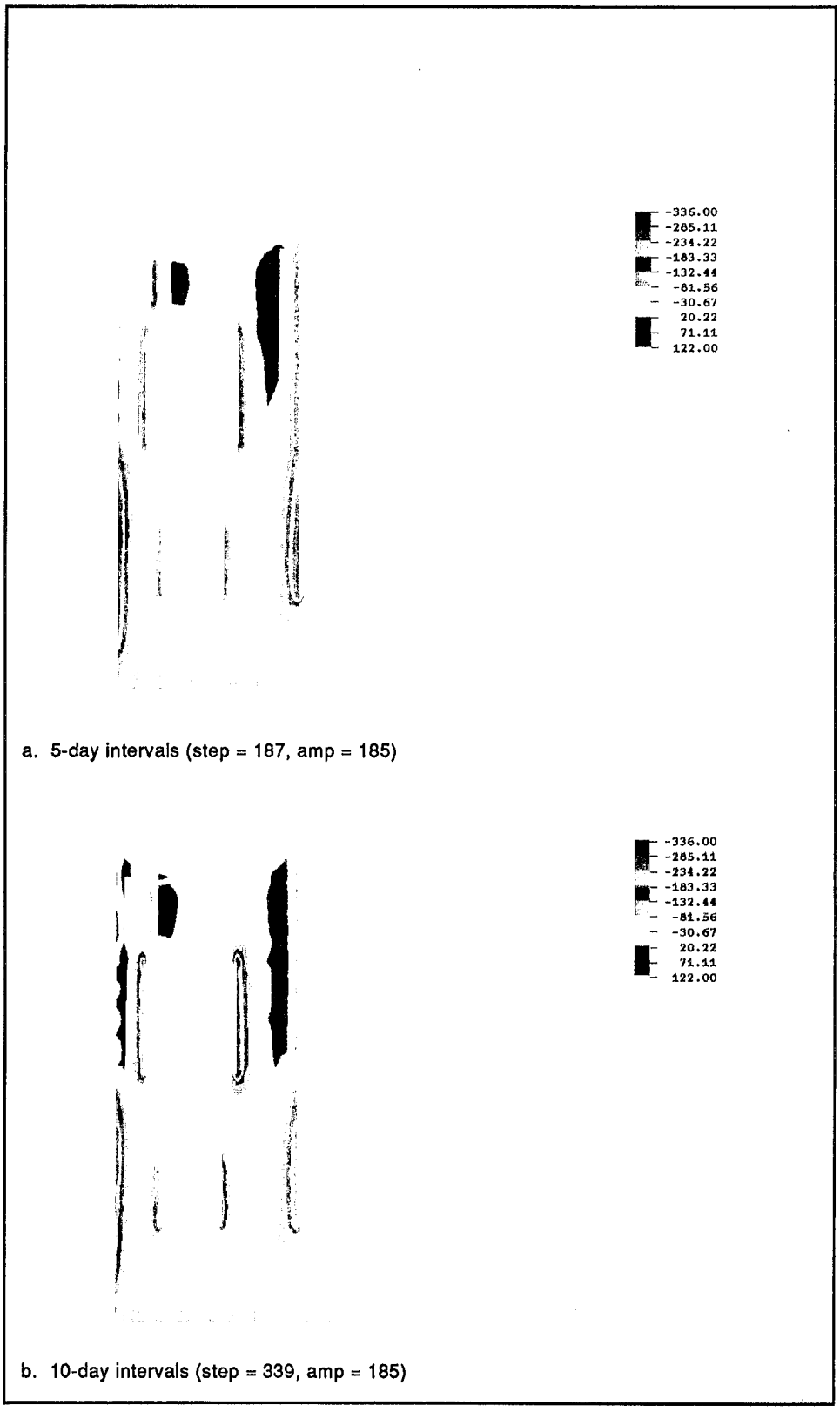

Figure 77. Vertical stress contours at 180 days after start of construction (Continued)

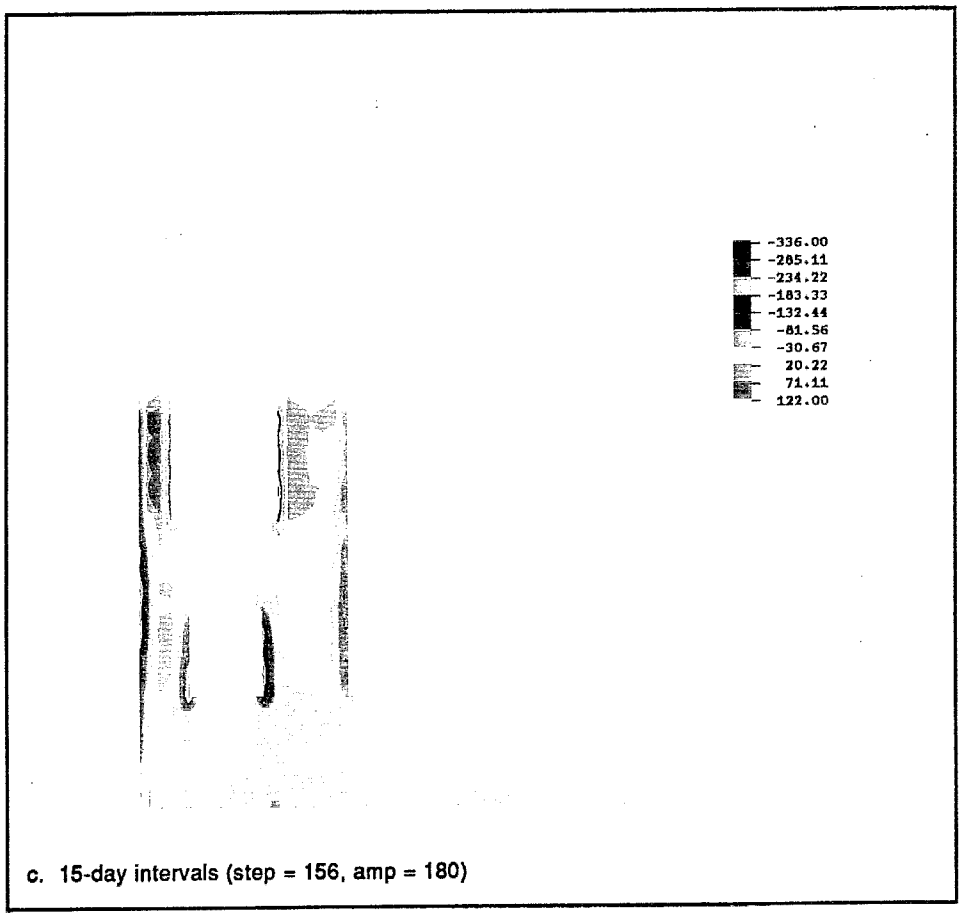

c. 15-day intervals (step = 156, amp = 180)

Figure 77. (Concluded)

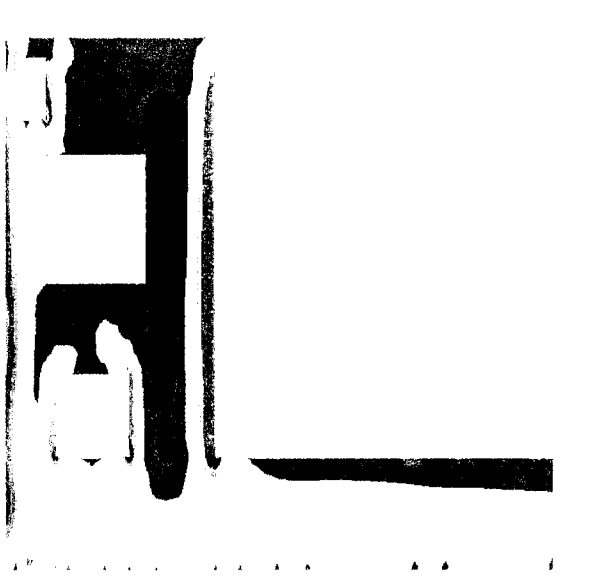

a. 5-day intervals (step = 205, amp = 365)

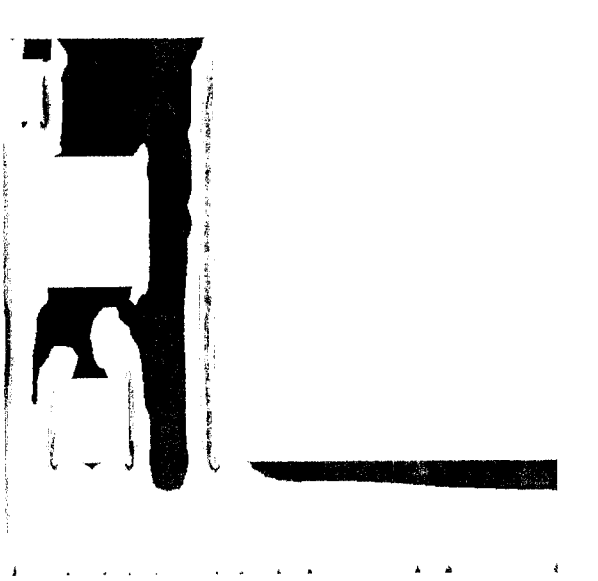

b. 10-day intervals (step = 354, amp = 360)

Figure 78. Vertical stress contours at 360 days after start of construction (Continued)

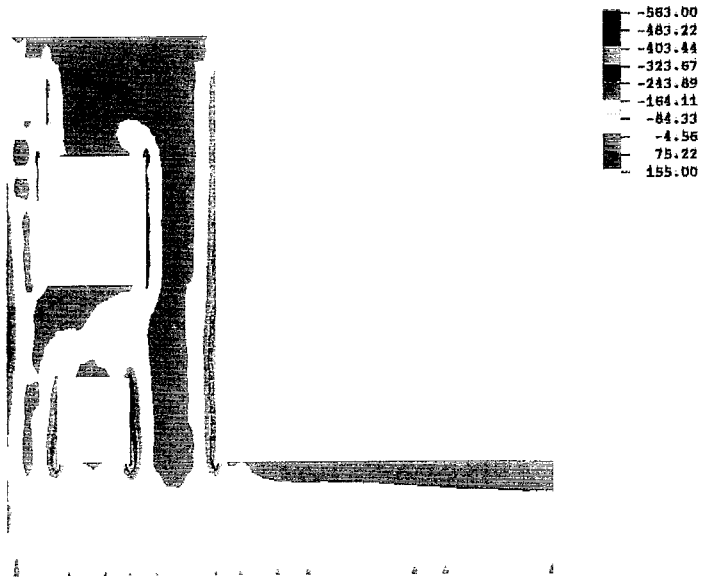

c. 15-day intervals (step = 218, amp = 360)

Figure 78. (Concluded)

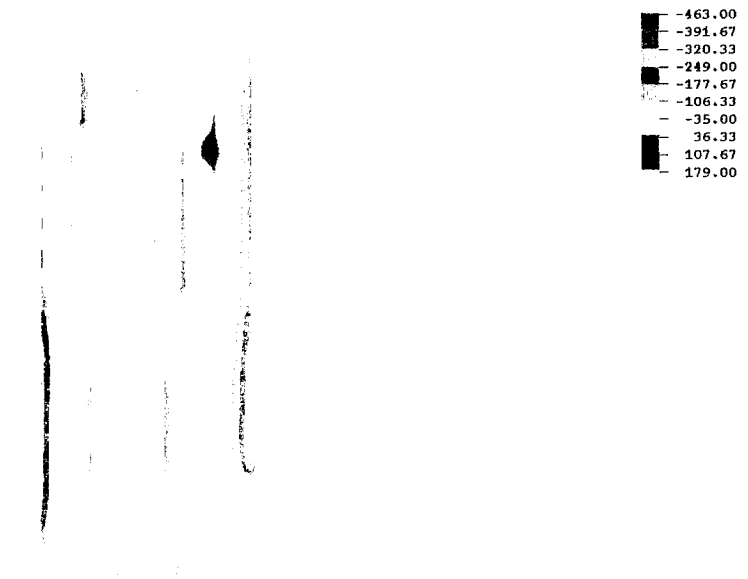

a. 5-day intervals (step = 223, amp = 545)

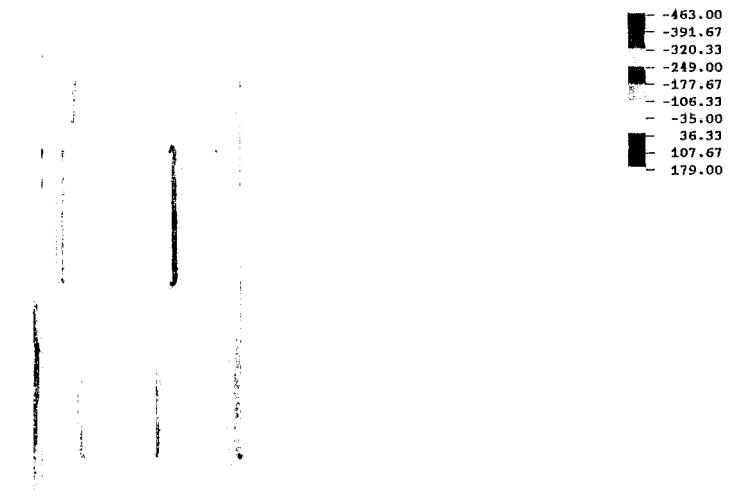

b. 10-day intervals (step = 363, amp = 540)

Figure 79. Vertical stress contours at 540 days after start of construction (Continued)

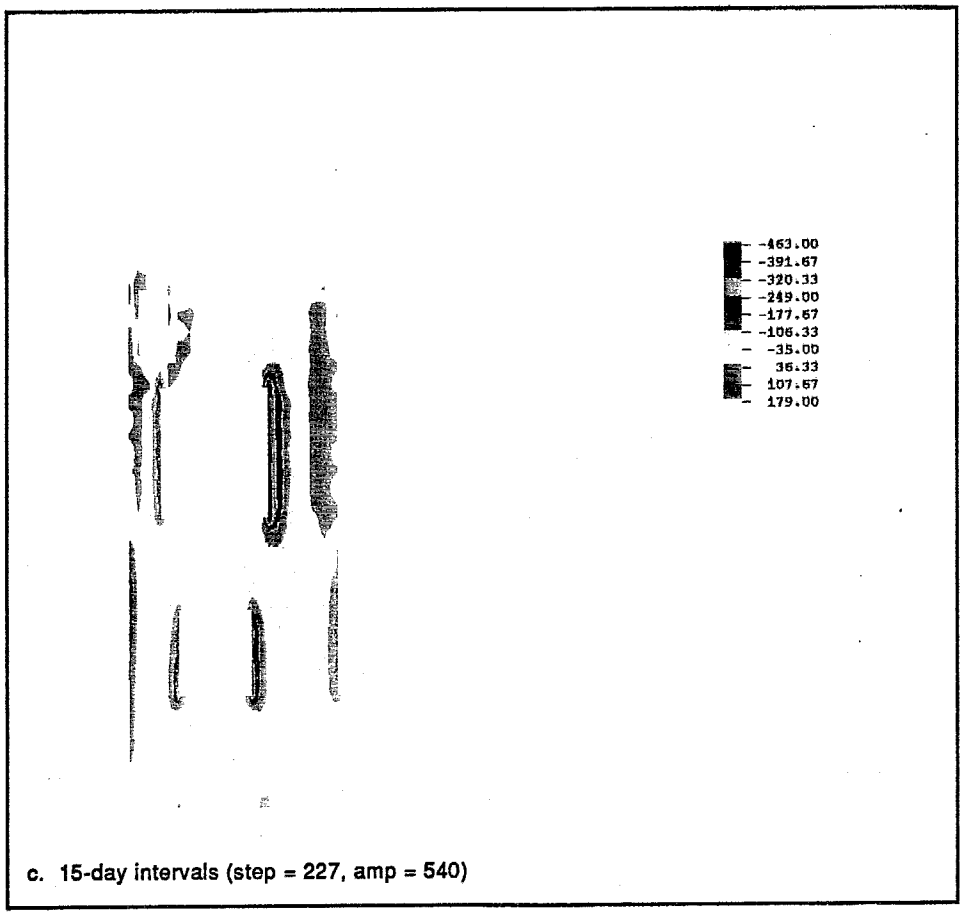

c. 15-day intervals (step = 227, amp = 540)

Figure 79. (Concluded)

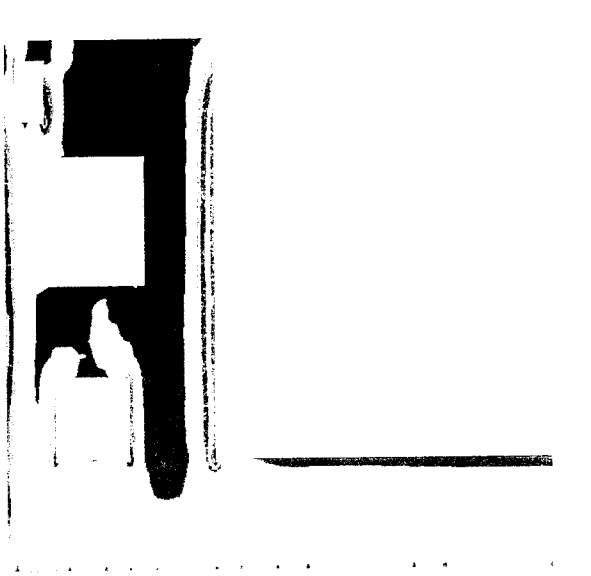

a. 5-day intervals (step = 241, amp = 725)

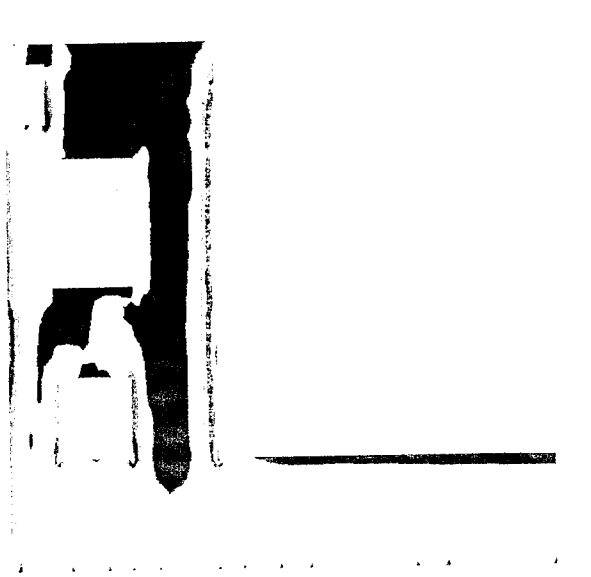

b. 10-day intervals (step = 372, amp = 720)

Figure 80. Vertical stress contours at 720 days after start of construction (Continued)

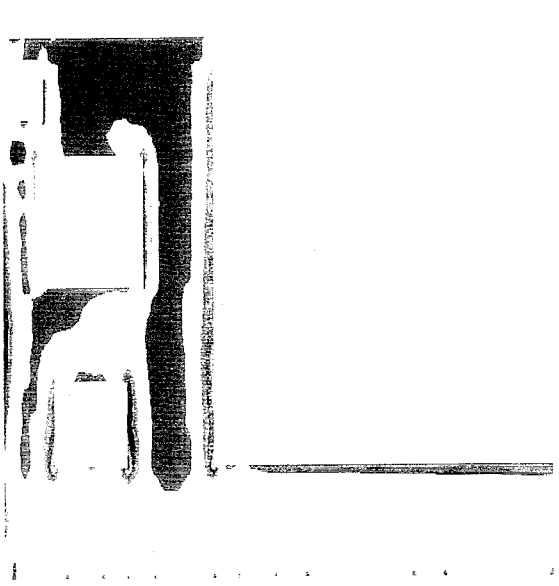

c. 15-day intervals (step = 236, amp = 720)

Figure 80. (Concluded)

than those in the horizontal direction. The difference in these directional stresses is even more pronounced when making the comparison for the base slab portion of the structure where there is up to an order of magnitude difference.

At day 180 (Figure 77), tensile stresses are generally low throughout the monolith. Comparing the three analyses, there are similarities particularly in the areas on either side of the culvert. The plots in Figure 78 (day 360) also have significant amount of resemblance to each other. The maximum stress is located in nearly the same location for all three analyses. This trend continues for day 540 (Figure 79) and day 720 (Figure 80) and, as was true for cracking potentials and horizontal stresses, the plots at day 360 are nearly identical to the plots at day 720.

Time-history plots

Figures 81 through 85 are time-history plots of the horizontal stress. One of the most notable items of these plots is that for all three cases the stresses cycle as a result of ambient air temperatures. While the case

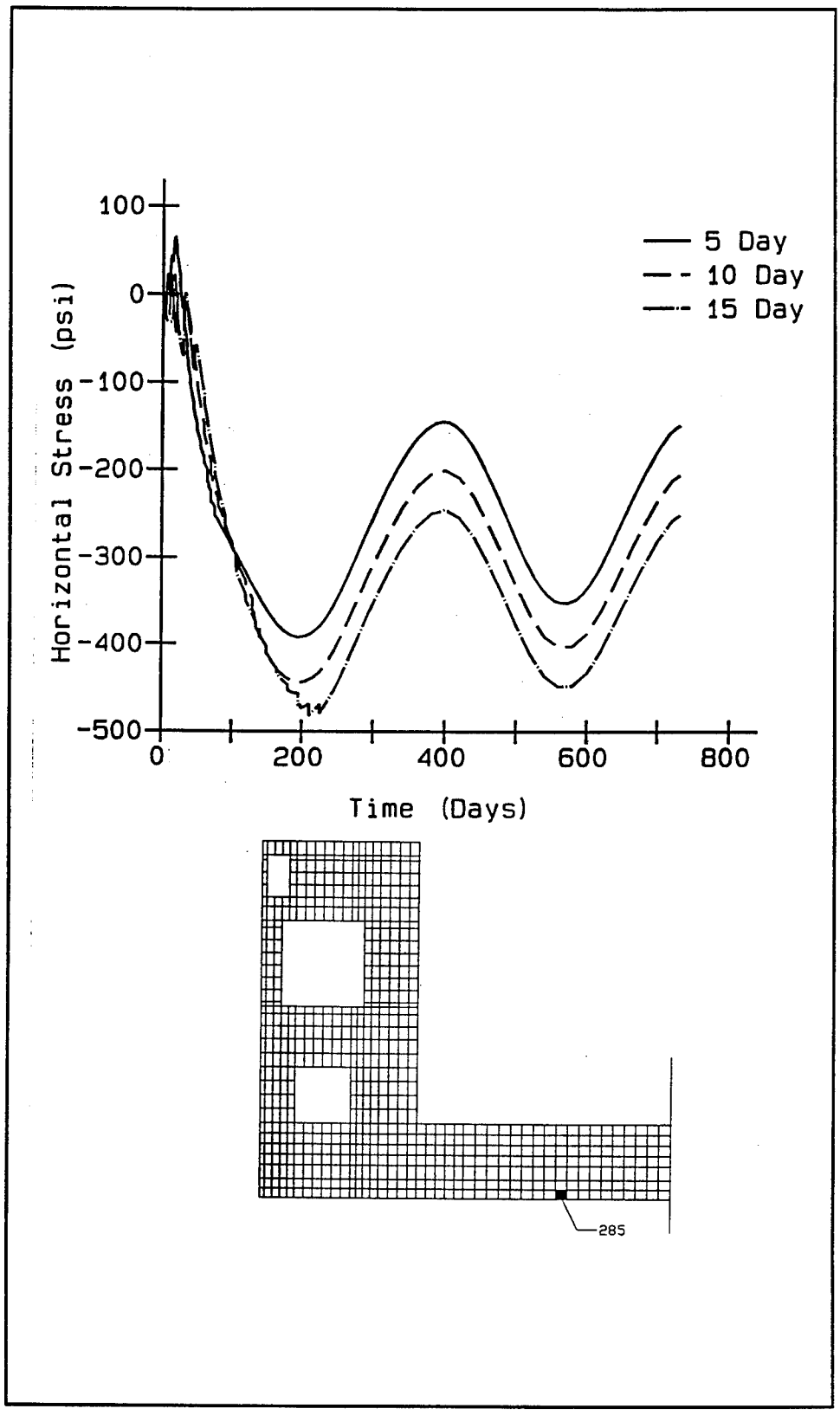

Figure 81. Horizontal stress time-histories at element 285

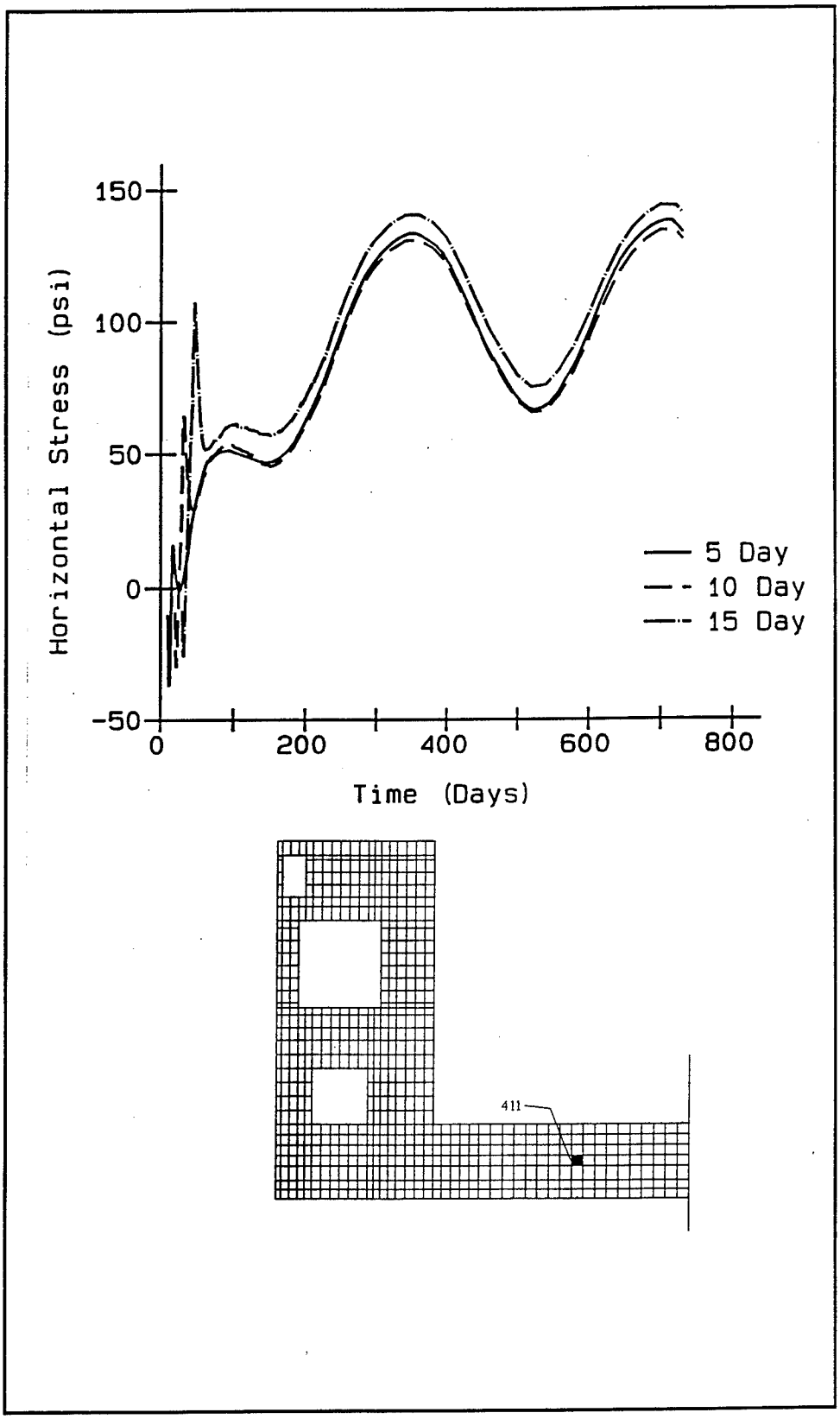

Figure 82. Horizontal stress time-histories at element 411

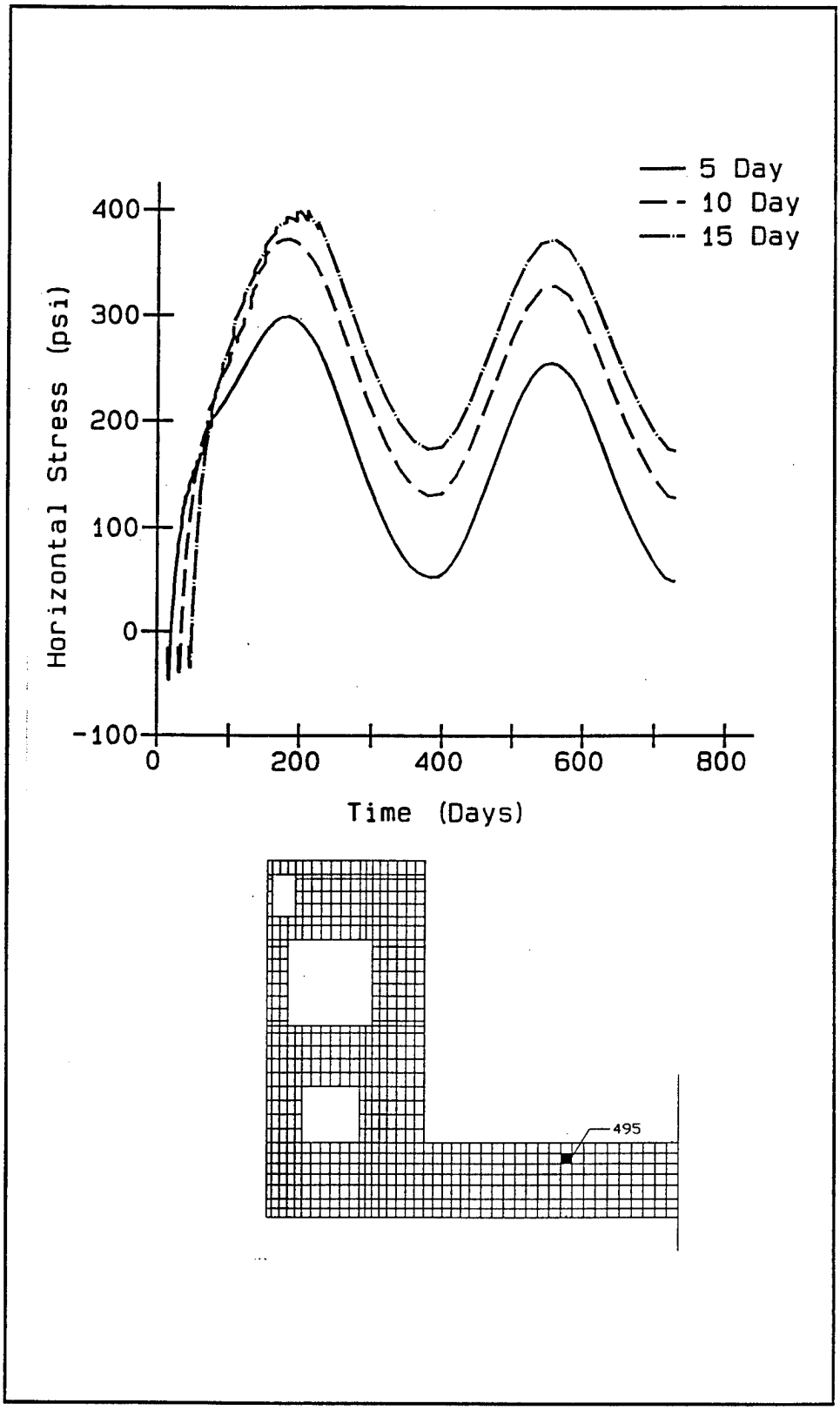

Figure 83. Horizontal stress time-histories at element 495

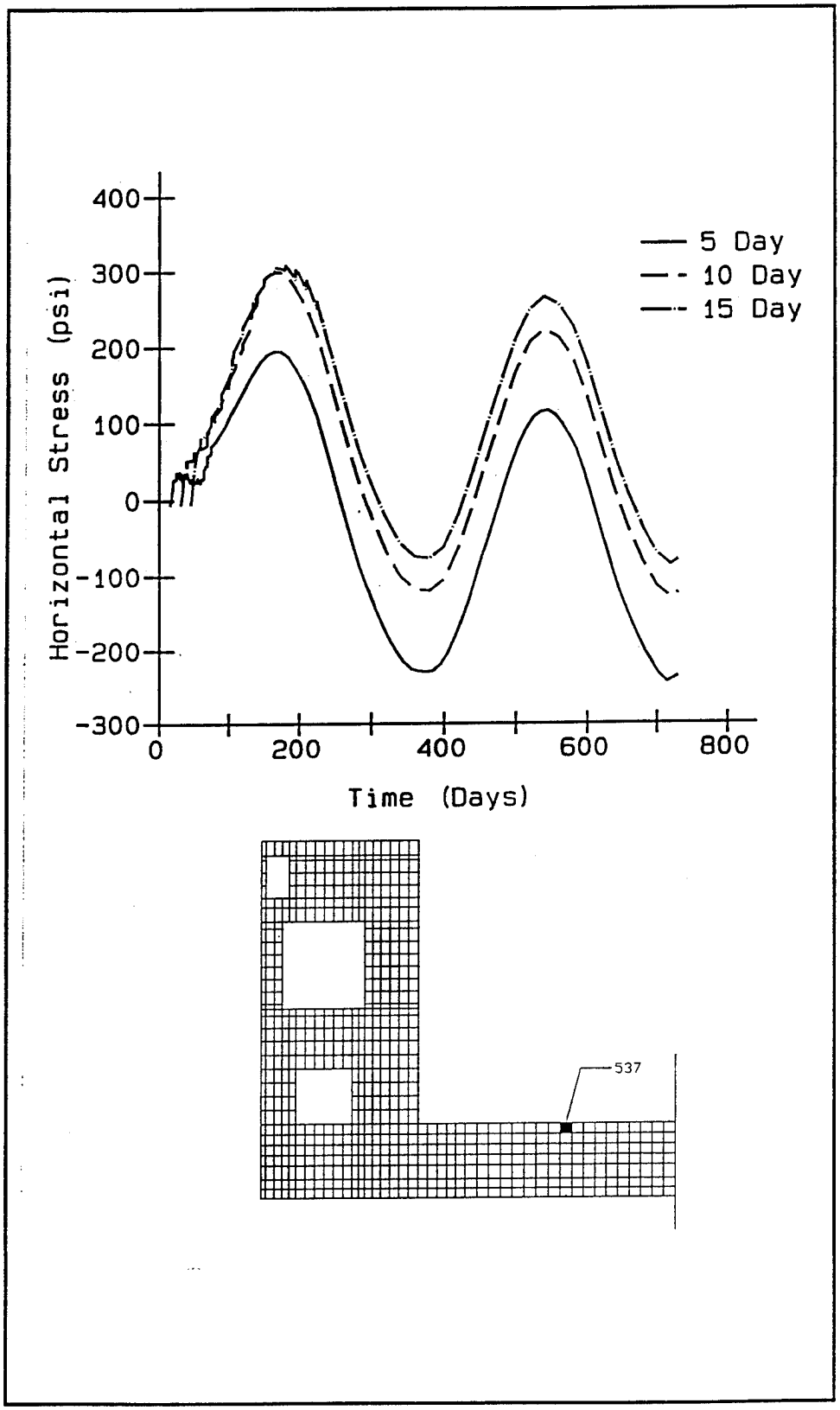

Figure 84. Horizontal stress time-histories at element 537

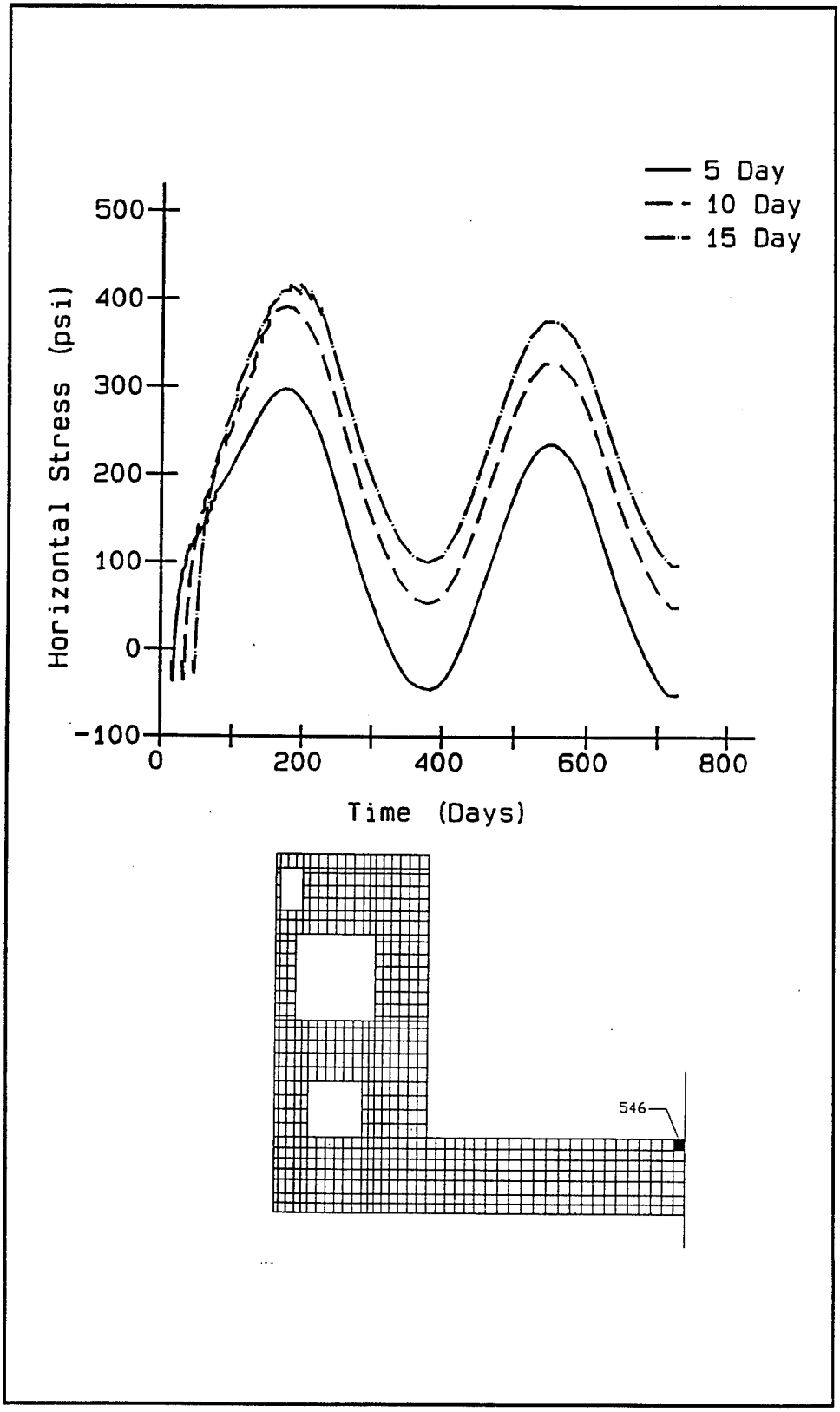

Figure 85. Horizontal stress time-histories at element 546

which used 15-day intervals appears to provide the worst condition, except possibly at very early times, the general shape of the curves in each of the plots are very similar after day 250. Differences in the curves prior to day 250 can be attributed to the fact that the longer the interval, the longer it takes to build the structure; for the 5-day case it requires 75 days to complete, but for the 15 day case it requires 225 days to complete. The long construction time for the 15-day case accounts for the perturbations in the plots until day 225, and these perturbations are the result of lifts being placed in the wall of the monolith. Another key item is that for the elements located at the top of the slab where the maximum tension occurs, the highest tensile stresses are a result of the changing ambient conditions. It should be noted even though the maximum stresses occur after several hundred days, lower levels of tensile stress occurring at early times in the construction process could in fact pose a higher threat of cracking due to the low strength of the concrete at early ages.

Figure 81 shows results at an element at the bottom of the slab where the slab is primarily in compression except for the early part of the analysis. This location is one point where the 5-day interval case has the highest tension, but it occurs within the first 20 days after the start of construction. The maximum compression of nearly 500 psi occurs from the 15-day case. Figure 82 is at an element located near the center of the slab which means it is located near the neutral axis of the slab and explains why the stresses are lower in this plot when compared to the others as well as why they are almost identical.

Figures 83 through 85 are elements located near the top of the slab and are very similar with some differences in the magnitudes of the stresses. In all three of the plots it can also be noted that the stresses from the 10- and 15-day cases are much closer together than the stresses from the 5-day case. Figure 83 shows an element which is the second element from the top of the slab, but its maximum tensile stresses are higher than stresses that result in the element adjacent to it at the top of the slab (Figure 84). Figure 85 is a plot taken at an element at the top of the slab right next to the line of symmetry of the model and shows the location of the maximum tensile stress (411 psi) which occurred in the structure.

Figures 86 through 88 are time-history plots of vertical stresses in the wall of the monolith. For these cases, the 5-day interval cases control in tension at two of the locations. As with the plots from the slab portion of the monolith, the ambient conditions control the shapes of the curves. Unlike the slab though, some of the maximum tensile stresses occur at early times as can be seen in Figure 86 for the 15-day case and in Figure 88 for the 5- and 10-day cases. It can also be seen that the starting times of the lifts in the walls are quite different between the analyses due to the fact that all three analyses started at the same time. As the construction continues, however, placement of the various lifts occur at different times as a result of the different placing schedules.

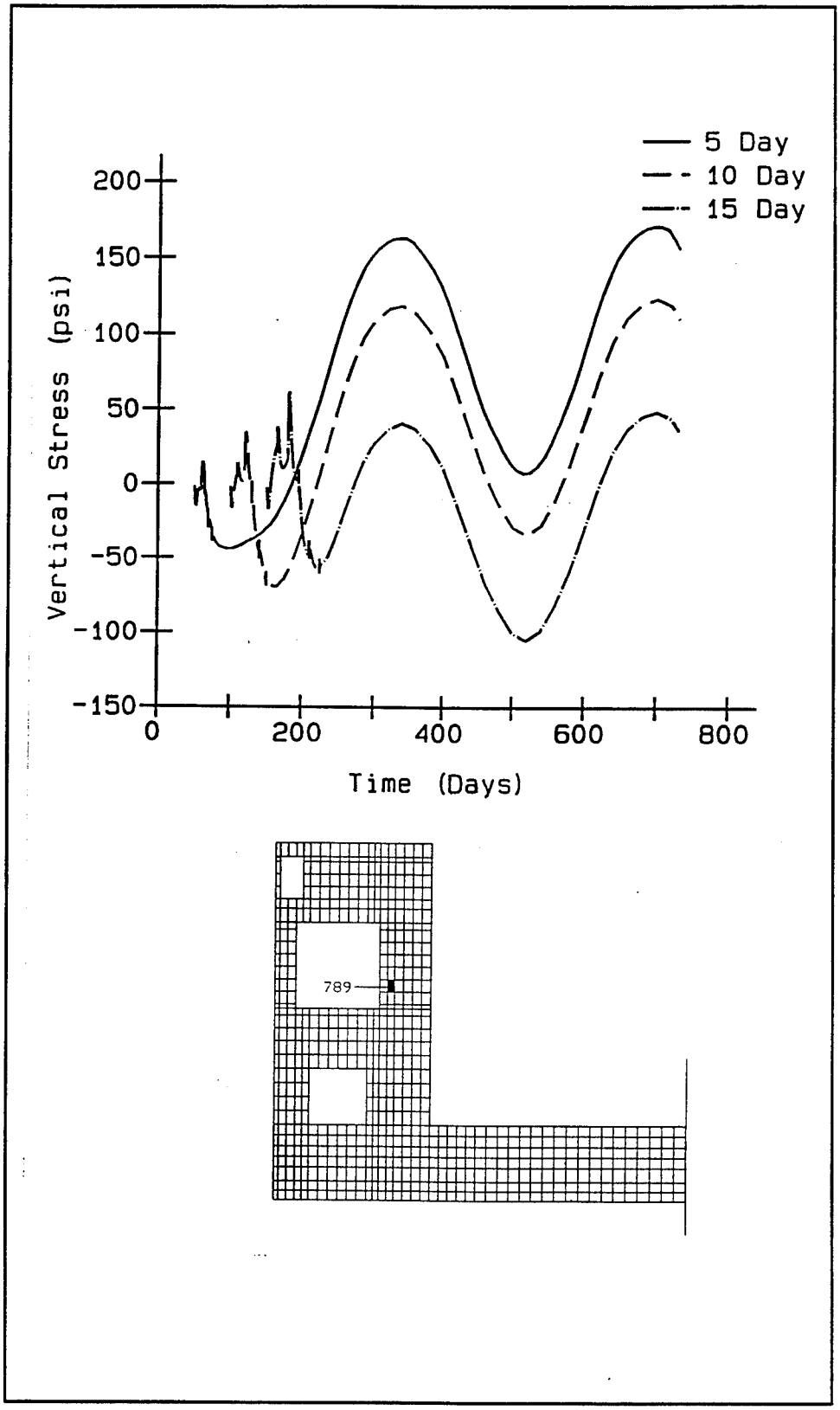

Figure 86. Vertical stress time-histories at element 789

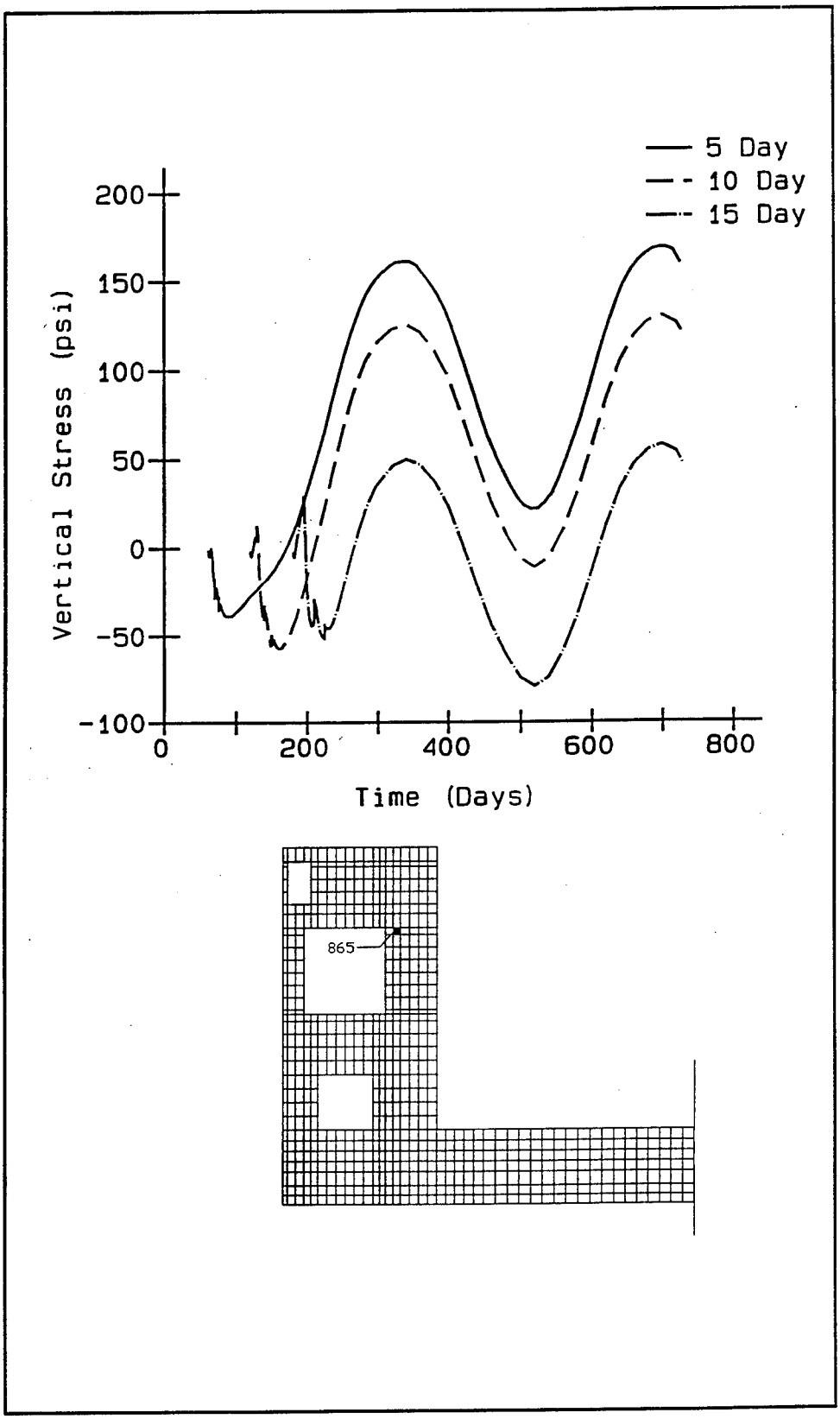

Figure 87. Vertical stress time-histories at element 865

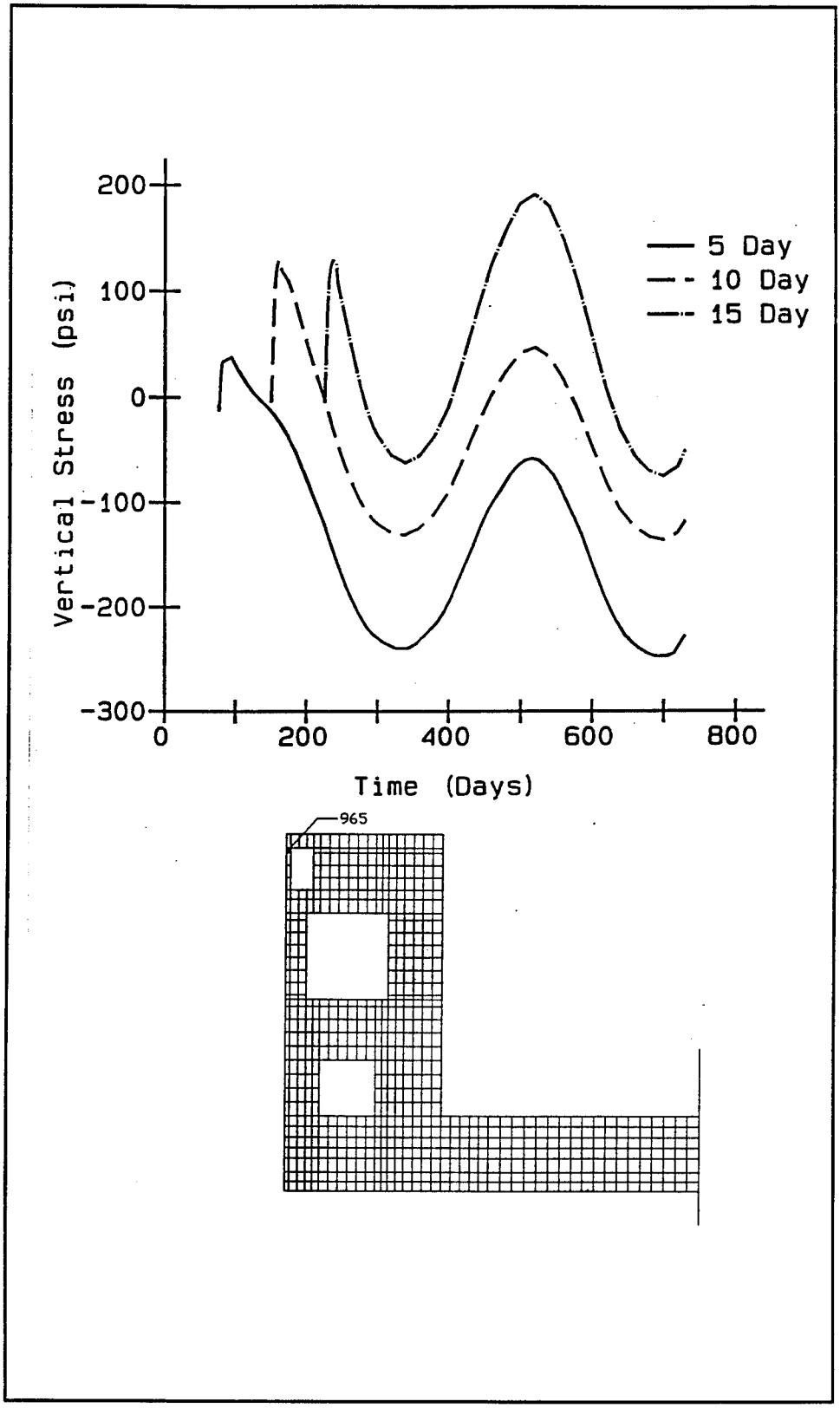

Figure 88. Vertical stress time-histories at element 965

Summary

The parametric study described in this chapter provided some interesting insight on the time interval assumed between lift placements when performing a NISA. Based on results shown for the slab portion of the monolith, it would appear that longer placing intervals would be the conservative assumption, but there are indications from the results in the wall portion of the monolith that this assumption would not always be conservative.

The temperature analyses showed that by 300 days after the start of construction that the temperatures throughout the structure were nearly identical. This observation indicates that the effects of the heat rise due to the heat of hydration are all dissipated by day 300 of the analyses regardless of the time between intervals used. A review of the time-history plots will also show that the heat generated by the concrete is dissipated within approximately 100 days after a lift is placed.

As mentioned in the introduction of this chapter, it was assumed that the heat of hydration was the primary source of high thermal stresses. The results of this study show that while the heat of hydration may create the highest temperatures, it is the ambient conditions that will create the highest stresses in many locations. This is demonstrated by the cyclic nature of the stresses in the time-history plots shown. Control of structural behavior by ambient temperatures has been shown also in NISA studies performed on Olmsted Locks (Garner et al. 1992) and McAlpine Lock Replacement (Fehl, Riveros, and Garner in preparation).

Based on the results presented in this chapter, questions may be raised as to why the longer the interval between placements created higher stresses in the slab. The cause for the higher stresses can be attributed to the fact that the longer the period between lift placements, a longer time is required for the existing lift to mature and hence gain strength. Additional gain in strength will translate into additional restraint to the newly placed lift. This can be demonstrated using plots of the aging modulus of the concrete as shown in Figure 89. The same aging modulus of elasticity curve is repeated three times at intervals of 5 days and a vertical line is placed at day 15 of the plot. As can be seen, Curve A of the plot has modulus of 3,839,000 psi at an age of 15 days, Curve B has a modulus of 3,459,000 psi at an age of 10 days, and Curve C has a modulus of 2,847,000 psi at an age of 5 days. Therefore, using 10-day intervals instead of 5-day intervals will allow the existing lift to increase in strength by 21 percent, and using 15-day intervals instead of 5-day intervals will permit an increase in the existing lift's strength of 35 percent. Increasing the length between lift placements has a significant effect on the stiffness that will be achieved prior to the placement of the next lift. The difference in modulus between 5 and 10 days and 10 and 15 days also can be used to explain why the curves for 10 and 15 days are closer together than the 5- and 10-day intervals. The same type of phenomena were also seen

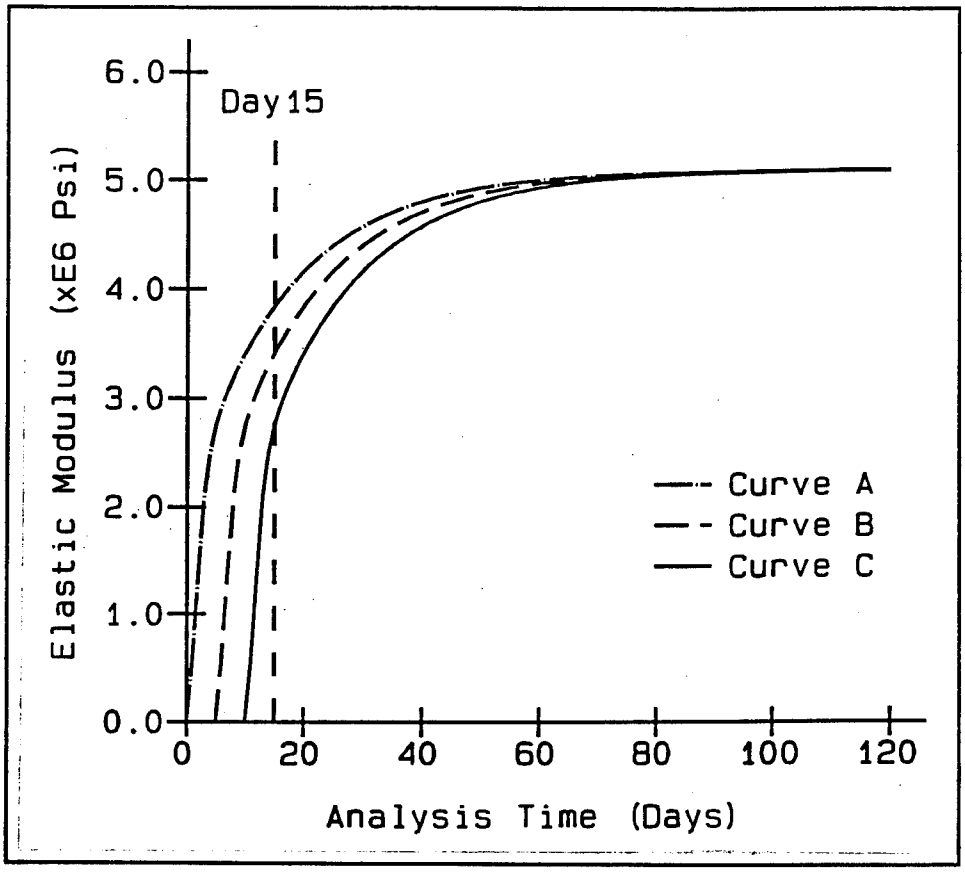

Figure 89. Plots of aging modulus of 5-day intervals for concrete mixture used in analyses

in a similar type of study performed during the Olmsted Locks NISA study (Merrill, Fehl, and Garner 1995).

In addition to the fact that the longer the interval between lifts, the stiffer the existing concrete will become, other aging parameters may likewise have an effect. Creep and shrinkage also are age dependent, so longer periods between placements will allow more creep and shrinkage effects to be dissipated in an existing lift. So, the shorter the time intervals between lifts, then the smaller the differences will be in the volume changes which will occur as a result of creep and shrinkage.

6 Ambient Temperature and Heat of Hydration Effects

Introduction

The parametric study discussed in Chapter 5 that looked at the time interval between lift placements in a lock monolith provided valuable insight into the behavior of the structure when these time intervals are varied. While the original intent of that study was to simply evaluate the effects of changing the time intervals, the results indicated that the behavior was highly dependent on the ambient temperature cycle. The indications from that study and other studies (Garner et al. 1992; Fehl, Riveros and Garner in preparation) were that ambient temperature changes produce the highest stresses, and further investigation of this phenomenon was warranted.

To study the effects of ambient temperature and the heat generated due to the heat of hydration, two additional analyses were performed varying the ambient and heat of hydration parameters. One analysis was performed in which the ambient temperature was held constant at 70 °F with normal heat generation. This analysis was performed so that the effects of the heat generated by the heat of hydration could be observed without taking into consideration the changing ambient temperatures. Another analysis was performed using the normal ambient temperature curve but allowing no heat to be generated. This analysis was performed so that the effects of ambient temperature could be observed without having to consider the effects of heat generated by the heat of hydration.

The analyses for the two cases just described will be compared to the analysis performed in Chapter 5. Since the results in Chapter 5 showed that the behavior of the monolith was controlled primarily by the construction condition of 15 days between lift placements, the comparison between the three cases will be made with 15-day intervals between lift placements. The only variations being made between the analyses will be to the ambient temperature curve and to the heat generation. Each case will be identified in the comparisons as follows:

Case a - variable ambient temperature + heat generated

Case b - constant ambient temperature + heat generated

Case c - variable ambient temperature + no heat generated

Comparisons between the three sets of analyses will include time-history plots of temperature, temperature contour plots, stress time-history plots, and contour plots of the cracking potentials. While it is obvious there will be differences in the results of the temperature analyses, the differences from the results of the stress analyses are not as intuitive.

Heat Transfer Analysis

Time-history plots

Figures 90 through 97 are time-history plots comparing the temperatures of the three different cases at various nodes throughout the structure. It is easy to identify the plot of Case b in all of the plots shown, since the line for Case b moves asymptotically to a single temperature while the other two curves change continually. The final temperature for Case b in each plot is slightly different depending on its location in the structure. Since node 1166 in Figure 90 is near the base of the structure, the foundation will have an effect on the temperature and actually create a constant temperature of approximately 65 °F. Temperatures for the other points generally reach an equilibrium of about 70 °F.

The plots also show that by the end of the analysis there is virtually no difference between the temperatures predicted by Cases a and c, an indication that the behavior is being driven by the ambient conditions. For node 2101 (Figure 92), located near a surface, Cases a and c converge approximately 50 days after the lift is placed, while for node 1166 located near the foundation, the two cases do not converge until about day 500. This range of times for convergence demonstrates how the distance from a surface affects the dissipation of the heat which is generated by the hydration of the concrete. While nodes 2101 and 1166 are the extremes when comparing Cases a and c, the remaining nodes all appear to converge at 200 to 300 days after a lift has been placed.

The final item of note regarding the time-history temperature plots are the early-time temperatures. Case c always has lower early-time temperatures than the other two cases due to the fact that no heat is generated. Peak temperatures at early times are very close for Cases a and b. Whether Case a or Case b has the highest early temperature is dependent on which portion of the structure is being evaluated. For nodes in the slab, Case a will have the highest early temperatures since the summer temperatures are higher than 70 °F. In the fall and winter where ambient

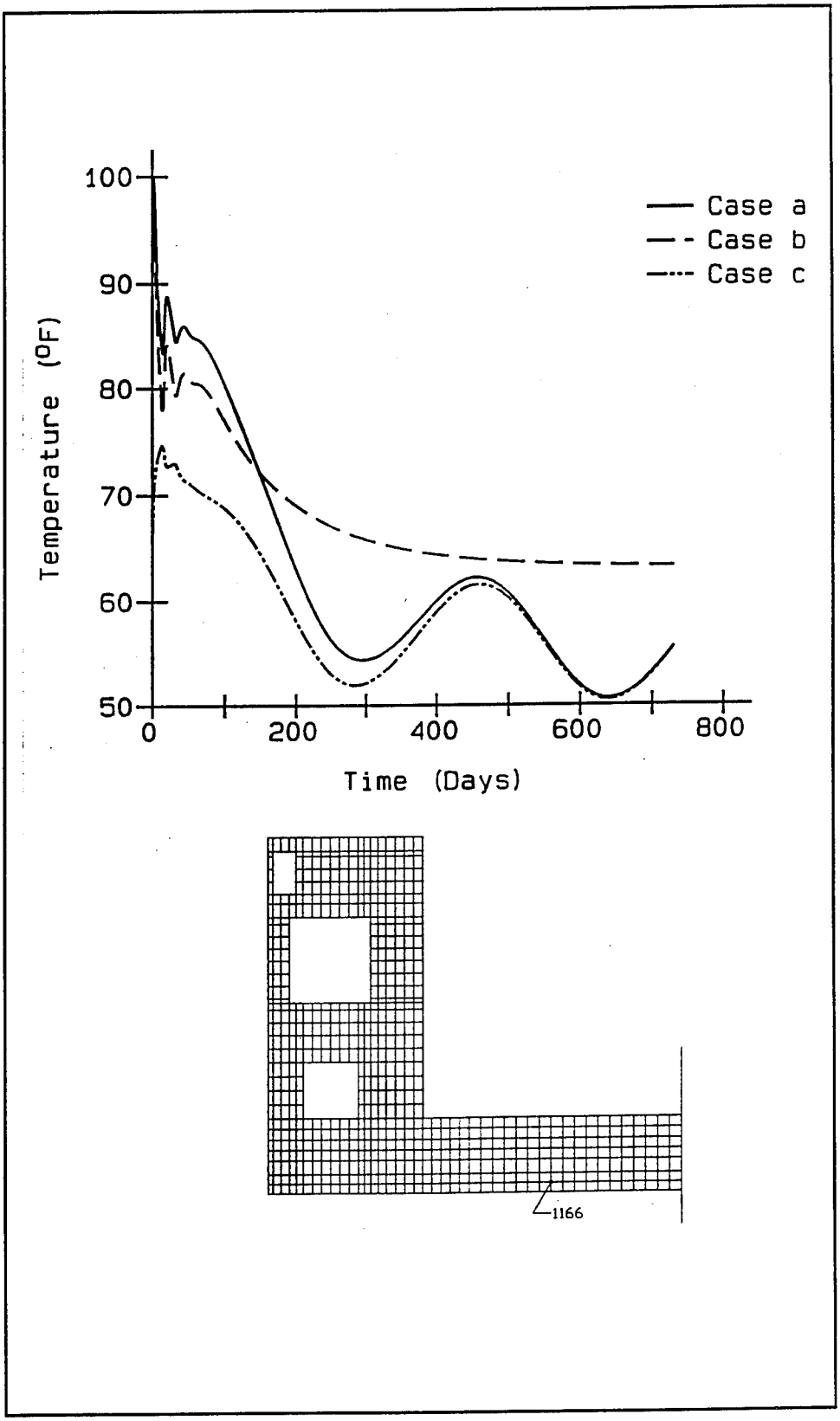

Figure 90. Temperature time-histories at node 1166

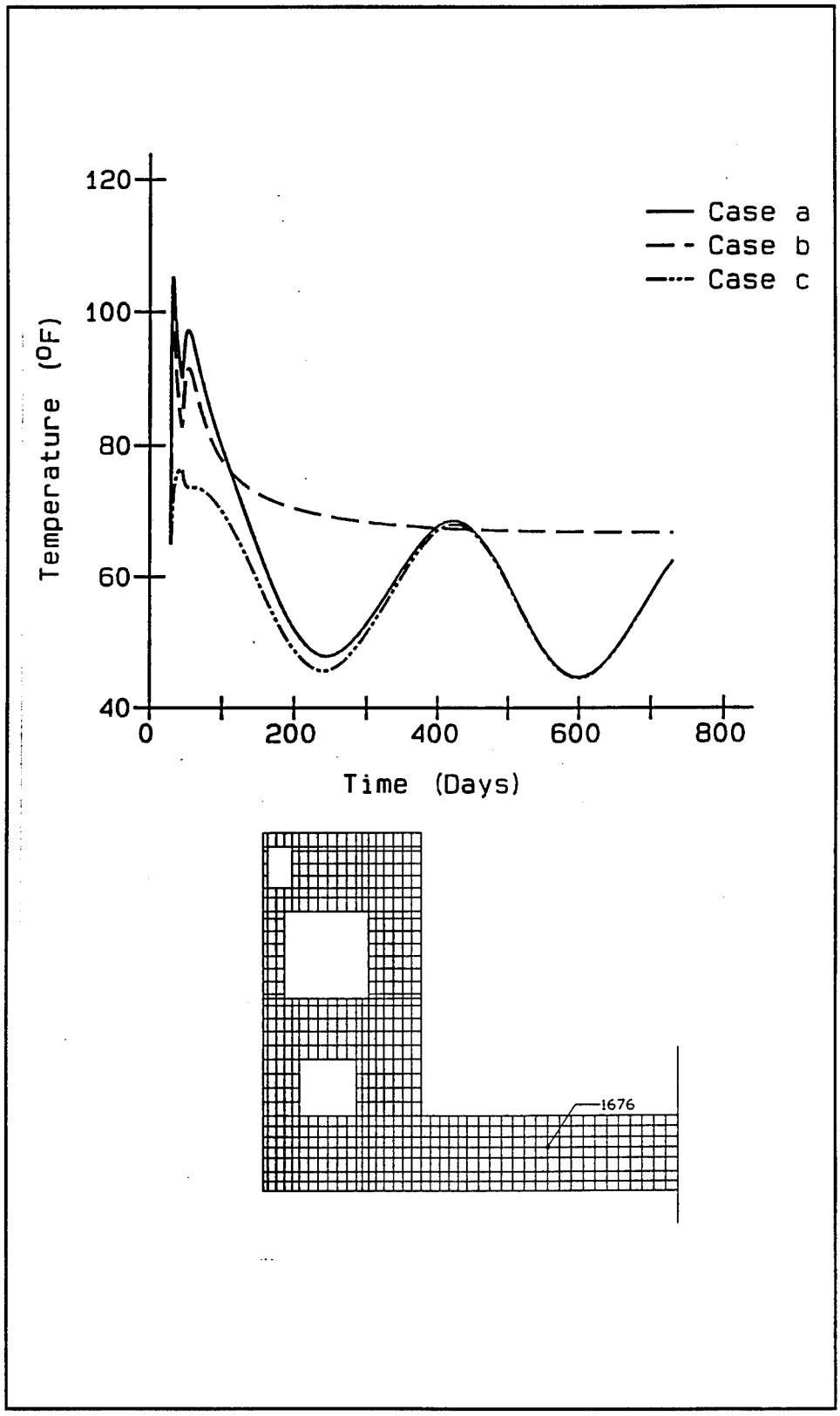

Figure 91. Temperature time-histories at node 1676

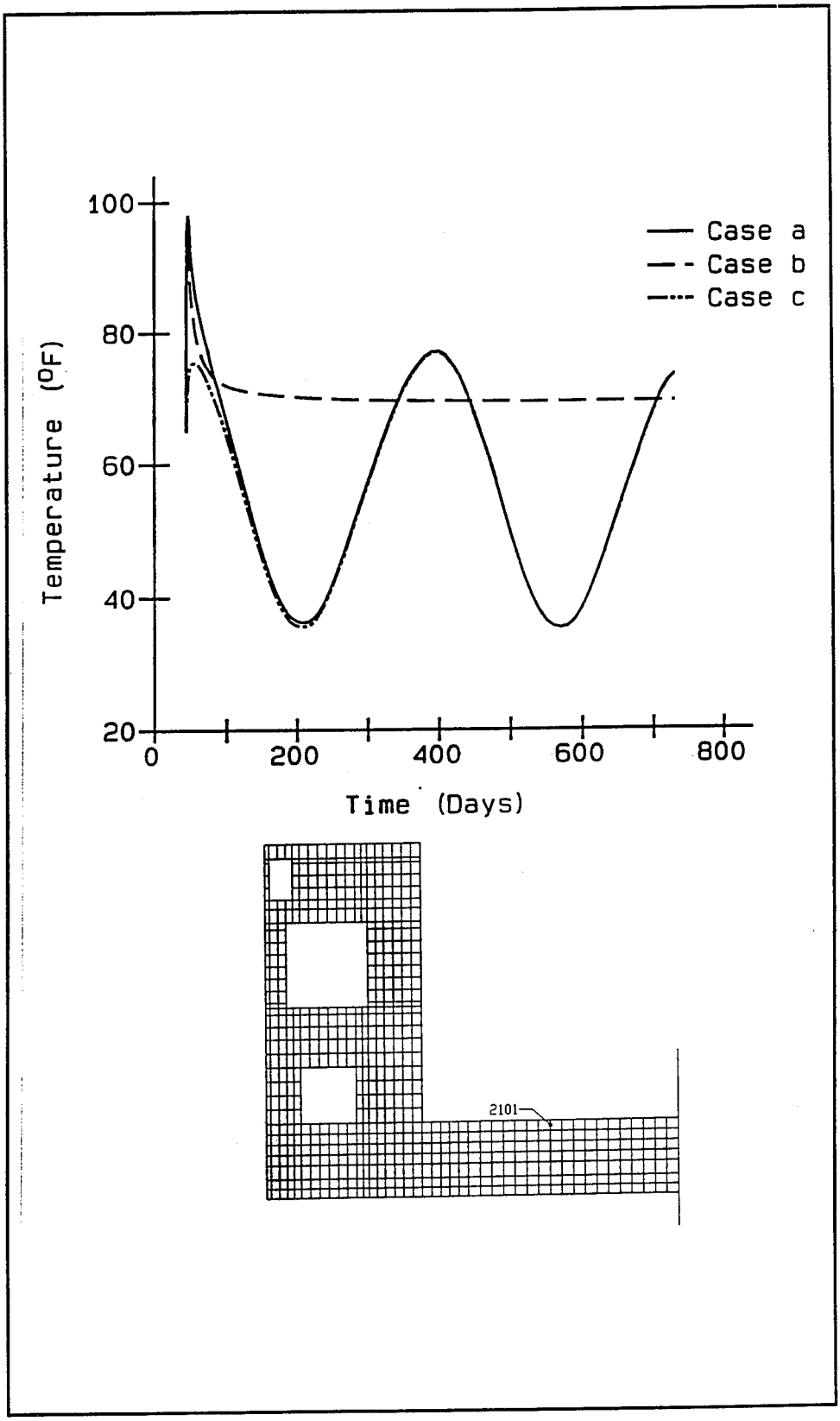

Figure 92. Temperature time-histories at node 2101

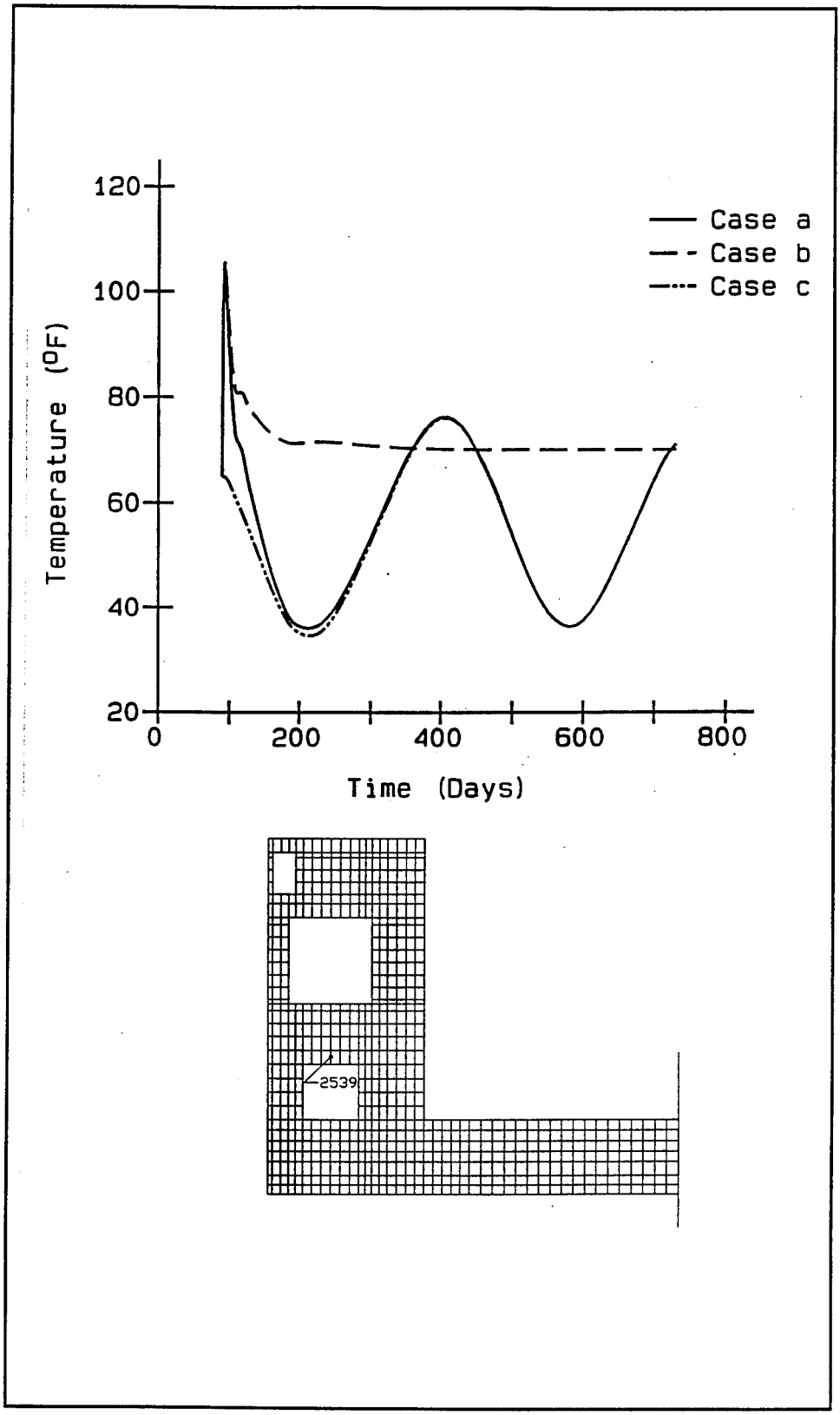

Figure 93. Temperature time-histories at node 2539

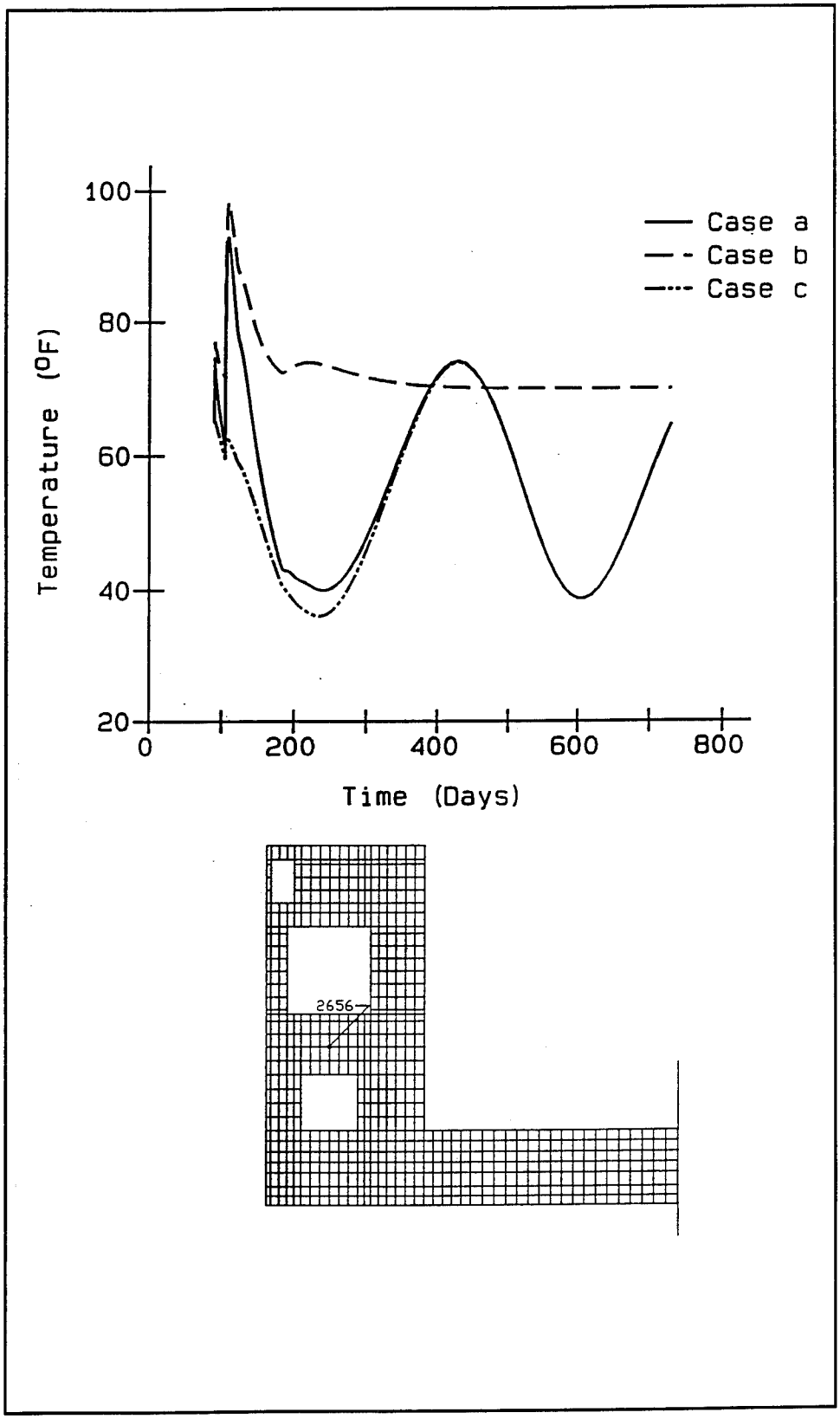

Figure 94. Temperature time-histories at node 2656

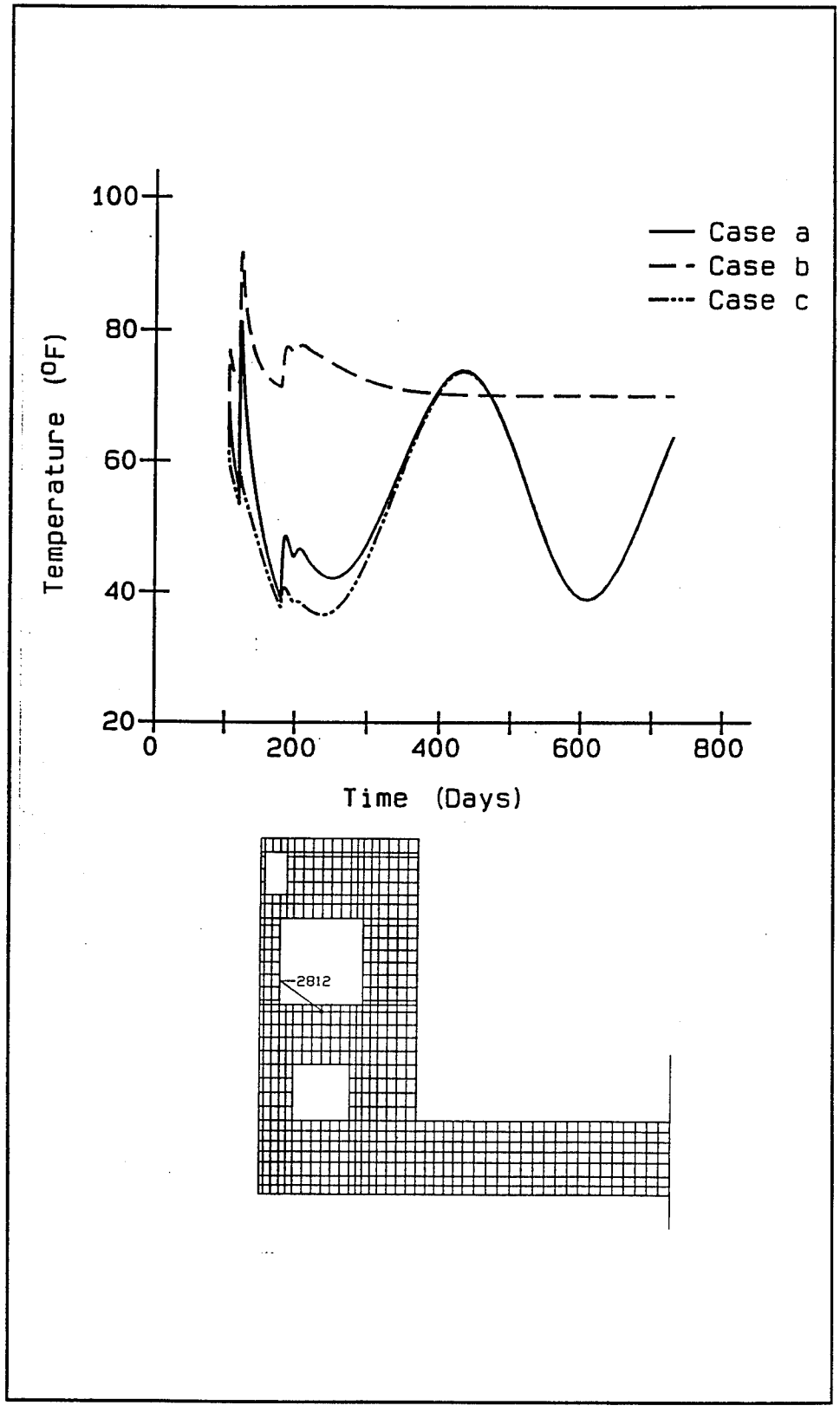

Figure 95. Temperature time-histories at node 2812

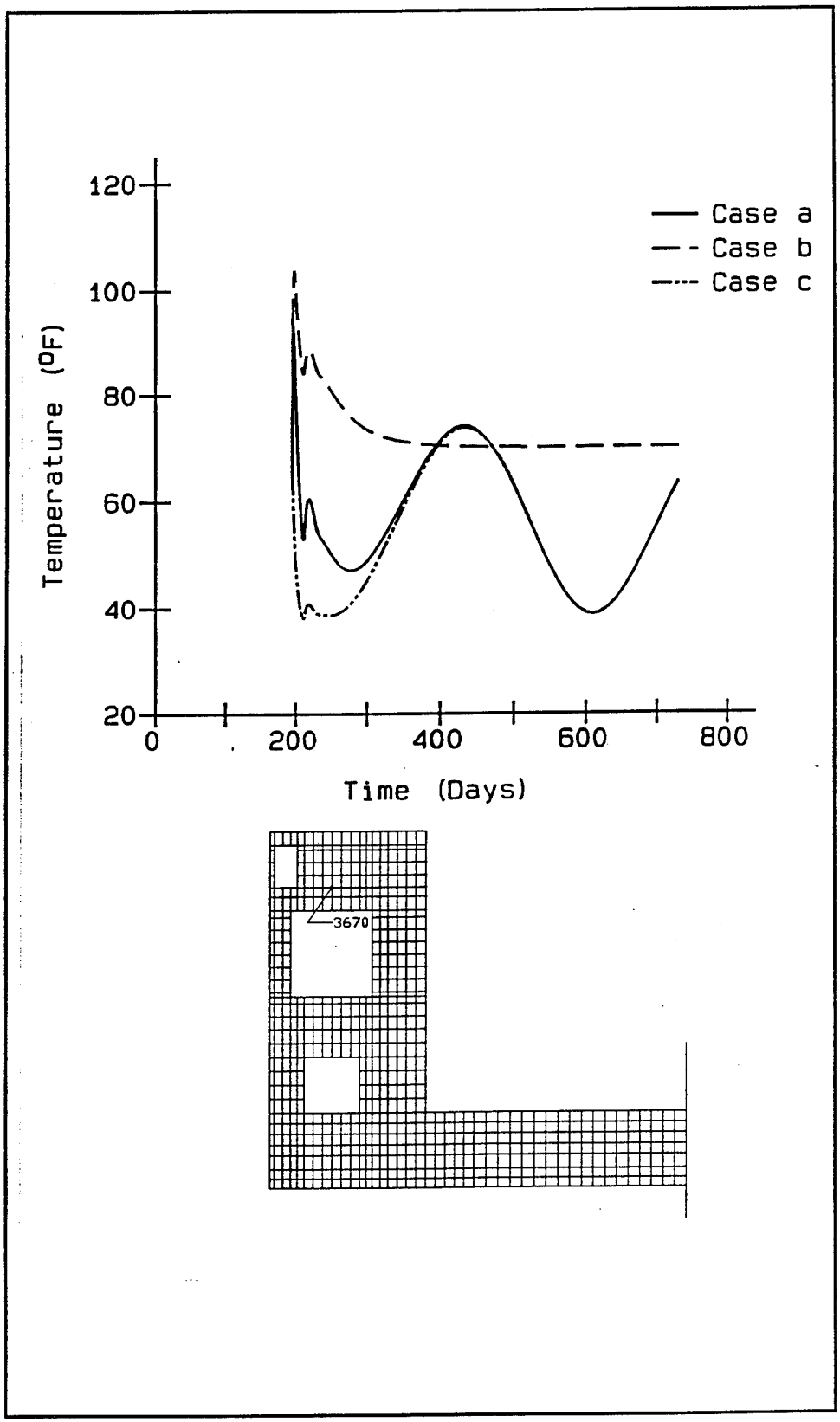

Figure 96. Temperature time-histories at node 3670

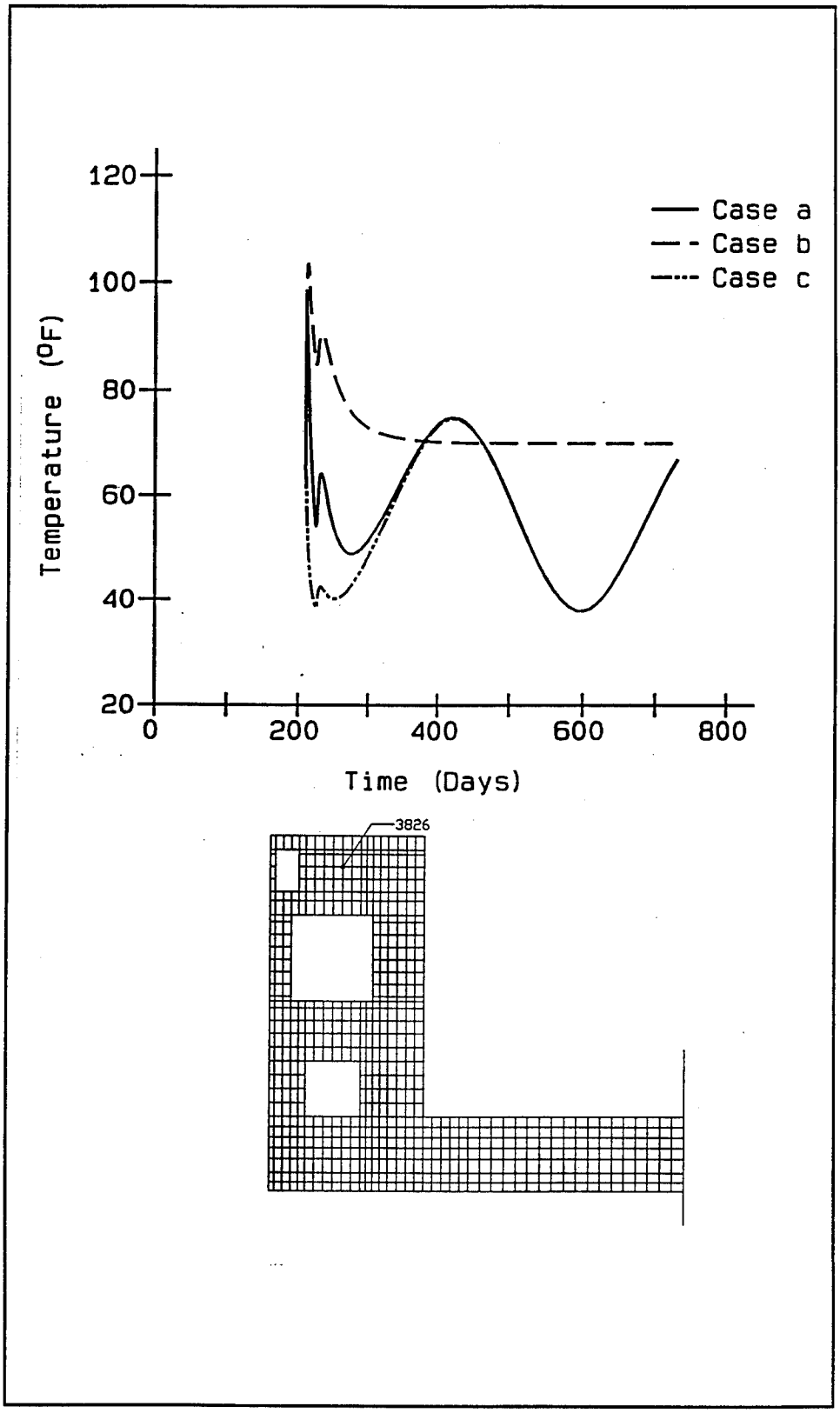

Figure 97. Temperature time-histories at node 3826

temperatures are lower than 70 °F, Case b will have higher early-time temperatures.

Temperature contours

Contours of temperature are presented for days 180, 360, 540, and 720 in Figures 98, 99, 100, and 101, respectively. Each figure presents a plot for Cases a, b, and c.

The three plots shown in Figure 98 at day 180 show significant differences between all three plots. Temperature gradients through the slab are similar for Cases a and c, but temperatures at the base of the slab are slightly higher for Case a. Temperatures in the slab and lower portions of the wall are nearly constant for Case b as they have nearly equilibrated to the ambient temperature of 70 °F. The lift above the void has just been placed at day 180, so Cases a and b have a buildup of heat at the lift interfaces that does not occur in Case c.

At day 370 (Figure 99) the difference in temperature contours for Cases a and c are very minimal. Case c does have a portion of the base slab at a lower temperature than Case a, and temperatures directly above and below the void in the wall also appear to be lower for Case c. Other than these differences though, Cases a and c are nearly identical. As would be expected, Case b is quite different from Cases a and c. Very little variation in temperature exists throughout the monolith for Case b.

Figures 100 and 101 at days 550 and 730, respectively, show how heat generated due to hydration has virtually no effect on the temperatures at these times as can be seen when comparing Cases a and c. This should have been expected from the results presented in the time-history temperature plots. Case b, as in Figure 99, is significantly different than the other two cases, with the wall temperatures having reached a constant. Figures 100b and 101b are actually identical but look different because different scales being used. If the interface between the red and orange contour, with a value of 65.78 °F, of Figure 100b is compared to the interface of the light green and medium green contour, with a value of 65.89 °F, of Figure 101b, the location of the interfaces are at approximately the same position.

Stress Analysis

Time-history plots

Time-history plots of the horizontal stress in the slab are presented at several locations in Figures 102 through 106. The only trend that can be seen in all five of these plots is that the peak stresses for Case a are always

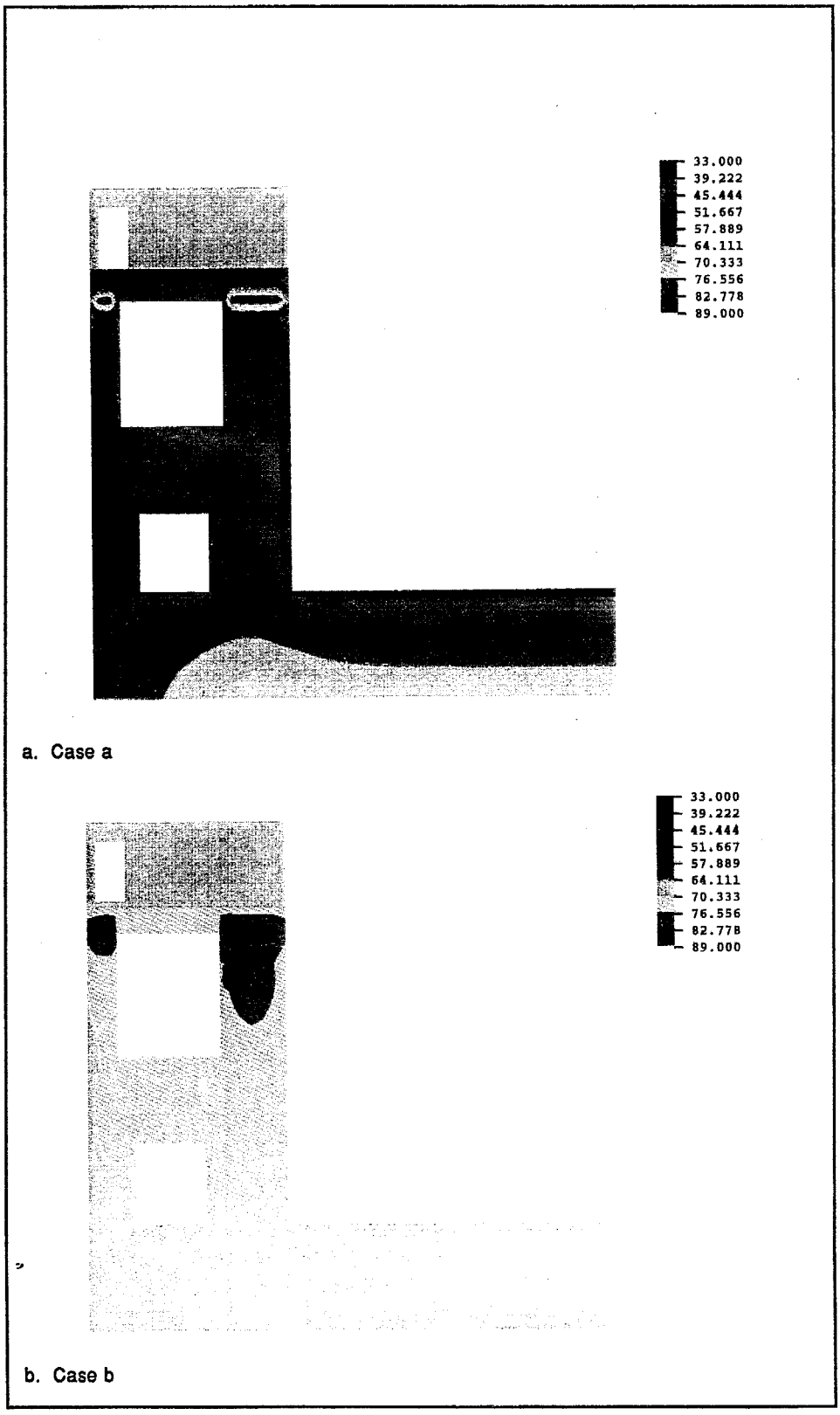

Figure 98. Temperature contours at 180 days after start of construction (step = 241, amp = 180) (Continued)

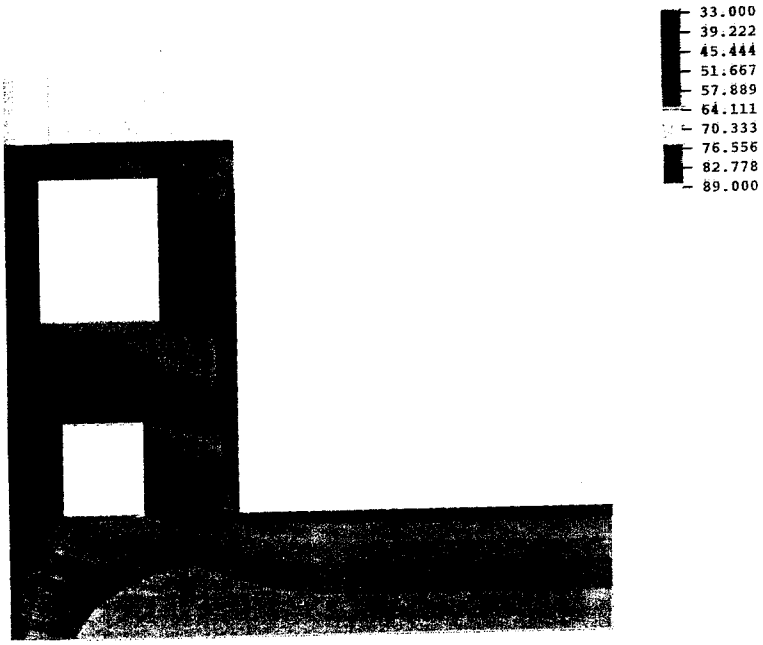

c. Case c

Figure 98. (Concluded)

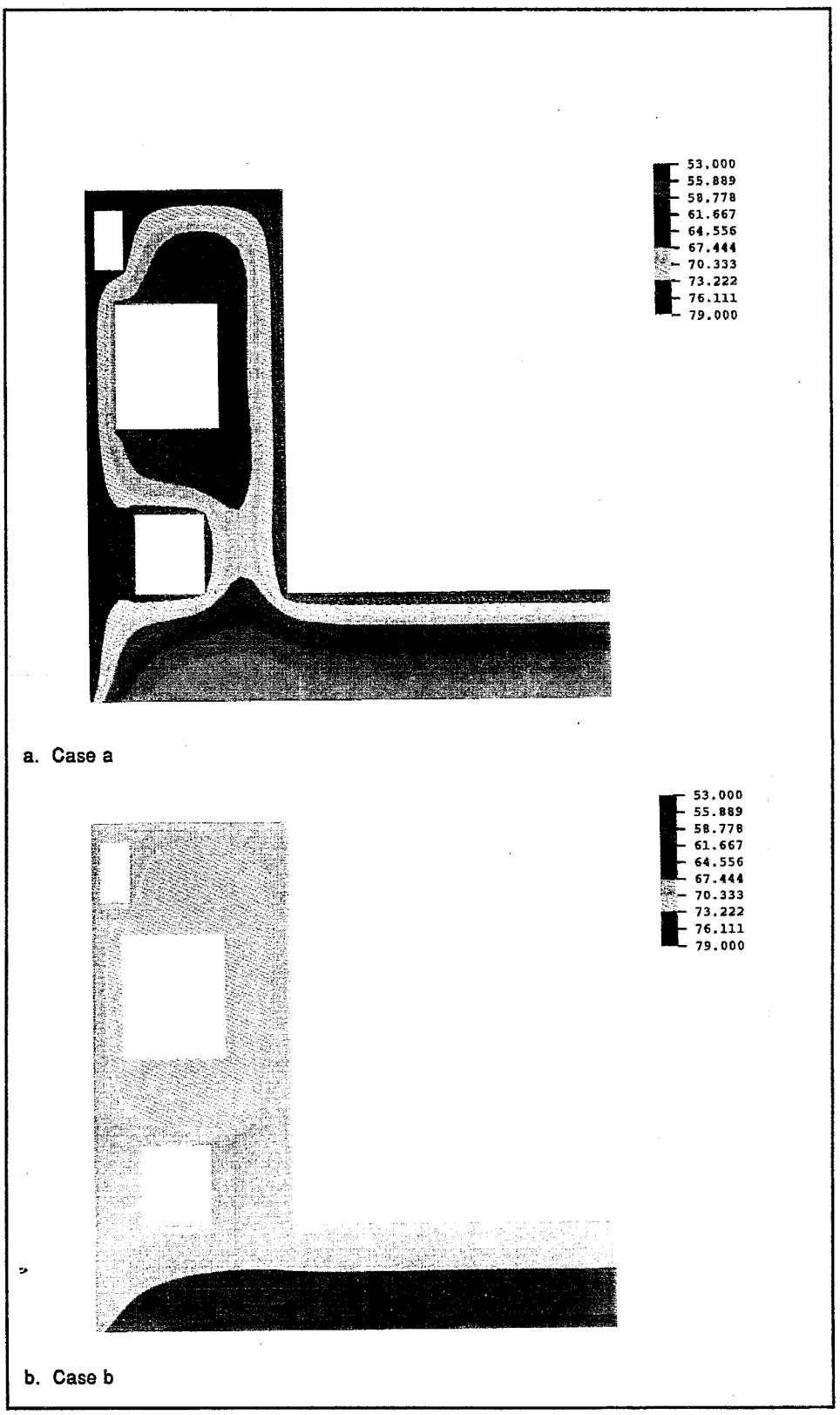

Figure 99. Temperature contours at 370 days after start of construction (step = 340, amp = 370) (Continued)

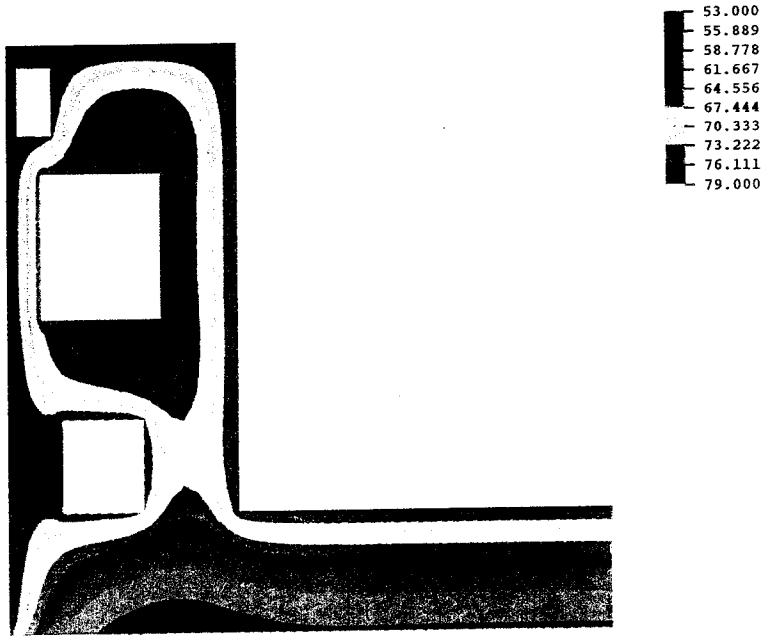

c. Case c

Figure 99. (Concluded)

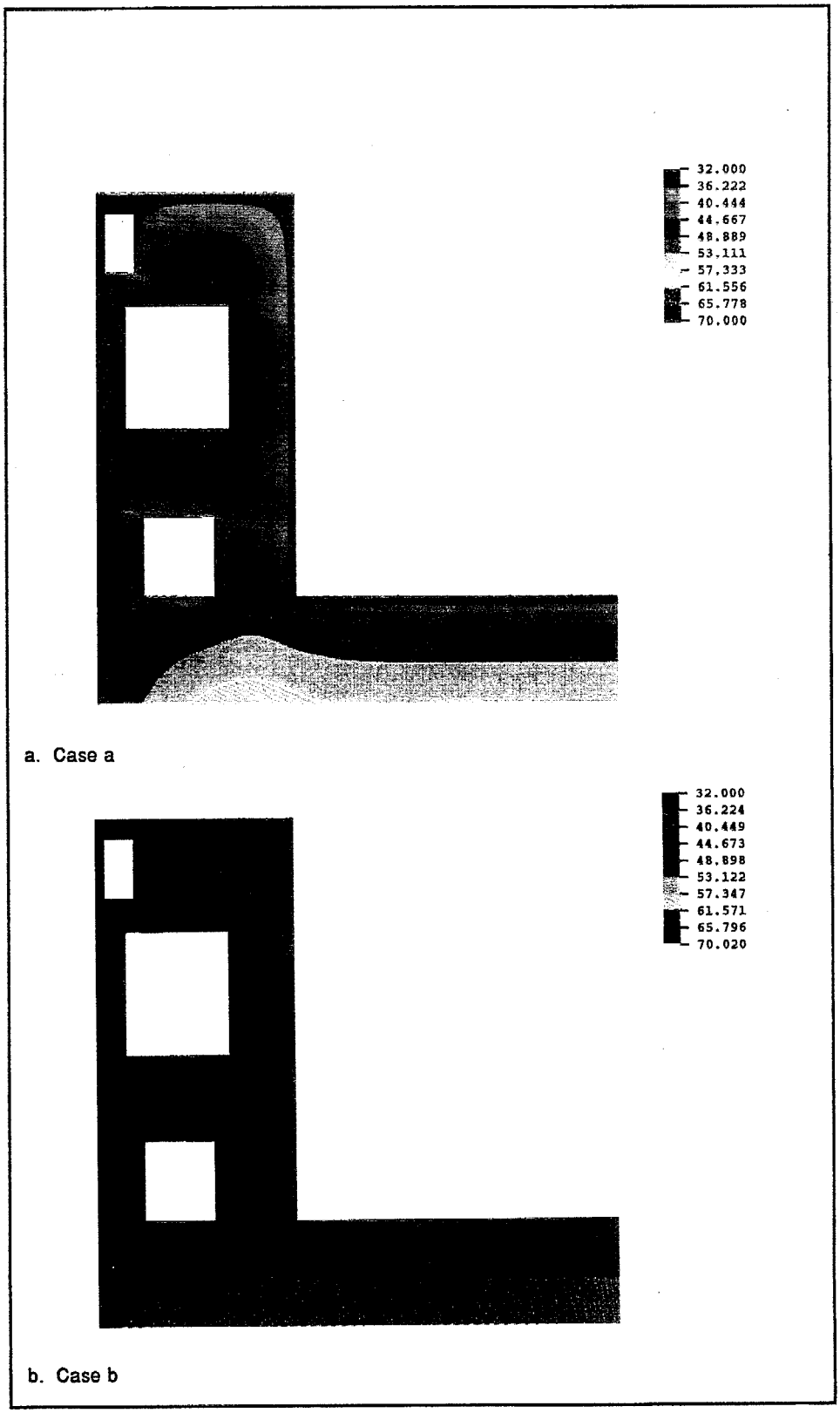

Figure 100. Temperature contours at 550 days after start of construction (step = 358, amp = 550) (Continued)

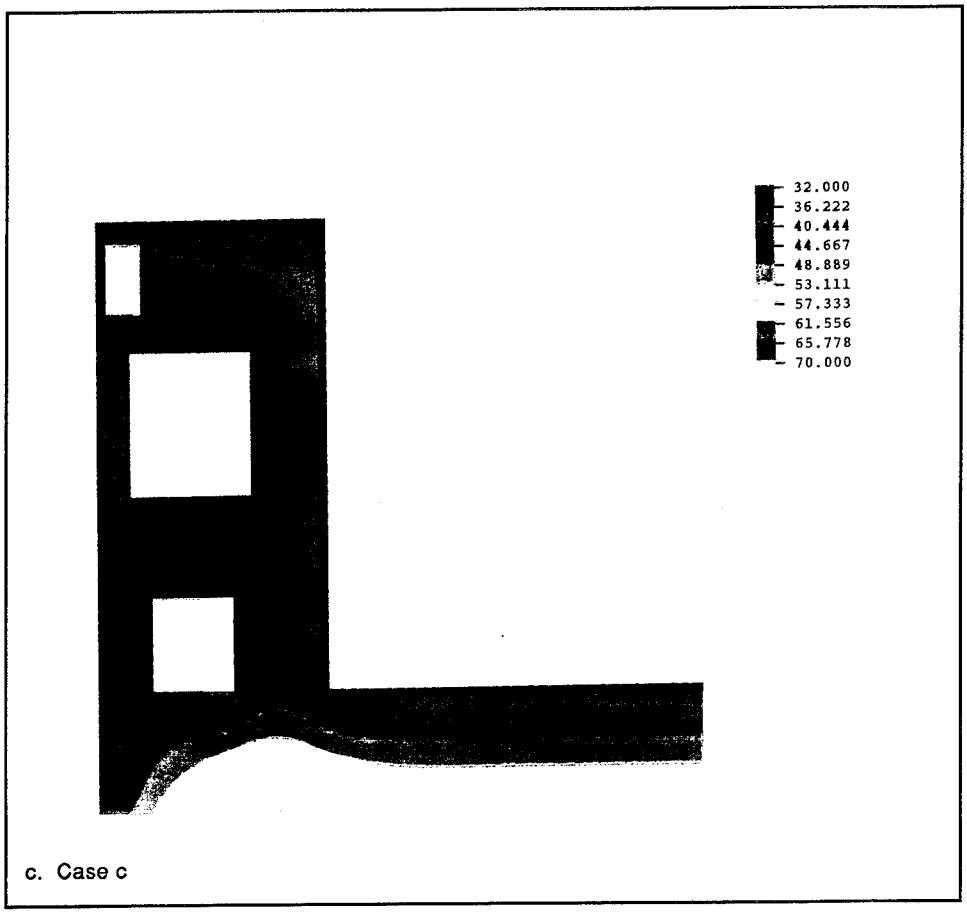

c. Case c

Figure 100. (Concluded)

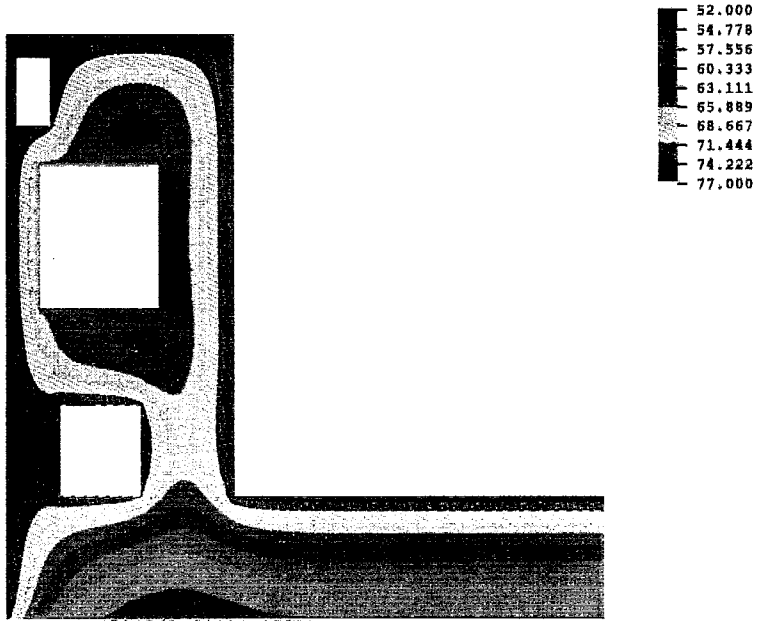

a. Case a (step = 376, amp = 730)

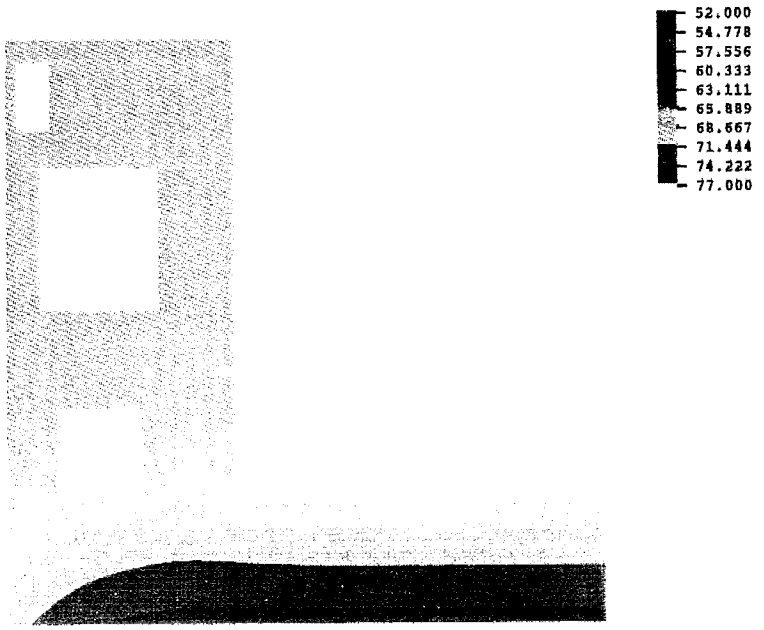

b. Case b (step = 373, amp = 700)

Figure 101. Temperature contours at 730 days after start of construction (Continued)

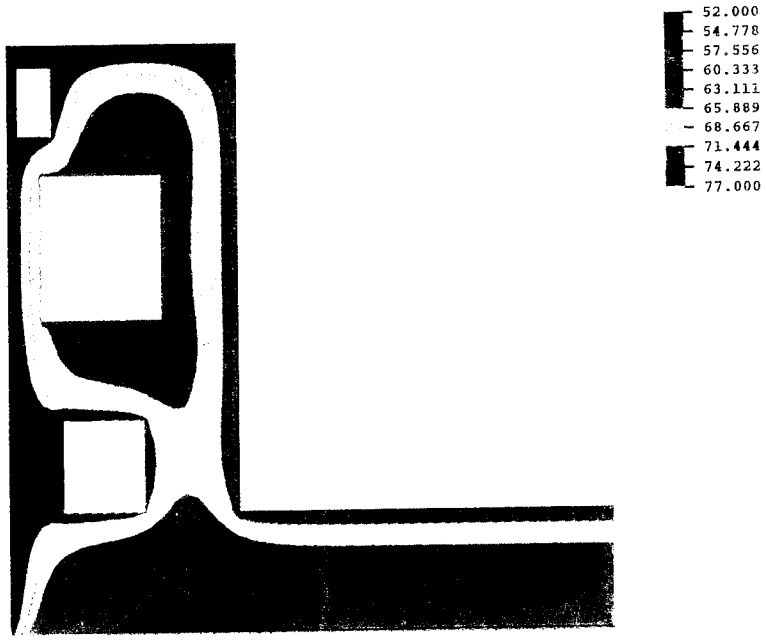

c. Case c (step = 376, amp 730)

Figure 101. (Concluded)

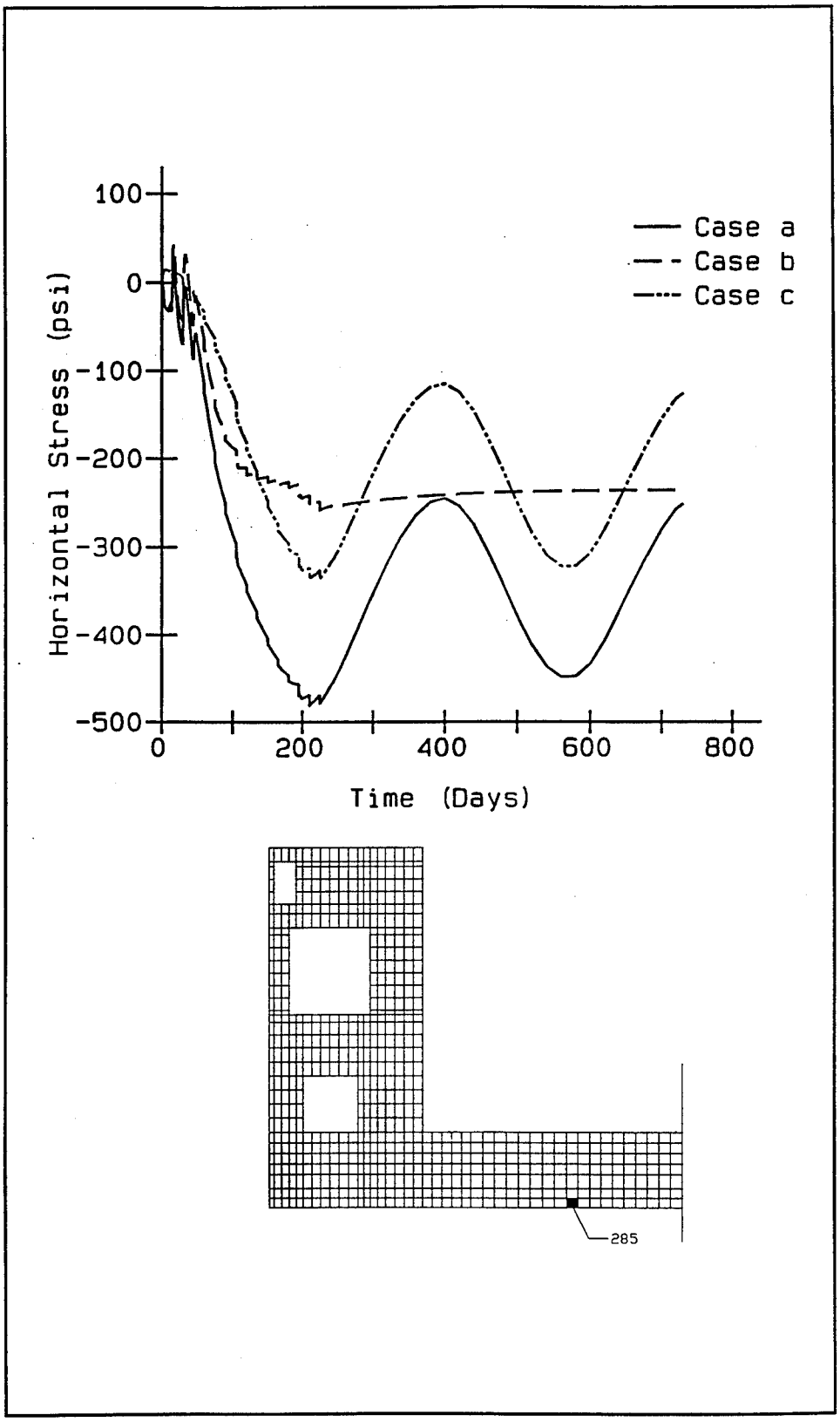

Figure 102. Horizontal stress time-histories at element 285

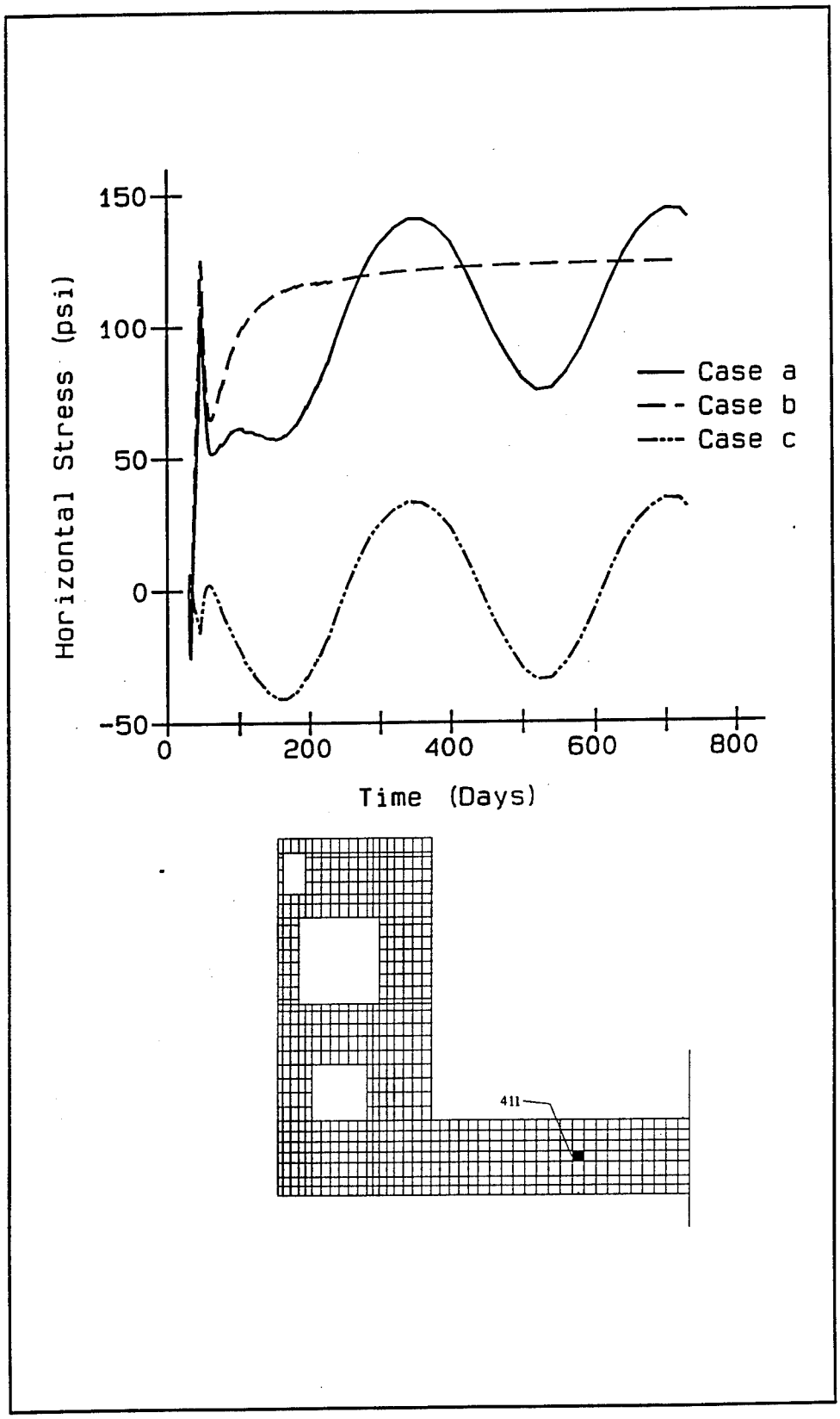

Figure 103. Horizontal stress time-histories at element 411

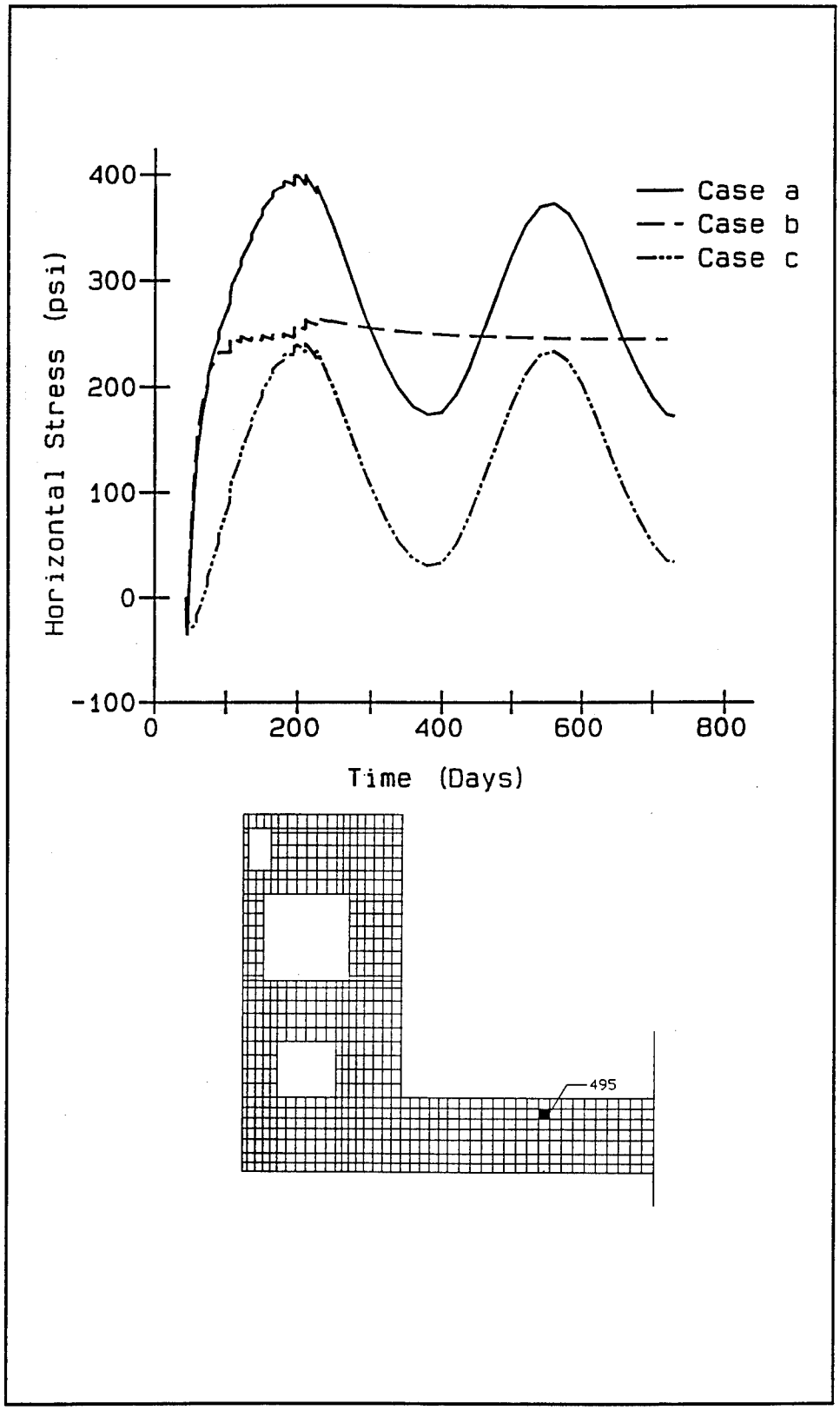

Figure 104. Horizontal stress time-histories at element 495

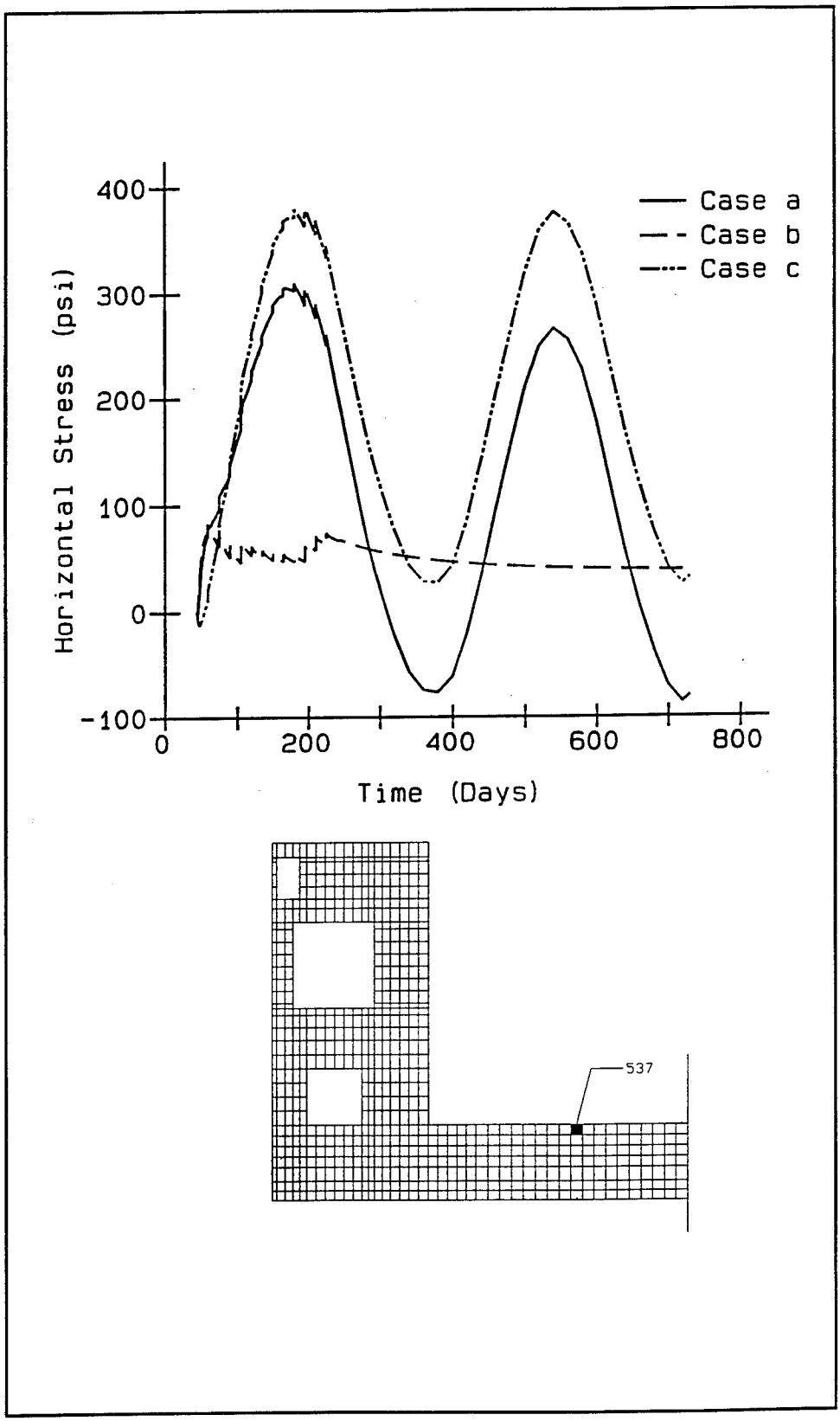

Figure 105. Horizontal stress time-histories at element 537

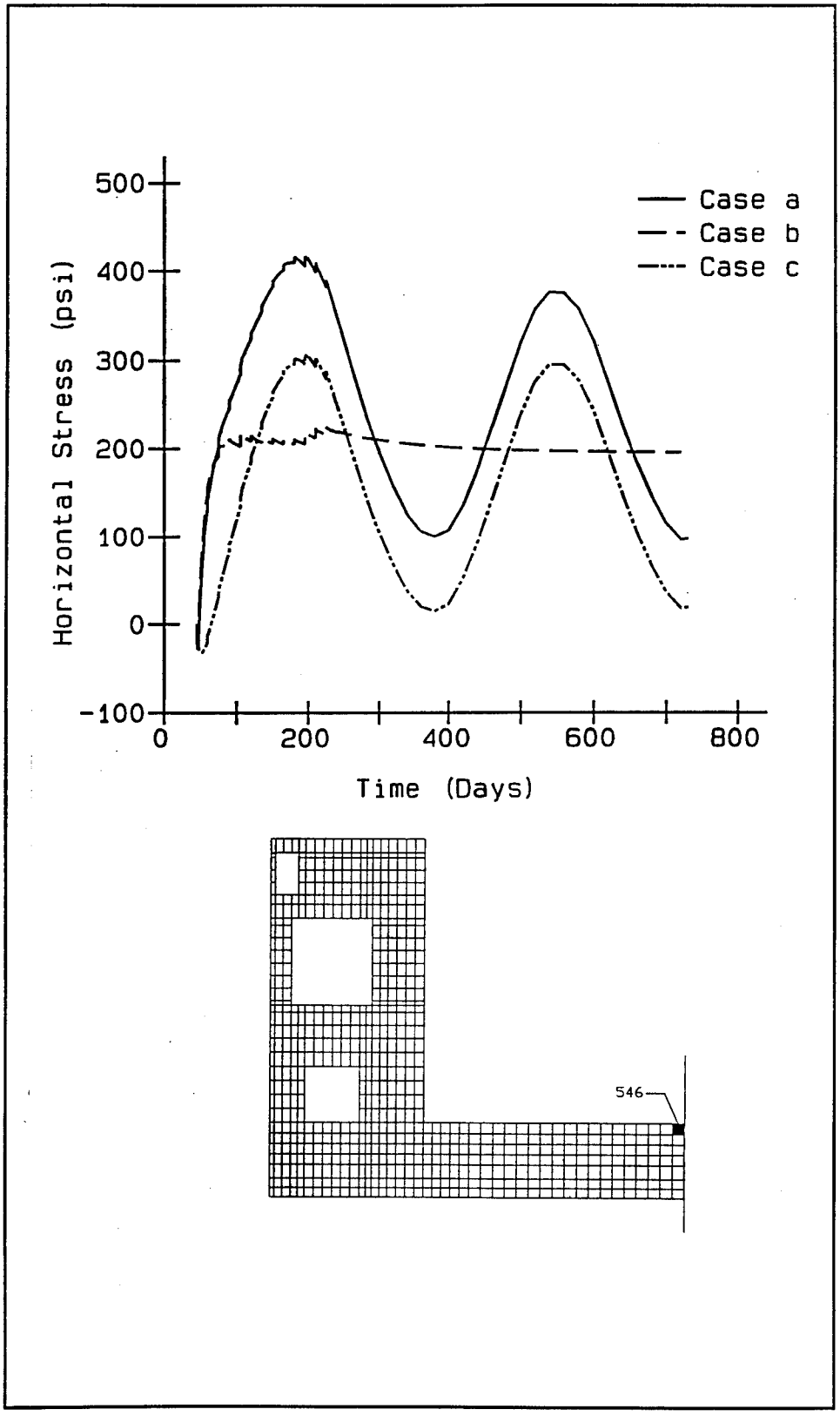

Figure 106. Horizontal stress time-histories at element 546

larger than the long-term stresses resulting from Case b. In general, the maximums that result (compressive in Figure 102, tensile elsewhere) occur due to conditions modeled in Case a, although at element 546, Case c provided the controlling condition. The effects of ambient temperature are obvious when comparing Cases a and c to Case b. Looking closely at Figures 102 through 106, at early times the heat due to hydration is the major factor, since initially Cases a and b follow nearly identical paths. Finally, it is also obvious that the heat of hydration is not a negligible effect, since significant differences do exist between plots for Cases a and c.

Many of the same observations made in the previous paragraph will apply to the plots of vertical stress shown in Figures 107 through 109. Again, Case a controls at locations of peak stress except for one location (element 965) where the maximum value for Case c slightly exceeds the maximum obtained from Case a. The primary point of note for Figures 107 through 109 is that once the stresses reach an equilibrium in Case b, the resulting stress is very near zero; thus, it appears that for wall portions of the monolith, heat of hydration effects in this portion of the structure are negligible. But if Cases a and c are compared, it shows that the combination of the heat of hydration and ambient does have an affect on the structural behavior.

Cracking potential contours

Figures 110, 111, 112, and 113 are cracking potential plots at days 180, 360, 540, and 720, respectively. Similarities exist, particularly in the slab, between all three cases, but the value of the percentages reported varies appreciably from case to case. At day 180 (Figure 110), the highest potentials reported are all at or near the top of the slab, but the shapes of the contours vary from case to case. For Case a, a ridge of high potentials occurs at a line below the top of the slab and the potential across the top of the slab varies along its length, while for Case b, the highest potentials also occur below the top of the slab but the potential at the top of the slab is fairly constant. Finally for Case c, the highest potentials occur directly at the top of the slab and vary along its length. The variation of the potentials across the top of the slab would seem to indicate that this condition is created by the ambient conditions since it does not occur for Case b. In addition, the fact that the maximum potentials occur at a point below the top of the slab would appear to demonstrate that this phenomenon is created by the heat of hydration since it does not occur in Case c.

Potentials in the walls are all low at day 180 (Figure 110), although there are considerable differences in the contours at the location near the top of the void where the most recently placed lift is located. The heat of hydration effects do have a definite influence on the stress states at the time of year this plot is shown.

At day 360 (Figure 111), shapes of contours in the slab for Cases a and b are similar, but the magnitudes are slightly different, while Case c has

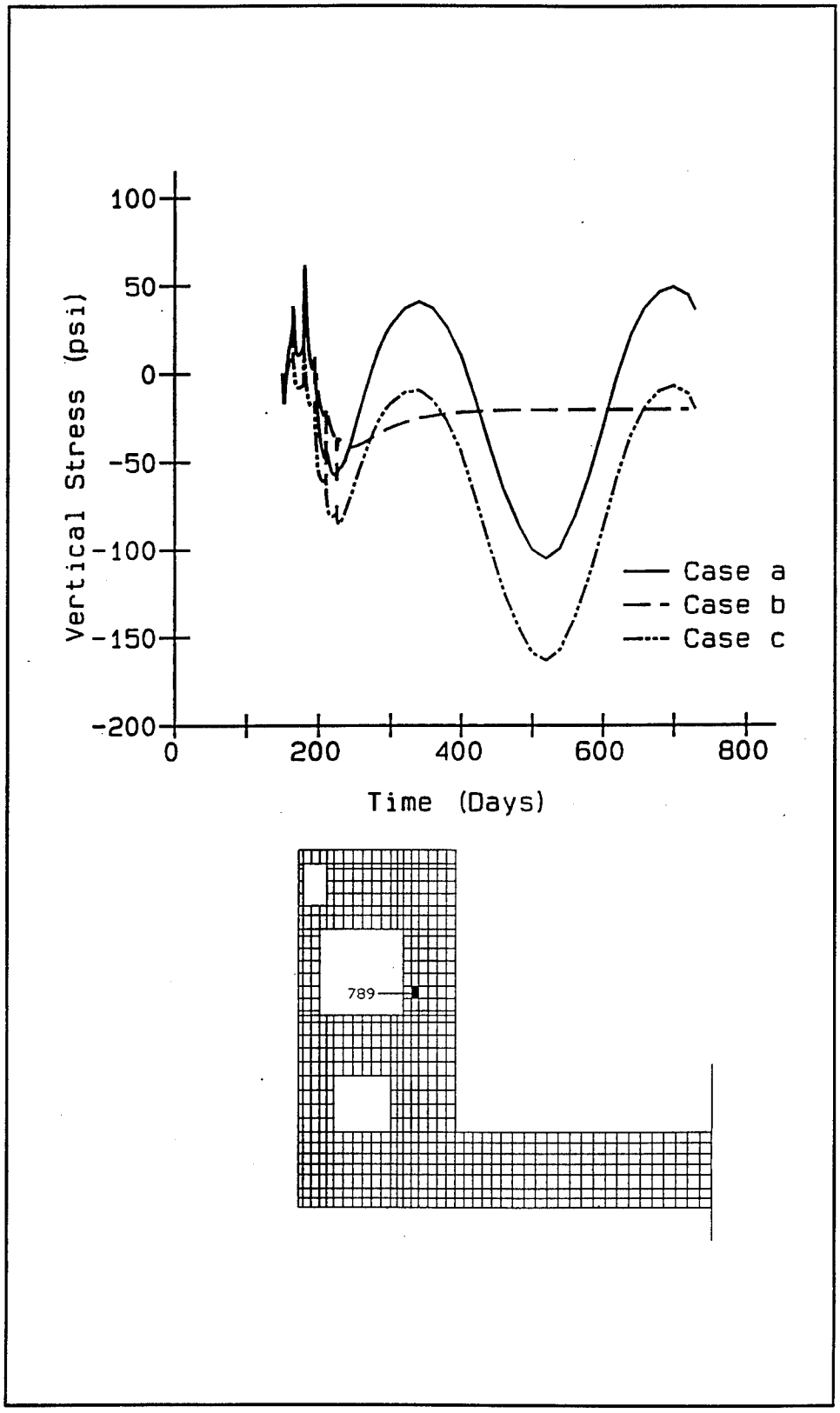

Figure 107. Vertical stress time-histories at element 789

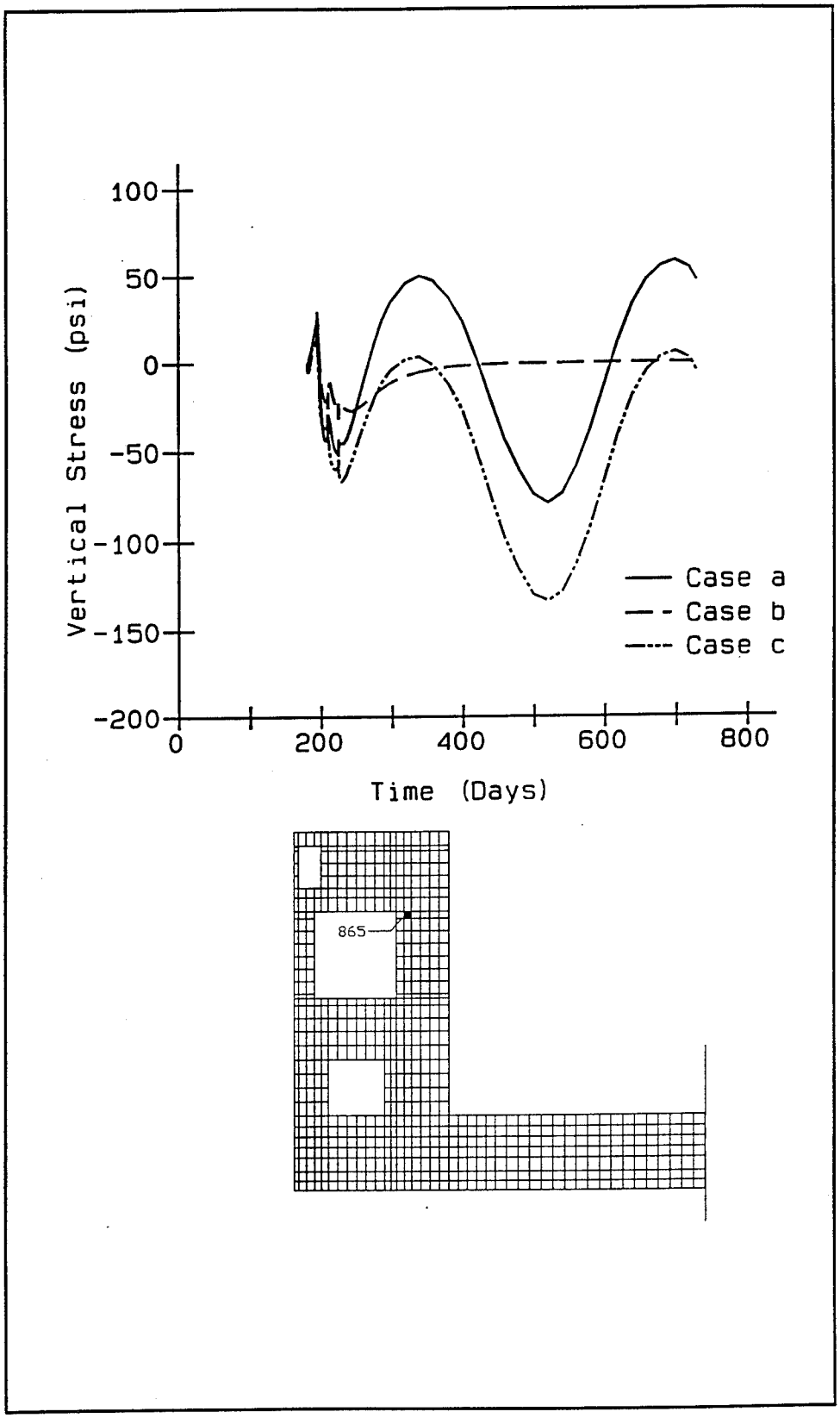

Figure 108. Vertical stress time-histories at element 865

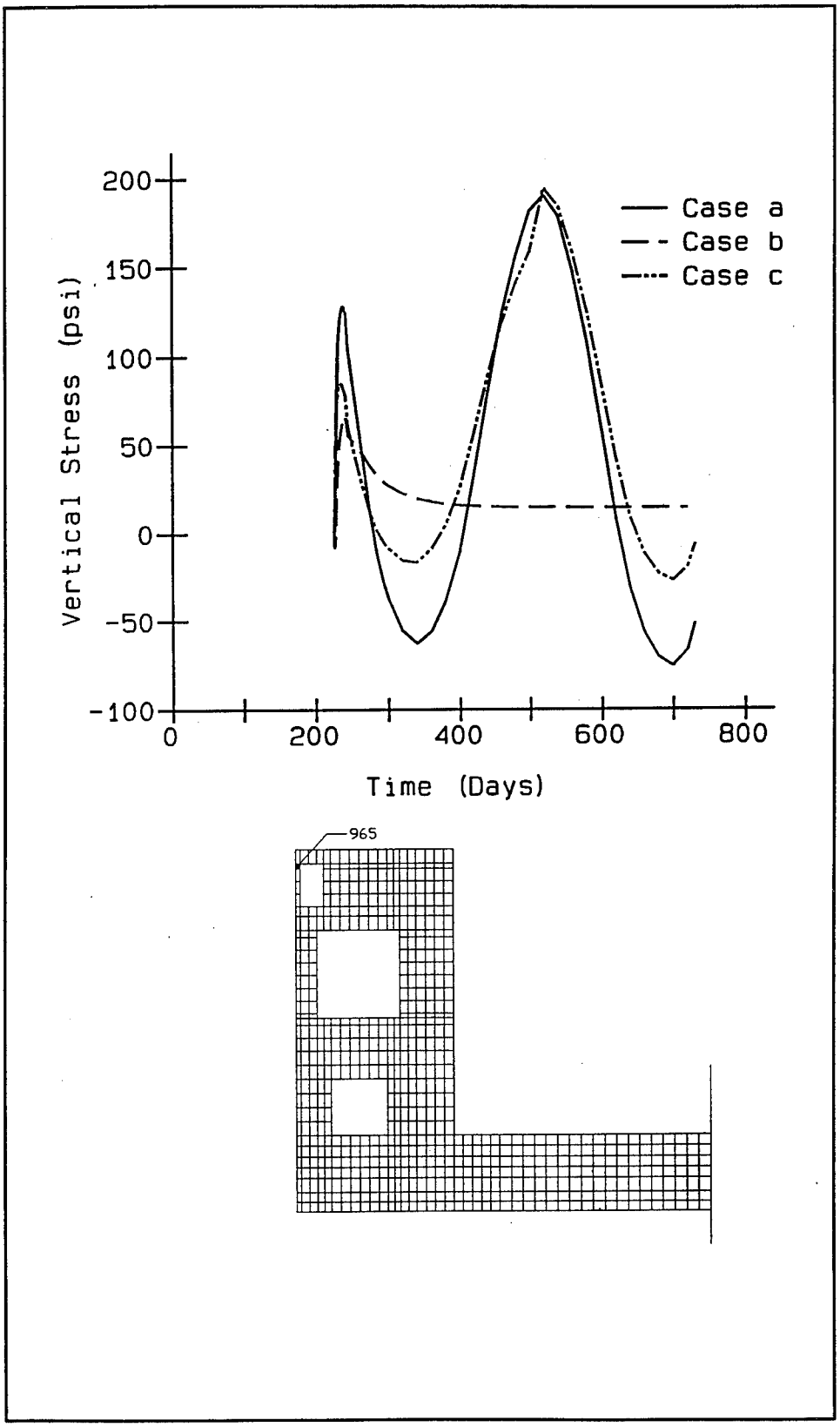

Figure 109. Vertical stress time-histories at element 965

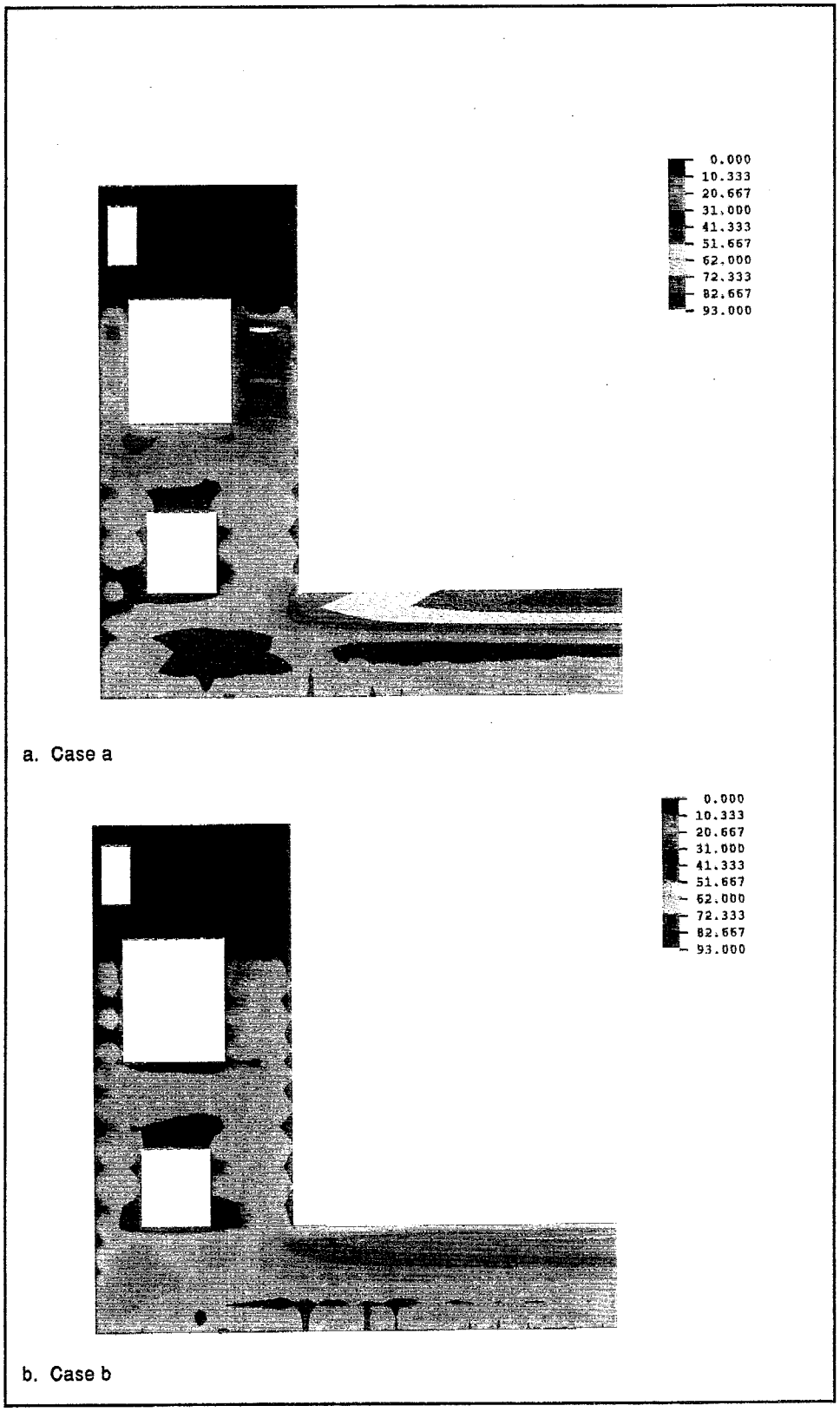

Figure 110. Cracking potential contours at 180 days after start of construction (step = 156, amp = 180) (Continued)

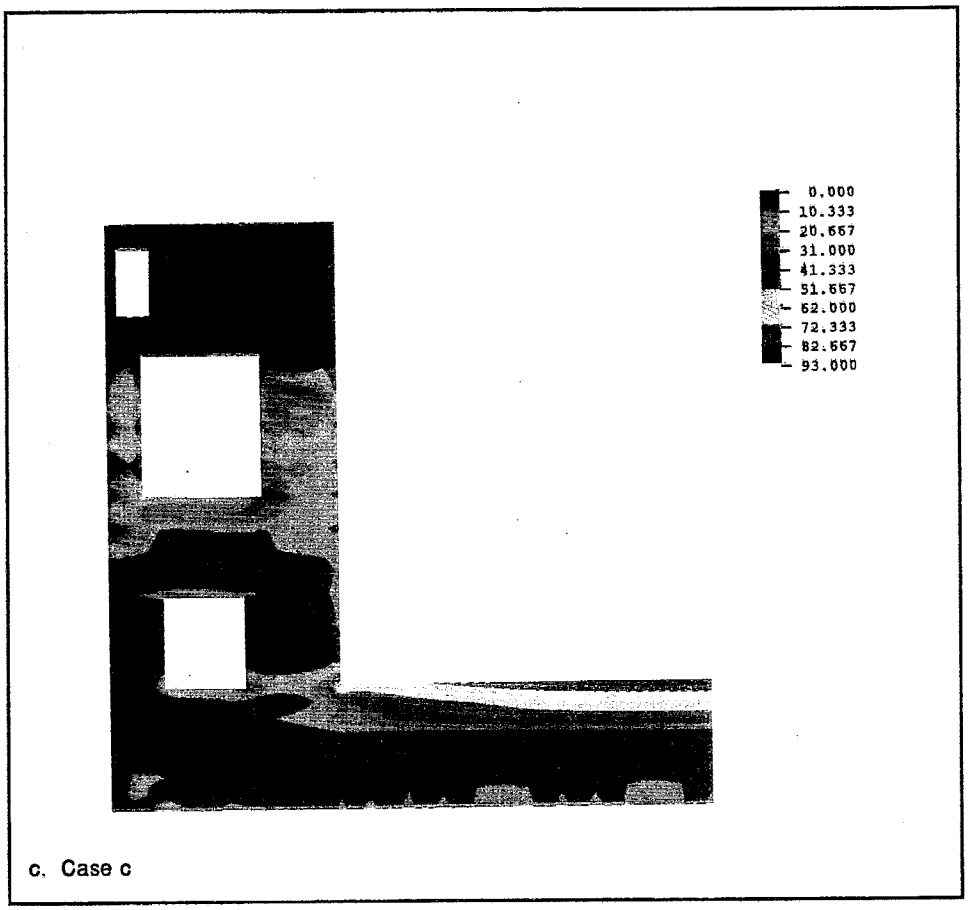

c. Case c

Figure 110. (Concluded)

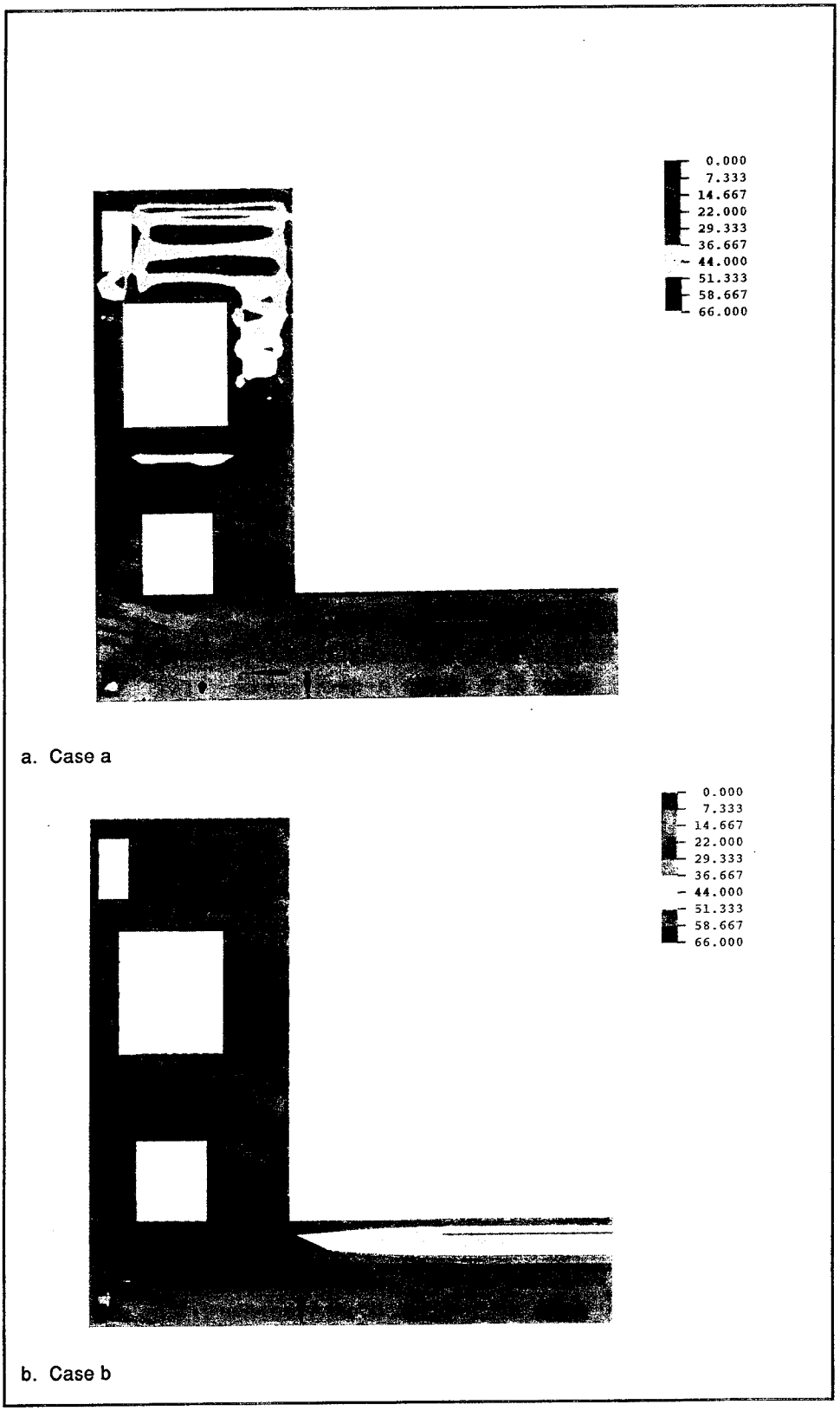

a. Case a

b. Case b

Figure 111. Cracking potential contours at 360 days after start of construction (step = 218, amp = 360) (Continued)

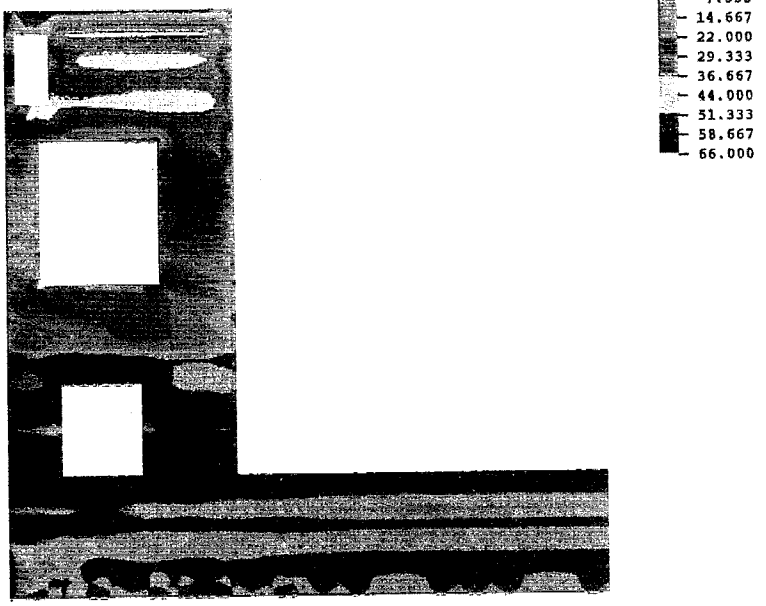

c. Case c

Figure 111. (Concluded)

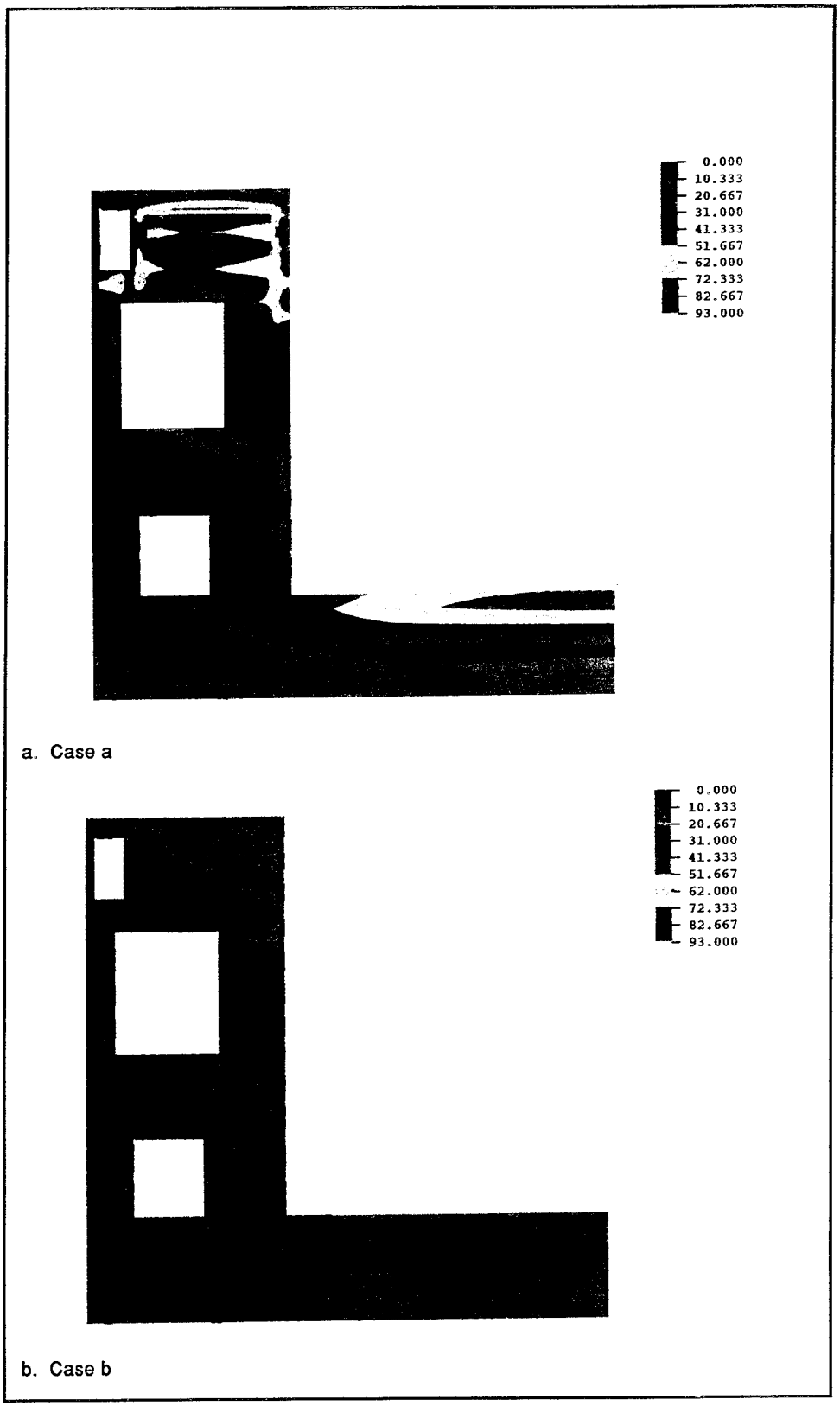

Figure 112. Cracking potential contours at 540 days after start of construction (step = 227, amp = 540) (Continued)

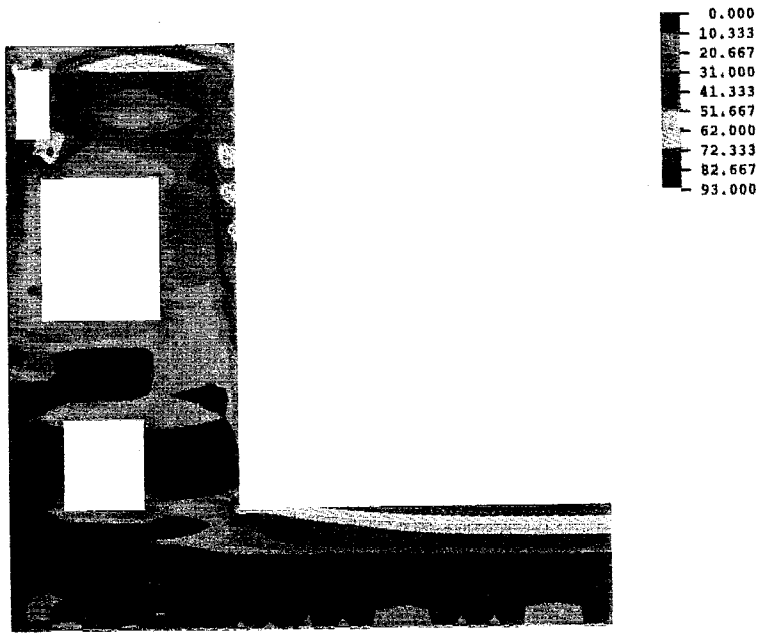

c. Case c

Figure 112. (Concluded)

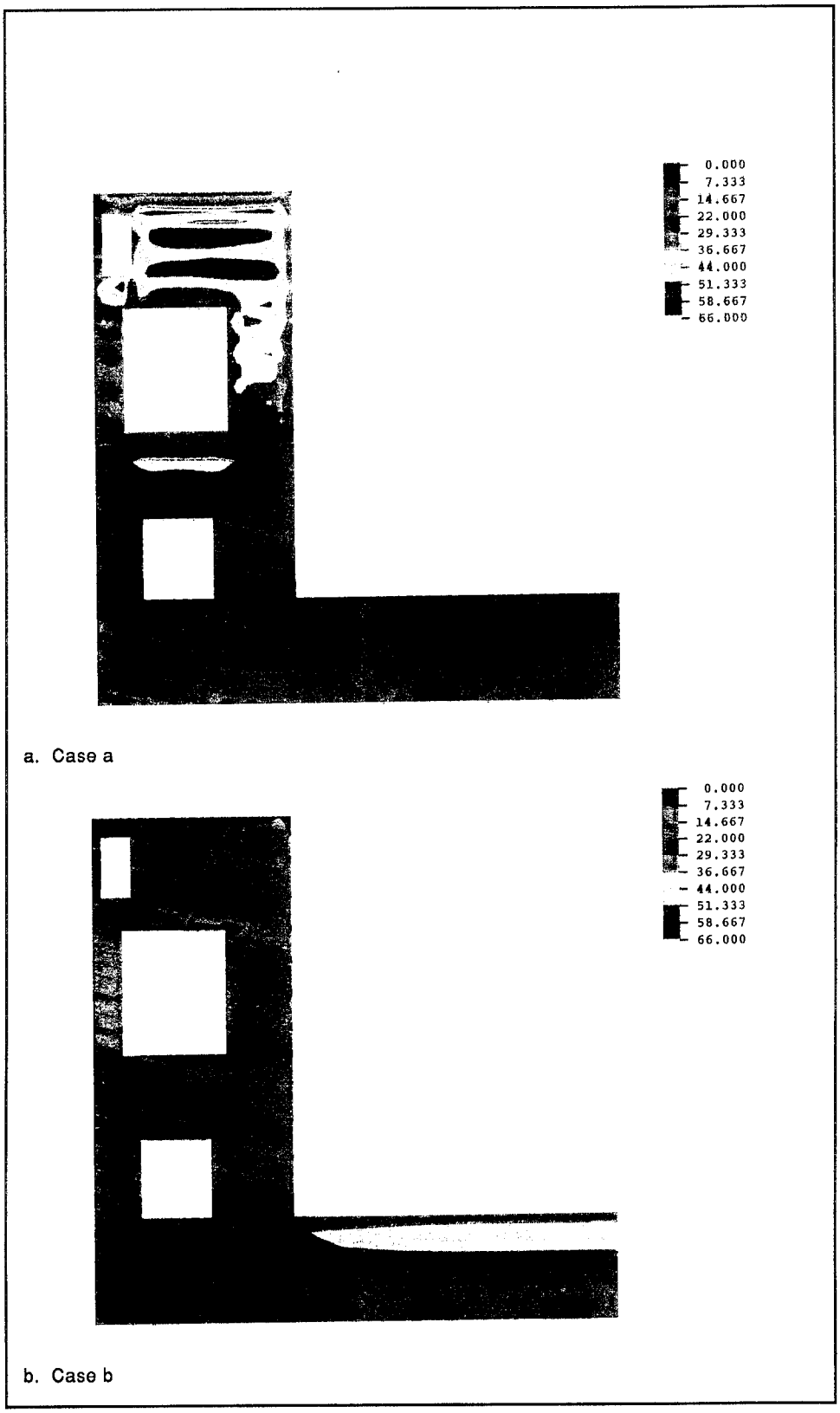

Figure 113. Cracking potential contours at 720 days after start of construction (step = 236, amp = 720) (Continued)

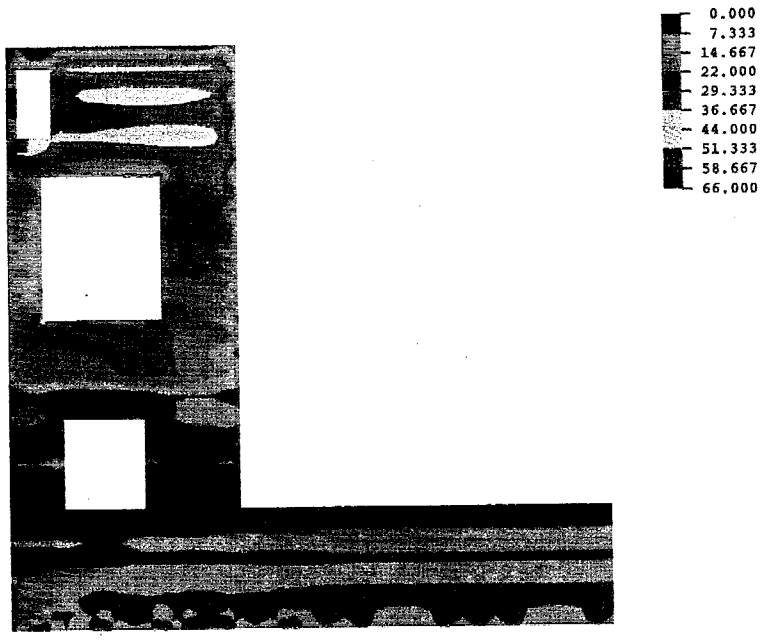

c. Case c

Figure 113. (Concluded)

considerably lower potentials than the other two cases. In the walls, Cases a and c have similarly shaped contours, but they also have different magnitudes. Contours in the top of the wall in Cases a and c are likely to be a result of the cold winter temperatures present at the time they were placed. Likewise, the contours observed in the base slab for Cases a and b would seem to be attributed to the heat of hydration.

At day 540 (Figure 112), contours in the base slab of the monolith are very similar to the contours seen in Figure 110 for day 180. There are small differences in the shapes and magnitudes of the contours, but in general the plots are very nearly the same. Crack potentials in the wall are in general very low except near the top of the wall for Cases a and c, which once again would indicate that the high potentials are being driven by the ambient conditions.

Finally, Figure 113 shows crack potentials at day 720. If these plots are compared for each case to the plots in Figure 111 (day 360), the differences are very small, and therefore the discussions of Figure 111 will apply to Figure 113 as well.

Summary

The results of the study presented in this chapter show that while the worst conditions result several months after the start of construction due to changing ambient conditions, the heat generated in the early portions of the analysis can significantly affect the long-term stresses. The heat generated when the concrete is placed causes the behavior of the structure to be different at early times, and this continues to be reflected at later ages in the life of the structure. Therefore, high stresses can not be attributed only to changing ambient conditions, since the results of this study show that neglecting the heat of hydration effects would be unconservative.

Examination of time-history stress plots also demonstrates how significant ambient effects are when comparing the case which includes changing ambient temperatures and the heat of hydration (Case a) to the case which used a constant ambient condition (Case b). The constant ambient condition demonstrates how important inclusion of the changing ambient conditions are, since the constant ambient condition results in a near constant stress level after 200 days and generally provides a lower maximum tensile stress than the changing ambient case. The time-history plots also show the stress varies by up to 300 psi for the changing ambient case.

7 Conclusions and Recommendations

Parametric studies are a valuable means for making evaluations of the various parameters which affect the behavior of the structure. The objective of the studies summarized in this report were to perform such an evaluation. The results of these parametric studies should be used in assisting designers in making decisions regarding NISA studies that may be performed in the future. The results described in this report provide information regarding the time of year to start an analysis, the lift interval placement rates to specify, and the type of analysis approach to use. The results presented in the report in conjunction with the conclusions and recommendations given in the following paragraphs provide knowledge which can be used by the designer to make informative decisions.

Conclusions

One of the primary conclusions that can be drawn is that ambient temperatures are a primary factor in the development of thermal stresses. This can be seen in the results reported in all of the analyses, particularly if the time-history plots of stress are reviewed. In these plots, the stresses peak during the cold winter months, and then during the summer months the stresses are at their lowest values. This trend has been observed in other studies as well (Garner et al. 1992; Fehl, Riveros, and Garner in preparation). Although the ambient temperature appears to control the time-of-peak stresses, stresses occurring at early times (0-20 days) should be observed closely as well. The strength of the concrete is lower at these times, and the stress and strain required to cause cracking is not as high. In addition, it was observed that while the colder winter temperatures may drive the maximum stresses in the concrete, neglecting the heat of hydration will have an unconservative effect on the maximums that do occur.

From the analyses evaluating different construction start times, it became clear that insulation is a critical component for winter placements, which is another item supported by other studies (Garner et al. 1992). It

was also seen in this set of studies that use of the proper values of placing temperatures can also be critical to the resulting structural behavior, i.e., using near ambient temperatures for winter placements.

The study evaluating the type of analysis to use in a NISA showed that the analysis using the generalized plane strain approach provided the worst case but was not significantly higher than the other two approaches. Very little difference was exhibited between the results of the plane stress and the plane strain analyses, which has been observed previously (Truman, Petruska, and Fehri 1992; Garner et al. 1992).

From the study on lift intervals, it can be noted that using longer intervals between placements for long, thin sections (such as U-frame lock slabs) may be the worst condition that can be specified. This conclusion does not necessarily apply to sections in the wall. In some locations, the longer intervals between lift placements produced higher stresses, but in other locations, it did not.

Recommendations

As a result of the studies in this report, there are a couple of general recommendations that should be considered when designers are considering the performance of a NISA:

a. Insulation should always be included in an analysis when ambient temperatures can be expected to be below 40 °F.

b. Analyses which are on the border line of creating critical conditions should consider a parametric study which uses extreme cases of lift interval placement schemes.

Other recommendations given below are for additional studies that should be considered in the future to supplement the work presented in this report.

a. The spring and fall analyses presented in Chapter 3 should be performed again. Placing temperatures should be used that coincide with the ambient conditions and insulation included for lifts placed when temperatures are below 40 °F.

b. Studies should be undertaken that use results from a 3-D analysis and correlate them to the results of 2-D analyses using the various analysis approaches.

c. Analyses evaluating lift placement intervals in wall sections should be performed for cases where the ambient conditions are nearly the same. The analyses performed in this report had large discrepancies in the ambient temperature by the time the top lifts of the monolith

were placed, because the construction of the monolith using 10- and 15-day lift intervals required considerably more time to construct than the 5-day case.

d. A lift interval study of a gravity structure (lock or dam) should be considered to determine if the behavior of this type of structure is similar to the behavior of the wall portion of a U-frame lock monolith.

References

Fehl, B. D., Garner, S. A., James, R. J., Dunham, R. S., and Zhang, L. "Nonlinear, incremental structural analysis for the lower miter gate monolith at Olmsted Locks and Dam," Technical Report in preparation, U.S. Army Engineer Waterways Experiment Station, Vicksburg, MS.

Fehl, B. D., and Merrill, C. A. "Three-dimensional nonlinear, incremental structural analysis of a culvert valve monolith wall, Olmsted Locks," Technical Report in preparation, U.S. Army Engineer Waterways Experiment Station, Vicksburg, MS.

Fehl, B. D., Riveros, G., and Garner, S. A. "Nonlinear, incremental structural analysis of the McAlpine Lock Replacement," Technical Report in preparation, U.S. Army Engineer Waterways Experiment Station, Vicksburg, MS.

Garner, S., Bombich, A. A., Norman, C. D., Merrill, C. A., Fehl, B. D., and Jones, H. W. (1992). "Nonlinear, incremental structural analysis of Olmsted Locks and Dams - volume I, main text," Technical Report SL-92-28, U.S. Army Engineer Waterways Experiment Station, Vicksburg, MS.

Garner, S., Hammons, M., and Bombich, A. (1991). "Red River Waterway thermal studies, report 2, thermal stress analyses," Technical Report SL-90-8, U.S. Army Engineer Waterways Experiment Station, Vicksburg, MS.

Hammons, M., Neeley, B., Alexander, M., Bombich, A., and Garner, S. (1991). "Concrete mixture selection and characterization study, Olmsted Locks and Dam, Ohio River," Technical Report SL-91-9, U.S. Army Engineer Waterways Experiment Station, Vicksburg, MS.

Headquarters, Department of the Army. (1990). "Special design provisions for massive concrete structures," Engineering Technical Letter 1110-2-324, Washington, DC.

Headquarters, Department of the Army. (1994). "Nonlinear, incremental structural analysis of massive concrete structures," Engineering Technical Letter 1110-2-365, Washington, DC.

Hibbitt, Karlsson, and Sorensen. (1989). *ABAQUS user's manual, version 4.8*, Providence, RI.

Merrill, C. A., Fehl, B. D., and Garner, S. A. (1995). "Nonlinear, incremental structural analysis of Olmsted Locks: phase III," Technical Report ITL-95-1, U.S. Army Engineer Waterways Experiment Station, Vicksburg, MS.

Truman, K. Z., and Fehl, B. D. "UMAT - a simplified overview," Technical Report in preparation, U.S. Army Engineer Waterways Experiment Station, Vicksburg, MS

Truman, K. Z., Petruska, D., and Ferhi, A. (1992). "Evaluation of thermal and incremental construction effects for monoliths AL-3 and AL-5 of the Melvin Price Locks and Dams," Contract Report ITL-92-3, U.S. Army Engineer Waterways Experiment Station, Vicksburg, MS.

REPORT DOCUMENTATION PAGE

Form Approved
OMB No. 0704-0188

1. AGENCY USE ONLY *(Leave blank)*	2. REPORT DATE	3. REPORT TYPE AND DATES COVERED
	June 1995	Final report

4. TITLE AND SUBTITLE
Parametric Evaluation of Construction and Analysis Procedures Using Nonlinear, Incremental Structural Analysis

5. FUNDING NUMBERS

6. AUTHOR(S)
Barry D. Fehl, Kevin Z. Truman, Gary Warmka

7. PERFORMING ORGANIZATION NAME(S) AND ADDRESS(ES)
U.S. Army Engineer Waterways Experiment Station
3909 Halls Ferry Road, Vicksburg, MS 39180-6199;
Washington University, Department of Civil Engineering
One Brookings Drive, St. Louis, MO 63130

8. PERFORMING ORGANIZATION REPORT NUMBER
Technical Report ITL-95-4

9. SPONSORING/MONITORING AGENCY NAME(S) AND ADDRESS(ES)
U.S. Army Corps of Engineers
Washington, DC 20314-1000

10. SPONSORING/MONITORING AGENCY REPORT NUMBER

11. SUPPLEMENTARY NOTES
Available from National Technical Information Service, 5285 Port Royal Road, Springfield, VA 22161.

12a. DISTRIBUTION/AVAILABILITY STATEMENT
Approved for public release; distribution is unlimited.

12b. DISTRIBUTION CODE

13. ABSTRACT *(Maximum 200 words)*

A series of parametric studies were conducted as part of the development of Engineering Technical Letter 1110-2-365, Nonlinear, Incremental Structural Analysis of Massive Concrete Structures, 31 August 1994. Parameters studied were construction start dates, intervals of lift placements, analysis procedure, and the ambient and heat of hydration effects. The studies were performed on a miter gate monolith from the Melvin Price Lock and Dam Project located on the Mississippi River.

The analyses of construction start dates compared construction starts in the winter, spring, summer, and fall to determine the most critical starting time. The study showed that spring and fall starts may produce the critical case and that insulation in the winter is absolutely critical.

The analysis procedures studied were plane stress, plane strain, and generalized plane strain, and the results showed little with respect to determining which procedure should be used. Further studies comparing to three-dimensional analyses are necessary.

Intervals of lift placements were varied between 5, 10, and 15 days. These lift placements showed that for long slabs, a longer interval may be the most critical case, but this may not hold true for wall sections. Results of comparing the ambient and heat of hydration effects show that the ambient is the main driver for thermal induced stresses but that the heat of hydration can have a significant effect on the resulting stresses.

14. SUBJECT TERMS
Aging materials
Cracking
Finite element
Incremental construction
Mass concrete

15. NUMBER OF PAGES
208

16. PRICE CODE

17. SECURITY CLASSIFICATION OF REPORT	18. SECURITY CLASSIFICATION OF THIS PAGE	19. SECURITY CLASSIFICATION OF ABSTRACT	20. LIMITATION OF ABSTRACT
UNCLASSIFIED	UNCLASSIFIED		